UNIVERSITY OF CALIFORNIA

Los Angeles

Targeting Metabolic Co-dependencies to Overcome Therapeutic Resistance in Cancer

A dissertation submitted in partial satisfaction of the

requirements for the degree Doctor of Philosophy

in Molecular and Medical Pharmacology

by

Yuchao Gu

2017

ABSTRACT OF THE DISSERTATION

Targeting Metabolic Co-dependencies to Overcome Therapeutic Resistance in Cancer

by

Yuchao Gu
Doctor of Philosophy in Molecular and Medical Pharmacology
University of California, Los Angeles, 2017
Professor Cauis Gabriel Radu, Co-Chair
Professor Paul Mischel, Co-Chair

Oncogenic mutations in cancer reprogram nutrient metabolism to drive tumor growth and survival under environmental stress and drug treatment, but the molecular mechanisms are not well understood. Using an unbiased proteomic screen, we identified mTORC2 as a critical regulator of amino acid metabolism in cancer via phosphorylation of the cystine-glutamate antiporter xCT. mTORC2 phosphorylates serine 26 at the cytosolic N-terminus of xCT, inhibiting its activity when nutrient is abundant to conserve glutamine-derived glutamate for biosynthesis. Genetic inhibition of mTORC2, or pharmacologic mTOR kinase inhibition, promotes glutamate secretion, cystine uptake and incorporation into glutathione. This adaptation renders tumor cells exquisitely sensitive to combined inhibition of glutathione synthesis and mTOR kinase, resulting in massive ferroptotic tumor cell death. These results identified an unanticipated mechanism of amino acid metabolic reprogramming in cancer, revealing a drug-induced metabolic co-dependency as a potentially exploitable therapeutic vulnerability.

The dissertation of Yuchao Gu is approved.

Heather R Christofk

Peter John Tontonoz

Cauis Gabriel Radu, Committee Co-Chair

Paul Mischel, Committee Co-Chair

University of California, Los Angeles

2017

For the Love of Science, My Dearest Family and Friends.

TABLE OF CONTENTS

LIST OF FIGURES

Chapter 1.

Chapter 2.

ACKNOWLEDGEMENTS

I was always amazed whenever I looked back and wondering how I have become who I am today, just like I've always been pondering on the question of how a normal cell transforms into a cancer cell. And I do very much believe that these two questions might share the similar answer with why everything else exist, why the universe exist, which was illustrated by Stephen Hawking when he was asked the question whether god created the universe, in which he said: Spontaneous creation is the reason there is something rather than nothing, why the universe exist, and why we exist.

Just like the creation of the universe, which is the consequence of random events albeit constrained by the laws of physics, the creation of the "me" today also involved randomness and spontaneity, including all of you who I want to express my greatest and deepest gratitude and thanks to.

First and the foremost, I want to convey my deepest loves and thanks to my wonderful parents and my family, who have really been the greatest support and inspiration throughout my life. I want to thank my dad, Zhengfei Gu, who is also a scientist himself, for all his advice of how to become a good scientist, and always pushing me to learn and think, and believing in me that I could achieve more than what I could imaging. Also I want to thank my mom, Ning Yang, for always being there, encouraging me and comforting me when life is hard, for telling me never to lose my confidence. And all my admiration goes to her for being a doctor and cancer survivor. Her lovingness and kindness to her patients and her bravery and courage to fight cancer have seeded my dream of studying cancer and amplified my desired to alleviate the pains and sorrows of cancer patients in the future.

Another important person I wanted to thank is my mentor Paul Mischel, for being the best mentor that I could ever have asked for. His passion for science, his unique and critical way of thinking, and his guidance to urge us to contemplate on the big and important questions has undoubtfully sculpted me into a better scientist. Thank you Paul for always having faith in me, for all the wonderful and inspiring discussions we had, for always being so supportive and encouraging both for my research and my life. I also want to thank all of my committee members, Heather Christofk, Cauis Radu and Peter Tontonoz, for being the most wonderful committee I could have ever had. Thank you Heather for all of your brilliant ideas and unique insights for my project, and showing the fascinating world of metabolism to me, and thank you for always welcoming me whenever I came back to UCLA for experiments and make your lab a second home to me. Thank you Cauis and Peter for your greatest and invaluable suggestions both for my project and my career, and thank you for always being so supportive. Also I want to express my thanks to Dr. Sam Chow, who have recruited me to this amazing Department of Molecular and Medical Pharmacology at UCLA, and opened for me the chances to explore a whole new world of possibilities. I would have never regretted coming all the way here.

And together I also want to thank all the past and present members of the Mischel lab, Ivan Babic, Kenta Masui, Beatrice Gini, David Nathanson, Genaro Villa, Junfeng Bi, Wendy Zhang, Sean Wu, Sudhir Chodhry, Feng Liu, Kristen Turner, Junho Ko, Akihisa Sakamoto, Shiro Ikegami, Tomoo Matsutani and Huijun Yang, without whom the work presented here wouldn't be possible. Thank you Ivan and Kenta for all the helpful discussions; thank you Beatrice and David Nathanson, for sharing all the happiness and sorrows in the lab with me; thank you Jerry, Junfeng and Wendy, for being such wonderful bay-mates, listening to my complains and excitements, and helping me

figure out what happened when experiments didn't work; and thank you Sean, Sudhir, Feng, Kristen, Junho, Aki, Shiro, Tomoo and Huijun, for all your help and discussions, and making the Mischel lab so wonderful. I also want to thank all of our collaborators that contributed to the work presented here, the members of Christofk lab, Minh Thai, Daniel Brass, Abby Krall, Carolina Jacobs, Wen Gu, and BJ Sullivan, for all your helpful discussion about metabolism and help with the experiments; members of the Zhou lab, Huilin Zhou and Claudio P. Albuquerque, for your help with the LC/MS phosphoproteomics studies; members from the Guan Lab, Zhipeng Meng, Haixin Yuan and Jenna Jewell for help with the in vitro kinase assay; Andrew Shiau and Tim Gahman from the small molecule group for providing compounds and reagents used in the experiments; as well as Kun-Liang Guan for help with the experiments, suggestions and insights for my project and paper.

Last but not the least, I want to express my many thanks to my dearest friends. First I want to thank my boyfriend Zhiping Feng, for always being so loving and caring, and always being there for me; and Briana Sullivan, my dearest roommate, thank you for being the best roommate ever, for always patiently listening to my endless science talks, and sharing with me your passions for workouts, baking and good food; and our cutest and cleverest and warmest kitty Mishka, for keeping me company throughout the lonely and cold winter days and making my thesis writing much less miserable; I also want to thank Rui Li, Ting Liu, Wenyuan Wang, Jie Li, Lydia Zheng and Niyati Metha who are the most amazing friends I could have ever had. It was all of you that made my life in grad school so much more fun and enjoyable, and I will always cherish the memories of our explorations, our challenges, our discussions about science and life, and our support for each other throughout my whole life.

Many others have also been an important part on my path of becoming who I am today, and even though I am not able to list out all the names, I still wanted to express my gratefulness and appreciation to everyone that made me and is making me who I am today. It is all of you that gave me the courage to embrace all the randomness in the future, and to become a better person, and a better scientist.

The work in this dissertation was performed under the direction of Dr. Paul S. Mischel and supported by grants from National Institute for Neurological Diseases and Stroke (NS73831), the Defeat GBM Program of the National Brain Tumor Society, the Ben and Catherine Ivy Foundation, and generous donations from the Ziering Family Foundation in memory of Sigi Ziering.

Part of this dissertation is based upon work from the manuscript:

Gu, Y., Albuquerque C.P., Braas, D., Zhang, W., Villa, G.R., Bi, J., Ikegami, S., Masui, K., Gini, B., Yang, H., Gahman, T.C., Shiau, A.K., Cloughesy, T.F., Christofk, H.R., Zhou, H., Guan, K., Mischel, P.S. mTORC2 reprograms amino acid metabolism in cancer by phosphorylation of the cystine-glutamate antiporter xCT. Submitted and currently under review at Molecular cell.

Y.G. and P.S.M. designed the experiments. Y.G. conducted most of the experiments and data analysis. Y.G. and C.P.A. performed SILAC labeling, LC/MS proteomic analysis, and in vitro kinase assay. H.Z. helped design the LC/MS proteomic experiment, in vitro kinase assay and data analysis. D.B. performed the metabolomics measurements and analyzed data. W.Z. conducted the Gene Ontology Analysis. G.R.V., J.B., S.I., B.G., K.M., H.Y. helped with conducting the experiments and data analysis. T.C.G., A.K.S., T.F.C., H.R.C., K.G. helped design the experiments and data interpretation. All authors discussed the results and helped revise the manuscript.

Vita

EDUCATION

2006-2010 B. S. School of Pharmaceutical Sciences,

Sun Yat-sen University

PUBLICATIONS

Gu, Y., Albuquerque C.P., Braas, D., Zhang, W., Villa, G.R., Bi, J., Ikegami, S., Masui, K., Gini, B., Yang, H., Gahman, T.C., Shiau, A.K., Cloughesy, T.F., Christofk, H.R., Zhou, H., Guan, K., Mischel, P.S. mTORC2 reprograms amino acid metabolism in cancer by phosphorylation of the cystine-glutamate antiporter xCT. Manuscript submitted and currently under review at Molecular cell.

Wei, W., Shin, Y.S., Xue, M., Matsutani, T., Masui, K., Yang, H., Ikegami, S., **Gu, Y.**, Herrmann, K., Johnson, D., Ding, X., Hwang, K., Kim, J., Zhou, J., Su, Y., Li, X., Bonetti, B., Chopra, R., James, C.D., Cavenee, W.K., Cloughesy, T.F., Mischel, P.S., Heath, J.R., and Gini, B. (2016). Single-Cell Phosphoproteomics Resolves Adaptive Signaling Dynamics and Informs Targeted Combination Therapy in Glioblastoma. Cancer cell 29, 563-573.

Villa, G.R., Hulce, J.J., Zanca, C., Bi, J., Ikegami, S., Cahill, G.L., **Gu, Y.**, Lum, K.M., Masui, K., Yang, H., Rong, X., Hong, C., Turner, K.M., Liu, F., Hon, G.C., Jenkins, D., Martini, M., Armando, A.M., Quehenberger, O., Cloughesy, T.F., Furnari, F.B., Cavenee, W.K., Tontonoz, P., Gahman, T.C., Shiau, A.K., Cravatt, B.F., and Mischel, P.S. (2016). An LXR-Cholesterol Axis Creates a Metabolic Co-Dependency for Brain Cancers. Cancer cell 30, 683-693.

Masui, K., Tanaka, K., Akhavan, D., Babic, I., Gini, B., Matsutani, T., Iwanami, A., Liu, F., Villa, G.R., **Gu, Y.**, Campos, C., Zhu, S., Yang, H., Yong, W.H., Cloughesy, T.F., Mellinghoff, I.K., Cavenee, W.K., Shaw, R.J., and Mischel, P.S. (2013). mTOR complex 2 controls glycolytic metabolism in glioblastoma through FoxO acetylation and upregulation of c-Myc. Cell metabolism 18, 726-739.

Gini, B., Zanca, C., Guo, D., Matsutani, T., Masui, K., Ikegami, S., Yang, H., Nathanson, D., Villa, G.R., Shackelford, D., Zhu, S., Tanaka, K., Babic, I., Akhavan, D., Lin, K., Assuncao, A., **Gu, Y.**, Bonetti, B., Mortensen, D.S., Xu, S., Raymon, H.K., Cavenee, W.K., Furnari, F.B., James, C.D., Kroemer, G., Heath, J.R., Hege, K., Chopra, R., Cloughesy, T.F., and Mischel, P.S. (2013). The mTOR kinase inhibitors, CC214-1 and CC214-2, preferentially block the growth of EGFRvIII-activated glioblastomas. Clinical cancer research : an official journal of the American Association for Cancer Research 19, 5722-5732.

Babic, I., Anderson, E.S., Tanaka, K., Guo, D., Masui, K., Li, B., Zhu, S., **Gu, Y.**, Villa, G.R., Akhavan, D., Nathanson, D., Gini, B., Mareninov, S., Li, R., Camacho, C.E., Kurdistani, S.K., Eskin, A., Nelson, S.F., Yong, W.H., Cavenee, W.K., Cloughesy, T.F., Christofk, H.R., Black, D.L., and Mischel, P.S. (2013). EGFR mutation-induced alternative splicing of Max contributes to growth of glycolytic tumors in brain cancer. Cell metabolism 17, 1000-1008.

Wang, J., Hwang, K., Braas, D., Dooraghi, A., Nathanson, D., Campbell, D.O., **Gu, Y.**, Sandberg, T., Mischel, P., Radu, C., Chatziioannou, A.F., Phelps, M.E., Christofk, H., and Heath, J.R. (2013). Fast metabolic response to drug intervention through analysis on a miniaturized, highly integrated molecular imaging system. Journal of nuclear medicine : official publication, Society of Nuclear Medicine 54, 1820-1824.

Chapter 1

Introduction

Deregulated Metabolism as a Hallmark of Cancer

In the 1956 *Science* paper: On the Origin of Cancer Cells (Warburg, 1956), Otto Warburg first proposed the theory that the fundamental cause of cell transformation and cancer is the forced adaptation to glycolysis-dependent energy generation as a consequence of impaired mitochondria respiration. And this was based on the observations of elevated fermentation across cancer cells, which is now also known as the Warburg effect (Otto, 2016). At the time his theory was met with strong opposing debates, as Sidney Weinhouse stated "…that there's no sound experimental basis for the believe that oxidative metabolism in tumors is impaired", and he argued that many cancers did not have decreased oxygen consumption despite elevated glycolysis (Weinhouse, 1956). Nevertheless, the important observation of elevated glycolysis across cancers remained inarguably true (Smith and Kenyon, 1973). These seemingly controversial observations raised two interesting questions. First, what is the real cause of elevated glycolysis in cancer cells? Sidney Weinhouse's denial of impaired respiration in cancer might not be 100% correct, as it was only based on no apparent changes in oxygen consumption observed in certain cancers. But increased glycolysis could also result from other changes in mitochondria metabolism that does not necessarily affect oxygen consumption, such as decoupling of mitochondria respiration with the TCA cycle. And the second question is how metabolic shift to elevated glycolysis led to neoplastic transformation? Considering that transformation of normal cells to neoplasia usually involves a series of genetic and epigenetic changes (Rangarajan et al., 2004), the question then lies in whether altered metabolism could lead to such changes and how. One possible mechanism might involve excess ROS produced as metabolic waste, which could potentially cause DNA mutations and increase genome instability. In addition, it was recently discovered that metabolism and epigenetics are intricately linked with each other. Metabolites such as α-ketoglutarate (α-KG), SAM, acetyl-CoA

and NAD+ are all important substrates and cofactors for epigenetic modifying enzymes, whereas metabolites that share similar chemical structures could act as inhibitors such as 2-hydroxyglutarate (2-HG), fumarate and succinate. Changes in intracellular levels of these metabolites could therefore affect the global epigenetic landscape of the cell, and increasing evidence have suggested that metabolism-mediated epigenetic changes are playing very important roles during neoplastic transformation (Flavahan et al., 2016; Janke et al., 2015; Kaelin and McKnight, 2013; Kottakis et al., 2016; Lu et al., 2016; Lu and Thompson, 2012).

Around the same time when Warburg's theory was proposed, in 1953, the DNA double helix structure was discovered by Watson and Crick (Watson and Crick, 1953), which revolutionized the whole field of cancer research. The following 50 years witnessed a booming era of cancer genetics together with the development of in-depth DNA sequencing technologies. As more and more cancers were being sequenced, accumulating findings of cancer-specific mutations has led to the general recognition that cancer is a genetic disease (Vogelstein et al., 2013), and therapies targeting these cancer-specific mutations could be a cure for cancer. It was not until the continuous failures of targeted therapies against oncogenic, or so-called "cancer-causing" mutations when people started to consider alternative perspectives of cancer in the hope to find better cures (Cloughesy et al., 2014; Huang et al., 2014; Vander Heiden, 2011).

In 2008, Christofk et al reported an intriguing discovery that almost all cancer cells and proliferating cells express the PKM2 isoform of pyruvate kinase, which is responsible for the metabolic shift to aerobic glycolysis, in other words, fermentation in the presence of oxygen (Christofk et al., 2008a; Christofk et al., 2008b). This important rediscovery of the Warburg effect

brought back attentions on the altered metabolism in cancer cells (Koppenol et al., 2011). As our knowledge of cancer metabolism increasingly grew in the last decade, deregulated metabolism is now recognized as one of the hallmarks of cancer (Fig. 1-1) (Hanahan and Weinberg, 2011; Pavlova and Thompson, 2016).

Deregulated Glucose Metabolism in Cancer

As Warburg observed as early as in the 1920s, cancer cells avidly take up glucose and generate lactate through glycolysis instead of using it for oxidative phosphorylation in the mitochondria (Warburg, 1956). It wasn't clear then how and why cancer cells revert back to this primitive form of glucose metabolism, which is normally seen in embryonic stem cells during early stages of development (Shyh-Chang et al., 2013). Although whether increased glycolysis is a forced adaptation to impaired mitochondria respiration still remained debatable, we now understand that certain oncogenic mutations could directly drive glucose uptake and glycolysis. Amplification or mutations of the epidermal growth factor receptor (EGFR) could result in hyperactivation of the PI3K-Akt-mTOR pathway, which upregulates expression and membrane levels of glucose transporters such as GLUT1 and GLUT3 (Babic et al., 2013). The oncogenic Ras protein also drives glucose uptake by increasing the expression of GLUT1 (Yun et al., 2009). In addition, oncogenic mutations could also elevate levels of key glycolytic enzymes such as hexokinase (HK2), aldolase, pyruvate kinase (PKM2) and lactate dehydrogenase (LDHA), as well as downstream mitochondria proteins and membrane transporters such as pyruvate dehydrogenase (PDK1) and monocarboxylate transporters (MCT1/4) (Cairns et al., 2011). Consequently, cancer cells are able to maintain a high rate of glycolytic flux, prevent glucose-derived pyruvate from entering the mitochondria, while diverting it for lactate production and secretion out of the cell.

So why glycolysis? Energetically, metabolizing glucose through fermentation and secreting it as lactate might seem a stupid choice, as glycolysis only generates 2 molecules of ATP from one molecule of glucose while oxidative phosphorylation could generate 36! But by taking up significantly larger amounts of glucose and metabolizing it at a much higher rate, cancer cells are actually able to generate more ATP through glycolysis than normal cells to support proliferation (Warburg, 1956). More importantly, starting from the very first steps of glycolysis, cancer cells could exploit glycolytic intermediates as precursors for biosynthesis and production of reducing equivalents (Pavlova and Thompson, 2016). For example, glucose-6-phosphate is diverted into the pentose phosphate pathway to generate NADPH and ribose-5-phosphate for nucleotide synthesis; fructose-6-phosphate is shunt into the hexosamine synthesis pathway to provide substrates for protein glycosylation; glyceralderhyde-3-phosphate (G3P) is converted to DHAP to synthesize glycerol-3-phosphate for phospholipids; 3-phosphoglycerate is used as the precursor for serine/glycine synthesis which also generates methyl donors and large amounts of NADPH as it is coupled with the folate and methionine cycle in one-carbon metabolism. While cancer cells mainly control flux of glycolytic intermediates into these branching pathways by upregulating the expression levels of corresponding metabolic enzymes, the unique expression of the special isoform of pyruvate kinase PKM2 in cancer controls the overall rate of glycolysis on the other end as it catalyzes the last step to generate pyruvate (Chaneton et al., 2012; Israelsen et al., 2013). The activity of PKM2 is regulated and inhibited by tyrosine phosphorylation downstream of growth factor signaling, allowing cancer cells to couple glycolytic flux to cellular growth demands (Christofk et al., 2008b). In the end, excess pyruvate is converted to lactate, which is important to maintain the cellular NAD+ pool to support glycolysis, and avoid overflow of NADH into the mitochondria which would exert an inhibition on the TCA cycle (Pavlova and Thompson, 2016).

Despite the significant increase in glycolysis, metabolic tracer analysis in cancer cells also revealed that glucose-derived pyruvate could be oxidized through the TCA cycle in the mitochondria (Marin-Valencia et al., 2012). It was found that cancer cells convert a large amount of glucose-derived pyruvate into citrate in the mitochondria, but instead of completing the TCA cycle, most of the citrate is secreted into the cytosol and broken down into acetyl-CoA and oxaloacetate to replenish the cytosolic acetyl-CoA pool for fatty acid synthesis and protein acetylation, while oxaloacetate is converted to malate and transported back to the mitochondria for anaplerosis (Pavlova and Thompson, 2016). Another interesting feature of mitochondria metabolism in cancer is that the electron transport chain in cancer cells could accept electrons from alternative sources to generate ATP, therefore the TCA cycle is no longer restricted for energy production, and TCA cycle intermediates could now be used to provide cancer cells with building blocks for fatty acid, amino acid and nucleotide synthesis (Pavlova and Thompson, 2016). And besides glucose, many cancers appear to utilize alternative carbon sources to fuel the TCA cycle such as glutamine or fatty acid (Carracedo et al., 2013; DeBerardinis et al., 2007). Essentially, the mitochondria in cancer cells have been reprogrammed to fully support biosynthesis instead of energy production.

Even though we are still on our way to fully understand why cancer cells perform aerobic glycolysis with the TCA cycle and oxidative phosphorylation remained intact, the reprogramming of glucose metabolism observed across cancer has already served as the foundation for tumor imaging using 18F-FDG PET. Meanwhile inhibitors targeting glycolytic enzymes such as hexokinase 2, PDK1 and MCT1 are currently being tested in the clinic as potential anti-cancer

therapeutics (Martinez-Outschoorn et al., 2017; Phelps, 2000), which we'll discuss more in the last part of this chapter.

Deregulated Amino Acid Metabolism in Cancer

Besides glucose metabolism, amino acid metabolism is also deregulated in cancer. Cancer cells commonly increase amino acid uptake through upregulation of specific amino acid transporters as well as downstream metabolic enzymes. For example, many cancers drive glutamine uptake and metabolism through c-myc mediated upregulation of glutamine transporters ASCT2 and SN2, as well as GLS1 - the enzyme that catalyze the very first step converting glutamine to glutamate. Glutamate is then fluxed into many critical metabolic pathways such as transamination, glutathione synthesis, serine-glycine synthesis, TCA cycle aneplerosis, and NADPH production through the malate-aspartate shuttle and malic enzyme (DeBerardinis et al., 2007). Glutamine metabolism is also essential for providing both the carbon backbones and nitrogen source for nucleotide synthesis, which is reflected by the coherent upregulation of downstream rate-limiting enzymes for de novo nucleotide synthesis such as phosphoribosyl pyrophosphate synthetase (PRPS2) and carbamoyl-phosphate synthetase 2 (CAD) (Ben-Sahra et al., 2013; Cunningham et al., 2014). In addition, glutamine and glutamate could also act as important exchangers for nutrient uptake through specific amino acid transporters such as SLC7A5 and xCT. (Chung et al., 2005; Nicklin et al., 2009; Takeuchi et al., 2012; Timmerman et al., 2013). Alternatively, mutant Ras or c-src was found to drive an opportunistic way of obtaining amino acids through micropinocytosis, in which cancer cells are able to engulfed extracellular proteins and nutrients by forming small vesicles, from which proteins could then be broken down in the lysosome to replenish the cellular amino acid pool (Commisso et al., 2013).

Deregulated Lipid Metabolism in Cancer

Sufficient lipid supply is also critical for rapidly proliferating cancer cells. Many cancers such as GBM rely on uptake of lipids from the extracellular environment generated by neighboring stromal cells in the form of protein-bound LDL or through specific transporters, as de novo lipid synthesis is both energetically consuming and requires a significant amount of reducing equivalents (Guo et al., 2009; Hayashi et al., 2004). Given the abundant lipid pool in the brain, GBM cells were found to become cholesterol auxotrophs and even lost the feedback inhibition mechanism to convert excess cholesterol to oxysterols, which are responsible for activating the liver X receptor to inhibit cholesterol uptake and promote cholesterol efflux in normal cells (Villa et al., 2016). But under a different context when extracellular lipids are scarce, tumor cells were also able to to ramp up de novo lipid synthesis from acetyl-CoA using citrate derived from glucose and aneplerotic glutamine metabolism in the mitochondria. Interestingly, under hypoxia, tumor cells were also found to undergo reductive carboxylation of glutamine to generate citrate through IDH1 for lipogenesis (Metallo et al., 2011). In addition, the cellular acetyl-CoA pool could also be replenished by catabolism of branch chain amino acids (BCAA) in certain cancers (Tonjes et al., 2013).

Not only does proliferation requires doubling of total membrane lipids, cancer cells also undergo membrane remodeling by changing the levels of different membrane lipid species, which also has significant functional importance (Beloribi-Djefaflia et al., 2016). For example, many oncogenic signaling proteins are localized on the plasma membrane, such as EGFR, Ras, Rac, PI3K and Akt. Membrane fluidity and formation of lipid clusters and micro-domains are crucial for protein oligomerization, proper conformational changes, as well as protein-protein interactions, which are

usually required for kinase activation and the occurrence of downstream signaling events (Zhou et al., 2015). Furthermore, membrane-bound organelles such as the mitochondria also rely on the membrane integrity for proper functioning (Betz et al., 2013). Therefore, it's not surprising that cancer cells display unique lipid profiles compared to normal cells, and the synthesis as well as remodeling of specific lipid species in cancer are usually in turn driven directly or indirectly downstream of oncogenic signaling pathways.

Current next-generation sequencing and metabolic studies in cancer has established a strong link between oncogenes, oncogenic mutations and metabolic reprogramming (Cairns et al., 2011). We now know that many oncogenes and oncogenic mutations directly drive metabolic reprogramming in cancer cells, supporting the perspective that cancer is a genetic disease, and that genetic mutations are responsible for metabolic reprogramming required for cellular transformation. Another branch of view that stems from the early Warburg's experiments instead were trying to argue that cancer is more likely a metabolic disease, in which neoplastic transformation is the consequence of forced metabolic reprogramming that happened in the first place and eventually resulted in irreversible epigenetic and genetic changes. Especially recent studies also suggested possible links between cancer and metabolic diseases such as diabetes and obesity (Thompson, 2011). But maybe these aren't two conflicting hypothesis after all. Early geneticists have long understood that phenotype = genotype + environment, which obviously puts genetic mutations and metabolic reprogramming on the same side of the equation. We hope that future studies could help us eventually understand the intricate links between genetic mutations and metabolism and how they both contribute to cancer, one and every step along the way.

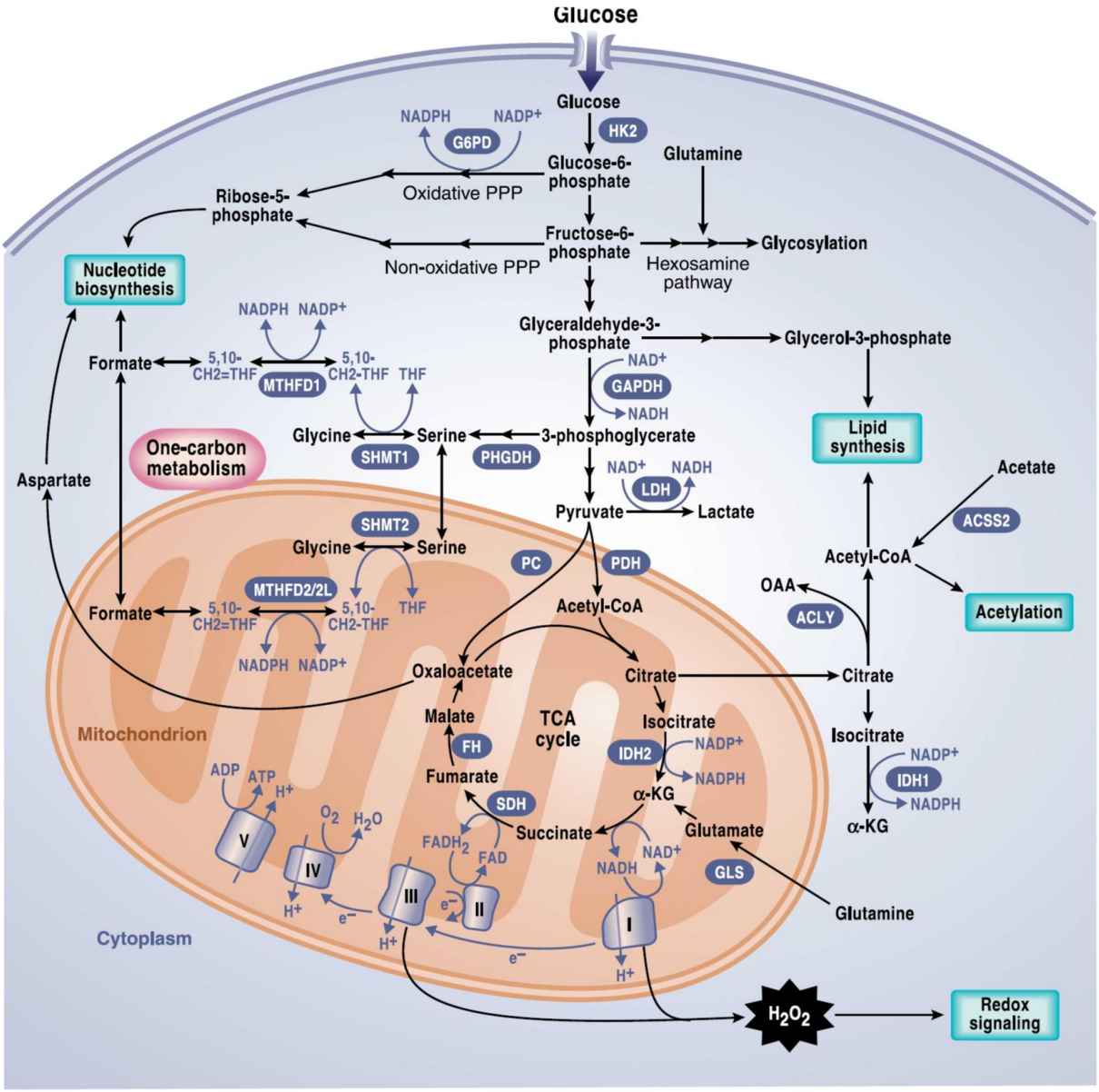

Fig. 1-1. Reprogrammed Metabolism in Cancer.

Glucose metabolism in cancer is reprogrammed to favor glycolysis as glycolytic intermediates provide substrates for biosynthesis of macromolecules as well as reductive NADPH. On the other hand, cancer cells utilize glutamine for TCA cycle, which decouples glucose metabolism from the mitochondria electron transport chain for energy production. Figure was originally published by DeBeradinis *et al* (DeBerardinis and Chandel, 2016).

mTOR - The Maestro of Cancer Cell Metabolism

Hyperactivation of mTOR signaling in Cancer

mTOR, also known as the mechanistic target of rapamycin, is an essential coordinator that integrates cellular energy, nutrient, stress status and growth factors signals with cell growth and division (Zoncu et al., 2011). Hyperactivation of mTOR is commonly seen across cancer, liberating cell growth from the requirement of extracellular growth factor signals (Guertin et al., 2009; Masri et al., 2007). This is usually achieved by amplification or activating mutations in upstream kinases such as EGFR, PI3K, Akt and Ras, which activates mTOR by phosphorylating specific components in the mTOR complexes or the mTOR-inhibitory TSC1/2 complex (Carriere et al., 2011; Gan et al., 2011; Liu et al., 2013; Ma et al., 2005a; Yuan and Cantley, 2008). Loss of tumor suppressor genes could also lead to aberrant activation of mTOR, such as the phosphatase and tensin homolog (PTEN) which is a negative regulator of the PI3K-Akt pathway, NF1 which inhibits Ras activation, LKB1 which activates AMPK that inhibit mTOR in response to energy stress, and TSC1/2 which negatively regulates mTOR through the small G protein Rheb (Banerjee et al., 2011; Huynh et al., 2015; Johannessen et al., 2005; Ma et al., 2005b; Shackelford and Shaw, 2009). Germ line mutations in these tumor suppressor genes usually give rise to tumor-associated syndromes, such as the PTEN harmatoma tumor syndrome, neurofibromatosis type 1 caused by NF1 deletion, Peutz-Jegher's syndrome in patients with LKB1 loss, as well as Tuberous sclerosis syndrome or lymphangioleimyomatosis (LAM) cause by TSC1/2 deletion, which are all commonly associated with mTOR hyperactivation (Nagy et al., 2004).

mTOR kinase is the catalytic subunit of two distinct complexes mTOR Complex 1 (mTORC1) and mTOR Complex 2 (mTORC2). Two distinct scaffold proteins, Raptor in mTORC1 and Rictor

mTORC2, differentiate the two complexes by recruiting different components for complex assembly and restricting substrate specificity. Other components in mTORC1 include PRAS40, DEPTOR and mLST8, whereas mTORC2 also contains mSIN1 and PROTOR in addition to DEPTOR and mLST8 (Fig. 1-2A) (Zoncu et al., 2011). Both mTORC1 and mTORC2 respond to upstream growth factor signals and promote cell growth and proliferation, albeit through different downstream effector kinases and proteins. mTORC1 phosphorylates two major substrates S6 kinase 1 (S6K1) and eIF4E-biniding protein 1 (4EBP1), which both induce protein synthesis by promoting mRNA translation initiation and elongation, and S6K1 also promotes ribosome biogenesis by upregulating the activity of rRNA polymerase RNA polymerase I (RNAP1) (Hsieh et al., 2010). mTORC2 on the other hand phosphorylates and activates a set of AGC family kinases including Akt, serum- and glucocorticoid- regulated kinase (SGK) and protein kinase C (PKC), which are involved in regulating cell cycle, survival and metabolism (Garcia-Martinez and Alessi, 2008; Hung et al., 2012; Pearce et al., 2010).

mTOR Complexes as nutrient sensors in cancer

Besides responding to upstream growth factor signals, both mTOR complexes also play the role as nutrient sensors in the cell through different mechanisms (Fig. 1-2B) (Efeyan et al., 2015; Zoncu et al., 2011). mTORC1 was identified as an essential component of a complex amino acid sensing machinery on the lysosome, which also involves Rag GTPases, Ragulator, v-ATPase, and amino acid transporters SLC38A9 and SLC36A1 (Fig. 1-3A) (Goberdhan et al., 2016). In addition, mTORC1 also senses amino acids through mechanisms mediated by the MAP kinase regulator MAP4K3 and the Class III PI3-kinase Vsp34 (Efeyan and Sabatini, 2010; Findlay et al., 2007; Nobukuni et al., 2005), as well as through Rag-independent mechanisms mediated by two

membrane trafficking proteins Arf1 and RabA1 involved in ER-Golgi transport (Li et al., 2010). mTORC1 also senses decreased cellular energy levels (ATP/AMP) , hypoxia and DNA damage in an AMPK-dependent manner (Hardie et al., 2012). mTORC2 on the other hand, was identified as an important glucose sensor in tumor cells. The availability of glucose-derived acetate turned out to be required for acetylation of Rictor to sustain consistent mTORC2 activation upon growth factor stimulation, which in turn further drives glycolysis through the Akt-FOXO-c-myc mediated upregulation of glycolytic genes (Fig.1-3B) (Babic et al., 2013; Masui et al., 2015). The fact that the nutrient and energy sensing role of mTOR is largely maintained in cancer along with its hyperactivation suggests that effective coupling of cell proliferation with cellular nutrient and energy status is also critical for cancer cells.

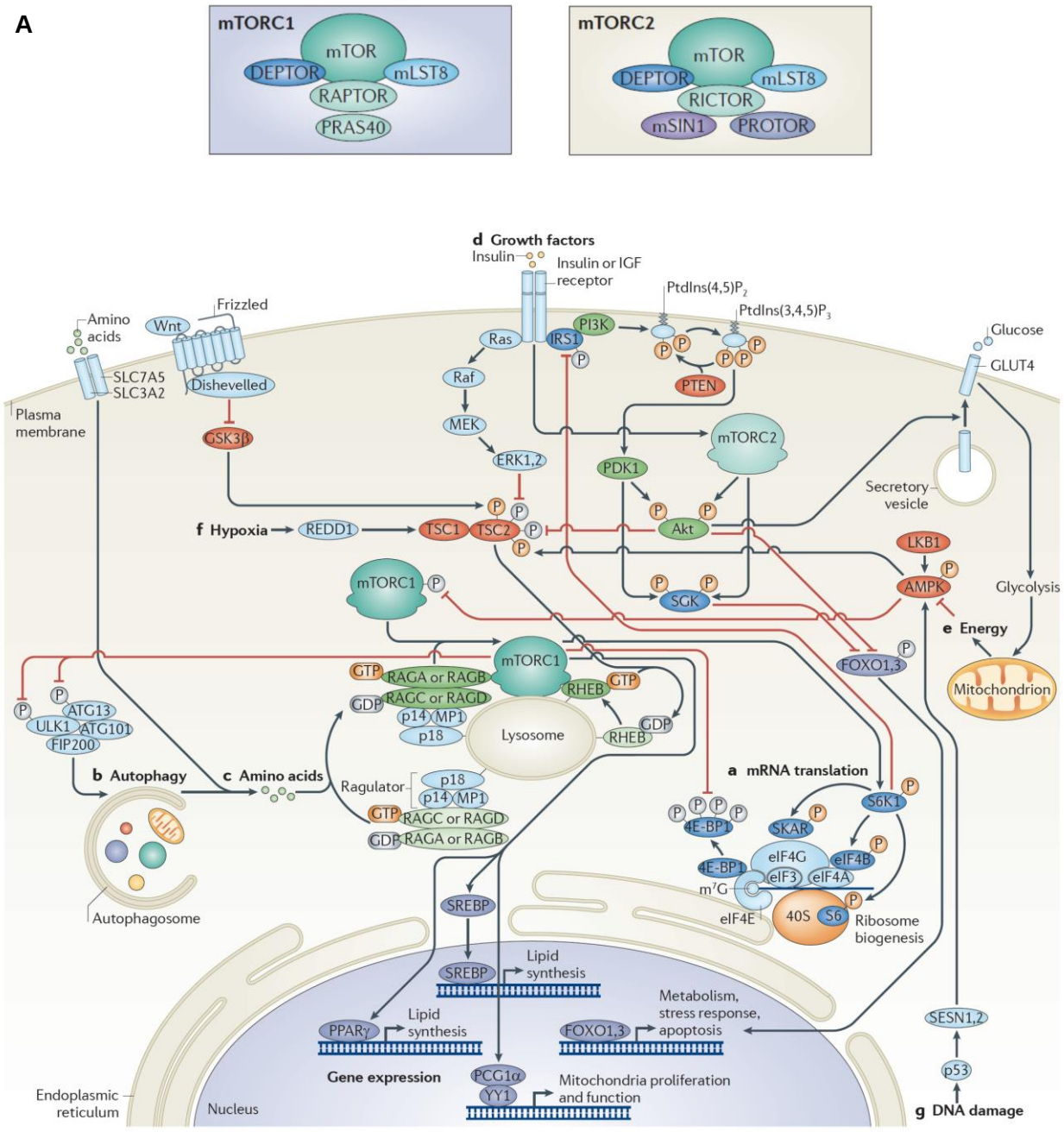

Fig. 1-2. Structure and Function of mTOR Complexes.

(A) mTORC1 and mTORC2 contains both shared and unique components.

(B) mTOR complexes are responsive to upstream signals from growth factors, nutrient and stress status as well as DNA damage, and control downstream protein synthesis, metabolism and autophagy. Figure was modified and originally published by Zoncu *et al* (Zoncu et al., 2011)**.**

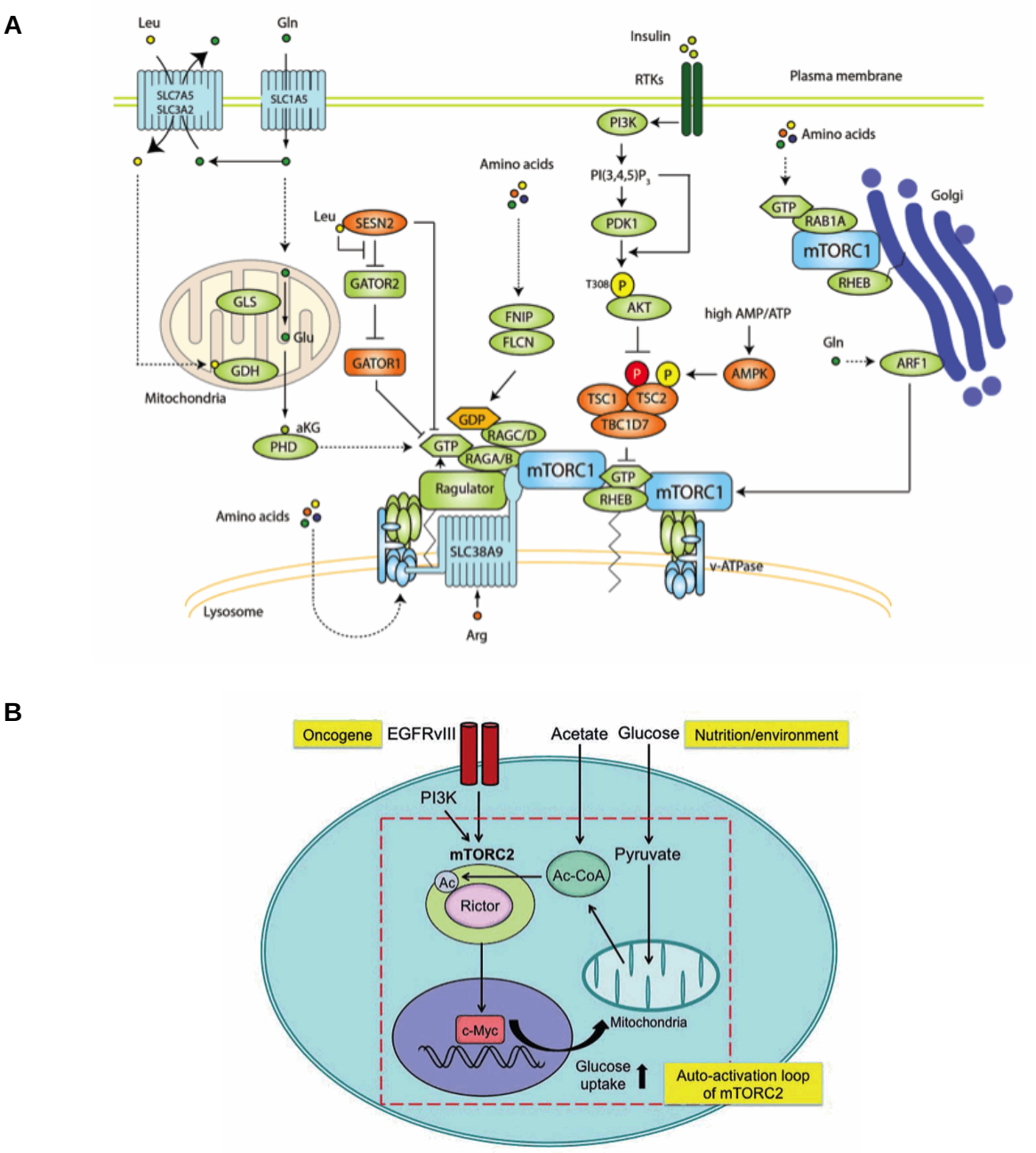

Fig. 1-3. Nutrient Sensing Mechanisms Mediated by mTOR Complexes.

(A) Amino acid sensing mechanisms by mTORC1. Figure was originally published by Shimobayashi *et al* (Shimobayashi and Hall, 2016). (B) mTORC2 senses cellular glucose and acetate levels through acetylation of Rictor. Figure was originally published by Masui *et al* (Masui et al., 2015).

mTOR mediates metabolic reprogramming in cancer

Upon receiving signals from growth factors and nutrients, mTOR not only drives protein synthesis, but also elevates cellular metabolism, powering biosynthesis by ensuring continuous supply of energy, substrates and reducing equivalents (Duvel et al., 2010). Both mTOR complexes are involved in mechanisms regulating glycolysis, mitochondria function, glutamine metabolism and lipogenesis (Fig. 1-4 and Fig. 1-5) (Masui et al., 2015; Wu et al., 2014). Hyperactivation of mTORC1 upregulates Hif-1 and c-myc, both of which promotes transcription of glycolytic genes (Yecies and Manning, 2011). mTORC2 on the other hand activates Akt, which induces expression of the rate limiting enzymes hexokinase (HK) and phospho-fructose kinase (PFK) in glycolysis, while inhibits gluconeogenesis through phosphorylation of GSK3β (Sarbassov et al., 2005; Thompson and Thompson, 2004; Vivanco and Sawyers, 2002). mTORC1 also regulates mitochondria function through PGC1α and YY1, which are both major transcription factors controlling expression of nuclear encoded mitochondria genes (Cunningham et al., 2007). mTORC2 instead has been shown to help maintain interaction between hexokinase 2 and the mitochondria voltage dependent anion channel (VDAC) through Akt-mediated mechanisms (Gottlob et al., 2001). In addition, mTORC2 is also required for maintaining the integrity of the mitochondria associated endoplasmic reticulum membrane (MAM), which is crucial for proper mitochondrial calcium flux and membrane potential (Betz et al., 2013).

Besides glucose metabolism, mTORC1 also regulates glutaminase (GLS) and glutamate dehydrogenase, which catalyze the first two steps in glutamine metabolism (Csibi et al., 2013). Several key transcription factors regulating amino acid transporters, such as c-myc, Hif1 and ATF4, are also regulated by mTORC1 to promote uptake of essential as well as nonessential amino acids,

especially leucine and glutamine (Csibi et al., 2014). Recent unpublished studies from our lab discovered an important role of mTORC2 in glutamate and redox metabolism through direct phosphorylation of the glutamate-cystine transporter xCT.

In addition, the expression and processing of SREBP1, which is an essential transcription factor controlling genes in core pathways of lipid metabolism, is also regulated by S6K1 and Akt downstream of mTORC1 an mTORC2 (Duvel et al., 2010; Hagiwara et al., 2012; Lamming and Sabatini, 2013; Porstmann et al., 2008). Furthermore, Akt is found to phosphorylate and activate ACLY to maintain the cytosolic acetyl-CoA pool for de novo lipogenesis (Berwick et al., 2002).

mTORC1 and mTORC2 also regulate distinct metabolic processes. mTORC1 is involved in regulating de novo pyrimidine synthesis through phosphorylation of carbomyl phosphate synthetase (CAD) by S6K1 (Ben-Sahra et al., 2013; Robitaille et al., 2013). Autophagy is also regulated by mTORC1-mediated phosphorylation of ATG proteins, through which cells could degrade and recycle intracellular components to provide sufficient nutrients for cell survival under starvation or stressful conditions (Chan, 2009). Likewise, mTORC2 also regulates cell survival, as well as cytoskeleton dynamics and ceramide/sphingolipid synthesis through downstream AGC family kinases SGK1 and PKC (Hung et al., 2012; Laplante and Sabatini, 2012).

Interestingly, recent studies also revealed an important role of mTOR in promoting cancer cell survival in nutrient-depleted conditions. It was observed that activation of mTORC1 on the contrary suppressed tumor growth in Ras-driven cancer cells, while mTORC1 inhibition promoted cell proliferation through induction of autophagy to facilitate catabolism of endocytosed proteins

from macropinocytosis (Palm et al., 2015). These together suggest that it will be crucial to fully understand how mTOR regulates metabolism in tumors with distinct genetic backgrounds, and under different microenvironment, before the correct decision could be made about whether targeting mTOR is the right treatment option for each individual patient.

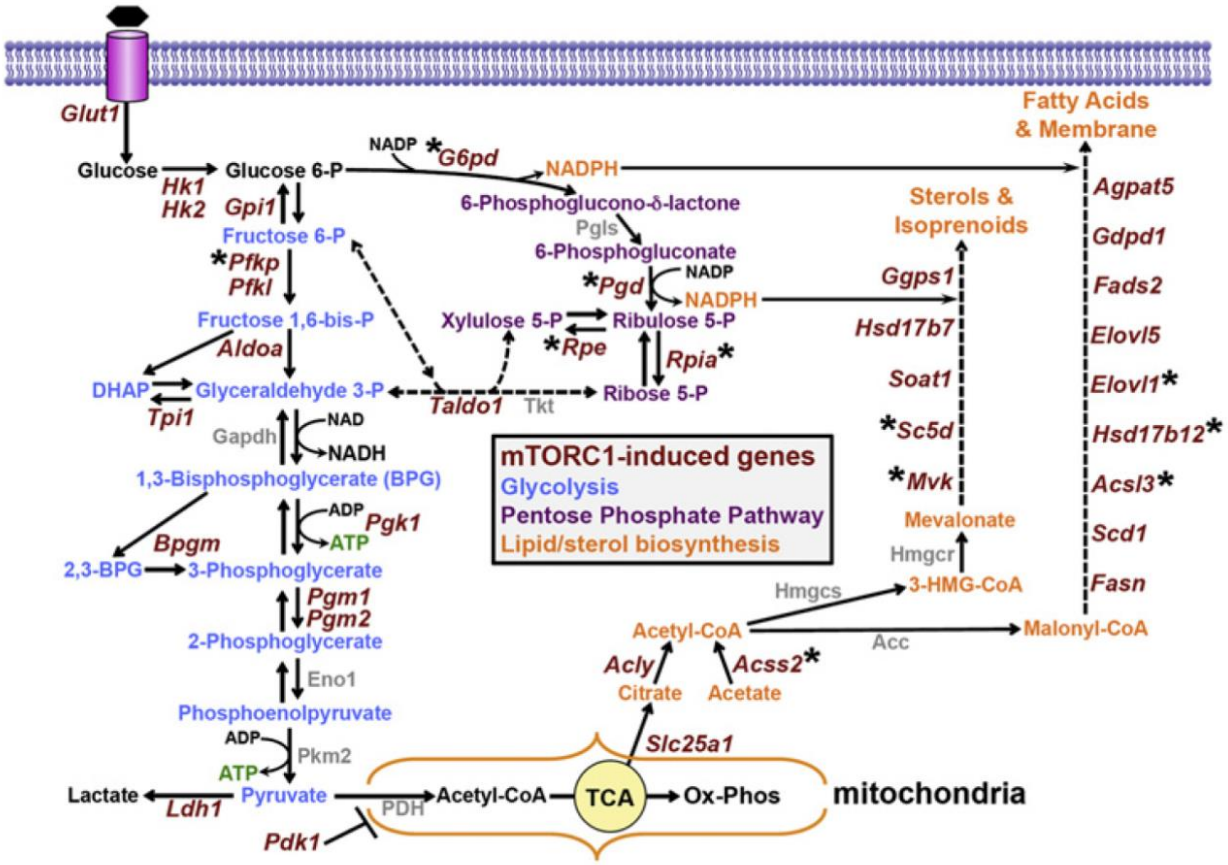

Fig. 1-4. mTOR Complex 1 Reprograms Metabolism in Cancer.

mTORC1 regulated metabolic enzymes are involved in glycolysis, pentose phosphate pathway and lipid biosynthesis. Figure was originally published by Duvel *et al*. (Duvel et al., 2010)

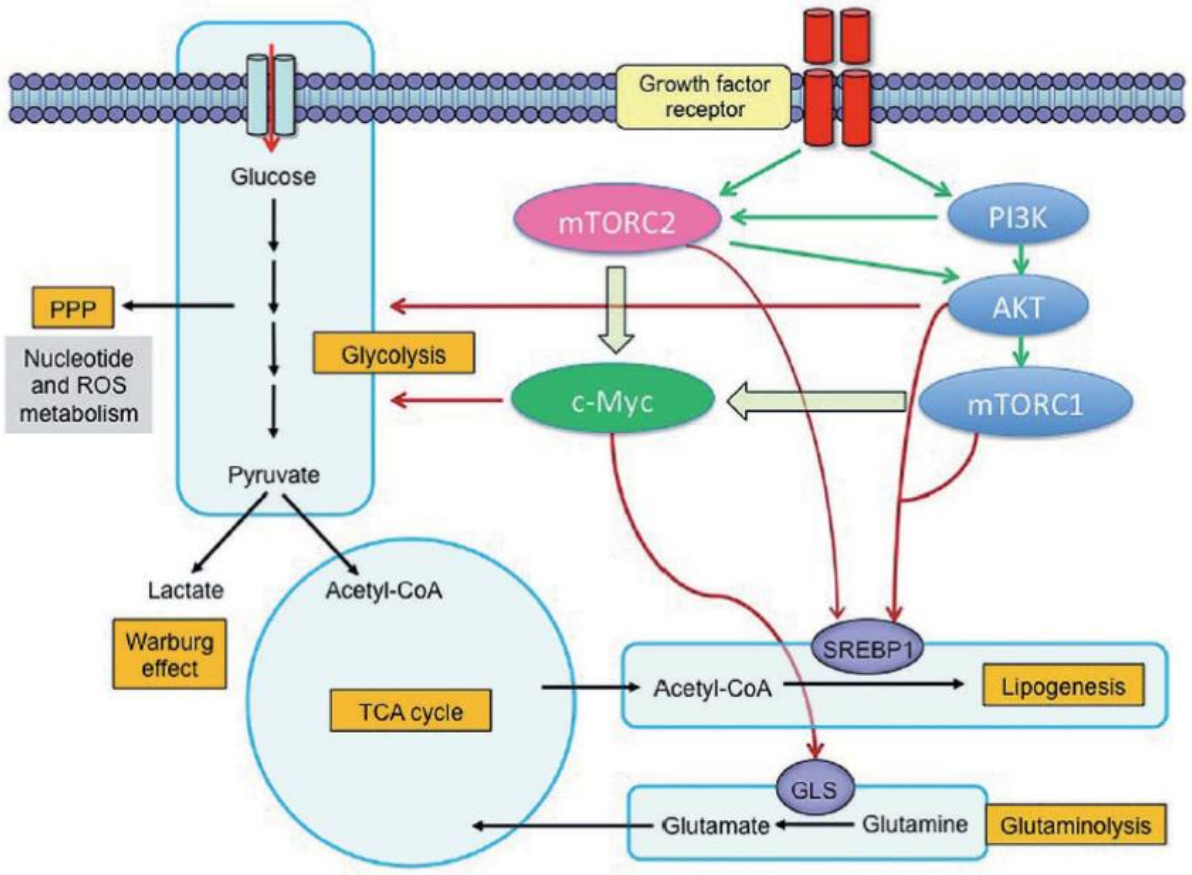

Fig. 1-5. mTOR Complex 2 Reprograms Metabolism in Cancer.

mTORC2 mediates metabolic reprogramming through transcription factors such as c-myc and SREBP1 which are involved in regulating glucose/glutamine metabolism and lipid metabolism. Figure was originally published by Masui *et al*. (Masui et al., 2015)

xCT - An Emerging Therapeutic Target for Cancer

Structure and Function of the xCT transporter

xCT was first discovered in the 1980s and characterized as a 12-transmembrane protein that belongs to the family of Heterodimeric Amino Acid Transporters (HAT) (Bannai and Kitamura, 1980). HAT family amino acid transporters usually consist of a functional light chain which determines the transporter's substrate specificity, and a heavily glycosylated heavy chain usually shared between different HAT family members (Chillaron et al., 2001). xCT is the light subunit of the cystine-glutamate antiporter system xC^-, which is linked to the heavy subunit 4F2hc (also known as CD98) through a disulfide bridge (Bassi et al., 2001). No crystal structure of xCT is available to date, but predicted structures of xCT have been proposed based on protein sequence analysis using membrane topology algorithmns. Additional studies using the cysteine accessibility strategy revealed that both the N- and C-terminus of xCT reside in the cytosol, and a re-entrant loop between the 2^{nd} and 3^{rd} transmembrane domain is involved in restricting substrate binding and specificity (Gasol et al., 2004). Interestingly, additional amino acid residues further away from the re-entrant loop were also identified to be required for substrate binding, suggesting that these substrate-docking sites might be spatially close to each other, which leads to the assumption that xCT likely adopts a barrel-like cylindrical structure with its N- and C-terminus close to each other rather than spreading apart in a linear fashion. Dimerization of xCT has also been suggested but whether it is required for transporter activity of is unknown (Gasol et al., 2004), whereas CD98 was suggested to be required for xCT function and recruitment onto the plasma membrane (Sato et al., 1999).

xCT functions as a cystine-glutamate antiporter, which exports glutamate and imports cystine both in the anion form in a 1:1 ratio, and in a Na^+-independent and Cl^- dependent manner. Although xCT is a bi-directional transporter, the direction of substrate transport through xCT is largely determined by the concentration gradient. Generally, extracellular glutamate level in the brain, where xCT is mainly found to be expressed, is around 2-9 μM, as neurons and astrocytes avidly take up glutamate through EAATs such as GLT1 and GLAST to prevent overactivation of post-synaptic neurons, while intracellular glutamate levels can reach as high as 10 mM. On the other hand, cystine is immediately reduced into cysteine upon entering the cell, and used for glutathione synthesis or involved in other redox reactions, therefore intracellular cystine level is usually much lower level compared to the extracellular environment (Lewerenz et al., 2012). Besides glutamate and cystine, aspartate and cystathionine were also identified as possible substrates of xCT (Kobayashi et al., 2015).

Mechanisms regulating xCT

As xCT is responsible for the uptake of cystine, which is the rate-limiting substrate for glutathione synthesis, it is not surprising that Nrf2 was first identified to bind to the antioxidant response element (ARE) in the xCT promoter and induces transcription of xCT in response to oxidative stress. (Ishii et al., 2000; Sasaki et al., 2002). In addition, amino acid starvation was also found to induce transcription of xCT through ATF4 binding onto the amino acid responsive element (AARE) in the xCT promoter. Activation of the amino acid sensor GCN2 in response to decreased amino acid levels in the cell phosphorylates eIF2α, which led to increased translation of ATF4 and xCT transcription. (Sato et al., 2004). Surprisingly, p53 was recently discovered as an xCT transcriptional repressor, which has been proposed to play an important role in inducing cell death

through ferroptosis in response to cellular stress during embryonic development and tumor suppression (Fig. 1-6) (Jiang et al., 2015). In contrast, post-translational mechanisms regulating xCT are largely unknown. Despite several potential phosphorylation sites, one N-glycosylation site (Bridges et al., 2001) and multiple ubiquitination sites have been detected on xCT based on cumulative data obtained from large-scale phosphoproteomic studies, validation of these phosphorylation events and identification of the responsible kinases still awaits. More importantly, we have yet to understand the functional importance of these post-translational modifications on xCT. Nevertheless, CD44v6, which is a variant form of CD44, has been shown to stabilize xCT on the plasma membrane in certain types of cancer (Ishimoto et al., 2011).

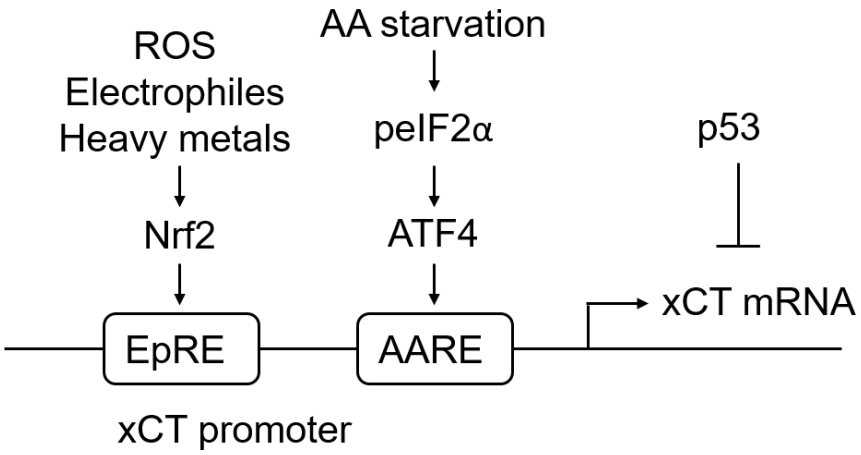

Fig. 1-6. Mechanisms Regulating xCT Transcription.

xCT transcription is induced by Nrf2 and ATF4 in response to oxidative stress and amino acid starvation, and suppressed by p53. Figure was modified based on originally published paper by Lewerenz *et al*. (Jiang et al., 2015; Lewerenz et al., 2012)

The Important Roles of xCT in Cancer

Uptake of extracellular cystine was essential for cell survival in many cancers. Systemic depletion of cystine with a genetically engineered human cyst(e)inase was recently reported to selectively kill cancer cells both in vitro and in vivo while it is very well tolerated in animals (Cramer et al., 2016). Cystine uptake is predominantly mediated by xCT in cancer, especially in glioblastoma (GBM), lymphoma and triple-negative breast cancer, where xCT is found to be significantly upregulated (Timmerman et al., 2013; Ye et al., 1999; Zhang et al., 2012). Interestingly, xCT is normally expressed in the brain, especially in astrocytes, and lymphoid organs such as the spleen and thymus, suggesting that the tissue of origin might also contribute to the unique dependence of xCT in different cancers (Lewerenz et al., 2012).

In GBM, tumor cells preferentially express xCT rather than the other two glutamate transporters GLT and GLAST normally seen in astrocytes and neurons (Fig. 1-7) (Savaskan and Eyupoglu, 2010). Genetic knockdown or pharmacological inhibition of xCT is sufficient to completely block glutamate secretion in GBM cells (Ye et al., 1999). Glutamate secreted by tumor cells through xCT accumulates in the tumor microenvironment and could reach to a level of several hundred-fold higher than in normal brain (Marcus et al., 2010; Ye and Sontheimer, 1999). High levels of extracellular glutamate promotes GBM cell proliferation and migration through activating the AMPA glutamate receptor, while inducing excitotoxicity and cell death of surrounding neurons and astrocytes, facilitating tumor expansion and resulting in epilepsy and brain edema (Buckingham et al., 2011; Chen et al., 2009; Chung et al., 2005; Ishiuchi et al., 2007; Savaskan et al., 2008). It was suggested that the differential expression levels of the AMPA and NMDA

glutamate receptors might explain the distinct effect of extracellular glutamate on normal brain and glioma cells (van Vuurden et al., 2009).

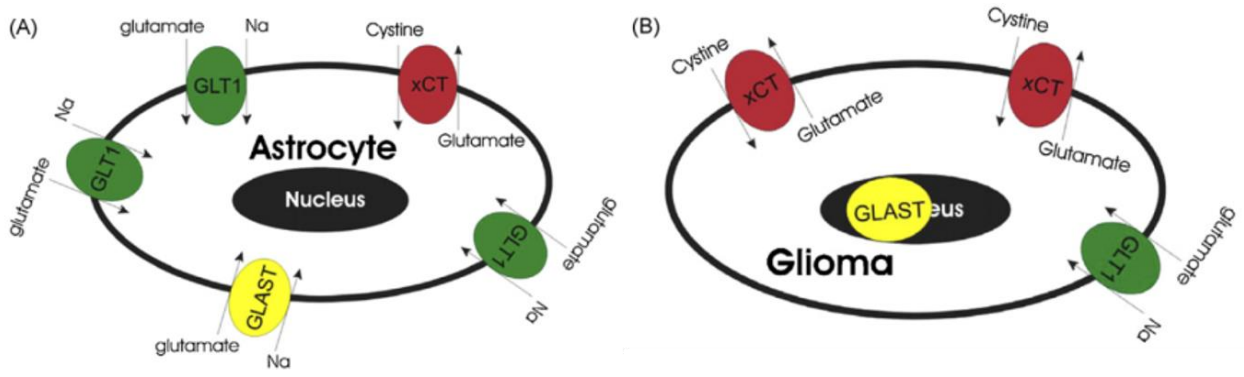

Fig. 1-7. xCT is Preferentially Expressed in Glioma Cells.

Astrocytes and neurons normally express GLT1 and GLAST which mediate sodium-dependent uptake of glutamate. Glioma cells on the contrary express the cystine/glutamate antiporter xCT, which is sodium-independent and mediates export of glutamate and uptake of cystine. Figure was modified and originally published by Savaskan *et al*. (Savaskan and Eyupoglu, 2010)

In chronic lymphocytic leukemia (CLL), tumor-associated stromal cells, rather than CLL cells, were found to express high levels of xCT. Stromal cells avidly take up cystine through xCT and provide the reduced form of cysteine to the neighboring CLL cells through the ASC1 transporter (Zhang et al., 2012). Inhibition of xCT in stromal cells significantly decreased glutathione levels in CLL cells while treating CLL cells alone with an xCT inhibitor had no effect on total cellular glutathione levels, suggesting that CLL cells are solely dependent on the cysteine provided by stromal cells for glutathione synthesis and cell survival.

Analysis of nutrient dependency in breast cancers identified a specific reliance on xCT in triple-negative breast cancer (TNBC). xCT expression level is significantly higher in TNBC compare to estrogen (ER)- or progesterone (PR) driven breast cancers (Timmerman et al., 2013). More interestingly, a recent study by Kaelin et al suggested that the high levels of xCT in TNBC cells is responsible for Hif1α induction under normoxia to drive tumor growth and metabolism. It was found that accumulation of extracellular glutamate secreted from xCT could feedback inhibit xCT activity and suppress cystine uptake, which eventually led to cysteine depletion in tumor cells. Cysteine depletion is responsible for oxidation of cystine residues on the prolyl hydroxylase domain (PHD) protein EgIN1, which inactivates EgIN1 and suppressed EgIN1-dependent Hif1α degradation (Briggs et al., 2016). As oxidation of cysteine residues is a common post-translational mechanism regulating protein function and activity of many redox-responsive proteins, we would expect that the importance of xCT in cancer cells might go far beyond maintaining glutathione synthesis. It will be interesting to look into how xCT is involved in regulating other important cellular functions through affecting cysteine residues oxidation of proteins in cancer cells.

Targeting xCT in Cancer

The unique dependence on xCT for cystine uptake suggests that cancer cells should be more sensitive to xCT inhibition compared to normal cells. Genetic knockdown as well as pharmacological inhibition of xCT in GBM significantly suppressed tumor growth, prevented tumor cell migration and helped alleviate brain edema and neurodegeneration by blocking glutamate secretion (Chen et al., 2009; Chung et al., 2005; Savaskan and Eyupoglu, 2010; Savaskan et al., 2008). In vivo administration of xCT inhibitors in CLL mouse models significantly decreased tumor cell viability and increased the cytotoxicity of standard chemotherapeutic agents

F-ara-A and oxaliplatin through suppressing glutathione synthesis (Huang et al., 2005; Zhang et al., 2012). In addition, inhibition of glutamine metabolism or direct inhibition of xCT was also shown to induce oxidative stress in TNBC cells and suppressed tumor growth in vivo (Briggs et al., 2016; Timmerman et al., 2013).

But xCT inhibition has not yet been successful in clinical studies due to low specificity or poor pharmacokinetic properties of currently available xCT inhibitors such as sulfasalazine (SAS) and (S)-4-caboxyphenylglycine [(S)-4CPG] (Griffith, 1982; Robe et al., 2009). A new category of compounds was recently identified from a synthetic lethal screen in RAS-driven cancer cells, which can induce an iron-dependent, non-apoptotic form of cell death (Dolma et al., 2003; Yang and Stockwell, 2008). Following studies identified erastin as one of the most promising candidate compound and it was found that erastin significantly inhibited cystine uptake through xCT, which led to glutathione depletion and lipid peroxidation in the cell and resulted in an iron-dependent form of cell death termed ferroptosis. But no direct binding between erastin and xCT was detected, suggesting that the inhibition of xCT and cystine uptake by erastin was likely a secondary effect (Dixon et al., 2012). Interestingly, another group of structurally related compounds were also identified as ferroptosis inducers, which target the phospholipid hydroperoxidase glutathione peroxidase 4 (GPX4) – an enzyme responsible for glutathione-mediated reduction of oxidized lipids (lipid peroxide) in the mitochondria (Yang et al., 2014). These together suggest that cancer cells might share the vulnerability towards glutathione depletion, and indicate that besides xCT, additional key players in glutathione metabolism such as GCLC and GPXs could also be potential drug targets. In fact, several glutathione depleting agents have already been evaluated in cancer, including a naturally-occurring compound phenethyl isothiocyanate (PEITC), which specifically

reacts with intracellular glutathione and transports it out of the cell; and L-Buthionine sulphoximine (BSO) – an inhibitor targeting the rate-limiting enzyme GCLC in glutathione synthesis. Both of them showed very promising anti-tumor effect (Bailey et al., 1994; Yuan et al., 2016). But so far, these candidate compounds including erastin, PEITC and BSO are still not optimal for use in the clinic due to undesired systemic toxicities or poor pharmacokinetic properties (Griffith, 1982).

Targeting Reprogrammed Metabolism in Cancer

To date, a total of 125 “driver” genes have been identified in cancer, including 54 oncogenes and 71 tumor suppressor genes (Vogelstein et al., 2013). Targeting oncogenic driver mutations was once believed to be the cure for cancer, until resistance invariably occurred as tumor cells become independent of the initial driver mutation for survival and proliferation. Unlike the diversity of oncogenic mutations in cancer, common metabolic phenotypes are usually seen in genetically distinct tumors and driven by different oncogenes, suggesting that cancer cells might be less flexible with metabolic perturbations. Metabolic reprogramming is thought to serve three major purposes in cancer: 1) catabolism of nutrients to meet bioenergetics needs; 2) anabolism of nutrients for biosynthesis; 3) maintaining cellular redox balance (Fig. 1-8) (DeBerardinis and Chandel, 2016). The metabolic reprogramming in cancer has been mostly described in the first part of this chapter. Here in the last section of the introduction we want to present some of the exciting recent findings and our current understanding of cancer-specific metabolic vulnerabilities for designing better therapeutic strategies targeting metabolism in cancer.

Targeting Bioenergetic Pathways in Cancer

Glycolysis and mitochondria OXPHOS are two major pathways generating ATP in cancer. Most cancer cells are dependent on the high rate of glycolysis for energy production, therefore inhibitors targeting key enzymes in glycolysis have been extensively studied and tested in cancer. 2-deoxyglucose (2-DG) and 3-bromopyruvate (3-BP) are potent inhibitors targeting hexokinase (HK2) in glycolysis, but both display systemic toxicities (Dwarakanath et al., 2009; Jae et al., 2009; Klippel et al., 2012; Shoshan, 2012). Inhibitors of lactate dehydrogenase (LDHA) as well as lactate transporters MCT1 and MCT4 on the other hand are very well tolerated and are currently being

evaluated in both preclinical and clinical studies (Doherty and Cleveland, 2013; Polanski et al., 2014). Dichloroacetate (DCA) is another glycolysis inhibitor currently being tested in clinical trials. DCA inhibits pyruvate dehydrogenase kinase (PDK1), which could revert the glycolytic phenotype in cancer cells by forcing pyruvate entry into the mitochondria and suppress lactate production (Dunbar et al., 2014; Michelakis et al., 2010).

On the other hand, a subset of cancer cells are found especially dependent on mitochondria metabolism and sensitive to mitochondria inhibitors, including cancer stem cells, tumor cells with limited access to glucose, as well as tumors treated with inhibitors targeting EGFR, PI3K, Akt or mTOR which suppress glycolysis (Birsoy et al., 2014; Hsu et al., 2015; Shackelford et al., 2013; Viale et al., 2014). Biguanides such as metformin and phenformin, which were initially used in patients with diabetes to inhibit gluconeogenesis, were identified as mitochondria inhibitors targeting Complex I in the electron transport chain (ETC) and both are currently involved in hundreds of ongoing clinical trials in different cancers as single therapy or in combination with standard chemotherapies and targeted therapies (Foretz et al., 2014; Kasznicki et al., 2014). Another famous mitochondria inhibitor is arsenic trioxide, which was initially identified to induce differentiation of leukemia cells and approved for clinical use in patients with relapsed or refractory acute promyelocytic leukemia (APL). Surprisingly it was later found that the real target of arsenic trioxide is the mitochondria Complex III (Lo-Coco et al., 2013; Pelicano et al., 2003).

In addition, glutamine also contributes to the TCA cycle and OXPHOS especially under hypoxia and glucose-limiting conditions. Enzymes in glutamine metabolism such as glutaminase and glutamate pyruvate transaminase (GPT) have also become potential therapeutic targets for cancer

(DeBerardinis et al., 2007). One small molecule glutaminase inhibitor CB-839 is currently undergoing clinical evaluation (Gross et al., 2014). It was also observed that when glucose is limited, tumor cells could obtain fatty acids from the microenvironment or from stromal cells to generate ATP and NADPH through β-oxidation, which suggest that the enzyme carnitine O-palmitoyltransferase (CPT) involved in fatty acid β-oxidation in the mitochondria could also be a potential drug target for cancer (Boroughs and DeBerardinis, 2015; Jeon et al., 2012; Nieman et al., 2011; Zaugg et al., 2011).

Targeting Biosynthesis Pathways in Cancer

A major advantage of elevated glycolysis and decoupling of the TCA cycle with OXPHOS observed in cancer cells is to provide precursors for biosynthesis of macromolecules. In fact, targeting biosynthesis has long been the rationale behind some of the most successful modern chemotherapies such as L-asparaginase, dihydrofolate reductase inhibitor pemetrexed and thymidylate inhibitor 5-fluorouracil (Wilson et al., 2014). In fact, many de novo amino acid, nucleotide and lipid synthesis pathways are dependent on metabolic intermediates from glycolysis and the TCA cycle, including the serine/glycine synthesis pathway, purine and pyrimidine synthesis pathways, as well as fatty acid and cholesterol synthesis pathways (DeBerardinis and Chandel, 2016). Therefore, the glycolysis and mitochondria inhibitors mentioned above as well as additional small molecule inhibitors targeting biosynthetic pathways have also been tested for their effect on inhibiting biosynthesis in cancer. For example, phosphoglycerate dehydrogenase (PHGDH) and serine hydroxymethyltransferase (SHMT2) are two major enzymes in the serine/glycine synthesis pathway highly amplified or upregulated in breast cancer and melanoma (DeNicola et al., 2015; Jain et al., 2012; Locasale et al., 2011; Mullarky et al., 2011; Possemato et

al., 2011; Yang and Vousden, 2016). Recently a small molecule inhibitor targeting PHGDH was reported and is currently undergoing further preclinical studies (Mullarky et al., 2016).

Another important biosynthetic process that we could potentially target in cancer involves nucleotide synthesis. The ribose-5-phosphate synthesized by the pentose phosphate pathway (PPP), aspartate derived from the TCA cycle through glutamine anaplerosis, and formate generated from one-carbon metabolism downstream of the serine/glycine synthesis pathway are all essential substrates for de novo nucleotide synthesis. Although few inhibitors targeting these pathways are available to date, several candidate enzymes have been suggested by RNAi studies as promising targets, including glucose-6-phosphate dehydrogenase (G6PD) and phosphoglycerate mutase (PGAM1) in the PPP, pyruvate carboxylase, α-ketoglutarate dehydrogenase, and glutaminase mediating TCA cycle anaplerosis, as well as methylenetetrahydrofolate dehydrogenase/cyclohydrolase (MTHFD2) and monofonctional C1-tetrahydrofolate synthase (MTHFD1L) involved in the mitochondrial one-carbon metabolism (Nilsson et al., 2014).

Acetyl-CoA is another important biosynthetic precursor, which is essential for de novo fatty acid and cholesterol synthesis as well as protein acetylation. Acetyl-CoA could be derived from citrate by ACLY, or from acetate by acetyl-CoA synthase (ACCS2). Genetic knockdown and pharmacological inhibition of ACLY and ACCS2 both suppressed tumor growth in vivo, possibly through inhibiting de novo lipogenesis and histone acetylation (Bauer et al., 2005; Schug et al., 2015; Schug et al., 2016). Other inhibitors targeting de novo lipid synthesis also include fatty acid synthase (FASN) inhibitor TVB-2640 and HMG-CoA reductase inhibitor statins (Nielsen et al., 2012; Rohrig and Schulze, 2016).

Targeting Redox Pathways in Cancer

A third major feature of metabolic reprogramming in cancer is upregulation of redox metabolism, including NADPH production, glutathione synthesis, thioredoxin pathway, as well as mitochondria superoxide dismutase (SOD). NADPH is one of the major reducing powers in cancer cells, and is also responsible for regenerating reduced glutathione and thioredoxin. The main pathways and enzymes contributing to cellular NADPH pool in cancer include the PPP pathway, one-carbon metabolism, malic enzyme (ME1) as well as cytosolic and mitochondria isocitrate dehydrogenase IDH1 and IDH2 (Fan et al., 2014; Jiang et al., 2016; Patra and Hay, 2014; Son et al., 2013). But since normal cells also share many of these common pathways to generate NADPH, inhibitors targeting these pathways will most likely encounter the problem of systemic toxicity. Two exceptions are G6PD in the PPP pathway and MTHFD2 in one-carbon metabolism, as systemic depletion of G6PD could be tolerated and MTHFD2 is found to be differentially upregulated in cancer cells but not in normal proliferating cells (Nilsson et al., 2014). In fact, normally NADPH does not directly react with oxidized proteins, but rather transfer its reducing power onto glutathione and thioredoxin by glutathione reductase (GR) and thioredoxin reductase (TXNR). The reduced glutathione and thioredoxin carrying the reductive thiol group then reduces oxidized proteins or lipids in the cell either by specific enzymes such as glutathione peroxidase (GPXs) or directly react with the substrates in the case of thioredoxin (Trachootham et al., 2009). Therefore, targeting glutathione and thioredoxin pathways might be an alternative way to inhibit redox metabolism in cancer. Sulfasalazine and erastin which inhibit xCT-mediated uptake of the rate-limiting substrate cystine, BSO which targets the rate limiting enzyme GCLC in glutathione synthesis, together with TXNR inhibitor PX-12 are examples of promising drug candidates targeting the glutathione and thioredoxin pathways in cancer (Chung et al., 2005; Dixon et al.,

2012; Trachootham et al., 2009). Another interesting idea to exhaust the reductive potential of cancer cells is by treating cells with the oxidized form of vitamin C – dehydroascorbate (DHA). In KRAS-driven tumors such as colorectal cancer where GLUT1 is highly expressed, DHA was shown to be preferentially taken up by cancer cells through GLUT1, which then rapidly depleted the NADPH and GSH pool and induced ROS-mediated tumor cell death (Yun et al., 2015).

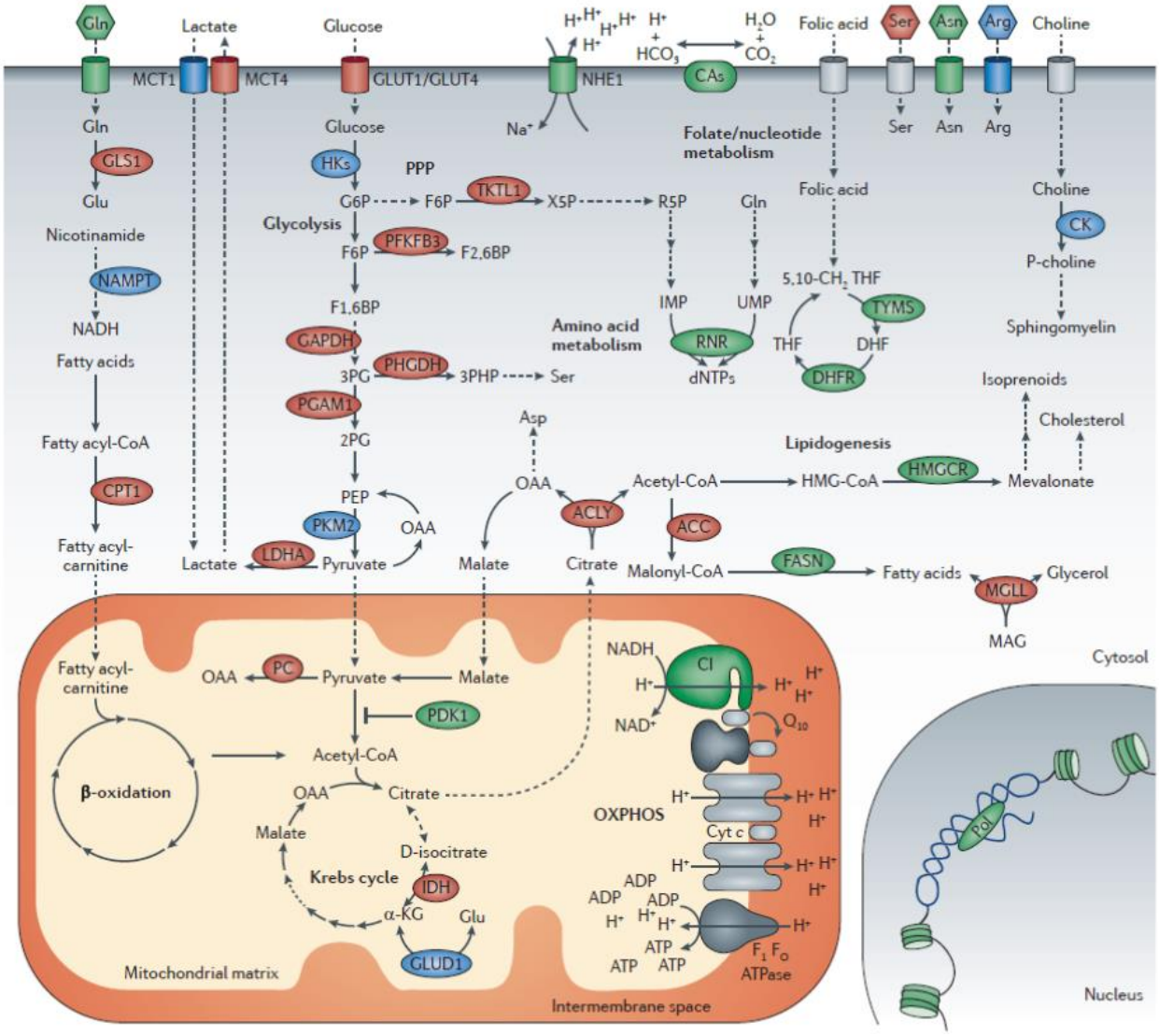

Fig. 1-8. Potential Therapeutic Targets in Cancer Metabolism.

Many metabolic enzymes involved in bioenergetics pathways, biosynthesis pathways and redox pathways are found differentially expressed in cancer and could be potential therapeutic targets. Figure was originally published by Galluzzi *et al* (Galluzzi et al., 2013).

Exploiting Cancer-specific Metabolic Co-dependencies

Oncogenic mutations, tumor microenvironment and drug treatments all contribute to the specific metabolic phenotypes and dependencies in cancer cells. For example, EGFR determines the specific dependence on uptake of exogenous lipids rather than de novo synthesis in GBM cells, rendering them specifically sensitive to LXR agonists which deplete intracellular cholesterol pool by inhibiting cholesterol uptake through LDLR and promotes cholesterol efflux through ABCA1, which significantly reduced tumor cell viability, while statins that inhibit de novo lipid synthesis had no effect in GBM (Villa et al., 2016). In colorectal cancer, glucose-limiting condition was found to select for a population of cancer cells harboring KRAS or BRAF mutations, as mutant KRAS or BRAF significantly upregulates the glucose transporter GLUT1 which allows tumor cells to compete for the limited glucose for survival. Targeting glycolysis using 2-DG or 3-BP preferentially inhibits tumor cells with KRAS or BRAF mutations while sparing those with wild type KRAS or BRAF (Yun et al., 2009). In addition, we also discovered a novel mechanism through which mTORC2 regulates glutathione metabolism by phosphorylation of xCT in response to nutrient and oxidative stress. Treatment with small molecule mTOR kinase inhibitors significantly increased tumor cell dependency on glutathione in GBM, due to a specific and significant induction of mitochondria ROS and lipid peroxidation by mTOR kinase inhibitors,

which eventually led to ferroptotic cell death if not resolved by glutathione. These suggest that Torin1-treated GBM cells are especially sensitive to glutathione depletion by the xCT inhibitor erastin or GCLC inhibitor BSO. In general, the above examples all emphasize the importance that we should carefully assess the context-specific metabolic phenotypes in different cancer before the right therapeutic targets can be chosen.

After almost a hundred years since Warburg first reported the differential metabolism in cancer, our knowledge and insights about cancer metabolism have greatly advanced, especially with the development of new technologies and better models made available in recent years. We now understand that besides oncogenic mutations, tumor microenvironment and treatment perturbations are also important determinants involved in the selection for the specific metabolic phenotypes seen in different cancers and even in different individuals with the same type of cancer. We also uncovered the link between metabolism and epigenetics, which might be the first step to cellular transformation and the underlying cause of cancer. In fact, studying metabolism in intact whole tumors as well as looking for tumor-stromal interactions have become two important current trends in cancer metabolism research (Hensley et al., 2016; McMillin et al., 2013). In addition, as metabolism in cancer cells is very flexible, development of new models and computational approaches would allow us to look at metabolic changes in real-time, in different cellular compartments and under specific drug treatments to explore better therapeutic strategies targeting metabolism in cancer.

REFERENCES

Babic, I., Anderson, E.S., Tanaka, K., Guo, D., Masui, K., Li, B., Zhu, S., Gu, Y., Villa, G.R., Akhavan, D., *et al.* (2013). EGFR mutation-induced alternative splicing of Max contributes to growth of glycolytic tumors in brain cancer. Cell metabolism *17*, 1000-1008.

Bailey, H.H., Mulcahy, R.T., Tutsch, K.D., Arzoomanian, R.Z., Alberti, D., Tombes, M.B., Wilding, G., Pomplun, M., and Spriggs, D.R. (1994). Phase I clinical trial of intravenous L-buthionine sulfoximine and melphalan: an attempt at modulation of glutathione. Journal of clinical oncology : official journal of the American Society of Clinical Oncology *12*, 194-205.

Banerjee, S., Crouse, N.R., Emnett, R.J., Gianino, S.M., and Gutmann, D.H. (2011). Neurofibromatosis-1 regulates mTOR-mediated astrocyte growth and glioma formation in a TSC/Rheb-independent manner. Proceedings of the National Academy of Sciences of the United States of America *108*, 15996-16001.

Bannai, S., and Kitamura, E. (1980). Transport interaction of L-cystine and L-glutamate in human diploid fibroblasts in culture. The Journal of biological chemistry *255*, 2372-2376.

Bassi, M.T., Gasol, E., Manzoni, M., Pineda, M., Riboni, M., Martin, R., Zorzano, A., Borsani, G., and Palacin, M. (2001). Identification and characterisation of human xCT that co-expresses, with 4F2 heavy chain, the amino acid transport activity system xc. Pflugers Archiv : European journal of physiology *442*, 286-296.

Bauer, D.E., Hatzivassiliou, G., Zhao, F., Andreadis, C., and Thompson, C.B. (2005). ATP citrate lyase is an important component of cell growth and transformation. Oncogene *24*, 6314-6322.

Beloribi-Djefaflia, S., Vasseur, S., and Guillaumond, F. (2016). Lipid metabolic reprogramming in cancer cells. Oncogenesis *5*, e189.

Ben-Sahra, I., Howell, J.J., Asara, J.M., and Manning, B.D. (2013). Stimulation of de novo pyrimidine synthesis by growth signaling through mTOR and S6K1. Science *339*, 1323-1328.

Berwick, D.C., Hers, I., Heesom, K.J., Moule, S.K., and Tavare, J.M. (2002). The identification of ATP-citrate lyase as a protein kinase B (Akt) substrate in primary adipocytes. The Journal of biological chemistry *277*, 33895-33900.

Betz, C., Stracka, D., Prescianotto-Baschong, C., Frieden, M., Demaurex, N., and Hall, M.N. (2013). Feature Article: mTOR complex 2-Akt signaling at mitochondria-associated endoplasmic reticulum membranes (MAM) regulates mitochondrial physiology. Proceedings of the National Academy of Sciences of the United States of America *110*, 12526-12534.

Birsoy, K., Possemato, R., Lorbeer, F.K., Bayraktar, E.C., Thiru, P., Yucel, B., Wang, T., Chen, W.W., Clish, C.B., and Sabatini, D.M. (2014). Metabolic determinants of cancer cell sensitivity to glucose limitation and biguanides. Nature *508*, 108-112.

Boroughs, L.K., and DeBerardinis, R.J. (2015). Metabolic pathways promoting cancer cell survival and growth. Nature cell biology *17*, 351-359.

Bridges, C.C., Kekuda, R., Wang, H., Prasad, P.D., Mehta, P., Huang, W., Smith, S.B., and Ganapathy, V. (2001). Structure, function, and regulation of human cystine/glutamate transporter in retinal pigment epithelial cells. Investigative ophthalmology & visual science *42*, 47-54.

Briggs, K.J., Koivunen, P., Cao, S., Backus, K.M., Olenchock, B.A., Patel, H., Zhang, Q., Signoretti, S., Gerfen, G.J., Richardson, A.L., *et al.* (2016). Paracrine Induction of HIF by Glutamate in Breast Cancer: EglN1 Senses Cysteine. Cell *166*, 126-139.

Buckingham, S.C., Campbell, S.L., Haas, B.R., Montana, V., Robel, S., Ogunrinu, T., and Sontheimer, H. (2011). Glutamate release by primary brain tumors induces epileptic activity. Nature medicine *17*, 1269-1274.

Cairns, R.A., Harris, I.S., and Mak, T.W. (2011). Regulation of cancer cell metabolism. Nature reviews Cancer *11*, 85-95.

Carracedo, A., Cantley, L.C., and Pandolfi, P.P. (2013). Cancer metabolism: fatty acid oxidation in the limelight. Nature reviews Cancer *13*, 227-232.

Carriere, A., Romeo, Y., Acosta-Jaquez, H.A., Moreau, J., Bonneil, E., Thibault, P., Fingar, D.C., and Roux, P.P. (2011). ERK1/2 phosphorylate Raptor to promote Ras-dependent activation of mTOR complex 1 (mTORC1). The Journal of biological chemistry *286*, 567-577.

Chan, E.Y. (2009). mTORC1 phosphorylates the ULK1-mAtg13-FIP200 autophagy regulatory complex. Science signaling *2*, pe51.

Chaneton, B., Hillmann, P., Zheng, L., Martin, A.C., Maddocks, O.D., Chokkathukalam, A., Coyle, J.E., Jankevics, A., Holding, F.P., Vousden, K.H., *et al.* (2012). Serine is a natural ligand and allosteric activator of pyruvate kinase M2. Nature *491*, 458-462.

Chen, R.S., Song, Y.M., Zhou, Z.Y., Tong, T., Li, Y., Fu, M., Guo, X.L., Dong, L.J., He, X., Qiao, H.X., *et al.* (2009). Disruption of xCT inhibits cancer cell metastasis via the caveolin-1/beta-catenin pathway. Oncogene *28*, 599-609.

Chillaron, J., Roca, R., Valencia, A., Zorzano, A., and Palacin, M. (2001). Heteromeric amino acid transporters: biochemistry, genetics, and physiology. American journal of physiology Renal physiology *281*, F995-1018.

Christofk, H.R., Vander Heiden, M.G., Harris, M.H., Ramanathan, A., Gerszten, R.E., Wei, R., Fleming, M.D., Schreiber, S.L., and Cantley, L.C. (2008a). The M2 splice isoform of pyruvate kinase is important for cancer metabolism and tumour growth. Nature *452*, 230-233.

Christofk, H.R., Vander Heiden, M.G., Wu, N., Asara, J.M., and Cantley, L.C. (2008b). Pyruvate kinase M2 is a phosphotyrosine-binding protein. Nature *452*, 181-186.

Chung, W.J., Lyons, S.A., Nelson, G.M., Hamza, H., Gladson, C.L., Gillespie, G.Y., and Sontheimer, H. (2005). Inhibition of cystine uptake disrupts the growth of primary brain tumors. The Journal of neuroscience : the official journal of the Society for Neuroscience *25*, 7101-7110.

Cloughesy, T.F., Cavenee, W.K., and Mischel, P.S. (2014). Glioblastoma: from molecular pathology to targeted treatment. Annual review of pathology *9*, 1-25.

Commisso, C., Davidson, S.M., Soydaner-Azeloglu, R.G., Parker, S.J., Kamphorst, J.J., Hackett, S., Grabocka, E., Nofal, M., Drebin, J.A., Thompson, C.B., *et al.* (2013). Macropinocytosis of protein is an amino acid supply route in Ras-transformed cells. Nature *497*, 633-637.

Cramer, S.L., Saha, A., Liu, J., Tadi, S., Tiziani, S., Yan, W., Triplett, K., Lamb, C., Alters, S.E., Rowlinson, S., *et al.* (2016). Systemic depletion of L-cyst(e)ine with cyst(e)inase increases reactive oxygen species and suppresses tumor growth. Nature medicine.

Csibi, A., Fendt, S.M., Li, C., Poulogiannis, G., Choo, A.Y., Chapski, D.J., Jeong, S.M., Dempsey, J.M., Parkhitko, A., Morrison, T., *et al.* (2013). The mTORC1 pathway stimulates glutamine metabolism and cell proliferation by repressing SIRT4. Cell *153*, 840-854.

Csibi, A., Lee, G., Yoon, S.O., Tong, H., Ilter, D., Elia, I., Fendt, S.M., Roberts, T.M., and Blenis, J. (2014). The mTORC1/S6K1 pathway regulates glutamine metabolism through the eIF4B-dependent control of c-Myc translation. Current biology : CB *24*, 2274-2280.

Cunningham, J.T., Moreno, M.V., Lodi, A., Ronen, S.M., and Ruggero, D. (2014). Protein and nucleotide biosynthesis are coupled by a single rate-limiting enzyme, PRPS2, to drive cancer. Cell *157*, 1088-1103.

Cunningham, J.T., Rodgers, J.T., Arlow, D.H., Vazquez, F., Mootha, V.K., and Puigserver, P. (2007). mTOR controls mitochondrial oxidative function through a YY1-PGC-1alpha transcriptional complex. Nature *450*, 736-740.

DeBerardinis, R.J., and Chandel, N.S. (2016). Fundamentals of cancer metabolism. Science advances *2*, e1600200.

DeBerardinis, R.J., Mancuso, A., Daikhin, E., Nissim, I., Yudkoff, M., Wehrli, S., and Thompson, C.B. (2007). Beyond aerobic glycolysis: transformed cells can engage in glutamine metabolism that exceeds the requirement for protein and nucleotide synthesis. Proceedings of the National Academy of Sciences of the United States of America *104*, 19345-19350.

DeNicola, G.M., Chen, P.H., Mullarky, E., Sudderth, J.A., Hu, Z., Wu, D., Tang, H., Xie, Y., Asara, J.M., Huffman, K.E., *et al.* (2015). NRF2 regulates serine biosynthesis in non-small cell lung cancer. Nat Genet *47*, 1475-1481.

Dixon, S.J., Lemberg, K.M., Lamprecht, M.R., Skouta, R., Zaitsev, E.M., Gleason, C.E., Patel, D.N., Bauer, A.J., Cantley, A.M., Yang, W.S., *et al.* (2012). Ferroptosis: an iron-dependent form of nonapoptotic cell death. Cell *149*, 1060-1072.

Doherty, J.R., and Cleveland, J.L. (2013). Targeting lactate metabolism for cancer therapeutics. The Journal of clinical investigation *123*, 3685-3692.

Dolma, S., Lessnick, S.L., Hahn, W.C., and Stockwell, B.R. (2003). Identification of genotype-selective antitumor agents using synthetic lethal chemical screening in engineered human tumor cells. Cancer cell *3*, 285-296.

Dunbar, E.M., Coats, B.S., Shroads, A.L., Langaee, T., Lew, A., Forder, J.R., Shuster, J.J., Wagner, D.A., and Stacpoole, P.W. (2014). Phase 1 trial of dichloroacetate (DCA) in adults with recurrent malignant brain tumors. Invest New Drugs *32*, 452-464.

Duvel, K., Yecies, J.L., Menon, S., Raman, P., Lipovsky, A.I., Souza, A.L., Triantafellow, E., Ma, Q., Gorski, R., Cleaver, S., *et al.* (2010). Activation of a metabolic gene regulatory network downstream of mTOR complex 1. Molecular cell *39*, 171-183.

Dwarakanath, B.S., Singh, D., Banerji, A.K., Sarin, R., Venkataramana, N.K., Jalali, R., Vishwanath, P.N., Mohanti, B.K., Tripathi, R.P., Kalia, V.K., *et al.* (2009). Clinical studies for improving radiotherapy with 2-deoxy-D-glucose: present status and future prospects. J Cancer Res Ther *5 Suppl 1*, S21-26.

Efeyan, A., Comb, W.C., and Sabatini, D.M. (2015). Nutrient-sensing mechanisms and pathways. Nature *517*, 302-310.

Efeyan, A., and Sabatini, D.M. (2010). mTOR and cancer: many loops in one pathway. Current opinion in cell biology *22*, 169-176.

Fan, J., Ye, J., Kamphorst, J.J., Shlomi, T., Thompson, C.B., and Rabinowitz, J.D. (2014). Quantitative flux analysis reveals folate-dependent NADPH production. Nature *510*, 298-302.

Findlay, G.M., Yan, L., Procter, J., Mieulet, V., and Lamb, R.F. (2007). A MAP4 kinase related to Ste20 is a nutrient-sensitive regulator of mTOR signalling. The Biochemical journal *403*, 13-20.

Flavahan, W.A., Drier, Y., Liau, B.B., Gillespie, S.M., Venteicher, A.S., Stemmer-Rachamimov, A.O., Suva, M.L., and Bernstein, B.E. (2016). Insulator dysfunction and oncogene activation in IDH mutant gliomas. Nature *529*, 110-114.

Foretz, M., Guigas, B., Bertrand, L., Pollak, M., and Viollet, B. (2014). Metformin: from mechanisms of action to therapies. Cell metabolism *20*, 953-966.

Galluzzi, L., Kepp, O., Vander Heiden, M.G., and Kroemer, G. (2013). Metabolic targets for cancer therapy. Nature reviews Drug discovery *12*, 829-846.

Gan, X., Wang, J., Su, B., and Wu, D. (2011). Evidence for direct activation of mTORC2 kinase activity by phosphatidylinositol 3,4,5-trisphosphate. The Journal of biological chemistry *286*, 10998-11002.

Garcia-Martinez, J.M., and Alessi, D.R. (2008). mTOR complex 2 (mTORC2) controls hydrophobic motif phosphorylation and activation of serum- and glucocorticoid-induced protein kinase 1 (SGK1). The Biochemical journal *416*, 375-385.

Gasol, E., Jimenez-Vidal, M., Chillaron, J., Zorzano, A., and Palacin, M. (2004). Membrane topology of system xc- light subunit reveals a re-entrant loop with substrate-restricted accessibility. The Journal of biological chemistry *279*, 31228-31236.

Goberdhan, D.C., Wilson, C., and Harris, A.L. (2016). Amino Acid Sensing by mTORC1: Intracellular Transporters Mark the Spot. Cell metabolism *23*, 580-589.

Gottlob, K., Majewski, N., Kennedy, S., Kandel, E., Robey, R.B., and Hay, N. (2001). Inhibition of early apoptotic events by Akt/PKB is dependent on the first committed step of glycolysis and mitochondrial hexokinase. Genes & development *15*, 1406-1418.

Griffith, O.W. (1982). Mechanism of action, metabolism, and toxicity of buthionine sulfoximine and its higher homologs, potent inhibitors of glutathione synthesis. The Journal of biological chemistry *257*, 13704-13712.

Gross, M.I., Demo, S.D., Dennison, J.B., Chen, L., Chernov-Rogan, T., Goyal, B., Janes, J.R., Laidig, G.J., Lewis, E.R., Li, J., *et al.* (2014). Antitumor activity of the glutaminase inhibitor CB-839 in triple-negative breast cancer. Mol Cancer Ther *13*, 890-901.

Guertin, D.A., Stevens, D.M., Saitoh, M., Kinkel, S., Crosby, K., Sheen, J.H., Mullholland, D.J., Magnuson, M.A., Wu, H., and Sabatini, D.M. (2009). mTOR complex 2 is required for the development of prostate cancer induced by Pten loss in mice. Cancer cell *15*, 148-159.

Guo, D., Prins, R.M., Dang, J., Kuga, D., Iwanami, A., Soto, H., Lin, K.Y., Huang, T.T., Akhavan, D., Hock, M.B., *et al.* (2009). EGFR signaling through an Akt-SREBP-1-dependent, rapamycin-resistant pathway sensitizes glioblastomas to antilipogenic therapy. Science signaling *2*, ra82.

Hagiwara, A., Cornu, M., Cybulski, N., Polak, P., Betz, C., Trapani, F., Terracciano, L., Heim, M.H., Ruegg, M.A., and Hall, M.N. (2012). Hepatic mTORC2 activates glycolysis and lipogenesis through Akt, glucokinase, and SREBP1c. Cell metabolism *15*, 725-738.

Hanahan, D., and Weinberg, R.A. (2011). Hallmarks of cancer: the next generation. Cell *144*, 646-674.

Hardie, D.G., Ross, F.A., and Hawley, S.A. (2012). AMPK: a nutrient and energy sensor that maintains energy homeostasis. Nature reviews Molecular cell biology *13*, 251-262.

Hayashi, H., Campenot, R.B., Vance, D.E., and Vance, J.E. (2004). Glial lipoproteins stimulate axon growth of central nervous system neurons in compartmented cultures. The Journal of biological chemistry *279*, 14009-14015.

Hensley, C.T., Faubert, B., Yuan, Q., Lev-Cohain, N., Jin, E., Kim, J., Jiang, L., Ko, B., Skelton, R., Loudat, L., *et al.* (2016). Metabolic Heterogeneity in Human Lung Tumors. Cell *164*, 681-694.

Hsieh, A.C., Costa, M., Zollo, O., Davis, C., Feldman, M.E., Testa, J.R., Meyuhas, O., Shokat, K.M., and Ruggero, D. (2010). Genetic dissection of the oncogenic mTOR pathway reveals druggable addiction to translational control via 4EBP-eIF4E. Cancer cell *17*, 249-261.

Hsu, C.C., Wu, L.C., Hsia, C.Y., Yin, P.H., Chi, C.W., Yeh, T.S., and Lee, H.C. (2015). Energy metabolism determines the sensitivity of human hepatocellular carcinoma cells to mitochondrial inhibitors and biguanide drugs. Oncol Rep *34*, 1620-1628.

Huang, M., Shen, A., Ding, J., and Geng, M. (2014). Molecularly targeted cancer therapy: some lessons from the past decade. Trends in pharmacological sciences *35*, 41-50.

Huang, Y., Dai, Z., Barbacioru, C., and Sadee, W. (2005). Cystine-glutamate transporter SLC7A11 in cancer chemosensitivity and chemoresistance. Cancer research *65*, 7446-7454.

Hung, C.M., Garcia-Haro, L., Sparks, C.A., and Guertin, D.A. (2012). mTOR-dependent cell survival mechanisms. Cold Spring Harb Perspect Biol *4*.

Huynh, H., Hao, H.X., Chan, S.L., Chen, D., Ong, R., Soo, K.C., Pochanard, P., Yang, D., Ruddy, D., Liu, M., *et al.* (2015). Loss of Tuberous Sclerosis Complex 2 (TSC2) Is Frequent in Hepatocellular Carcinoma and Predicts Response to mTORC1 Inhibitor Everolimus. Mol Cancer Ther *14*, 1224-1235.

Ishii, T., Itoh, K., Takahashi, S., Sato, H., Yanagawa, T., Katoh, Y., Bannai, S., and Yamamoto, M. (2000). Transcription factor Nrf2 coordinately regulates a group of oxidative stress-inducible genes in macrophages. The Journal of biological chemistry *275*, 16023-16029.

Ishimoto, T., Nagano, O., Yae, T., Tamada, M., Motohara, T., Oshima, H., Oshima, M., Ikeda, T., Asaba, R., Yagi, H., *et al.* (2011). CD44 variant regulates redox status in cancer cells by stabilizing the xCT subunit of system xc(-) and thereby promotes tumor growth. Cancer cell *19*, 387-400.

Ishiuchi, S., Yoshida, Y., Sugawara, K., Aihara, M., Ohtani, T., Watanabe, T., Saito, N., Tsuzuki, K., Okado, H., Miwa, A., *et al.* (2007). Ca2+-permeable AMPA receptors regulate growth of human glioblastoma via Akt activation. The Journal of neuroscience : the official journal of the Society for Neuroscience *27*, 7987-8001.

Israelsen, W.J., Dayton, T.L., Davidson, S.M., Fiske, B.P., Hosios, A.M., Bellinger, G., Li, J., Yu, Y., Sasaki, M., Horner, J.W., *et al.* (2013). PKM2 isoform-specific deletion reveals a differential requirement for pyruvate kinase in tumor cells. Cell *155*, 397-409.

Jae, H.J., Chung, J.W., Park, H.S., Lee, M.J., Lee, K.C., Kim, H.C., Yoon, J.H., Chung, H., and Park, J.H. (2009). The antitumor effect and hepatotoxicity of a hexokinase II inhibitor 3-bromopyruvate: in vivo investigation of intraarterial administration in a rabbit VX2 hepatoma model. Korean journal of radiology *10*, 596-603.

Jain, M., Nilsson, R., Sharma, S., Madhusudhan, N., Kitami, T., Souza, A.L., Kafri, R., Kirschner, M.W., Clish, C.B., and Mootha, V.K. (2012). Metabolite profiling identifies a key role for glycine in rapid cancer cell proliferation. Science *336*, 1040-1044.

Janke, R., Dodson, A.E., and Rine, J. (2015). Metabolism and epigenetics. Annual review of cell and developmental biology *31*, 473-496.

Jeon, S.M., Chandel, N.S., and Hay, N. (2012). AMPK regulates NADPH homeostasis to promote tumour cell survival during energy stress. Nature *485*, 661-665.

Jiang, L., Kon, N., Li, T., Wang, S.J., Su, T., Hibshoosh, H., Baer, R., and Gu, W. (2015). Ferroptosis as a p53-mediated activity during tumour suppression. Nature *520*, 57-62.

Jiang, L., Shestov, A.A., Swain, P., Yang, C., Parker, S.J., Wang, Q.A., Terada, L.S., Adams, N.D., McCabe, M.T., Pietrak, B., *et al.* (2016). Reductive carboxylation supports redox homeostasis during anchorage-independent growth. Nature *532*, 255-258.

Johannessen, C.M., Reczek, E.E., James, M.F., Brems, H., Legius, E., and Cichowski, K. (2005). The NF1 tumor suppressor critically regulates TSC2 and mTOR. Proceedings of the National Academy of Sciences of the United States of America *102*, 8573-8578.

Kaelin, W.G., Jr., and McKnight, S.L. (2013). Influence of metabolism on epigenetics and disease. Cell *153*, 56-69.

Kasznicki, J., Sliwinska, A., and Drzewoski, J. (2014). Metformin in cancer prevention and therapy. Ann Transl Med *2*, 57.

Klippel, S., Jakubikova, J., Delmore, J., Ooi, M., McMillin, D., Kastritis, E., Laubach, J., Richardson, P.G., Anderson, K.C., and Mitsiades, C.S. (2012). Methyljasmonate displays in vitro and in vivo activity against multiple myeloma cells. Br J Haematol *159*, 340-351.

Kobayashi, S., Sato, M., Kasakoshi, T., Tsutsui, T., Sugimoto, M., Osaki, M., Okada, F., Igarashi, K., Hiratake, J., Homma, T., *et al.* (2015). Cystathionine is a novel substrate of cystine/glutamate transporter: implications for immune function. The Journal of biological chemistry *290*, 8778-8788.

Koppenol, W.H., Bounds, P.L., and Dang, C.V. (2011). Otto Warburg's contributions to current concepts of cancer metabolism. Nature reviews Cancer *11*, 325-337.

Kottakis, F., Nicolay, B.N., Roumane, A., Karnik, R., Gu, H., Nagle, J.M., Boukhali, M., Hayward, M.C., Li, Y.Y., Chen, T., *et al.* (2016). LKB1 loss links serine metabolism to DNA methylation and tumorigenesis. Nature *539*, 390-395.

Lamming, D.W., and Sabatini, D.M. (2013). A Central role for mTOR in lipid homeostasis. Cell metabolism *18*, 465-469.

Laplante, M., and Sabatini, D.M. (2012). mTOR signaling in growth control and disease. Cell *149*, 274-293.

Lewerenz, J., Hewett, S.J., Huang, Y., Lambros, M., Gout, P.W., Kalivas, P.W., Massie, A., Smolders, I., Methner, A., Pergande, M., *et al.* (2012). The Cystine/Glutamate Antiporter System x(c)(-) in Health and Disease: From Molecular Mechanisms to Novel Therapeutic Opportunities. Antioxidants & redox signaling.

Li, L., Kim, E., Yuan, H., Inoki, K., Goraksha-Hicks, P., Schiesher, R.L., Neufeld, T.P., and Guan, K.L. (2010). Regulation of mTORC1 by the Rab and Arf GTPases. The Journal of biological chemistry *285*, 19705-19709.

Liu, P., Gan, W., Inuzuka, H., Lazorchak, A.S., Gao, D., Arojo, O., Liu, D., Wan, L., Zhai, B., Yu, Y., *et al.* (2013). Sin1 phosphorylation impairs mTORC2 complex integrity and inhibits downstream Akt signalling to suppress tumorigenesis. Nature cell biology *15*, 1340-1350.

Lo-Coco, F., Avvisati, G., Vignetti, M., Thiede, C., Orlando, S.M., Iacobelli, S., Ferrara, F., Fazi, P., Cicconi, L., Di Bona, E., *et al.* (2013). Retinoic acid and arsenic trioxide for acute promyelocytic leukemia. N Engl J Med *369*, 111-121.

Locasale, J.W., Grassian, A.R., Melman, T., Lyssiotis, C.A., Mattaini, K.R., Bass, A.J., Heffron, G., Metallo, C.M., Muranen, T., Sharfi, H., *et al.* (2011). Phosphoglycerate dehydrogenase diverts glycolytic flux and contributes to oncogenesis. Nat Genet *43*, 869-874.

Lu, C., Jain, S.U., Hoelper, D., Bechet, D., Molden, R.C., Ran, L., Murphy, D., Venneti, S., Hameed, M., Pawel, B.R., *et al.* (2016). Histone H3K36 mutations promote sarcomagenesis through altered histone methylation landscape. Science *352*, 844-849.

Lu, C., and Thompson, C.B. (2012). Metabolic regulation of epigenetics. Cell metabolism *16*, 9-17.

Ma, L., Chen, Z., Erdjument-Bromage, H., Tempst, P., and Pandolfi, P.P. (2005a). Phosphorylation and functional inactivation of TSC2 by Erk implications for tuberous sclerosis and cancer pathogenesis. Cell *121*, 179-193.

Ma, L., Teruya-Feldstein, J., Behrendt, N., Chen, Z., Noda, T., Hino, O., Cordon-Cardo, C., and Pandolfi, P.P. (2005b). Genetic analysis of Pten and Tsc2 functional interactions in the mouse reveals asymmetrical haploinsufficiency in tumor suppression. Genes & development *19*, 1779-1786.

Marcus, H.J., Carpenter, K.L., Price, S.J., and Hutchinson, P.J. (2010). In vivo assessment of high-grade glioma biochemistry using microdialysis: a study of energy-related molecules, growth factors and cytokines. Journal of neuro-oncology *97*, 11-23.

Marin-Valencia, I., Yang, C., Mashimo, T., Cho, S., Baek, H., Yang, X.L., Rajagopalan, K.N., Maddie, M., Vemireddy, V., Zhao, Z., *et al.* (2012). Analysis of tumor metabolism reveals mitochondrial glucose oxidation in genetically diverse human glioblastomas in the mouse brain in vivo. Cell metabolism *15*, 827-837.

Martinez-Outschoorn, U.E., Peiris-Pages, M., Pestell, R.G., Sotgia, F., and Lisanti, M.P. (2017). Cancer metabolism: a therapeutic perspective. Nature reviews Clinical oncology *14*, 11-31.

Masri, J., Bernath, A., Martin, J., Jo, O.D., Vartanian, R., Funk, A., and Gera, J. (2007). mTORC2 activity is elevated in gliomas and promotes growth and cell motility via overexpression of rictor. Cancer research *67*, 11712-11720.

Masui, K., Cavenee, W.K., and Mischel, P.S. (2015). mTORC2 and Metabolic Reprogramming in GBM: at the Interface of Genetics and Environment. Brain pathology *25*, 755-759.

McMillin, D.W., Negri, J.M., and Mitsiades, C.S. (2013). The role of tumour-stromal interactions in modifying drug response: challenges and opportunities. Nature reviews Drug discovery *12*, 217-228.

Metallo, C.M., Gameiro, P.A., Bell, E.L., Mattaini, K.R., Yang, J., Hiller, K., Jewell, C.M., Johnson, Z.R., Irvine, D.J., Guarente, L., *et al.* (2011). Reductive glutamine metabolism by IDH1 mediates lipogenesis under hypoxia. Nature *481*, 380-384.

Michelakis, E.D., Sutendra, G., Dromparis, P., Webster, L., Haromy, A., Niven, E., Maguire, C., Gammer, T.L., Mackey, J.R., Fulton, D., *et al.* (2010). Metabolic modulation of glioblastoma with dichloroacetate. Sci Transl Med *2*, 31ra34.

Mullarky, E., Lucki, N.C., Beheshti Zavareh, R., Anglin, J.L., Gomes, A.P., Nicolay, B.N., Wong, J.C., Christen, S., Takahashi, H., Singh, P.K., *et al.* (2016). Identification of a small molecule inhibitor of 3-phosphoglycerate dehydrogenase to target serine biosynthesis in cancers. Proceedings of the National Academy of Sciences of the United States of America *113*, 1778-1783.

Mullarky, E., Mattaini, K.R., Vander Heiden, M.G., Cantley, L.C., and Locasale, J.W. (2011). PHGDH amplification and altered glucose metabolism in human melanoma. Pigment Cell Melanoma Res *24*, 1112-1115.

Nagy, R., Sweet, K., and Eng, C. (2004). Highly penetrant hereditary cancer syndromes. Oncogene *23*, 6445-6470.

Nicklin, P., Bergman, P., Zhang, B., Triantafellow, E., Wang, H., Nyfeler, B., Yang, H., Hild, M., Kung, C., Wilson, C., *et al.* (2009). Bidirectional transport of amino acids regulates mTOR and autophagy. Cell *136*, 521-534.

Nielsen, S.F., Nordestgaard, B.G., and Bojesen, S.E. (2012). Statin use and reduced cancer-related mortality. N Engl J Med *367*, 1792-1802.

Nieman, K.M., Kenny, H.A., Penicka, C.V., Ladanyi, A., Buell-Gutbrod, R., Zillhardt, M.R., Romero, I.L., Carey, M.S., Mills, G.B., Hotamisligil, G.S., *et al.* (2011). Adipocytes promote ovarian cancer metastasis and provide energy for rapid tumor growth. Nature medicine *17*, 1498-1503.

Nilsson, R., Jain, M., Madhusudhan, N., Sheppard, N.G., Strittmatter, L., Kampf, C., Huang, J., Asplund, A., and Mootha, V.K. (2014). Metabolic enzyme expression highlights a key role for MTHFD2 and the mitochondrial folate pathway in cancer. Nat Commun *5*, 3128.

Nobukuni, T., Joaquin, M., Roccio, M., Dann, S.G., Kim, S.Y., Gulati, P., Byfield, M.P., Backer, J.M., Natt, F., Bos, J.L., *et al.* (2005). Amino acids mediate mTOR/raptor signaling through activation of class 3 phosphatidylinositol 3OH-kinase. Proceedings of the National Academy of Sciences of the United States of America *102*, 14238-14243.

Otto, A.M. (2016). Warburg effect(s)-a biographical sketch of Otto Warburg and his impacts on tumor metabolism. Cancer & metabolism *4*, 5.

Palm, W., Park, Y., Wright, K., Pavlova, N.N., Tuveson, D.A., and Thompson, C.B. (2015). The Utilization of Extracellular Proteins as Nutrients Is Suppressed by mTORC1. Cell *162*, 259-270.

Patra, K.C., and Hay, N. (2014). The pentose phosphate pathway and cancer. Trends in biochemical sciences *39*, 347-354.

Pavlova, N.N., and Thompson, C.B. (2016). The Emerging Hallmarks of Cancer Metabolism. Cell metabolism *23*, 27-47.

Pearce, L.R., Komander, D., and Alessi, D.R. (2010). The nuts and bolts of AGC protein kinases. Nature reviews Molecular cell biology *11*, 9-22.

Pelicano, H., Feng, L., Zhou, Y., Carew, J.S., Hileman, E.O., Plunkett, W., Keating, M.J., and Huang, P. (2003). Inhibition of mitochondrial respiration: a novel strategy to enhance drug-induced apoptosis in human leukemia cells by a reactive oxygen species-mediated mechanism. The Journal of biological chemistry *278*, 37832-37839.

Phelps, M.E. (2000). Positron emission tomography provides molecular imaging of biological processes. Proceedings of the National Academy of Sciences of the United States of America *97*, 9226-9233.

Polanski, R., Hodgkinson, C.L., Fusi, A., Nonaka, D., Priest, L., Kelly, P., Trapani, F., Bishop, P.W., White, A., Critchlow, S.E., *et al.* (2014). Activity of the monocarboxylate transporter 1 inhibitor AZD3965 in small cell lung cancer. Clinical cancer research : an official journal of the American Association for Cancer Research *20*, 926-937.

Porstmann, T., Santos, C.R., Griffiths, B., Cully, M., Wu, M., Leevers, S., Griffiths, J.R., Chung, Y.L., and Schulze, A. (2008). SREBP activity is regulated by mTORC1 and contributes to Akt-dependent cell growth. Cell metabolism *8*, 224-236.

Possemato, R., Marks, K.M., Shaul, Y.D., Pacold, M.E., Kim, D., Birsoy, K., Sethumadhavan, S., Woo, H.K., Jang, H.G., Jha, A.K., *et al.* (2011). Functional genomics reveal that the serine synthesis pathway is essential in breast cancer. Nature *476*, 346-350.

Rangarajan, A., Hong, S.J., Gifford, A., and Weinberg, R.A. (2004). Species- and cell type-specific requirements for cellular transformation. Cancer cell *6*, 171-183.

Robe, P.A., Martin, D.H., Nguyen-Khac, M.T., Artesi, M., Deprez, M., Albert, A., Vanbelle, S., Califice, S., Bredel, M., and Bours, V. (2009). Early termination of ISRCTN45828668, a phase 1/2 prospective, randomized study of sulfasalazine for the treatment of progressing malignant gliomas in adults. BMC cancer *9*, 372.

Robitaille, A.M., Christen, S., Shimobayashi, M., Cornu, M., Fava, L.L., Moes, S., Prescianotto-Baschong, C., Sauer, U., Jenoe, P., and Hall, M.N. (2013). Quantitative phosphoproteomics reveal mTORC1 activates de novo pyrimidine synthesis. Science *339*, 1320-1323.

Rohrig, F., and Schulze, A. (2016). The multifaceted roles of fatty acid synthesis in cancer. Nature reviews Cancer *16*, 732-749.

Sarbassov, D.D., Guertin, D.A., Ali, S.M., and Sabatini, D.M. (2005). Phosphorylation and regulation of Akt/PKB by the rictor-mTOR complex. Science *307*, 1098-1101.

Sasaki, H., Sato, H., Kuriyama-Matsumura, K., Sato, K., Maebara, K., Wang, H., Tamba, M., Itoh, K., Yamamoto, M., and Bannai, S. (2002). Electrophile response element-mediated induction of the cystine/glutamate exchange transporter gene expression. The Journal of biological chemistry *277*, 44765-44771.

Sato, H., Nomura, S., Maebara, K., Sato, K., Tamba, M., and Bannai, S. (2004). Transcriptional control of cystine/glutamate transporter gene by amino acid deprivation. Biochemical and biophysical research communications *325*, 109-116.

Sato, H., Tamba, M., Ishii, T., and Bannai, S. (1999). Cloning and expression of a plasma membrane cystine/glutamate exchange transporter composed of two distinct proteins. The Journal of biological chemistry *274*, 11455-11458.

Savaskan, N.E., and Eyupoglu, I.Y. (2010). xCT modulation in gliomas: relevance to energy metabolism and tumor microenvironment normalization. Annals of anatomy = Anatomischer Anzeiger : official organ of the Anatomische Gesellschaft *192*, 309-313.

Savaskan, N.E., Heckel, A., Hahnen, E., Engelhorn, T., Doerfler, A., Ganslandt, O., Nimsky, C., Buchfelder, M., and Eyupoglu, I.Y. (2008). Small interfering RNA-mediated xCT silencing in gliomas inhibits neurodegeneration and alleviates brain edema. Nature medicine *14*, 629-632.

Schug, Z.T., Peck, B., Jones, D.T., Zhang, Q., Grosskurth, S., Alam, I.S., Goodwin, L.M., Smethurst, E., Mason, S., Blyth, K., *et al.* (2015). Acetyl-CoA synthetase 2 promotes acetate utilization and maintains cancer cell growth under metabolic stress. Cancer cell *27*, 57-71.

Schug, Z.T., Vande Voorde, J., and Gottlieb, E. (2016). The metabolic fate of acetate in cancer. Nature reviews Cancer *16*, 708-717.

Shackelford, D.B., Abt, E., Gerken, L., Vasquez, D.S., Seki, A., Leblanc, M., Wei, L., Fishbein, M.C., Czernin, J., Mischel, P.S., *et al.* (2013). LKB1 inactivation dictates therapeutic response of non-small cell lung cancer to the metabolism drug phenformin. Cancer cell *23*, 143-158.

Shackelford, D.B., and Shaw, R.J. (2009). The LKB1-AMPK pathway: metabolism and growth control in tumour suppression. Nature reviews Cancer *9*, 563-575.

Shimobayashi, M., and Hall, M.N. (2016). Multiple amino acid sensing inputs to mTORC1. Cell Res *26*, 7-20.

Shoshan, M.C. (2012). 3-Bromopyruvate: targets and outcomes. J Bioenerg Biomembr *44*, 7-15.

Shyh-Chang, N., Daley, G.Q., and Cantley, L.C. (2013). Stem cell metabolism in tissue development and aging. Development *140*, 2535-2547.

Smith, A.E., and Kenyon, D.H. (1973). A unifying concept of carcinogenesis and its therapeutic implications. Oncology *27*, 459-479.

Son, J., Lyssiotis, C.A., Ying, H., Wang, X., Hua, S., Ligorio, M., Perera, R.M., Ferrone, C.R., Mullarky, E., Shyh-Chang, N., *et al.* (2013). Glutamine supports pancreatic cancer growth through a KRAS-regulated metabolic pathway. Nature *496*, 101-105.

Takeuchi, S., Wada, K., Toyooka, T., Shinomiya, N., Shimazaki, H., Nakanishi, K., Nagatani, K., Otani, N., Osada, H., Uozumi, Y., *et al.* (2012). Increased xCT Expression Correlates with Tumor Invasion and Outcome in Patients with Glioblastoma. Neurosurgery.

Thompson, C.B. (2011). Rethinking the regulation of cellular metabolism. Cold Spring Harbor symposia on quantitative biology *76*, 23-29.

Thompson, J.E., and Thompson, C.B. (2004). Putting the rap on Akt. Journal of clinical oncology : official journal of the American Society of Clinical Oncology *22*, 4217-4226.

Timmerman, L.A., Holton, T., Yuneva, M., Louie, R.J., Padro, M., Daemen, A., Hu, M., Chan, D.A., Ethier, S.P., van 't Veer, L.J., *et al.* (2013). Glutamine sensitivity analysis identifies the xCT antiporter as a common triple-negative breast tumor therapeutic target. Cancer cell *24*, 450-465.

Tonjes, M., Barbus, S., Park, Y.J., Wang, W., Schlotter, M., Lindroth, A.M., Pleier, S.V., Bai, A.H., Karra, D., Piro, R.M., *et al.* (2013). BCAT1 promotes cell proliferation through amino acid catabolism in gliomas carrying wild-type IDH1. Nature medicine *19*, 901-908.

Trachootham, D., Alexandre, J., and Huang, P. (2009). Targeting cancer cells by ROS-mediated mechanisms: a radical therapeutic approach? Nature reviews Drug discovery *8*, 579-591.

van Vuurden, D.G., Yazdani, M., Bosma, I., Broekhuizen, A.J., Postma, T.J., Heimans, J.J., van der Valk, P., Aronica, E., Tannous, B.A., Wurdinger, T., *et al.* (2009). Attenuated AMPA receptor expression allows glioblastoma cell survival in glutamate-rich environment. PloS one *4*, e5953.

Vander Heiden, M.G. (2011). Targeting cancer metabolism: a therapeutic window opens. Nature reviews Drug discovery *10*, 671-684.

Viale, A., Pettazzoni, P., Lyssiotis, C.A., Ying, H., Sanchez, N., Marchesini, M., Carugo, A., Green, T., Seth, S., Giuliani, V., *et al.* (2014). Oncogene ablation-resistant pancreatic cancer cells depend on mitochondrial function. Nature *514*, 628-632.

Villa, G.R., Hulce, J.J., Zanca, C., Bi, J., Ikegami, S., Cahill, G.L., Gu, Y., Lum, K.M., Masui, K., Yang, H., *et al.* (2016). An LXR-Cholesterol Axis Creates a Metabolic Co-Dependency for Brain Cancers. Cancer cell *30*, 683-693.

Vivanco, I., and Sawyers, C.L. (2002). The phosphatidylinositol 3-Kinase AKT pathway in human cancer. Nature reviews Cancer *2*, 489-501.

Vogelstein, B., Papadopoulos, N., Velculescu, V.E., Zhou, S., Diaz, L.A., Jr., and Kinzler, K.W. (2013). Cancer genome landscapes. Science *339*, 1546-1558.

Warburg, O. (1956). On the origin of cancer cells. Science *123*, 309-314.

Watson, J.D., and Crick, F.H. (1953). Molecular structure of nucleic acids; a structure for deoxyribose nucleic acid. Nature *171*, 737-738.

Weinhouse, S. (1956). On respiratory impairment in cancer cells. Science *124*, 267-269.

Wilson, P.M., Danenberg, P.V., Johnston, P.G., Lenz, H.J., and Ladner, R.D. (2014). Standing the test of time: targeting thymidylate biosynthesis in cancer therapy. Nature reviews Clinical oncology *11*, 282-298.

Wu, S.H., Bi, J.F., Cloughesy, T., Cavenee, W.K., and Mischel, P.S. (2014). Emerging function of mTORC2 as a core regulator in glioblastoma: metabolic reprogramming and drug resistance. Cancer biology & medicine *11*, 255-263.

Yang, M., and Vousden, K.H. (2016). Serine and one-carbon metabolism in cancer. Nature reviews Cancer *16*, 650-662.

Yang, W.S., SriRamaratnam, R., Welsch, M.E., Shimada, K., Skouta, R., Viswanathan, V.S., Cheah, J.H., Clemons, P.A., Shamji, A.F., Clish, C.B., *et al.* (2014). Regulation of ferroptotic cancer cell death by GPX4. Cell *156*, 317-331.

Yang, W.S., and Stockwell, B.R. (2008). Synthetic lethal screening identifies compounds activating iron-dependent, nonapoptotic cell death in oncogenic-RAS-harboring cancer cells. Chemistry & biology *15*, 234-245.

Ye, Z.C., Rothstein, J.D., and Sontheimer, H. (1999). Compromised glutamate transport in human glioma cells: reduction-mislocalization of sodium-dependent glutamate transporters and

enhanced activity of cystine-glutamate exchange. The Journal of neuroscience : the official journal of the Society for Neuroscience *19*, 10767-10777.

Ye, Z.C., and Sontheimer, H. (1999). Glioma cells release excitotoxic concentrations of glutamate. Cancer research *59*, 4383-4391.

Yecies, J.L., and Manning, B.D. (2011). Transcriptional control of cellular metabolism by mTOR signaling. Cancer research *71*, 2815-2820.

Yuan, J.M., Stepanov, I., Murphy, S.E., Wang, R., Allen, S., Jensen, J., Strayer, L., Adams-Haduch, J., Upadhyaya, P., Le, C., *et al.* (2016). Clinical Trial of 2-Phenethyl Isothiocyanate as an Inhibitor of Metabolic Activation of a Tobacco-Specific Lung Carcinogen in Cigarette Smokers. Cancer prevention research *9*, 396-405.

Yuan, T.L., and Cantley, L.C. (2008). PI3K pathway alterations in cancer: variations on a theme. Oncogene *27*, 5497-5510.

Yun, J., Mullarky, E., Lu, C., Bosch, K.N., Kavalier, A., Rivera, K., Roper, J., Chio, II, Giannopoulou, E.G., Rago, C., *et al.* (2015). Vitamin C selectively kills KRAS and BRAF mutant colorectal cancer cells by targeting GAPDH. Science *350*, 1391-1396.

Yun, J., Rago, C., Cheong, I., Pagliarini, R., Angenendt, P., Rajagopalan, H., Schmidt, K., Willson, J.K., Markowitz, S., Zhou, S., *et al.* (2009). Glucose deprivation contributes to the development of KRAS pathway mutations in tumor cells. Science *325*, 1555-1559.

Zaugg, K., Yao, Y., Reilly, P.T., Kannan, K., Kiarash, R., Mason, J., Huang, P., Sawyer, S.K., Fuerth, B., Faubert, B., *et al.* (2011). Carnitine palmitoyltransferase 1C promotes cell survival and tumor growth under conditions of metabolic stress. Genes & development *25*, 1041-1051.

Zhang, W., Trachootham, D., Liu, J., Chen, G., Pelicano, H., Garcia-Prieto, C., Lu, W., Burger, J.A., Croce, C.M., Plunkett, W., *et al.* (2012). Stromal control of cystine metabolism promotes cancer cell survival in chronic lymphocytic leukaemia. Nature cell biology *14*, 276-286.

Zhou, Y., Wong, C.O., Cho, K.J., van der Hoeven, D., Liang, H., Thakur, D.P., Luo, J., Babic, M., Zinsmaier, K.E., Zhu, M.X., *et al.* (2015). SIGNAL TRANSDUCTION. Membrane potential modulates plasma membrane phospholipid dynamics and K-Ras signaling. Science *349*, 873-876.

Zoncu, R., Efeyan, A., and Sabatini, D.M. (2011). mTOR: from growth signal integration to cancer, diabetes and ageing. Nature reviews Molecular cell biology *12*, 21-35.

Chapter 2

Growth Factor Signaling and mTOR Mediates Metabolic Reprograming in Cancer

mTOR Reprograms Amino Acid Metabolism in Cancer through Phosphorylation of xCT

INTRODUCTION

Dysregulated amino acid metabolism is an emerging hallmark of cancer (Hanahan and Weinberg, 2011; Pavlova and Thompson, 2016). Tumor cells take up amino acids from the extracellular environment as a carbon and nitrogen source for protein and nucleotide synthesis (DeBerardinis et al., 2007). Uptake of amino acids from the tumor microenvironment also contributes to one-carbon metabolism and redox maintenance (Altman et al., 2016; Yang and Vousden, 2016). Tumor cells take up amino acids either through specific amino acid transporters (Bhutia et al., 2015), or through macropinocytosis, a recently described opportunistic pathway of amino acid uptake (Commisso et al., 2013; Pavlova and Thompson, 2016). Currently, the underlying molecular mechanisms of amino acid transporter regulation in cancer are not well understood.

The cystine-glutamate antiporter xCT encoded by the *SLC7A11* gene, is highly expressed in multiple human cancer types, including triple negative breast cancer and glioblastoma (GBM) (Chung et al., 2005; Takeuchi et al., 2012; Timmerman et al., 2013). xCT is responsible for the uptake of cystine, the oxidized dimeric form of cysteine, in exchange for glutamate, contributing to tumor growth (Bassi et al., 2001; Lewerenz et al., 2012). In nutrient depleted conditions, cystine uptake is critical for glutathione synthesis to buffer reactive oxygen species (ROS), whereas in nutrient repleted conditions, glutamate can contribute to many anabolic reactions (Conrad and Sato, 2012; DeBerardinis et al., 2008; Kim et al., 2001; Son et al., 2013). Thus,

post-translational mechanisms of xCT regulation may be important for enabling tumor cells to rapidly respond to changing environmental conditions. We hypothesized that cell autonomous signaling mechanisms could provide an additional route of xCT regulation.

To identify complementary pathways of xCT regulation, we performed an unbiased mass spectrometry proteomics screen to identify xCT binding partners. Here we discovered an unanticipated mechanism of cross talk between altered growth factor receptor signaling and glutamate-cystine metabolism in tumor cells, linking growth factor receptor signaling with amino acid metabolism in cancer.

RESULTS

mTORC2 Phosphorylates xCT on Serine 26

Unbiased screen identifies mTORC2 as a binding partner of xCT

We stably expressed a FLAG-tagged xCT or vector control in GBM cells and used Stable Isotope Labeling in Cell culture (SILAC) (Ong and Mann, 2006) coupled to mass spectrometry to identify xCT binding partners. xCT-bound complexes were immunoprecipitated and subjected to quantitative LC/MS-MS (Fig. 2-1A), revealing 125 potential xCT binding proteins with a median fold enrichment of xCT/vector >10 (Fig. 2-1B and Supplementary Table 1). DAVID (Huang da et al., 2009) Gene Ontology (GO) analysis showed enrichment in pathways involved in cellular and protein metabolism (Fig. 2-1C and Supplementary Table 2). Established xCT binding partners including CD98 (*SLC3A2*) and CD44 (Ishimoto et al., 2011), were identified as well as the epidermal growth factor receptor (EGFR) (Tsuchihashi et al., 2016). Surprisingly, Rictor and mTOR, which are core components of mTOR complex 2 (mTORC2), were also identified as potential xCT binding proteins (Fig. 2-1B).

In GBM, lung cancer and triple-negative breast cancer cell lines, Co-Immunoprecipitation (Co-IP) experiments confirmed the physical association between xCT and endogenous mTORC2 components mTOR and Rictor. Importantly, Raptor, which is specific to mTORC1 (Fig. 2-2A), was not identified in the SILAC screen and was not detected by Co-IP analysis, thus confirming that the physical association with xCT was specific to mTORC2. Reverse Co-IP confirmed the binding of xCT to both a FLAG-tagged mTOR and a myc-tagged Rictor, in GBM cells (Fig. 2-2B). These data demonstrate that xCT specifically interacts with mTORC2, but not mTORC1, in GBM cells.

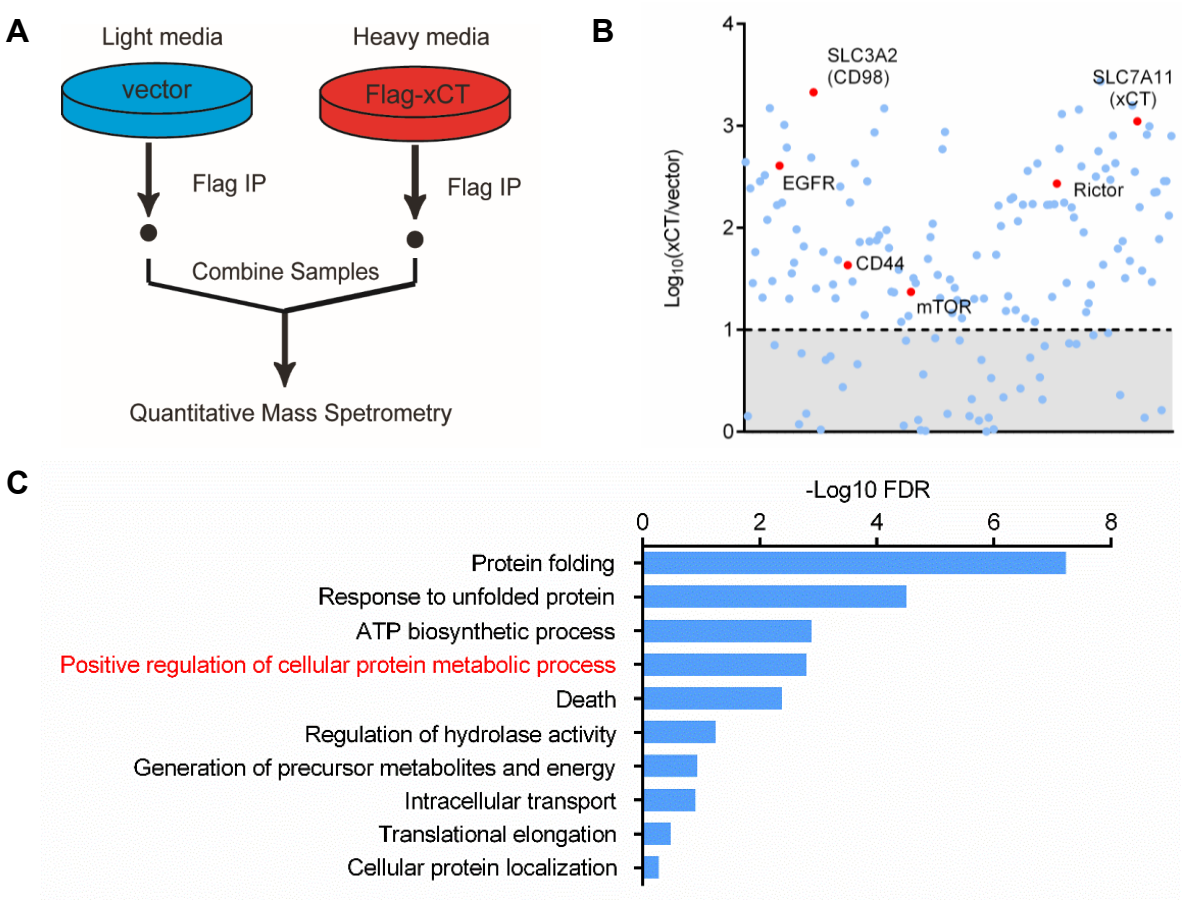

Fig. 2-1. mTORC2 is Identified as an xCT Binding Protein.

(A) A brief schematic of the SILAC Mass Spectrometry experiment performed to identify xCT specific binding proteins in U87EGFRvIII cells.

(B) The median fold enrichment of the identified proteins was plotted on a Log_{10} scale as xCT versus vector. A cutoff of Log_{10} (xCT/vector) <1 was applied and indicated by the dash line. Known xCT binding proteins as well as mTOR and Rictor were labeled in red. The complete list of proteins identified can be found in Table. 1.

(C) DAVID gene ontology (GO) analysis of the 125 potential xCT binding proteins identified in (B). Top 10 enriched biological pathways were plotted using the – (Log_{10} FDR). The enriched pathways that contain both mTOR and Rictor were indicated in red and the full gene list of each pathway can be found in Table. 2.

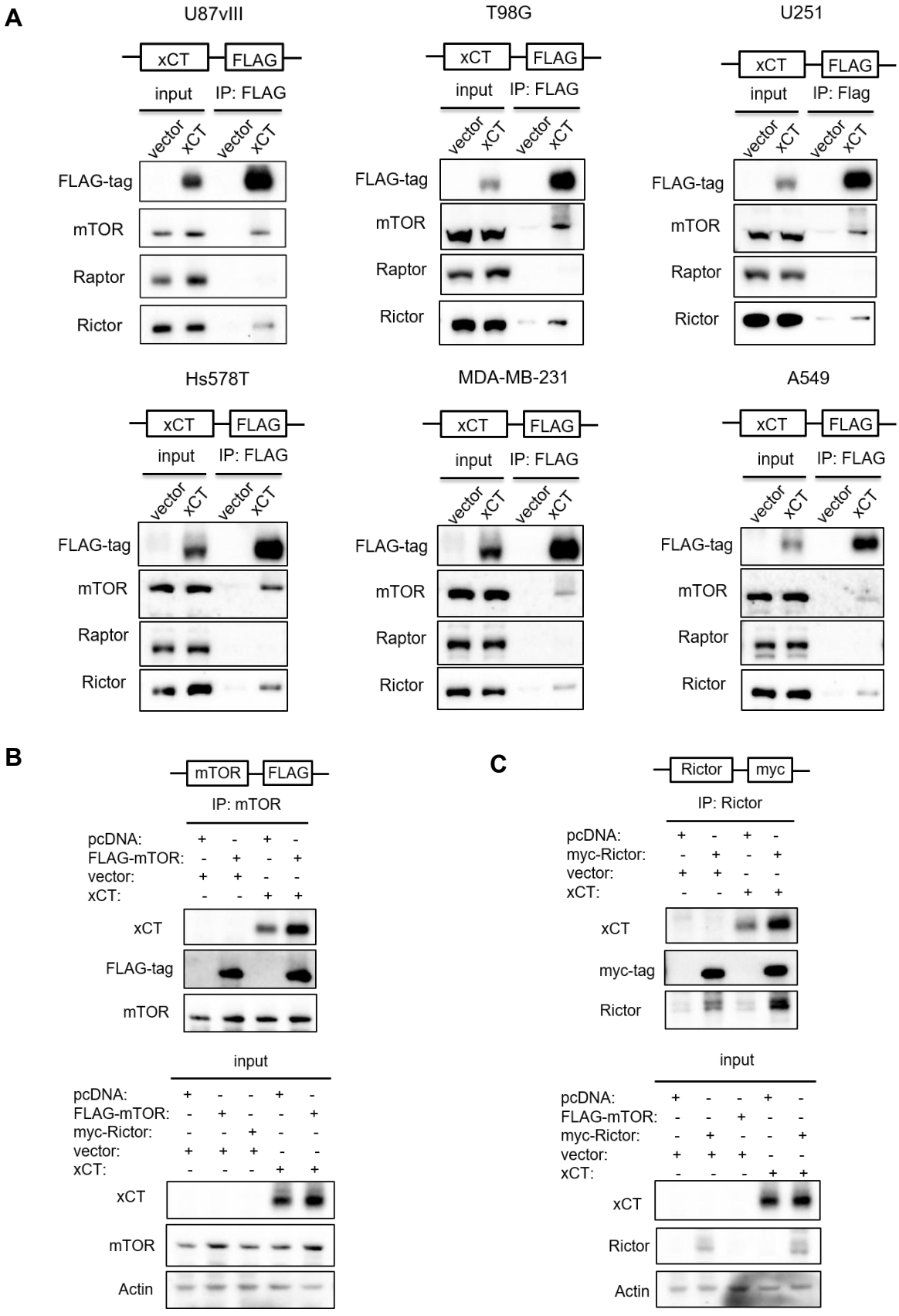
A
U87vIII
T98G
U251
Hs578T
MDA-MB-231
A549
xCT
FLAG
input
IP: FLAG
IP: Flag
vector
xCT
FLAG-tag
mTOR
Raptor
Rictor
B
mTOR
FLAG
IP: mTOR
pcDNA:
FLAG-mTOR:
vector:
xCT:
xCT
FLAG-tag
mTOR
input
myc-Rictor:
Actin
C
Rictor
myc
IP: Rictor
myc-tag

Fig. 2-2. mTORC2 Physically Interacts with xCT in Cancer Cells.

(A) Co-immunoprecipitation (Co-IP) was performed to validate mTOR and Rictor as xCT binding proteins in GBM (U87vIII, U251, T98G), triple-negative cancer (MDA-MB-231, Hs578T) and lung cancer (A549) cell lines stably overexpressing the FLAG-tagged xCT or vector control.

(B-C) Reverse Co-IP was performed to verify mTOR and Rictor as xCT binding proteins. U87EGFRvIII cells with stable xCT overexpression or vector control were transiently transfected with pcDNA vector control, FLAG-mTOR (A) or myc-Rictor (B). After 48 h of transfection, protein lysates were collected and incubated with Dynabeads Protein A pre-incubated with mTOR or Rictor specific antibodies. Eluates were subjected to immunoblotting to probe for xCT, mTOR, Rictor and corresponding tags.

mTORC2 phosphorylates xCT downstream of growth factor signaling in cancer

mTORC2 is a serine/threonine kinase that is a core-component of altered growth factor receptor signaling in some cancer types, including GBM (Masui et al., 2015a; Masui et al., 2013; Tanaka et al., 2011). EGFRvIII mutation in GBM cells, or ligand stimulation of EGFR and/or PTEN loss, activates mTORC2 to promote tumor growth (Tanaka et al., 2011), potentially by phosphorylating AGC kinases (Jacinto and Lorberg, 2008; Pearce et al., 2010). mTORC2 has recently been shown to regulate a number of essential metabolic pathways in cancer, including glycolysis, glutaminolysis, de novo lipid synthesis and nucleotide and ROS metabolism (Aramburu et al., 2014; Dang, 2012; Lamming and Sabatini, 2013; Masui et al., 2013). Rictor overexpression did not affect the levels of xCT mRNA, excluding effects of mTORC2 on xCT transcription, at least in the time course studied (Fig. 2-3A). Therefore, we hypothesized that mTORC2 could possibly regulate xCT activity through phosphorylation. A number of serine and threonine residues on xCT that have been previously reported to be potential phosphorylation sites including S26, S51 and S481 (Hornbeck et al., 2015; Lundby et al., 2012; Schweppe et al., 2013; Yu et al., 2011; Zhou et al., 2013), which could potentially serve as targets of mTORC2. Importantly, S26, S51 and S481 are all preceded by an arginine at the -3 position (RXXS/T) (Fig. 2-3B), suggesting that they might belong to the broad category of AGC kinase family substrates (Alessi et al., 1996; Pearce et al., 2010).

To test the hypothesis that mTORC2 regulates xCT phosphorylation in response to growth factor signaling, we knocked down Rictor or Raptor with siRNAs in GBM cells stably expressing wild-type EGFR, and examined xCT phosphorylation after stimulation with EGF. To broadly monitor the state of xCT serine/threonine phosphorylation, we performed immunoprecipitation of cellular

lysates using phospho-RXXS/T antibody conjugated beads, followed by immunoblotting for myc-tagged xCT. As shown in Fig. 2-3C, EGF stimulation increased xCT phosphorylation, which was abrogated by Rictor knockdown, demonstrating that EGF signaling promotes xCT serine/threonine phosphorylation in an mTORC2-dependent manner. In contrast to Rictor, Raptor knockdown increased xCT phosphorylation (Fig. 2-3C), which is consistent with the hyperactivation of mTORC2 that commonly occurs as a consequence of mTORC1 inhibition due to the mTORC1-medidated negative feedback regulation (Dibble et al., 2009). In addition, the mTOR kinase inhibitor Torin1, which blocks both mTORC1 and mTORC2 activity (Liu et al., 2010), significantly inhibited xCT phosphorylation on RXXS/T motifs in GBM cells (Fig. 2-3D).

mTORC2 phosphorylates and activates downstream AGC kinases including PKCα, Akt and SGK1, amplifying the signaling cascade by phosphorylating a much broader range of downstream substrates involved in various cellular processes (Laplante and Sabatini, 2009, 2012). Therefore, we tested the possibility of whether xCT phosphorylation was regulated by any of the AGC kinases downstream of mTORC2. Surprisingly, we did not detect physical interaction between any AGC kinases including PKCα, Akt or SGK1 and xCT in either the SILAC or Co-IP experiments (Table 1 and Fig. 2-4). Furthermore, neither siRNA-mediated genetic knockdown, nor pharmacological inhibition of PKCα, Akt and SGK1 suppressed xCT phosphorylation upon EGF stimulation (Fig. 2-5 and 2-6), suggesting that downstream effector AGC kinases are not required for mTORC2-mediated xCT phosphorylation.

A

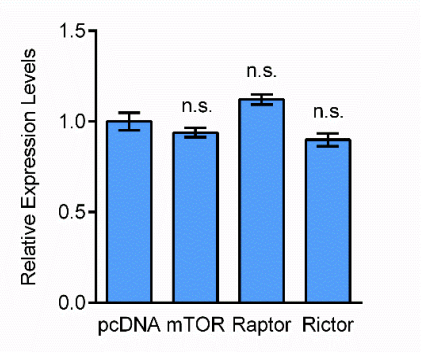

B

RXXS/T sites in xCT:

S26: NVNGRLPSLGNKEPP (cytoplasmic)
T45: VQLKRKVTLLRGVSI (transmembrane)
S51: VTLLRGVSIIIGTII (transmembrane)
S231: AFSGRDSSITRLPLA (extracellular)
T364: MIHVRKHTPLPAVIV (cytoplasmic/next to transmembrane)
S481: PRWFRIMSEKITRTL (cytoplasmic)

C

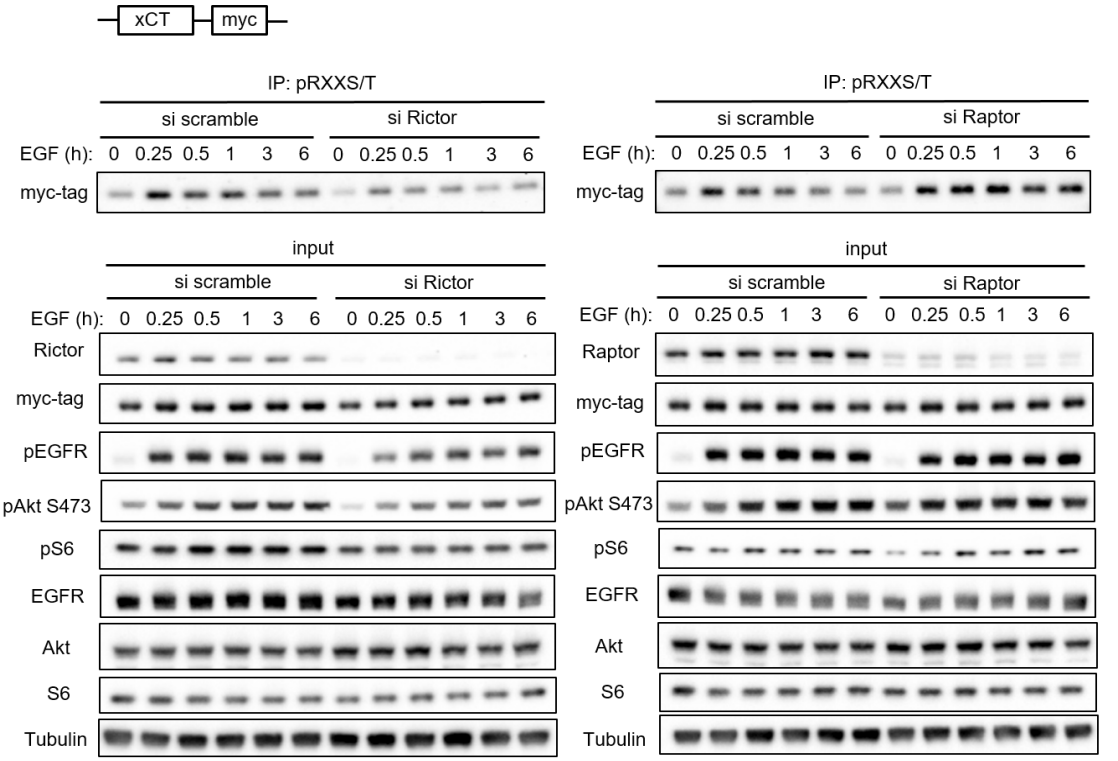

D

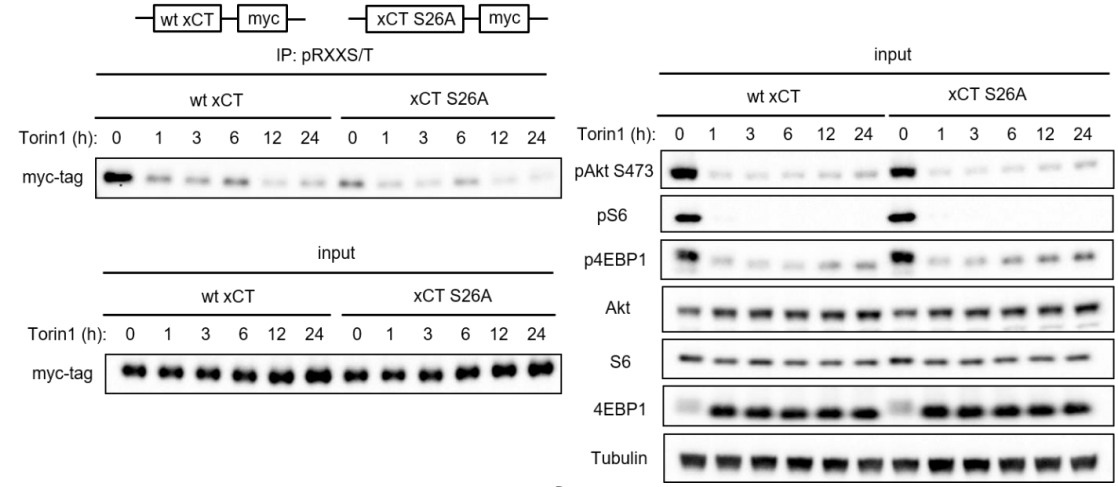

Fig. 2-3. mTORC2 Phosphorylates xCT Downstream of Growth Factor Signaling.

(A) RT-PCR analysis of xCT mRNA levels in U87 cells transiently transfected with vector (pcDNA) control, mTOR, Raptor or Rictor. Cells were collected after 72 h of transfection and mRNAs were extracted. Results were calculated from four independent replicates and data were shown as mean ± SEM. Statistical analysis was performed using one-way ANOVA and compared to the mean of pcDNA as control. n.s. refers to not statistically significant.

(B) RXXS/T motifs on xCT were listed by analyzing xCT protein sequence. S26 (in red) phosphorylation was detected in our study and has been reported by others. S51 and S481 (in blue) phosphorylation were reported on PhosphoSitePlus but were not detected in our experiments. Phosphorylation of the remaining RXXS/T sites (in black) on xCT has not been reported in any other studies or observed in our experiments (Hornbeck et al., 2015). (http://www.phosphosite.org/uniprotAccAction?id=Q9UPY5.)

(C) Immunoprecipitation (IP) - western blot was performed in U87 cells stably expressing EGFR and myc-tagged xCT. Cells were serum starved for 24 h post 24 h of transfection with siRNA before stimulated with 25 ng/ml EGF. Cell lysates were collected at indicated time points and subjected to pRXXS/T IP and western blotting analysis.

(D) U87EGFRvIII cells stably overexpressing xCT or vector control were treated with 250 nM Torin1. Protein lysates were collected over a time course of 24 h for IP-western blot to determine xCT phosphorylation on RXXS/T motifs.

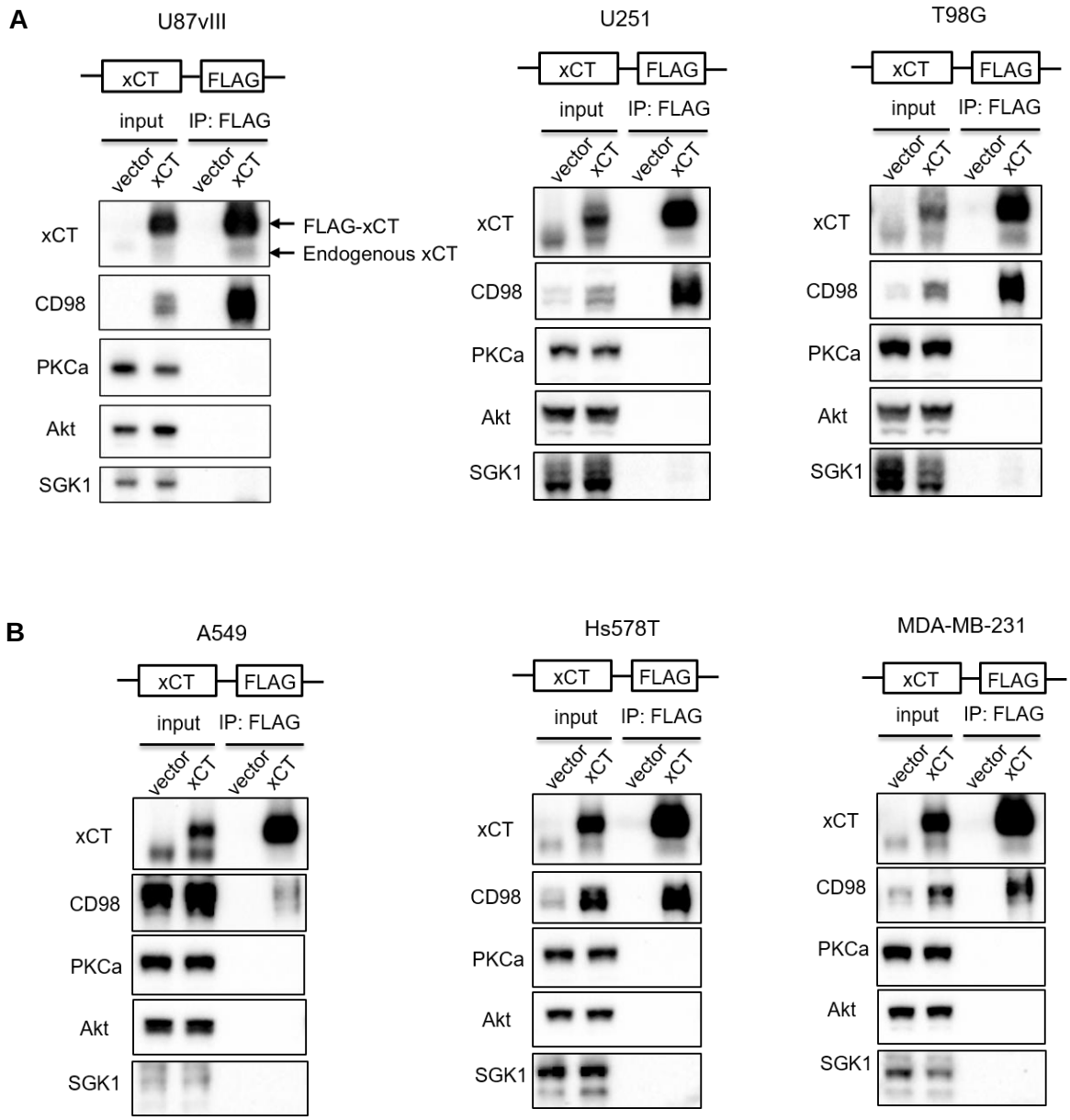

Fig. 2-4. AGC Kinases Downstream of mTORC2 Does Not Bind to xCT.

(A-B) Co-IP experiment was performed using (A) GBM cell lines U87EGFRvIII, U251 and T98G, and lung cancer cell line A549, as well as triple negative breast cancer cell lines Hs578T and MDA-MB-231 (B) stably overexpressing FLAG-tagged xCT or vector control to detect xCT binding with PKCα, Akt and SGK1.

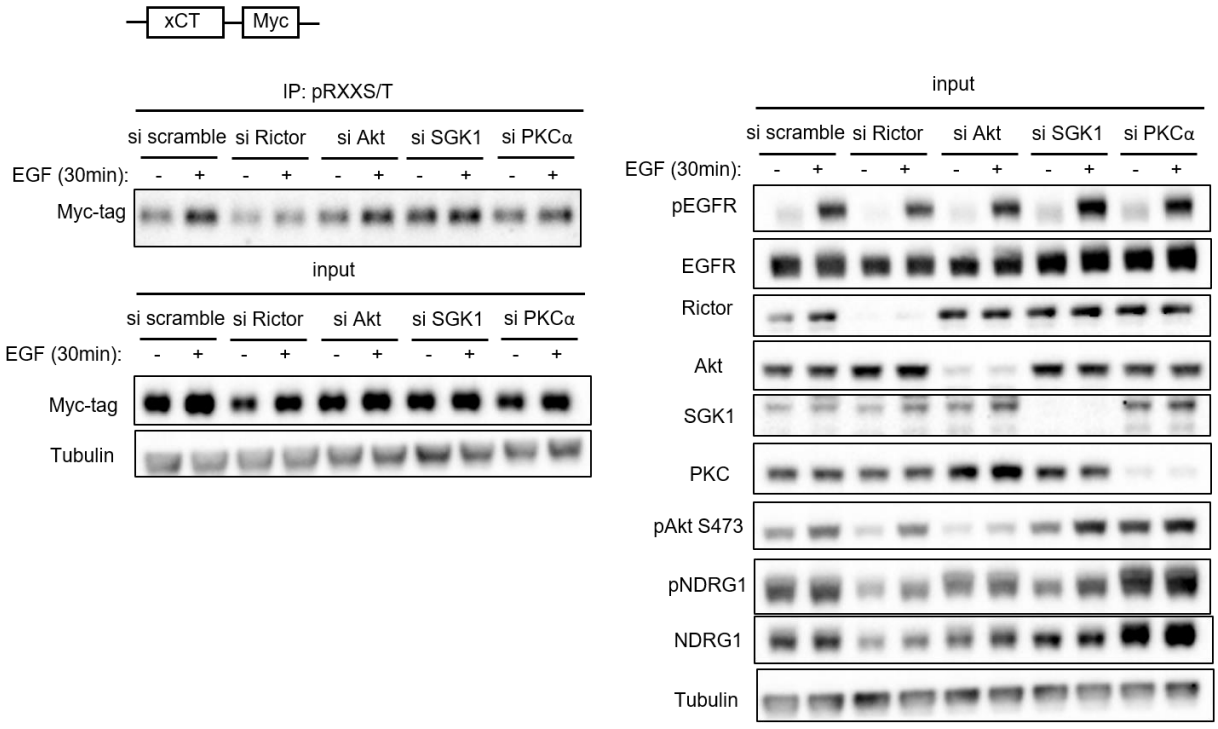

Fig. 2-5. Knockdowns of AGC Kinases Downstream of mTORC2 Do Not Affect xCT Phosphorylation on RXXS/T Motifs.

U87 cells stably expressing wt EGFR and myc-tagged xCT were transfected with indicated siRNA targeting Rictor or mTORC2 downstream AGC kinases. 24 h post-transfection cells were serum starved for an additional 24 h and then stimulated with 25 ng/ml EGF for 30 min before protein lysates were collected and subjected to pRXXS/T IP and western blotting analysis.

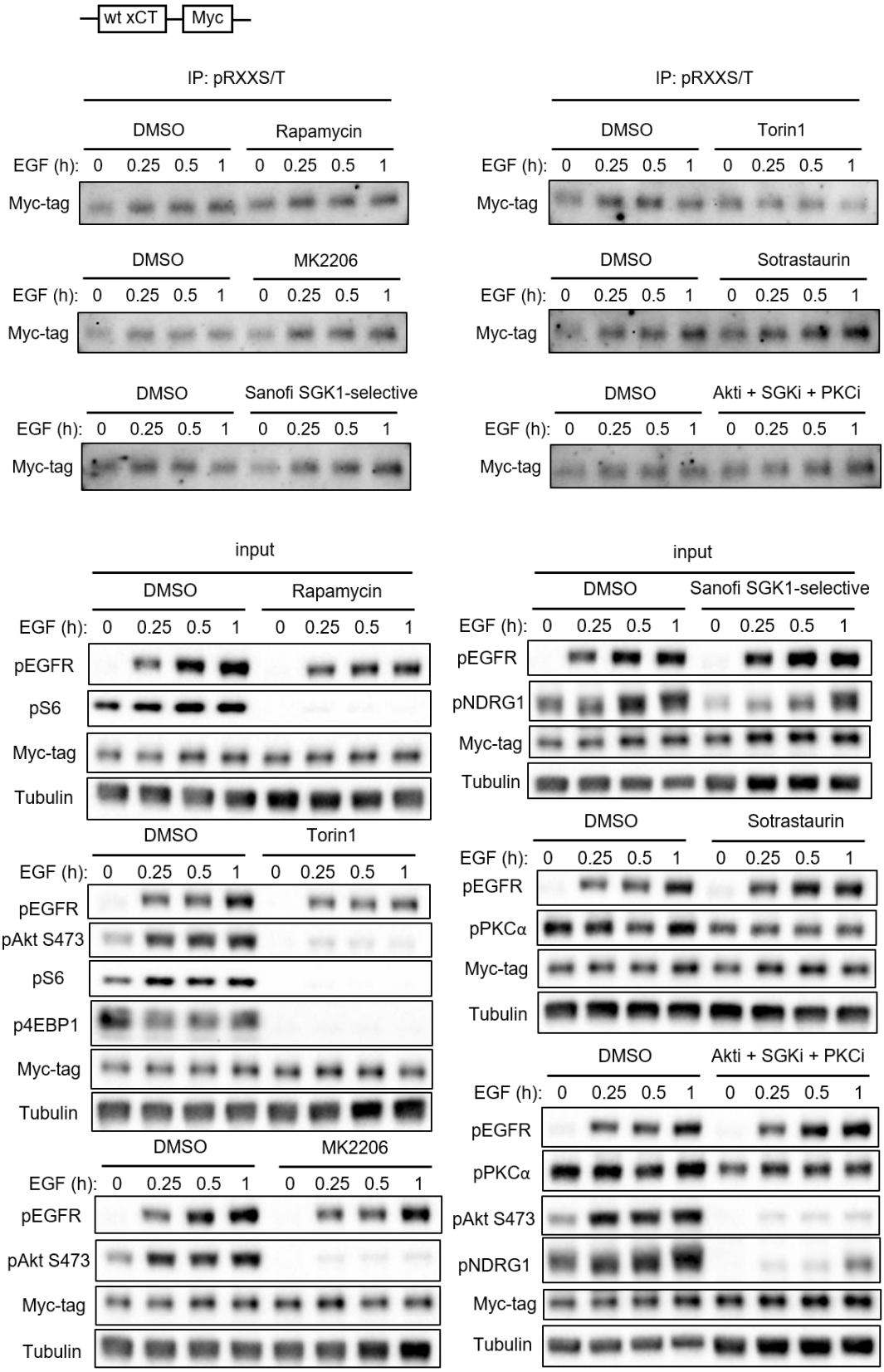
wt xCT
Myc
IP: pRXXS/T
DMSO
Rapamycin
EGF (h): 0 0.25 0.5 1 0 0.25 0.5 1
Myc-tag
DMSO
Torin1
EGF (h): 0 0.25 0.5 1 0 0.25 0.5 1
Myc-tag
DMSO
MK2206
EGF (h): 0 0.25 0.5 1 0 0.25 0.5 1
Myc-tag
DMSO
Sotrastaurin
EGF (h): 0 0.25 0.5 1 0 0.25 0.5 1
Myc-tag
DMSO
Sanofi SGK1-selective
EGF (h): 0 0.25 0.5 1 0 0.25 0.5 1
Myc-tag
DMSO
Akti + SGKi + PKCi
EGF (h): 0 0.25 0.5 1 0 0.25 0.5 1
Myc-tag
input
DMSO
Rapamycin
EGF (h): 0 0.25 0.5 1 0 0.25 0.5 1
pEGFR
pS6
Myc-tag
Tubulin
input
DMSO
Sanofi SGK1-selective
EGF (h): 0 0.25 0.5 1 0 0.25 0.5 1
pEGFR
pNDRG1
Myc-tag
Tubulin
DMSO
Torin1
EGF (h): 0 0.25 0.5 1 0 0.25 0.5 1
pEGFR
pAkt S473
pS6
p4EBP1
Myc-tag
Tubulin
DMSO
Sotrastaurin
EGF (h): 0 0.25 0.5 1 0 0.25 0.5 1
pEGFR
pPKCα
Myc-tag
Tubulin
DMSO
MK2206
EGF (h): 0 0.25 0.5 1 0 0.25 0.5 1
pEGFR
pAkt S473
Myc-tag
Tubulin
DMSO
Akti + SGKi + PKCi
EGF (h): 0 0.25 0.5 1 0 0.25 0.5 1
pEGFR
pPKCα
pAkt S473
pNDRG1
Myc-tag
Tubulin

Fig. 2-6. Pharmacological Inhibition of Neither mTORC1 Nor AGC Kinases Downstream of mTORC2 Affect xCT Phosphorylation on RXXS/T Motifs.

U87 cells stably expressing wt EGFR and myc-tagged xCT were serum starved for 24 h in the presence of DMSO or indicated kinase inhibitors (Rapamycin: 10 nM, Torin1: 250 nM; MK2206: 1 μM; Sanofi-SGK1-selective compound: 2 μM; Sotrastaurin: 5 μM; Akti + SGKi +PKCi refers to combination treatment with MK2206, Sanofi-SGK1-selective compound and Sotrastaurin at the same concentration as individual drug treatment mentioned above) and then stimulated with 25 ng/ml EGF before protein lysates were collected at indicated time points and subjected to pRXXS/T IP and western blotting analysis. Inhibition of kinase activity were also analyzed by western blot as shown in the input panels.

xCT is phosphorylated at serine 26 in the cytosolic N-terminus by mTORC2

xCT is a twelve-transmembrane protein (Gasol et al., 2004). We hypothesized that mTORC2-dependent phosphorylation of xCT would be more likely to occur on cytosolic domains, which are more accessible to kinases including mTORC2 (Fig. 2-7A). Consistent with this hypothesis, deletion of xCT's cytosolic N-terminus completely abrogated the phosphorylation of xCT on RXXS/T motifs. In contrast, deletion of xCT's cytosolic C-terminus had no effect on xCT phosphorylation (Fig. 2-7B). Several previous large-scale quantitative LC/MS-MS phosphoproteomic studies identified phosphorylation of xCT on serine 26 at the cytosolic N-terminus (Schweppe et al., 2013; Zhou et al., 2013), including the demonstration that xCT serine 26 phosphorylation was decreased by an mTOR kinase inhibitor Ku but not rapamycin in mouse embryonic fibroblasts (Yu et al., 2011). In addition, xCT serine 26 is resided within an mTOR substrate motif defined in part by a proline or glycine at -1 position and a phenylalanine, proline or leucine at the +1 position previously identified by Hsu et al (Hsu et al., 2011). These data raised the possibility that mTORC2 might regulate xCT by phosphorylating serine 26 of xCT's N-terminus cytosolic domain. Serine 26 of xCT is largely conserved across species (Fig. 2-8A) (Hornbeck et al., 2015), suggesting that it may be a biologically important phosphorylation site.

To test the hypothesis that mTORC2 regulates xCT by phosphorylating it on serine 26, we immunoprecipitated the FLAG-tagged xCT protein, and subjected samples to LC/MS-MS analysis after peptide fractionation by hydrophilic interaction chromatography (HILIC). As shown in Fig. 2-8B, xCT phosphorylation on serine 26 was detected in GBM cells. To determine whether serine 26 of xCT is indeed an mTORC2 substrate, we performed an in vitro kinase assay using purified mTORC2 and peptides containing the xCT serine 26 sequence (Fig. 2-8C and 2-

8F). xCT S26 (serine 26) phosphorylation at even higher levels compared to Akt S473 (serine 473), an established mTORC2 substrate (Sarbassov et al., 2005), was detected. Further, the phosphorylation resistant mutant xCT S26A (serine 26 to alanine mutation) was not phosphorylated by mTOR (Fig. 2-8C and 2-8F). In contrast, xCT S26 could not be phosphorylated by SGK1 (Fig. 2-8D and 2-8F), and phosphorylation of xCT S26 by Akt1 was markedly less than that of GSK3β, a known Akt1 substrate (Fig. 2-8E and 2-8F). Importantly, xCT S26A mutant could no longer be phosphorylated upon growth factor stimulation in GBM cells (Fig. 2-8G) and phosphorylation of the S26A xCT did not change in response to Torin1 treatment (Fig. 2-3D). Taken together, these data suggest that mTORC2 phosphorylates xCT on serine 26 in response to EGFR signaling.

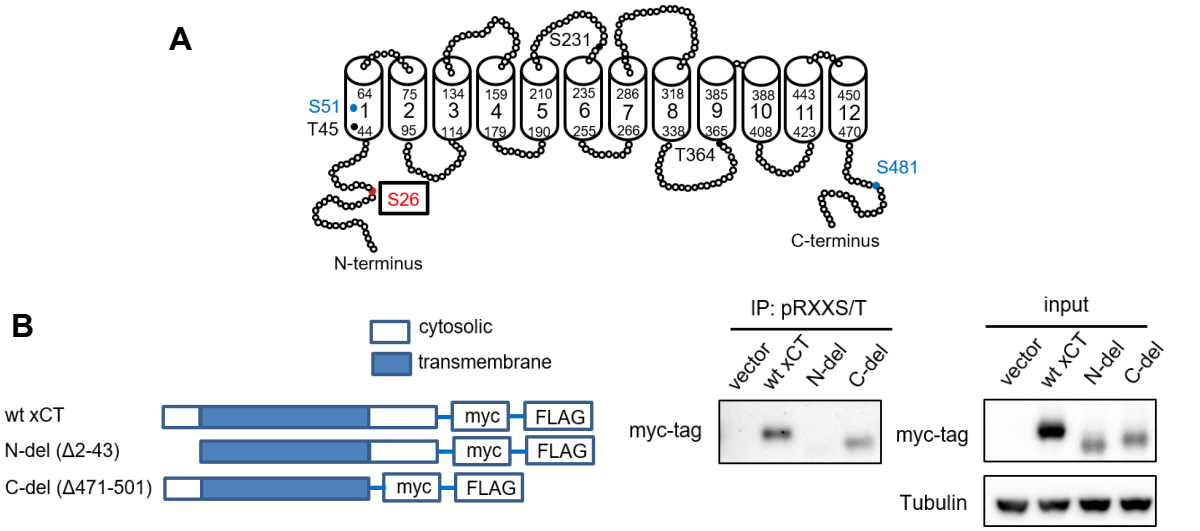

Fig. 2-7. xCT Phosphorylation on RXXS/T Motifs Occurs on the Cytosolic N-terminus.

(A) xCT 2D structure constructed based on sequence and predicted domains of xCT obtained from UniProt-KB. Transmembrane domains were shown as cylinders. Potential phosphorylation sites within RXXS/T motifs were labeled with the same color code as in Fig.2A.

(B) Phosphorylation on RXXS/T motifs in wt xCT and cytosolic N- and C-terminus deletion mutants were analyzed by pRXXS/T IP and western blot.

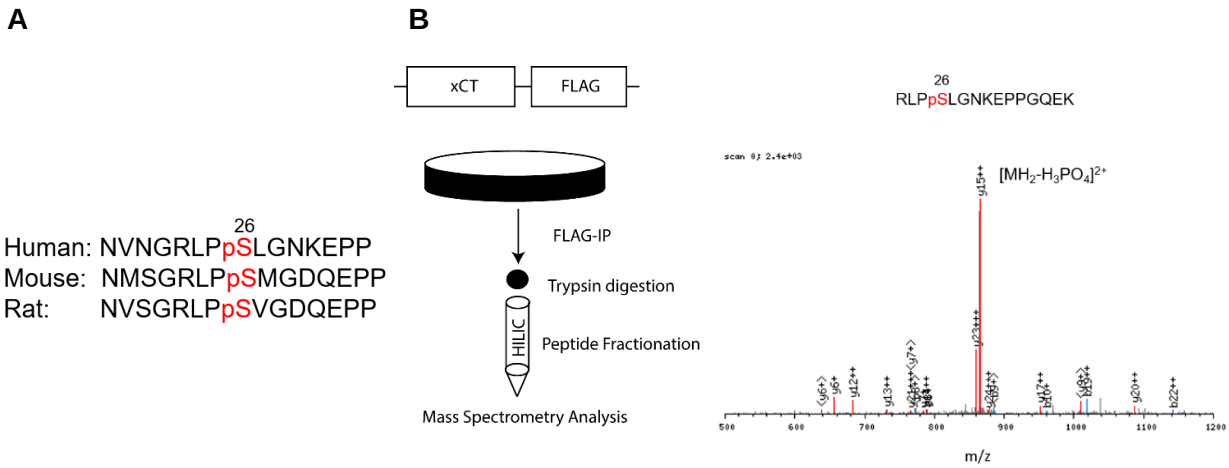

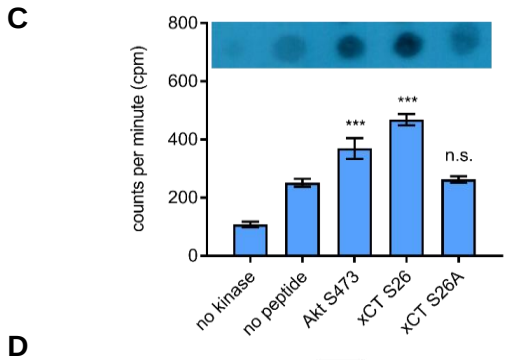

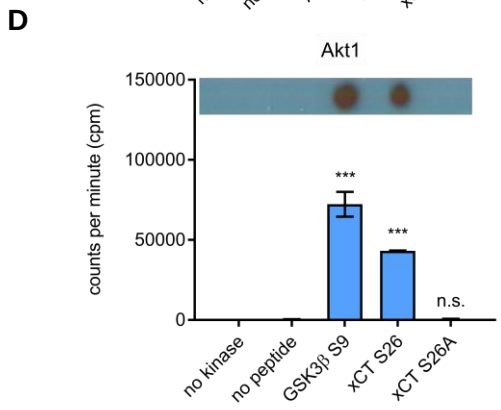

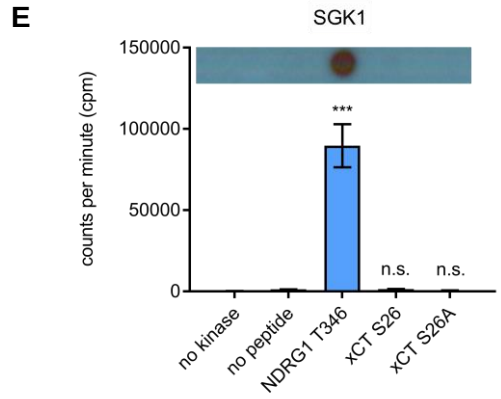

F

Akt S473: GYFPQFSYSASGRRRRR
GSK3β S9: GYGRPRTTSFAGRRRRR
NDRG1 T346: GYTRSRSHTSEGRRRRR
xCT S26: GYGRLPSLGNKGRRRRR
xCT S26A: GYGRLPALGNKGRRRRR

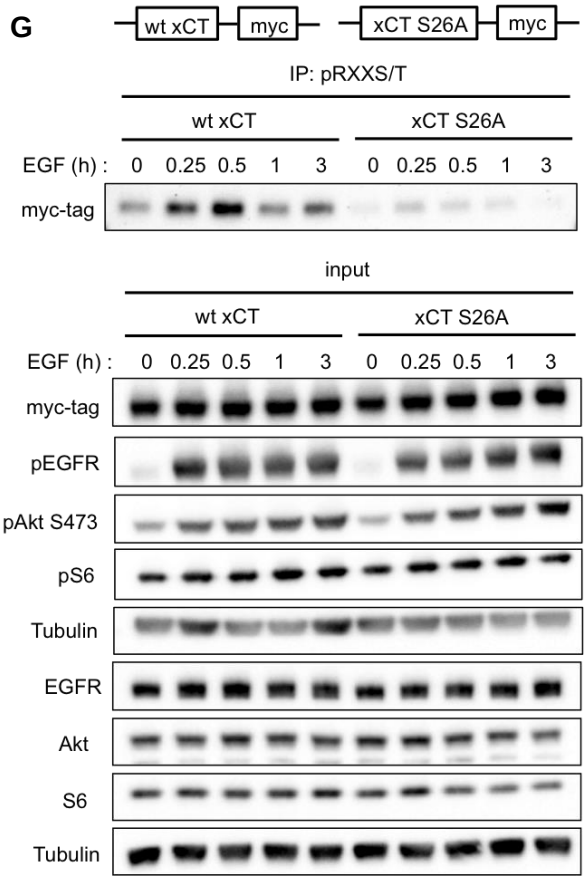

Fig. 2-8. mTORC2 Phosphorylates xCT on Serine 26.

(A) Phosphorylation on xCT serine 26 is conserved across species. (Hornbeck et al., 2015). (http://www.phosphosite.org/uniprotAccAction?id=Q9UPY5.)

(B) LC-MS/MS identified phosphorylation of xCT on serine 26 in U87EGFRvIII cells. A brief schematic of the experiment and the identification of phosphorylated xCT serine 26 peptide was shown.

(C-F) In vitro kinase assay was carried out by incubating IP-purified mTORC2 from HEK293T cells (C), recombinant Akt1 (D), SGK1 (E), and peptides with corresponding substrate sequences (F) and [γ-32P]-ATP. A representative dot plot of autoradiography was shown and radioactivity was quantified as scintillation counts from three independent replicates and presented as mean counts per minute (cpm) ± SEM. Statistical analysis was performed using one-way ANOVA.

(G) IP-western blot detecting wild-type or S26A mutant xCT phosphorylation on RXXS/T motifs upon EGF stimulation.

mTORC2 Fine-tunes xCT Activity through Phosphorylation in Response to Growth Factor and Nutrient

Phosphorylation resistant mutation S26A increases xCT activity

To examine the effect of mTORC2-dependent phosphorylation of serine 26 on xCT function, we measured glutamate secretion using a series of strategic mutants. First, we deleted either the cytosolic N or C terminus of xCT, revealing that both domains were important for xCT function, as measured by glutamate secretion (Fig. 2-9A). Although both N- and C-terminus deletion mutants were still localized on the plasma membrane, the mechanisms by which each domain regulates xCT activity seemed to differ (Fig. 2-9B and C). Deletion of the C-terminus of xCT prevented it from binding to CD98, which is required for xCT recruitment onto the plasma membrane (Bassi et al., 2001). In contrast, the interaction between CD98 and xCT remained intact in the N-terminus deletion mutant, indicating that the cytosolic N-terminus regulates xCT function through alternative mechanisms (Fig. 2-9B and C). This prompted us to test whether serine 26 phosphorylation could be the point of regulation at the N-terminus of xCT.

In the previous Co-IP experiment, we observed that the endogenous xCT could bind to the exogenously overexpressed xCT protein (Fig. 2-4A). Thus, to exclude potential effects of endogenous xCT binding, we obtained xCT knockout MEFs and generated stable cell lines expressing the wild-type xCT, or the phosphorylation resistant mutant S26A. Since the glutamate transport function of xCT is Na^+ independent and requires the presence of extracellular cystine, we measured glutamate secretion in xCT KO MEF cell lines in a Na^+ free PBS buffer system (Kobayashi et al., 2015), and compared glutamate secretion in the absence or presence of cystine as well as the xCT inhibitor sulfasalazine (SAS) (Gout et al., 2001) to exclude possible glutamate

efflux through other transporters. The phosphorylation resistant mutant S26A significantly increased glutamate secretion (Fig. 2-9D and E). Together, these data suggest that xCT activity is increased when mTORC2 mediated phosphorylation on serine 26 is ablated.

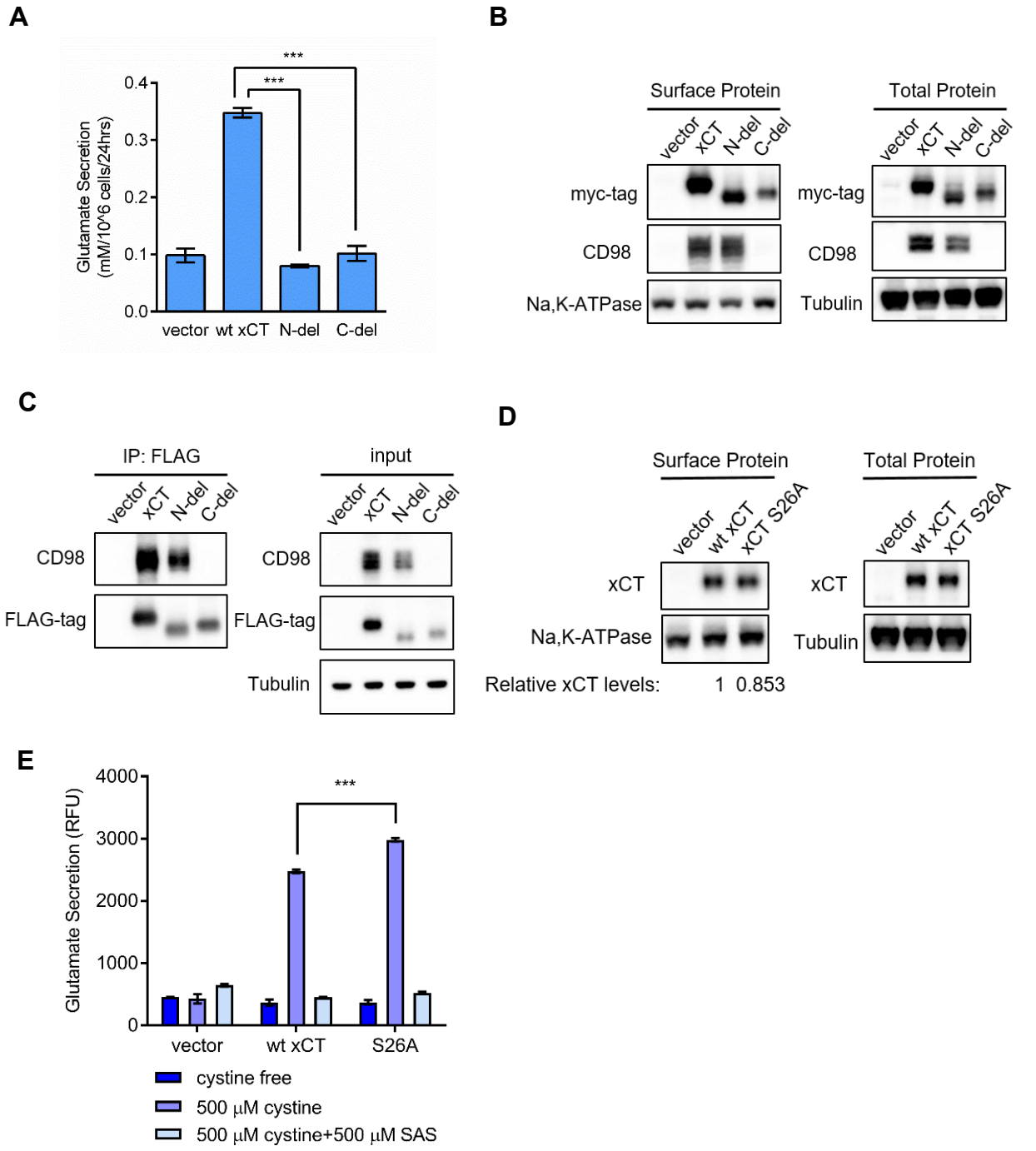

Fig. 2-9. Phosphorylation-resistant Mutation on xCT serine 26 Increased xCT Activity.

(A) Glutamate secretion was measured and in U87EGFRvIII cells stably overexpressing vector, wt xCT or N-del and C-del mutant xCT. Statistical analysis was performed using one-way ANOVA.

(B) Cell surface and total protein levels of wt xCT and N-del and C-del mutant xCT were analyzed by western blotting.

(C) Co-IP-western blot to detect binding of wt xCT or N-del and C-del mutant xCT with CD98.

(D) Cell surface and total protein levels of xCT were analyzed by western blotting in xCT KO MEFs stably overexpressing vector control, wt xCT and xCT S26A. Band intensities were quantified by densitometry and relative surface xCT levels was calculated, and normalized to Na,K-ATPase as loading control of cell surface proteins.

(E) xCT activity assay was perfomed in xCT KO MEFs stably overexpressing vector control, wt xCT and xCT S26A. Glutamate secretion was measured using the AmplexRed glutamate assay kit, calculated and normalized to cell counts and cell surface xCT protein levels. Statistical analysis was performed using one-way ANOVA.

mTORC2 inhibition increases xCT activity

Having shown that ablation of the mTORC2-mediated phosphorylation on serine 26 increases xCT activity, we hypothesized that inhibition of mTORC2 should also result in increased xCT activity. Inhibition of mTORC2 by two different Rictor shRNAs significantly increased glutamate secretion through xCT (Fig. 2-10A and B), which is consistent with decreased xCT phosphorylation (Fig. 2-10C). On the other hand, overexpression of Rictor activated mTORC2 and significantly decreased glutamate secretion in U87 cells (Fig. 2-10D), albeit the decrease was not as dramatic since basal mTORC2 activity is already high in U87 cells due to PTEN deletion. Treatment with Torin1 phenocopied Rictor knockdown, and significantly increased xCT-specific cystine uptake and glutamate secretion in multiple GBM cell lines, patient-derived neurosphere lines, as well as in triple negative breast cancer and lung cancer cell lines - which have high levels of xCT and mTORC2 activity (Fig. 2-10 E, F and Fig. 2-11) (Briggs et al., 2016; Masui et al., 2013). siRNA knockdown of xCT prevented the increase in glutamate secretion upon inhibition of mTORC2, demonstrating xCT specifically mediated the increased glutamate secretion (Fig. 2-10A, E and Fig. 2-11B). In addition, glucose deprivation has previously been shown to inhibit mTORC2 by depleting cellular acetyl-CoA pool, which is required for acetylation of Rictor and sustained activation of mTORC2 upon growth factor stimulation (Masui et al., 2015b). Therefore we tested whether glucose deprivation could also result in decreased xCT phosphorylation and increased xCT activity. As we expected, depletion of glucose in GBM cells significantly inhibited mTORC2 activity, xCT phosphorylation on RXXS/T motifs and increased glutamate secretion upon growth factor stimulation, which could be partially rescued by acetate (Fig. 2-12). These results demonstrate that genetic inhibition of mTORC2 or pharmacological inhibition of mTOR kinase, as well as glucose-deprivation induced

mTORC2 inhibition all increase xCT activity potentially through suppression of xCT phosphorylation on serine 26.

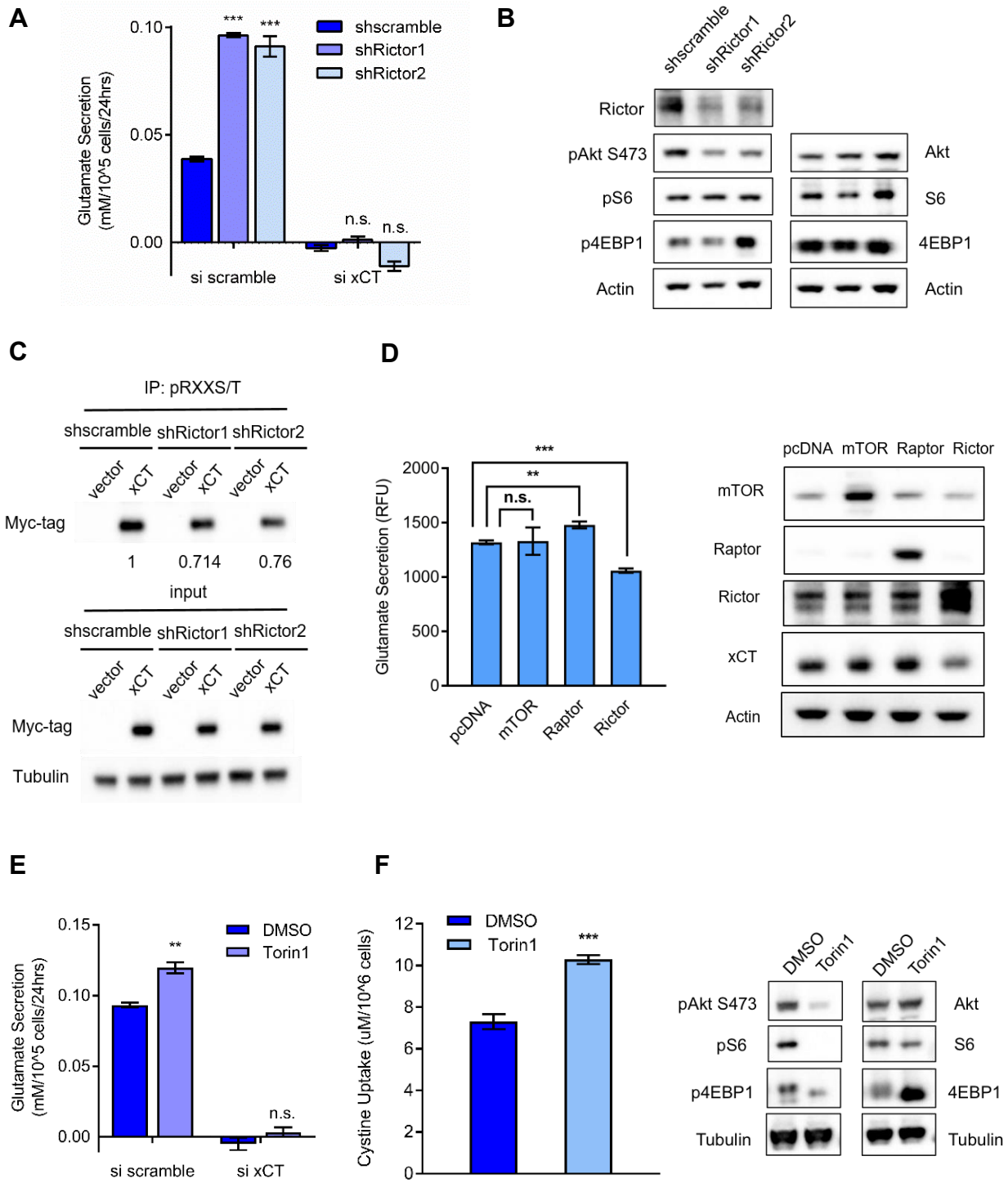

Fig. 2-10. mTORC2 Inhibition Increases xCT-dependent Glutamate Secretion and Cystine Uptake in U87EGFRvIII Cells.

(A-B) Glutamate secretion was measured by NOVA Bioprofile 400 analyzer in U87EGFRvIII cells with stable Rictor knockdown using two different shRNAs and after 72h of transfection with an xCT or scramble control siRNA. Statistical analysis was performed using two-way ANOVA. Western blot was performed to confirm knockdown of Rictor and suppression of downstream signaling pathways.

(C) Immunoprecipitation (IP) - western blot was performed in U87EGFRvIII with stable Rictor knockdown using two different shRNAs and stable overexpression of either vector control and wt xCT to detect xCT phosphorylation on RXXS/T motifs. Band intensity was quantified using ImageLab^{TM} Software.

(D) Glutamate secretion was measured using the AmplexRed glutamate assay kit in U87 cells 48h after transfection to transiently overexpress mTOR, Raptor and Rictor. Statistical analysis was performed using two-way ANOVA comparing the mean of mTOR, Raptor and Rictor to vector control. Western blot was performed to confirm overexpression.

(E) Cystine uptake was measured in U87EGFRvIII cells after treatment with 250 nM Torin1 for 24 h using a sodium cyanide and sodium nitroprusside based assay (Egea et al., 2015; Nakagawa and Coe, 1999). Results were obtained from seven replicates and data are presented as mean ± SEM.

(F) Glutamate secretion after 72h of transfection with an xCT or scramble control siRNA and 24 h of Torin1 treatment was measured in U87EGFRvIII cells using NOVA Bioprofile 400 analyzer. Inhibition of mTOR and downstream signaling pathways by Torin1 was confirmed by western blot.

A

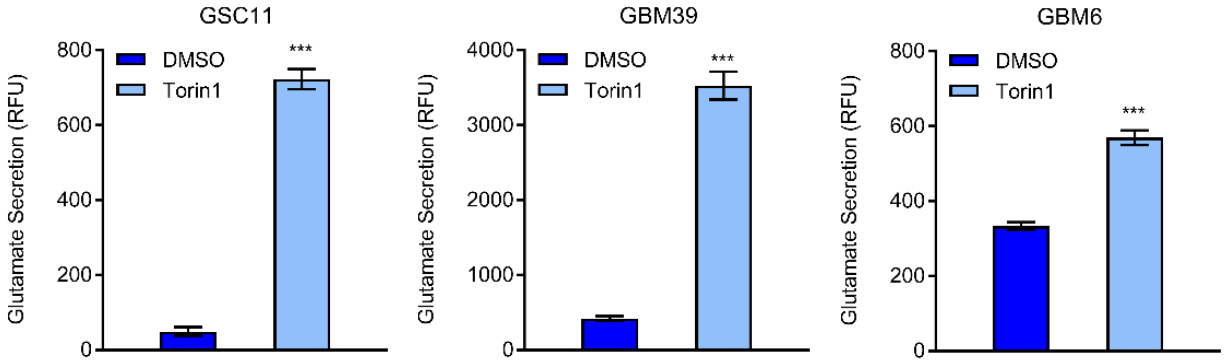
GSC11
GBM39
GBM6
Glutamate Secretion (RFU)
DMSO
Torin1
***
800
600
400
200
0
4000
3000
2000
1000

B

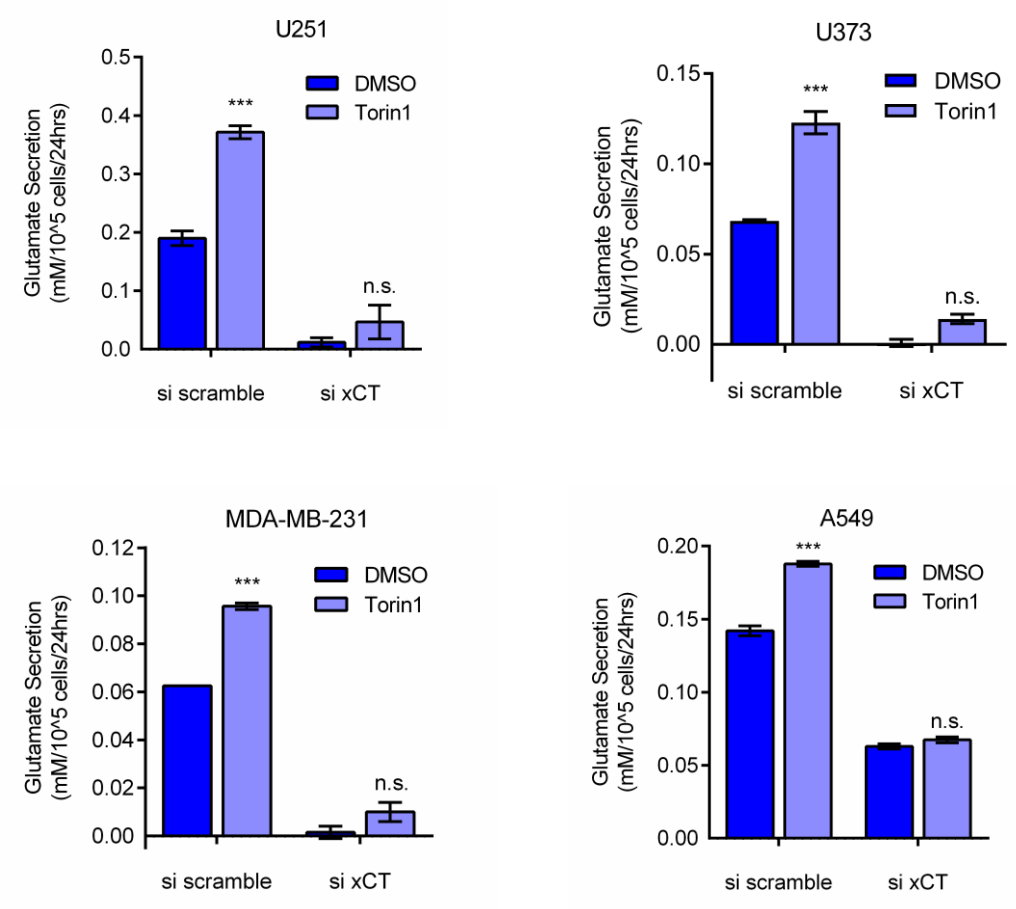
U251
U373
MDA-MB-231
A549
Glutamate Secretion (mM/10^5 cells/24hrs)
DMSO
Torin1
***
n.s.
si scramble
si xCT
0.5
0.4
0.3
0.2
0.1
0.0
0.15
0.10
0.05
0.00
0.12
0.08
0.06
0.04
0.02
0.20

Fig. 2-11. mTORC2 Inhibition Increases xCT-dependent Glutamate Secretion in GBM Patient-derived Neurosphere Lines, Triple-negative Breast Cancer and Lung Cancer Cell Lines.

(A) Glutamate secretion after 24 h of Torin1 treatment in patient-derived neurosphere lines were measured using the AmplexRed glutamate assay kit.

(B) The specificity of increased glutamate secretion through xCT upon Torin1 treatment in different cell lines was confirmed by xCT knockdown. Glutamate secretion was measured using NOVA Bioprofile 400 analyzer after 24 h of Torin1 treatment and 72h of transfection with an xCT or scramble control siRNA. Statistical analysis was performed using two-way ANOVA comparing the mean of Torin1 to DMSO control.

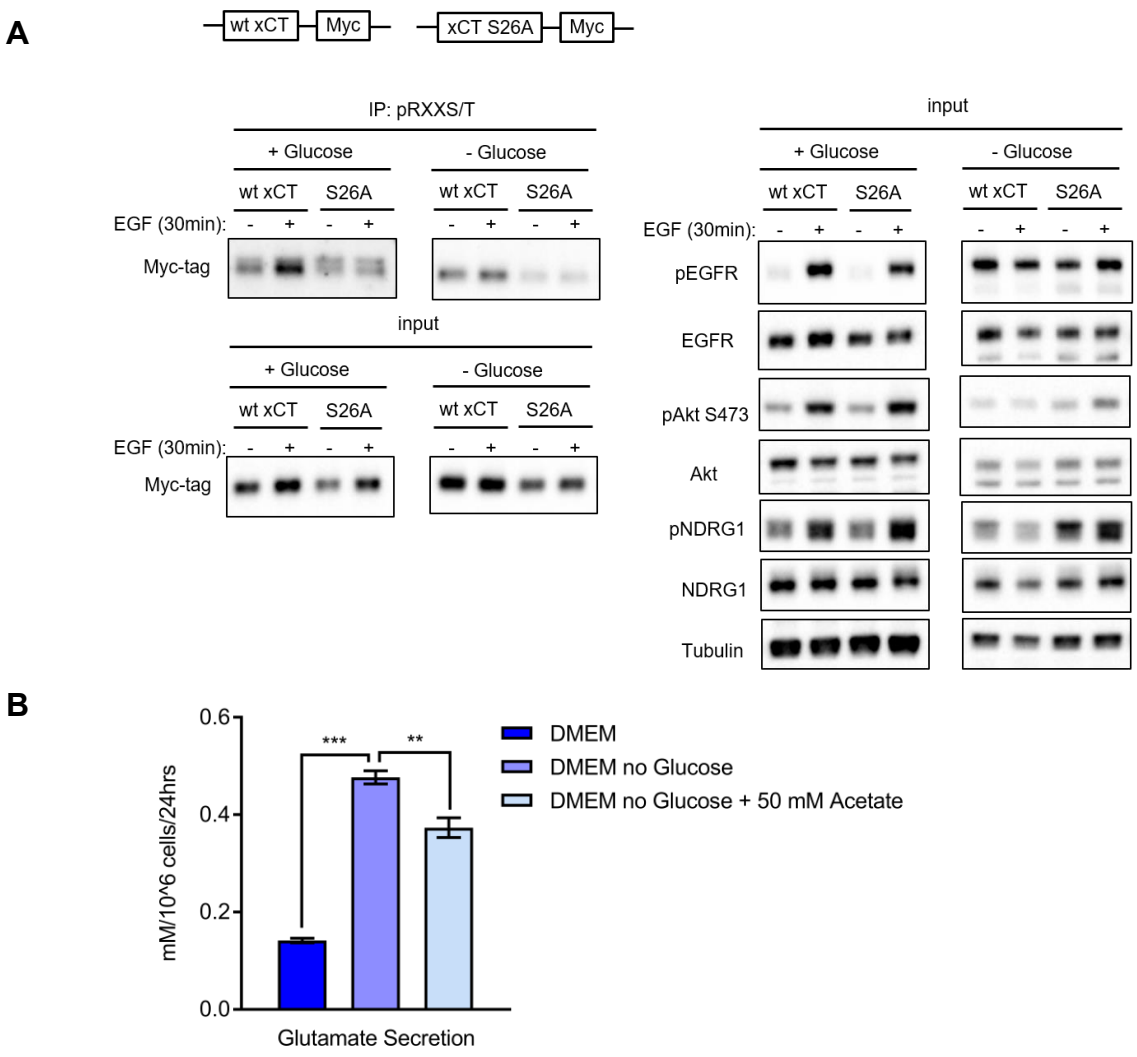

Fig. 2-12. Glucose Depletion Inhibited mTORC2-mediated xCT Phosphorylation on Serine 26 and Increased Glutamate Secretion in GBM Cells.

(A) U87 cells expressing wt EGFR were starved in glucose/pyruvate free DMEM media for 24 h before cells were stimulated with 25 ng/ml EGF for 30 min and cell lysates were collected and subjected to IP and western blotting to detect xCT phosphorylation on RXXS/T motifs.

(B) Glutamate secretion was measured using NOVA Bioprofile 400 analyzer after incubating U87vIII cells in DMEM (4.5 g/l glucose), glucose / pyruvate free DMEM, or glucose / pyruvate free DMEM with 50 mM acetate for 24 h. Statistical analysis was performed using one-way ANOVA.

DISCUSSION

By using an unbiased proteomic screen for xCT binding partners, followed by functional validation, we have made the surprising discovery that mTORC2 reprograms amino acid metabolism in tumor cells by phosphorylating serine 26 of the cystine-glutamate antiporter xCT on its cytosolic N-terminus to suppress glutamate secretion. Aberrant growth factor receptor signaling and or c-MYC activation increase glutamine uptake, converting it to glutamate to provide tumor cells with a carbon source for TCA anaplerosis as well as a nitrogen source for protein and nucleotide synthesis (Altman et al., 2016; DeBerardinis et al., 2007; Masui et al., 2015a). Thus, when microenvironmental nutrient levels are sufficient to support tumor cell proliferation, it would be disadvantageous for cancer cells to secrete glutamate. The mechanism identified here ensures that glutamine-derived glutamate can be used primarily for tumor growth when extracellular nutrient levels can support it. However, when nutrients become scarce, tumor cells increase xCT-dependent cystine uptake at the expense of glutamate efflux, possibly to enable tumor cells to buffer cellular redox stress by synthesizing glutathione from xCT-derived cystine. Therefore, the mechanism described here enables tumor cells to adapt to changing nutrient levels, linking proliferative signals to environmental conditions. It is interesting to note that mTORC2 requires either glucose or acetate derived acetyl-CoA to stay active and phosphorylate its downstream substrates (Masui et al., 2015b), raising the possibility that under nutrient poor conditions, lower mTORC2 signaling could tilt the balance from proliferation to survival, as we also discovered that glucose deprivation induced mTORC2 inhibition drives xCT-mediated glutamate efflux and cystine uptake, providing substrates for glutathione synthesis to protect tumor cells from cellular stress.

High xCT levels are associated with poor outcome in a number of cancer types, including glioblastoma (Robert et al., 2015) and triple negative breast cancer (Timmerman et al., 2013). The mTORC2-dependent mechanism reported here, in addition to a recently described paracrine mechanism of xCT reported by by Briggs and colleagues (Briggs et al., 2016), suggests that regulation of xCT function by post-translational modification may be critical for its tumor promoting effects. In triple negative breast cancer cells, high extracellular glutamate levels were demonstrated to suppress xCT function, depleting tumor cells of intracellular cysteine. Intracellular cysteine depletion was shown to cause oxidation of specific cysteine residues of the prolyl hydroxylase EglN1, thereby suppressing EglN1-dependent HIF1α degradation, thus elevating intra-tumoral HIF1α levels to drive tumor growth (Briggs et al., 2016). Our results provided a complementary mechanism of xCT post-translational inhibitory modification as a direct molecular link between pro-proliferative growth factor signaling with metabolic adaptation that favors anapleurotic flux through phosphorylation of xCT on serine 26. Future studies will be needed to determine whether there is any cooperation between these complementary post-translational regulatory mechanisms.

xCT is a 12 pass transmembrane protein that has two serine residues preceded by an arginine at the -3 position (RXXS/T) , S26, S51 on its N-terminus that may serve as consensus phosphorylation sites for mTORC2. Unlike S51, which lies in the transmembrane domain, S26 is predicted to reside on the cytoplasmic face of the membrane, where it could be engaged by mTORC2 (Gasol et al., 2004; UniProt, 2015). Interestingly, in a SILAC-based mass spectrometric screen of TSC null MEFs to identify mTOR regulated proteins which identified Grb10 as an mTORC1 substrate, Yu and colleagues identified serine 26 of xCT as a site whose

phosphorylation is inhibited by the mTOR kinase inhibitor Ku-0062794, but not by rapamycin (Yu et al., 2011), consistent with our finding that xCT serine 26 is an mTORC2 substrate. mTORC2 is thought to promote its biological activity by phosphorylating AGC kinases AKT, PKC and SGK1 which in turn phosphorylate other substrates (Laplante and Sabatini, 2009, 2012). It is interesting to note that we found no evidence of these other AGC kinases either by SILAC-Mass Spectrometry, or in the Co-IP studies, suggesting that mTORC2 may regulate xCT serine 26 phosphorylation directly.

The diversity of metabolic adaptations employed by cancer cells in response to rapidly changing conditions, contributes to their biological aggressiveness and therapeutic resistance by enabling them to proliferate when nutrients are plentiful and to shift their resources to survival when nutrients are scarce (Palm et al., 2015). The results presented here demonstrate that mTORC2 controls cystine uptake and glutamate secretion by directly phosphorylating xCT, thus linking altered growth factor receptor signaling with amino acid metabolism and ROS buffering in cancer.

EXPERIMENTAL PROCEDURES

Cell Culture

Human cancer cell lines (U87, U251, T98G, U373, Hs578T, MDA-MB-231, A549) were purchased from ATCC. xCT KO MEFs were a kind gift from Dr. Hideyo Sato, Yamagata University, Japan (Kobayashi et al., 2015). U87wtEGFR and U87EGFRvIII isogenic cell lines were established as described previously (Wang et al., 2006). All the above listed cells were cultured in DMEM (CORNING, 10-013) supplemented with 10% FBS (Omega Scientific) in a humidified incubator with 5% CO2 at 37 °C. Glucose depletion experiments were performed using glucose / pyruvate free DMEM (ThermoFisher Scientific, 11966025) without serum. xCT KO MEFs were additionally supplemented with 50uM β-mercaptoethanol (Gibico, 31350010). GBM39, GBM6 and GSC11 patient-derived neurosphere lines were cultured in NeuroCult medium (STEMCELL Technologies, 05751) supplemented with epidermal growth factor (Sigma, E9644), fibroblast growth factor (Sigma, F0291), and heparin (Sigma, H3149).

Antibodies and Reagents

Antibodies used include: anti-FLAG®M2 (Sigma, F3165), mTOR (Cell Signaling, 2972), Raptor (Cell Signaling, 2280), Rictor (Cell Signaling, 9476), Actin (Sigma, A4700), Myc-tag (Cell Signaling, 2276), EGFR (Millipore, 06-874), pEGFR-Y1068 (Cell Signaling, 3777), Akt (Cell Signaling, 9272), pAkt-S473 (Cell Signaling, 4060), NDRG1 (Cell Signaling, 9485), pNDRG1-T346 (Cell Signaling, 5482), S6 (Cell Signaling, 2317), pS6-S235/236 (Cell Signaling, 4858), 4EBP1 (Cell Signaling, 9644), p4EBP1-T37/46 (Cell Signaling, 2855), Tubulin (Sigma, T6074), xCT/SLC7A11 (Cell Signaling, 13691), 4F2hc/CD98 (Cell Signaling, 13180), PKCα (Cell

Signaling, 2056), pPKCα-S657 (Santa Cruz, sc12356), SGK1 (Cell Signaling, 12103), anti-rabbit IgG (Cell Signaling, 7074), anti-mouse IgG (Cell Signaling, 7076).

Reagents and drugs used include: FLAG® peptide (Sigma, F3290), anti-FLAG®M2 affinity gel (Sigma, A2220), phospho-Akt substrate (RXXS*/T*) magnetic bead conjugate (Cell Signaling, 8050), Sulfasalazine (SAS, Sigma, S0883), Torin1 (Tocris Bioscience, 4247), Rapamycin (Sigma, R0395), MK2206, Sanofi SGK1-selective inhibitor and Sotrastaurin were kindly provided by SMD lab in LICR San Diego.

SILAC Labeling and Mass Spectrometry Analysis

U87EGFRvIII cells stably expressing the vector control or FLAG-xCT were cultured in SILAC media (Thermo Scientific) that lack lysine and arginine and supplemented with 10% dialyzed FBS (Gibico). 12C6-L-arginine and 12C6-L-lysine (Sigma) were supplemented to the vector control cells and 13C6-L-arginine and 13C6-L-lysine (Cambridge Isotope Laboratories) were supplemented to the FLAG-xCT cells. Cells were passaged at least five times to ensure complete labeling (Ong and Mann, 2006). SILAC labelled cells were lysed in Pierce IP lysis buffer (Thermo Scientific) supplemented with 100x Halt Protease and Phosphatase cocktail (Thermo Scientific). Protein lysates were cleared by centrifugation and incubated with anti-FLAG M2 affinity gel (Sigma) overnight at 4 °C. FLAG-xCT and its binding proteins were eluted with 0.1 M glycine, pH 2.5 at room temperature with rotation for 2 min and then neutralized with 1 M Tris-HCl, pH 7.8. The eluted proteins were then reduced, alkylated and digested with 1 µg of trypsin. Digested peptides were desalted using a 50mg Sep-Pak C18 cartridge, fractionated on a TSKgel Amide-80 (1.0-mm inner diameter) column (TOSOH Bioscience), and analyzed by an Orbitrap-LTQ mass spectrometer as previously described (Albuquerque CP MCP 2008). MS

data were searched on Sorcerer-SEQUEST using the reviewed Swiss-prot human database. The identified peptides were quantified using XPRESS and a minimal ion intensity of 1.0E3 was used to calculate the abundance ratio. At least three unique peptides were required for a protein or a protein complex to be identified as xCT binding protein, and the median abundance ratio for each identified protein was calculated and plotted.

Gene Ontology (GO) Analysis

The enrichment of GO terms (http://www.geneontology.org/) of xCT physically interacted proteins were calculated by Fisher's exact test using the DAVID software (https://david.ncifcrf.gov/home.jsp). A Benjamini-Hochberg-corrected false discovery rate (FDR) ≤ 0.05 was used to determine the enriched functions.

Western Blotting

Cultured cells were lysed with RIPA lysis buffer containing 50 mM Tris-HCl, 150 mM NaCl, 1% NP-40, 0.5% sodium deoxycholate, and 0.1% SDS (Boston BioProducts, BP-115), and supplemented with protease and phosphatase inhibitor cocktail (ThermoFisher Scientific, 78842). Protein concentration of each sample was determined with Bradford Assay using the Protein Assay Dye Reagent Concentrate (Bio-Rad, 5000006). Equal amounts of protein extracts were mixed with 4 x Laemmli sample buffer (Bio-Rad, 161-0747) and separated by electrophoresis on 4-12% NuPAGE Bis-Tris Mini Gel (Invitrogen, NP0336), and then transferred using the Trans-Blot® Turbo™ Transfer System (Bio-Rad) onto nitrocellulose membranes (Bio-Rad, 1704159). Membranes were blocked with 5% bovine serum albumin (BSA) and incubated with corresponding primary antibodies and horseradish peroxidase-conjugated secondary antibodies.

The immunoreactivity was detected with SuperSignal™ West Pico Chemiluminescent Substrate (ThermoFisher Scientific, 34080) or SuperSignal™ West Femto maximum Sensitivity Substrate (ThermoFisher Scientific, 34096). Signals were captured and analyzed using the Bio-Rad ChemiDoc™ MP Imaging system and the Image Lab™ Software (Bio-Rad).

Co-immunoprecipitation (Co-IP) and Immunoprecipitation (IP)

Cells were lysed with IP lysis buffer containing 25 mM Tris-HCl pH 7.4, 150 mM NaCl, 1% NP-40, 1 mM EDTA, 5% glycerol (ThermoFisher Scientific, 87787), and supplemented with protease and phosphatase inhibitor cocktail (ThermoFisher Scientific, 78842). Protein concentrations were determined for each sample and equal amounts of protein lysates were incubated with antibody-conjugated beads as indicated at 4 °C overnight with end-to-end rotation. Protein-bound beads were then washed 3-4 times with wash buffer according to manufacturer's instructions provided for different beads used in the experiment. Proteins were then eluted with 3 x FLAG peptide for Co-IP with the anti-FLAG®M2 affinity gel; or with 0.1 M glycine, pH2.5 at room temperature with rotation for 2 min and then neutralized with 1 M Tris-HCl, pH7.8 for all the other Co-IP and IP experiments. Both input and eluate samples were analyzed by SDS-PAGE and immunoblotting.

DNA Constructs and Generation of xCT mutants

FLAG-mTOR (Cat. No. 26603), myc-Rictor (Cat. No.11367), HA-Raptor DNA (Cat. No. 8513) plasmids were obtained from Addgene. Lentiviral shRNA plasmids shcramble, shRictor1 and shRictor2 were obtained from Addgene. myc-FLAG-tagged xCT plasmid were obtained from Origene (RC204136) and the myc-FLAG-tagged xCT ORF was cloned into the lentiviral

expression vector pLVX-Puro (Clontech, 632164). The xCT point mutants S26A, S26D were generated using the QuikChange Multi Site-Directed Mutagenesis Kit (Agilent, 200514). The xCT N- and C-terminus deletion mutants were generated by PCR.

DNA plasmid, siRNA, shRNA transfection and generation of stable cell lines

Transfection of DNA plasmids were performed using X-tremeGENE HP (Roche, 06366236001) in DMEM supplemented with 10% FBS. Media were changed after 24 h of transfection and cells were harvested 48 h post-transfection for transient overexpression experiments. Transfection of siRNA into cells were performed using Lipofectamine® RNAiMAX Transfection Reagent (ThermoFisher Scientific, 13778150) in DMEM supplemented with 10% FBS. Media were changed after 24 h of transfection and cells were harvested 48 h post-transfection or with an additional 24 h of drug treatment. siRNA for Rictor was obtained from ThermoSCIENTIFIC (L-016984-00-0005), and siRNA for xCT was customed synthesized by ThermoSCIENTIFIC with the sequence: Sense: 5'-AGAAAUCUGGAGGUCAUUAdTdT-3', Antisense: 5'-UAAUGACCUCCAGAUUUCUdTdT-3'. Generation of stable cell lines was performed using the lentiviral delivering system. Lentivirus was packaged using 293T cells by co-transfecting cells with lentiviral packaging plasmid and DNA constructs containing gene of interest. Virus were collected and used to infect GBM cells in the presence of 12.5 μg/ml Polybrene Infection / Transfection Reagent (EMD Millipore, TR-1003-G). Media were changed after 24 h and cells were selected for one week before used for experiments and maintained cultured with 1 μg/ml puromycin.

Real-Time PCR (RT-PCR)

Total RNA was extracted using the RNeasy Mini Kit (Qiagen, 74106). RNA concentrations were measured and 1 µg of RNA was used from each sample for cDNA synthesis using the SuperScript® VILO™ cDNA Synthesis Kit (ThermoFisher Scientific, 11754050). RT-PCR was performed using the 2 x SYBR Green qPCR Master Mix (Bimake, B21202) on the CFX96 Real-Time PCR Detection System (Bio-Rad) following the manufacturer's instructions. Results were analyzed using the delta delta Ct method and TPB was used as the reference gene. Primer sequences used are:

xCT forward: 5'-CAGGAGAAAGTGCAGCTGAA-3',

xCT reverse: 5'-CTCCAATGATGGTGCCAATG-3',

TBP forward: 5'-GAGCTGTGATGTGAAGTTTCC-3'

TBP reverse: 5'-TCTGGGTTTGATCATTCTGTAG-3'.

Protein Sequence Analysis

Human xCT protein sequence was downloaded from UniProtKB with the accession number Q9UPY5. The complete sequence was scanned through for serine/threonine residues proceeded with arginine at the -3 position, hence the RXXS/T motif. xCT 2D structure was constructed based on the sequence analysis and predicted topology information available on UniProtKB (UniProt, 2015).

In Vitro Kinase Assay

mTORC2 was purified by IP from HEK293T cells transiently overexpressing FLAG-Rictor using anti-FLAG®M2 affinity gel. Recombinant Akt1 (#A16-10G) and SGK1 (#S06-10G) were

purchased from SignalChem. Biotinylated Peptide substrates [GYXXXX(S/A)XXXXGRRRRR] were synthesized and purchased from EZBiolab. Peptide phosphorylation by mTOR kinase was determined by incubating 0.1 mM peptide with kinase in reaction buffer (25 mM HEPES pH 7.4, 50 mM KCl, 10 mM $MgCl_2$) with 50 μM cold ATP and 5 μCi [γ-^{32}P]ATP for 1 h at room temperature and terminated with 0.5 volume of 7.5 M guanidine hydrochloride. Each reaction was performed in triplicates and 5 μl of reaction mix was spotted onto SAM$^{2®}$ Biotin Capture Membrane (Promega, V2861). Membranes were washed and dried according to manufacturer's instructions. Radioactivity was determined by autoradiography and quantified by scintillation counting.

Glutamate Secretion Assays

Glutamate secretion from cells were measured using a Nova BioProfile Basic Analyzer (Nova Biomedical), or with the Amplex® Red Glutamic Acid/Glutamate Oxidase Kit (ThermoFisher Scientific, A12221). Briefly cells were seeded in triplicates in 6-well plates at optimal density, and 24 h before measurement cells were washed three times with 1 x PBS and changed to 1 ml fresh DMEM media supplemented with 5% dialyzed FBS (Gibico), including three wells without cells as blank control. After incubation media were collected from each well and analyzed according to manufacturer's instructions. Cell numbers were determined using the TC20^{TM} Automated Cell Counter (Bio-Rad). Glutamate secretion was calculated by subtracting the levels of glutamate in the blank control and normalized to cell counts for each sample.

xCT activity assay

Glutamate secretion in xCT KO MEF cell lines were measured using a Na+ free PBS buffer system to exclude other glutamate transporter activity as reported (Kobayashi et al., 2015). Briefly, cells were seeded in 6-well plates at optimal density, washed three times with prewarmed Na+ free PBS buffer (137 mM choline chloride, 3 mM KCl, 0.01% CaCl2, 0.01% MgCl2 and 0.1% glucose, pH 7.4) and incubated in 1 ml same Na+ free PBS buffer without cystine, with 500 µM cystine, or with 500 µM cystine and 500 µM SAS at 37 °C for 1 h. After incubation, supernatants were collected from each well and analyzed using the Amplex® Red Glutamic Acid/Glutamate Oxidase Kit. Glutamate secretion was calculated by subtracting the blank control, normalized to cell counts as well as cell surface xCT levels for each sample.

Cell Surface Protein Purification

Cell Surface proteins were purified using the Pierce™ Cell Surface Protein Isolation Kit (ThermoFisher Scientific, 89881) according to manufacturer's instructions. Briefly, cells were washed with cold PBS and incubated with Sulfo-NHS-SS-Biotin at 4°C for 30min to label cell surface proteins. After labeling the reaction was quenched and cells were collected and lysed. Protein concentrations of lysates were determined using Bradford assay and equal amount of proteins from each sample were incubated with NeutrAvidin Agarose gels at 4 °C overnight to purify labeled cell surface proteins. After incubation proteins were eluted and subject to electrophoresis and immunoblotting analysis.

Cystine Uptake Assay

Sodium-independent cystine uptake through xCT was measure using a sodium nitroprusside based assay as described previously (Nakagawa and Coe, 1999). Briefly, cells were seeded at optimal confluency in 6-well plates and treated with drugs as indicated in the paper. After drug treatment, cells were first washed three times with 1 x PBS at room temperature, and pre-incubated in 1 ml cystine uptake buffer (122 mM choline chloride,1.8 mM KCl,1.3 mM $CaCl_2$,1.2 mM potassium phosphate,25 mM Triethylammonium bicarbonate,10 mM glucose, 0.4 mM $MgSO_4$, pH7.4) for 15 min before 1 µM L-cystine (MP BIOMEDICALS, 02194946) was added and further incubated for 1 h at 37 °C. 500 µl uptake buffer was collected from each well and centrifuged at 14,000 x rpm for 2 min. 400 µl of the supernatant was added to cuvettes containing 300 µl 10% NaCN, 100 µl ddH2O and 1 ml 150 mM choline chloride, pipetted to mix and incubated at room temperature for 20 min. Then 100 µl of 20% sodium nitroprusside solution was added to the cuvette, mixed and absorbance was read at 521 nm using a NanoDrop 2000c Spectrometer immediately within 1 min. Cystine concentrations was calculated using a standard curve and cystine uptake was calculated by subtracting from blank controls without cells and normalized to cell counts from each well.

Statistical Analysis

Data were all collected from at least three independent replicates and presented as mean ± SEM unless otherwise indicated. Statistical analysis was performed using unpaired Student's t test unless otherwise indicated. Statistical significance was indicated as * $p < 0.05$, ** $p < 0.01$, *** $p < 0.001$, and n.s. as not statistically significant.

Growth Factor Signaling Reprograms Glucose and Lipid Metabolism in GBM

See Appendix I

REFERENCES

Alessi, D.R., Caudwell, F.B., Andjelkovic, M., Hemmings, B.A., and Cohen, P. (1996). Molecular basis for the substrate specificity of protein kinase B; comparison with MAPKAP kinase-1 and p70 S6 kinase. FEBS letters *399*, 333-338.

Altman, B.J., Stine, Z.E., and Dang, C.V. (2016). From Krebs to clinic: glutamine metabolism to cancer therapy. Nature reviews Cancer *16*, 619-634.

Aramburu, J., Ortells, M.C., Tejedor, S., Buxade, M., and Lopez-Rodriguez, C. (2014). Transcriptional regulation of the stress response by mTOR. Science signaling *7*, re2.

Bassi, M.T., Gasol, E., Manzoni, M., Pineda, M., Riboni, M., Martin, R., Zorzano, A., Borsani, G., and Palacin, M. (2001). Identification and characterisation of human xCT that co-expresses, with 4F2 heavy chain, the amino acid transport activity system xc. Pflugers Archiv : European journal of physiology *442*, 286-296.

Bhutia, Y.D., Babu, E., Ramachandran, S., and Ganapathy, V. (2015). Amino Acid transporters in cancer and their relevance to "glutamine addiction": novel targets for the design of a new class of anticancer drugs. Cancer research *75*, 1782-1788.

Briggs, K.J., Koivunen, P., Cao, S., Backus, K.M., Olenchock, B.A., Patel, H., Zhang, Q., Signoretti, S., Gerfen, G.J., Richardson, A.L., *et al.* (2016). Paracrine Induction of HIF by Glutamate in Breast Cancer: EglN1 Senses Cysteine. Cell *166*, 126-139.

Chung, W.J., Lyons, S.A., Nelson, G.M., Hamza, H., Gladson, C.L., Gillespie, G.Y., and Sontheimer, H. (2005). Inhibition of cystine uptake disrupts the growth of primary brain tumors. The Journal of neuroscience : the official journal of the Society for Neuroscience *25*, 7101-7110.

Commisso, C., Davidson, S.M., Soydaner-Azeloglu, R.G., Parker, S.J., Kamphorst, J.J., Hackett, S., Grabocka, E., Nofal, M., Drebin, J.A., Thompson, C.B., *et al.* (2013). Macropinocytosis of protein is an amino acid supply route in Ras-transformed cells. Nature *497*, 633-637.

Conrad, M., and Sato, H. (2012). The oxidative stress-inducible cystine/glutamate antiporter, system x (c) (-) : cystine supplier and beyond. Amino acids *42*, 231-246.

Dang, C.V. (2012). MYC on the path to cancer. Cell *149*, 22-35.

DeBerardinis, R.J., Lum, J.J., Hatzivassiliou, G., and Thompson, C.B. (2008). The biology of cancer: metabolic reprogramming fuels cell growth and proliferation. Cell metabolism *7*, 11-20.

DeBerardinis, R.J., Mancuso, A., Daikhin, E., Nissim, I., Yudkoff, M., Wehrli, S., and Thompson, C.B. (2007). Beyond aerobic glycolysis: transformed cells can engage in glutamine metabolism that exceeds the requirement for protein and nucleotide synthesis. Proceedings of the National Academy of Sciences of the United States of America *104*, 19345-19350.

Dibble, C.C., Asara, J.M., and Manning, B.D. (2009). Characterization of Rictor phosphorylation sites reveals direct regulation of mTOR complex 2 by S6K1. Molecular and cellular biology *29*, 5657-5670.

Egea, J., Buendia, I., Parada, E., Navarro, E., Rada, P., Cuadrado, A., Lopez, M.G., Garcia, A.G., and Leon, R. (2015). Melatonin-sulforaphane hybrid ITH12674 induces neuroprotection in oxidative stress conditions by a 'drug-prodrug' mechanism of action. British journal of pharmacology *172*, 1807-1821.

Gasol, E., Jimenez-Vidal, M., Chillaron, J., Zorzano, A., and Palacin, M. (2004). Membrane topology of system xc- light subunit reveals a re-entrant loop with substrate-restricted accessibility. The Journal of biological chemistry *279*, 31228-31236.

Gout, P.W., Buckley, A.R., Simms, C.R., and Bruchovsky, N. (2001). Sulfasalazine, a potent suppressor of lymphoma growth by inhibition of the x(c)- cystine transporter: a new action for an old drug. Leukemia : official journal of the Leukemia Society of America, Leukemia Research Fund, UK *15*, 1633-1640.

Hanahan, D., and Weinberg, R.A. (2011). Hallmarks of cancer: the next generation. Cell *144*, 646-674.

Hornbeck, P.V., Zhang, B., Murray, B., Kornhauser, J.M., Latham, V., and Skrzypek, E. (2015). PhosphoSitePlus, 2014: mutations, PTMs and recalibrations. Nucleic acids research *43*, D512-520.

Hsu, P.P., Kang, S.A., Rameseder, J., Zhang, Y., Ottina, K.A., Lim, D., Peterson, T.R., Choi, Y., Gray, N.S., Yaffe, M.B., *et al.* (2011). The mTOR-regulated phosphoproteome reveals a mechanism of mTORC1-mediated inhibition of growth factor signaling. Science *332*, 1317-1322.

Huang da, W., Sherman, B.T., and Lempicki, R.A. (2009). Systematic and integrative analysis of large gene lists using DAVID bioinformatics resources. Nature protocols *4*, 44-57.

Ishimoto, T., Nagano, O., Yae, T., Tamada, M., Motohara, T., Oshima, H., Oshima, M., Ikeda, T., Asaba, R., Yagi, H., *et al.* (2011). CD44 variant regulates redox status in cancer cells by stabilizing the xCT subunit of system xc(-) and thereby promotes tumor growth. Cancer cell *19*, 387-400.

Jacinto, E., and Lorberg, A. (2008). TOR regulation of AGC kinases in yeast and mammals. The Biochemical journal *410*, 19-37.

Kim, J.Y., Kanai, Y., Chairoungdua, A., Cha, S.H., Matsuo, H., Kim, D.K., Inatomi, J., Sawa, H., Ida, Y., and Endou, H. (2001). Human cystine/glutamate transporter: cDNA cloning and upregulation by oxidative stress in glioma cells. Biochimica et biophysica acta *1512*, 335-344.

Kobayashi, S., Sato, M., Kasakoshi, T., Tsutsui, T., Sugimoto, M., Osaki, M., Okada, F., Igarashi, K., Hiratake, J., Homma, T., *et al.* (2015). Cystathionine is a novel substrate of cystine/glutamate transporter: implications for immune function. The Journal of biological chemistry *290*, 8778-8788.

Lamming, D.W., and Sabatini, D.M. (2013). A Central role for mTOR in lipid homeostasis. Cell metabolism *18*, 465-469.

Laplante, M., and Sabatini, D.M. (2009). mTOR signaling at a glance. Journal of cell science *122*, 3589-3594.

Laplante, M., and Sabatini, D.M. (2012). mTOR signaling in growth control and disease. Cell *149*, 274-293.

Lewerenz, J., Hewett, S.J., Huang, Y., Lambros, M., Gout, P.W., Kalivas, P.W., Massie, A., Smolders, I., Methner, A., Pergande, M., *et al.* (2012). The Cystine/Glutamate Antiporter System x(c)(-) in Health and Disease: From Molecular Mechanisms to Novel Therapeutic Opportunities. Antioxidants & redox signaling.

Liu, Q., Chang, J.W., Wang, J., Kang, S.A., Thoreen, C.C., Markhard, A., Hur, W., Zhang, J., Sim, T., Sabatini, D.M., *et al.* (2010). Discovery of 1-(4-(4-propionylpiperazin-1-yl)-3-(trifluoromethyl)phenyl)-9-(quinolin-3-yl)benz o[h][1,6]naphthyridin-2(1H)-one as a highly potent, selective mammalian target of rapamycin (mTOR) inhibitor for the treatment of cancer. Journal of medicinal chemistry *53*, 7146-7155.

Lundby, A., Secher, A., Lage, K., Nordsborg, N.B., Dmytriyev, A., Lundby, C., and Olsen, J.V. (2012). Quantitative maps of protein phosphorylation sites across 14 different rat organs and tissues. Nature communications *3*, 876.

Masui, K., Cavenee, W.K., and Mischel, P.S. (2015a). mTORC2 and Metabolic Reprogramming in GBM: at the Interface of Genetics and Environment. Brain pathology *25*, 755-759.

Masui, K., Tanaka, K., Akhavan, D., Babic, I., Gini, B., Matsutani, T., Iwanami, A., Liu, F., Villa, G.R., Gu, Y., *et al.* (2013). mTOR complex 2 controls glycolytic metabolism in glioblastoma through FoxO acetylation and upregulation of c-Myc. Cell metabolism *18*, 726-739.

Masui, K., Tanaka, K., Ikegami, S., Villa, G.R., Yang, H., Yong, W.H., Cloughesy, T.F., Yamagata, K., Arai, N., Cavenee, W.K., *et al.* (2015b). Glucose-dependent acetylation of Rictor promotes targeted cancer therapy resistance. Proceedings of the National Academy of Sciences of the United States of America *112*, 9406-9411.

Nakagawa, Y., and Coe, F.L. (1999). A modified cyanide-nitroprusside method for quantifying urinary cystine concentration that corrects for creatinine interference. Clinica chimica acta; international journal of clinical chemistry *289*, 57-68.

Ong, S.E., and Mann, M. (2006). A practical recipe for stable isotope labeling by amino acids in cell culture (SILAC). Nature protocols *1*, 2650-2660.

Palm, W., Park, Y., Wright, K., Pavlova, N.N., Tuveson, D.A., and Thompson, C.B. (2015). The Utilization of Extracellular Proteins as Nutrients Is Suppressed by mTORC1. Cell *162*, 259-270.

Pavlova, N.N., and Thompson, C.B. (2016). The Emerging Hallmarks of Cancer Metabolism. Cell metabolism *23*, 27-47.

Pearce, L.R., Komander, D., and Alessi, D.R. (2010). The nuts and bolts of AGC protein kinases. Nature reviews Molecular cell biology *11*, 9-22.

Robert, S.M., Buckingham, S.C., Campbell, S.L., Robel, S., Holt, K.T., Ogunrinu-Babarinde, T., Warren, P.P., White, D.M., Reid, M.A., Eschbacher, J.M., *et al.* (2015). SLC7A11 expression is associated with seizures and predicts poor survival in patients with malignant glioma. Science translational medicine *7*, 289ra286.

Sarbassov, D.D., Guertin, D.A., Ali, S.M., and Sabatini, D.M. (2005). Phosphorylation and regulation of Akt/PKB by the rictor-mTOR complex. Science *307*, 1098-1101.

Schweppe, D.K., Rigas, J.R., and Gerber, S.A. (2013). Quantitative phosphoproteomic profiling of human non-small cell lung cancer tumors. Journal of proteomics *91*, 286-296.

Son, J., Lyssiotis, C.A., Ying, H., Wang, X., Hua, S., Ligorio, M., Perera, R.M., Ferrone, C.R., Mullarky, E., Shyh-Chang, N., *et al.* (2013). Glutamine supports pancreatic cancer growth through a KRAS-regulated metabolic pathway. Nature *496*, 101-105.

Takeuchi, S., Wada, K., Toyooka, T., Shinomiya, N., Shimazaki, H., Nakanishi, K., Nagatani, K., Otani, N., Osada, H., Uozumi, Y., *et al.* (2012). Increased xCT Expression Correlates with Tumor Invasion and Outcome in Patients with Glioblastoma. Neurosurgery.

Tanaka, K., Babic, I., Nathanson, D., Akhavan, D., Guo, D., Gini, B., Dang, J., Zhu, S., Yang, H., De Jesus, J., *et al.* (2011). Oncogenic EGFR signaling activates an mTORC2-NF-kappaB pathway that promotes chemotherapy resistance. Cancer discovery *1*, 524-538.

Timmerman, L.A., Holton, T., Yuneva, M., Louie, R.J., Padro, M., Daemen, A., Hu, M., Chan, D.A., Ethier, S.P., van 't Veer, L.J., *et al.* (2013). Glutamine sensitivity analysis identifies the xCT antiporter as a common triple-negative breast tumor therapeutic target. Cancer cell *24*, 450-465.

Tsuchihashi, K., Okazaki, S., Ohmura, M., Ishikawa, M., Sampetrean, O., Onishi, N., Wakimoto, H., Yoshikawa, M., Seishima, R., Iwasaki, Y., *et al.* (2016). The EGF Receptor Promotes the Malignant Potential of Glioma by Regulating Amino Acid Transport System xc(-). Cancer research *76*, 2954-2963.

UniProt, C. (2015). UniProt: a hub for protein information. Nucleic acids research *43*, D204-212.

Wang, M.Y., Lu, K.V., Zhu, S., Dia, E.Q., Vivanco, I., Shackleford, G.M., Cavenee, W.K., Mellinghoff, I.K., Cloughesy, T.F., Sawyers, C.L., *et al.* (2006). Mammalian target of rapamycin inhibition promotes response to epidermal growth factor receptor kinase inhibitors in PTEN-deficient and PTEN-intact glioblastoma cells. Cancer research *66*, 7864-7869.

Yang, M., and Vousden, K.H. (2016). Serine and one-carbon metabolism in cancer. Nature reviews Cancer *16*, 650-662.

Yu, Y., Yoon, S.O., Poulogiannis, G., Yang, Q., Ma, X.M., Villen, J., Kubica, N., Hoffman, G.R., Cantley, L.C., Gygi, S.P., *et al.* (2011). Phosphoproteomic analysis identifies Grb10 as an mTORC1 substrate that negatively regulates insulin signaling. Science *332*, 1322-1326.

Zhou, H., Di Palma, S., Preisinger, C., Peng, M., Polat, A.N., Heck, A.J., and Mohammed, S. (2013). Toward a comprehensive characterization of a human cancer cell phosphoproteome. Journal of proteome research *12*, 260-271.

Chapter 3

Identifying Metabolic Vulnerabilities Induced by mTOR Inhibition

INTRODUCTION

The PI3K-Akt-mTOR pathway downstream of growth factor signaling is commonly hyperactivated in many cancers due to amplification, kinase domain mutations or loss of negative regulators such as AMPK and PTEN (Grabiner et al., 2014; Hollander et al., 2011; Iyer et al., 2012; Shackelford and Shaw, 2009; Yuan and Cantley, 2008). As the core signaling pathway driving tumor cell proliferation and survival, components of this pathway such as mTOR are among some of the most promising drug targets for cancer. First generation mTOR inhibitors such as Rapamycin and Rapalogs have been successfully approved by the FDA for the treatment of renal cell carcinoma and certain types of pancreatic and breast cancer (Wander et al., 2011). Second-generation mTOR inhibitors, which directly bind to the kinase domain of mTOR, and inhibit both mTOR complexes in an ATP-competitive manner were also developed. Compounds such as Torin1/2, AZD2014, MLN028 and CC-223, as well as dual PI3K-mTOR inhibitors such as BEZ-235 and GDC-0980 are currently being evaluated in preclinical studies with a few entering early clinical trials (Dienstmann et al., 2014; Faivre et al., 2006; Fruman and Rommel, 2014).

Although first- and second-generation mTOR inhibitors both showed great tumor-inhibitory effect in many cancers, variations in drug sensitivity and development of drug resistance remained two major unsolved problems for expanding their use in cancer treatment. For example, a phase I clinical trial testing the effect of Rapamycin in PTEN-deficient recurrent GBM patients showed that treatment with Rapamycin in fact accelerated the disease progression due to ablation of the feedback inhibition from S6K to IRS1 which led to reactivation of Akt and mTOR (Cloughesy et al., 2008). In addition, Rapamycin-insenstive components downstream of

mTORC1 such as 4EBP1, preexisting mutations in FKBP12 and mTOR kinase that interfere with drug binding or increase intrinsic kinase activity, as well as mTOR-independent mechanisms such as activation of complementary signaling pathways and induction of autophagy are all potential mechanisms contributing to mTOR inhibitor resistance in cancer (Gini et al., 2013; Grabiner et al., 2014; Lorenz and Heitman, 1995; Thoreen et al., 2009; Wagle et al., 2014; Wei et al., 2016). But currently the underlying determinants of drug sensitivity and mechanisms of resistance to mTOR inhibitors in different cancers still need to be better understood.

In GBM, treatment with mTOR kinase inhibitors only induced cytostatic effects in in vitro cell cultures, and in vivo tumor xenografts invariably developed drug resistance after prolonged treatment (Wei et al., 2016). To identify potential survival mechanisms and targetable vulnerabilities in cancer cells induced by mTOR inhibition, we specifically chose to focus on cellular metabolism and performed LC-MS/MS metabolomics analysis on GBM cells upon genetic or pharmacological inhibition of specific mTOR complexes. Consistent with the important role of mTOR as a major regulator of cancer cell metabolism, significant changes in many important metabolic pathways were observed, especially ones involved in biosynthesis and redox metabolism. Further studies on affected redox metabolic pathways revealed that mTOR inhibition significantly suppressed glutathione and NADPH production, disrupted mitochondria function and cellular ROS homeostasis, indicating that mTOR inhibition might have rendered cancer cells specifically sensitive to glutathione depletion and ROS-mediated cell death.

RESULTS

mTOR Inhibition Induced Global Metabolic Changes in GBM Cells

To better understand how mTOR inhibition affects metabolism, especially nutrient utilization in GBM cells, we performed metabolic tracer analysis by labeling U87EGFRvIII cells with either [U-13C6]-D-Glucose or [U-13C5]-L-Glutamine for 24 h in the presence or absence of an EGFR inhibitor Erlotinib or an mTOR kinase inhibitor Torin1. Total cellular metabolites were extracted and subjected to LC-MS/MS analysis, in which total amounts, percent labeling and labeling patterns of each metabolite by 13C6-Glucose or 13C5-Glutamine were quantified and complete data analysis was included in Appendix II. Two independent labeling experiments with [U-13C6]-D-Glucose or [U-13C5]-L-Glutamine identified similar changes in total cellular metabolite levels. Especially, Torin1 significantly decreased levels of glycolysis, pentose phosphate pathway and TCA cycle metabolites, glutathione, ATP, as well as nucleotides. Certain amino acids including 2-HG, glutamate, glycine and valine were also decreased by Torin1 (Fig. 3-1A and B). Interestingly, when we analyzed labeling patterns of metabolites by 13C6-Glucose or 13C5-Glutamine, it appeared that de novo synthesis of nucleotides and certain amino acids was strongly suppressed, suggesting that tumor cells might become more dependent on uptake of exogenous nutrients. Both glucose and glutamine labeling of purines and pyrimidines were significantly decreased, as well as glucose labeling of serine/glycine, which also led to a significant reduction of the important methyl donor SAM that could potentially affect protein and DNA methylation (Yang and Vousden, 2016). In addition, we also observed a strong inhibition of glutamine labeling of glutamate, asparagine and proline (Fig. 3-2A and B). Moreover, M4 labeling of TCA cycle metabolites such as citrate, malate, succinate and fumarate

by 13C5-glutamine were all significantly decreased, suggesting that mTOR inhibition by Torin1 also suppressed glutaminolysis as well as glutamine anaplerosis into the TCA cycle.

Recent studies from our lab suggest that mTORC2 plays a very important role in sensing nutrient status and promoting glycolysis in GBM cells (Masui et al., 2015; Masui et al., 2013), but whether mTORC2 is also involved in regulating other metabolic pathways in cancer remained largely unknown. To gain further insights into how inhibition of different mTOR complexes affects GBM cell metabolism, especially inhibition of mTORC2, we performed metabolomics analysis in GBM cells after 72 h of transfection with siRNAs targeting Rictor as well as mTORC2 downstream AGC kinases Akt and SGK1. siRNA-mediated knockdowns of Rictor and mTORC2 downstream kinases largely phenocopied the effect of Torin1, suppressing glycolysis, mitochondria TCA cycle, as well as decreasing levels of many amino acids and nucleotides (Fig. 3-3). Although further studies are still needed to understand the detailed mechanisms responsible for these changes, these results strongly support the important role of mTORC2 in cancer metabolism.

To complement the above metabolomics studies, we also measured glucose and glutamine uptake as well as lactate and glutamate secretion in GBM cells upon genetic or pharmacological inhibition of specific mTOR complexes (Fig. 3-4). Inhibition of mTORC1 or mTORC2 with Raptor or Rictor shRNA or complex-specific inhibitors both significantly suppressed glycolysis indicated by glucose uptake and lactate secretion, consistent with our previous findings that both mTORC1 and mTORC2 drives glycolysis downstream of growth factor signaling through c-Myc in cancer (Babic et al., 2013; Masui et al., 2013). Glutamine uptake was also suppressed upon

inhibition of mTORC1 or mTORC2, albeit not as significant as glucose. In addition, only inhibition of mTORC2 increased glutamate secretion, while inhibition of mTORC1 showed the opposite effect, further supporting our previous findings that it is specifically mTORC2, but not mTORC1 that regulate xCT activity through phosphorylation.

The global metabolomics analysis together with nutrient uptake measurements in GBM cells showed that inhibition of mTOR had profound effects on tumor cell metabolism, especially metabolism of glucose and glutamine that cancer cells mostly rely on. Glucose and glutamine are the two major carbon and nitrogen sources for biosynthetic reactions and are both involved in redox-related pathways generating reducing equivalents such as NADPH (Alberghina and Gaglio, 2014; Altman et al., 2016; Vander Heiden et al., 2009). Therefore, mTOR inhibition could have rendered cancer cells more sensitive to certain metabolic perturbations, which we could take advantage of to achieve tumor-killing effects.

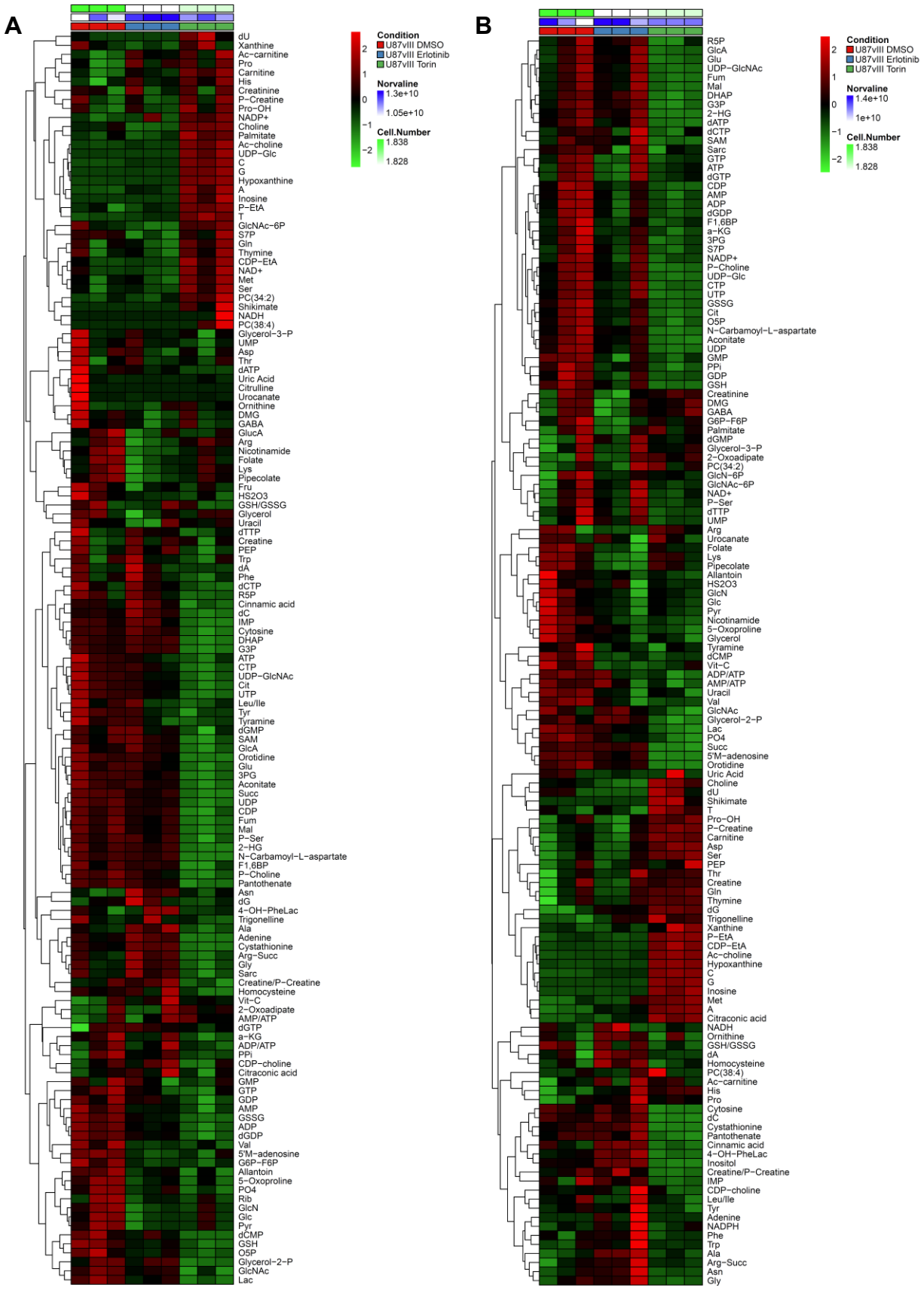
A
B
Condition
U87vIII DMSO
U87vIII Erlotinib
U87vIII Torin
Norvaline
1.3e+10
1.05e+10
Cell.Number
1.838
1.828
dU
Xanthine
Ac−carnitine
Pro
Carnitine
His
Creatinine
P−Creatine
Pro−OH
NADP+
Choline
Palmitate
Ac−choline
UDP−Glc
C
G
Hypoxanthine
A
Inosine
P−EtA
T
GlcNAc−6P
S7P
Gln
Thymine
CDP−EtA
NAD+
Met
Ser
PC(34:2)
Shikimate
NADH
PC(38:4)
Glycerol−3−P
UMP
Asp
Thr
dATP
Uric Acid
Citrulline
Urocanate
Ornithine
DMG
GABA
GlucA
Arg
Nicotinamide
Folate
Lys
Pipecolate
Fru
HS2O3
GSH/GSSG
Glycerol
Uracil
dTTP
Creatine
PEP
Trp
dA
Phe
dCTP
R5P
Cinnamic acid
dC
IMP
Cytosine
DHAP
G3P
ATP
CTP
UDP−GlcNAc
Cit
UTP
Leu/Ile
Tyr
Tyramine
dGMP
SAM
GlcA
Orotidine
Glu
3PG
Aconitate
Succ
UDP
CDP
Fum
Mal
P−Ser
2−HG
N−Carbamoyl−L−aspartate
F1,6BP
P−Choline
Pantothenate
Asn
dG
4−OH−PheLac
Trigonelline
Ala
Adenine
Cystathionine
Arg−Succ
Gly
Sarc
Creatine/P−Creatine
Homocysteine
Vit−C
2−Oxoadipate
AMP/ATP
dGTP
a−KG
ADP/ATP
PPi
CDP−choline
Citraconic acid
GMP
GTP
GDP
AMP
GSSG
ADP
dGDP
Val
5'M−adenosine
G6P−F6P
Allantoin
5−Oxoproline
PO4
Rib
GlcN
Glc
Pyr
dCMP
GSH
O5P
Glycerol−2−P
GlcNAc
Lac
R5P
GlcA
Glu
UDP−GlcNAc
Fum
Mal
DHAP
G3P
2−HG
dATP
dCTP
SAM
Sarc
GTP
ATP
dGTP
CDP
AMP
ADP
dGDP
F1,6BP
a−KG
3PG
S7P
NADP+
P−Choline
UDP−Glc
CTP
UTP
GSSG
Cit
O5P
N−Carbamoyl−L−aspartate
Aconitate
UDP
GMP
PPi
GDP
GSH
Creatinine
DMG
GABA
G6P−F6P
Palmitate
dGMP
Glycerol−3−P
2−Oxoadipate
PC(34:2)
GlcN−6P
GlcNAc−6P
NAD+
P−Ser
dTTP
UMP
Arg
Urocanate
Folate
Lys
Pipecolate
Allantoin
HS2O3
GlcN
Glc
Pyr
Nicotinamide
5−Oxoproline
Glycerol
Tyramine
dCMP
Vit−C
ADP/ATP
AMP/ATP
Uracil
Val
GlcNAc
Glycerol−2−P
Lac
PO4
Succ
5'M−adenosine
Orotidine
Uric Acid
Choline
dU
Shikimate
T
Pro−OH
P−Creatine
Carnitine
Asp
Ser
PEP
Thr
Creatine
Gln
Thymine
dG
Trigonelline
Xanthine
P−EtA
CDP−EtA
Ac−choline
Hypoxanthine
C
G
Inosine
Met
A
Citraconic acid
NADH
Ornithine
GSH/GSSG
dA
Homocysteine
PC(38:4)
Ac−carnitine
His
Pro
Cytosine
dC
Cystathionine
Pantothenate
Cinnamic acid
4−OH−PheLac
Inositol
Creatine/P−Creatine
IMP
CDP−choline
Leu/Ile
Tyr
Adenine
NADPH
Phe
Trp
Ala
Arg−Succ
Asn
Gly

Fig. 3-1. mTOR Kinase Inhibitor Torin1 Induced Global Metabolic Changes in GBM Cells. (A-B) Heatmap showing steady state metabolite levels in U87vIII cells treated with DMSO, 5 μM Erlotinib or 250 nM Torin1 for 24 h. LC-MS/MS was performed on cellular metabolites extracted from two independent experiments and results were normalized to norvaline as internal standard and cell counts. For detailed methods please refer to experimental procedures.

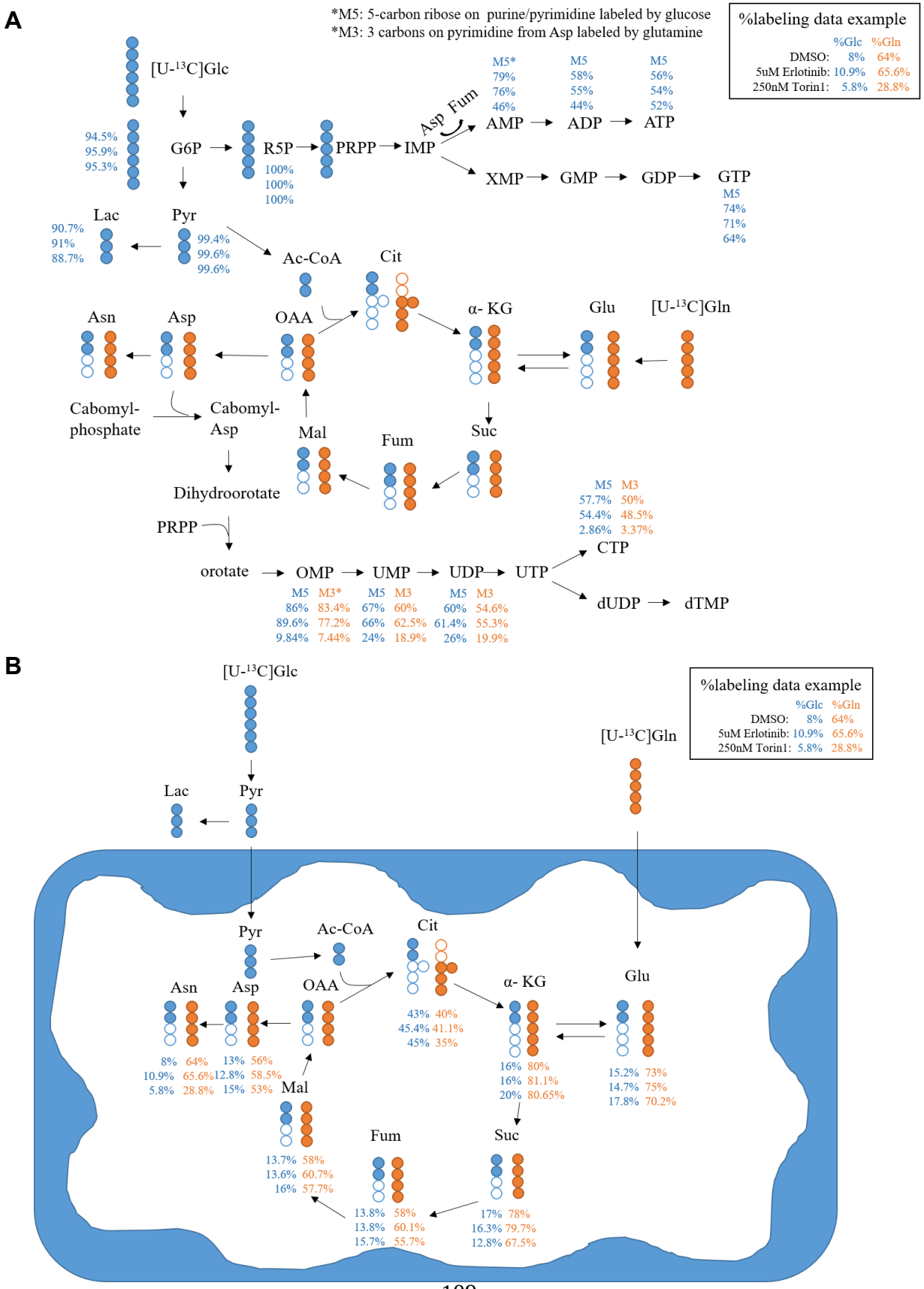
A
*M5: 5-carbon ribose on purine/pyrimidine labeled by glucose
*M3: 3 carbons on pyrimidine from Asp labeled by glutamine
%labeling data example
%Glc %Gln
DMSO: 8% 64%
5uM Erlotinib: 10.9% 65.6%
250nM Torin1: 5.8% 28.8%
[U-13C]Glc
94.5% 95.9% 95.3%
G6P
R5P
100% 100% 100%
PRPP
IMP
Asp Fum
M5* 79% 76% 46%
AMP
M5 58% 55% 44%
ADP
M5 56% 54% 52%
ATP
XMP
GMP
GDP
GTP
M5 74% 71% 64%
Lac
90.7% 91% 88.7%
Pyr
99.4% 99.6% 99.6%
Ac-CoA
Cit
Asn
Asp
OAA
α- KG
Glu
[U-13C]Gln
Cabomyl-phosphate
Cabomyl-Asp
Mal
Fum
Suc
Dihydroorotate
PRPP
orotate
OMP
UMP
UDP
UTP
M5 M3* 86% 83.4% 89.6% 77.2% 9.84% 7.44%
M5 M3 67% 60% 66% 62.5% 24% 18.9%
M5 M3 60% 54.6% 61.4% 55.3% 26% 19.9%
M5 M3 57.7% 50% 54.4% 48.5% 2.86% 3.37%
CTP
dUDP
dTMP
B
[U-13C]Glc
[U-13C]Gln
%labeling data example
%Glc %Gln
DMSO: 8% 64%
5uM Erlotinib: 10.9% 65.6%
250nM Torin1: 5.8% 28.8%
Lac
Pyr
Pyr
Ac-CoA
Cit
Asn
Asp
OAA
α- KG
Glu
43% 40% 45.4% 41.1% 45% 35%
8% 64% 10.9% 65.6% 5.8% 28.8%
13% 56% 12.8% 58.5% 15% 53%
16% 80% 16% 81.1% 20% 80.65%
15.2% 73% 14.7% 75% 17.8% 70.2%
Mal
Fum
Suc
13.7% 58% 13.6% 60.7% 16% 57.7%
13.8% 58% 13.8% 60.1% 15.7% 55.7%
17% 78% 16.3% 79.7% 12.8% 67.5%

Fig. 3-2. mTOR Inhibition Altered Nutrient Utilization in GBM Cells.

(A-B) Glucose and glutamine labeling patterns of metabolites in major metabolic pathways including glycolysis, pentose phosphate pathway and purine/pyrimidine synthesis pathways (A), as well as mitochondrial TCA cycle (B) are depicted with %labeled data obtained from the same experiment in Fig 3-1. Cells were treated with DMSO, 5 μM Erlotinib or 250 nM Torin1 and together incubated with 4.5 g/l [U-13C6]-D-Glucose or [U-13C5]-L-Glutamine for 24 h to reach steady state labeling. %labeled data for all metabolites measured is presented in Appendix II.

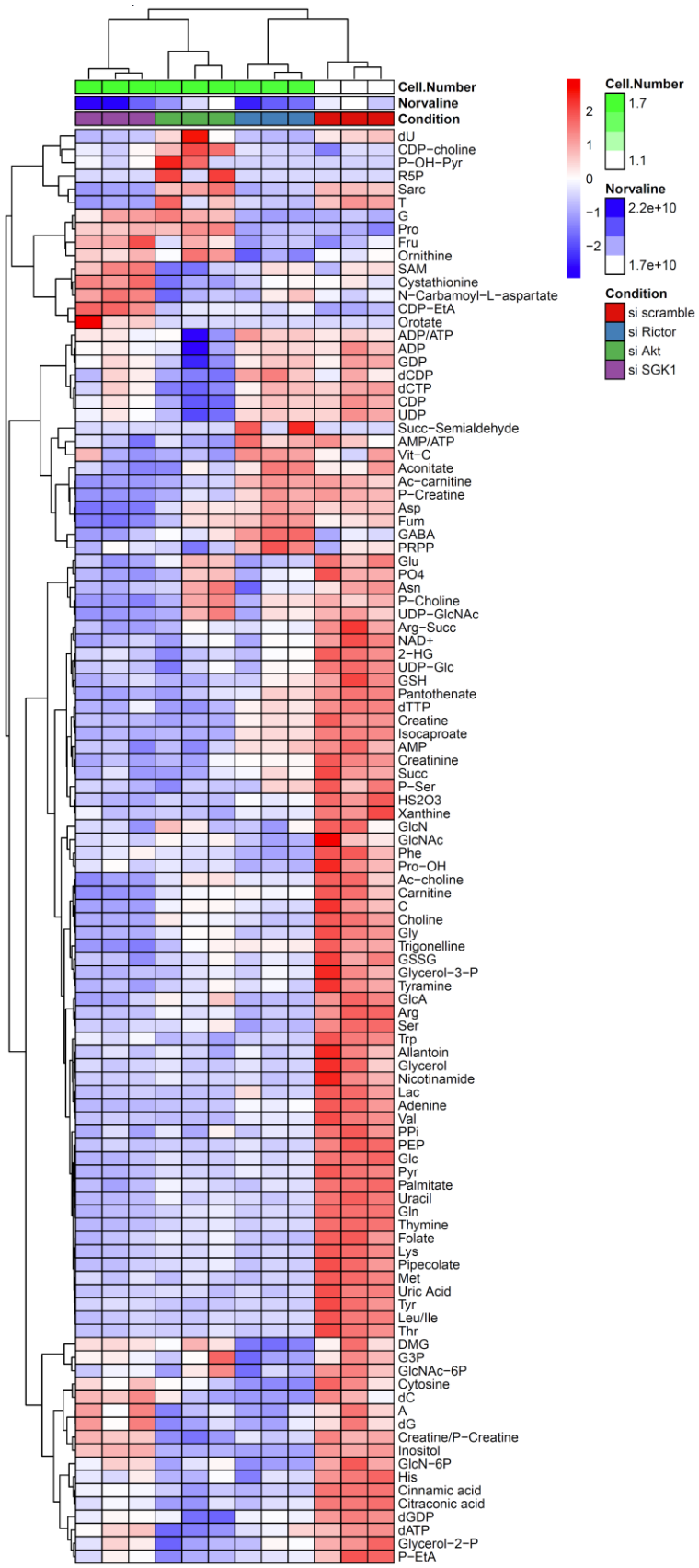
Cell.Number
Norvaline
Condition
dU
CDP−choline
P−OH−Pyr
R5P
Sarc
T
G
Pro
Fru
Ornithine
SAM
Cystathionine
N−Carbamoyl−L−aspartate
CDP−EtA
Orotate
ADP/ATP
ADP
GDP
dCDP
dCTP
CDP
UDP
Succ−Semialdehyde
AMP/ATP
Vit−C
Aconitate
Ac−carnitine
P−Creatine
Asp
Fum
GABA
PRPP
Glu
PO4
Asn
P−Choline
UDP−GlcNAc
Arg−Succ
NAD+
2−HG
UDP−Glc
GSH
Pantothenate
dTTP
Creatine
Isocaproate
AMP
Creatinine
Succ
P−Ser
HS2O3
Xanthine
GlcN
GlcNAc
Phe
Pro−OH
Ac−choline
Carnitine
C
Choline
Gly
Trigonelline
GSSG
Glycerol−3−P
Tyramine
GlcA
Arg
Ser
Trp
Allantoin
Glycerol
Nicotinamide
Lac
Adenine
Val
PPi
PEP
Glc
Pyr
Palmitate
Uracil
Gln
Thymine
Folate
Lys
Pipecolate
Met
Uric Acid
Tyr
Leu/Ile
Thr
DMG
G3P
GlcNAc−6P
Cytosine
dC
A
dG
Creatine/P−Creatine
Inositol
GlcN−6P
His
Cinnamic acid
Citraconic acid
dGDP
dATP
Glycerol−2−P
P−EtA
2
1
0
−1
−2
Cell.Number
1.7
1.1
Norvaline
2.2e+10
1.7e+10
Condition
si scramble
si Rictor
si Akt
si SGK1

Fig. 3-3. Genetic Knockdown of mTORC2 and Downstream Kinases Resulted in Significant Alterations in Cellular Metabolism.

Heat map showing steady state metabolite levels in U87vIII cells after 72 h of transfection with si scramble control or siRNAs targeting Rictor, Akt1/2/3, or SGK1. LC-MS/MS was performed and results were normalized to norvaline as internal standard and cell counts. For detailed methods please refer to experimental procedures.

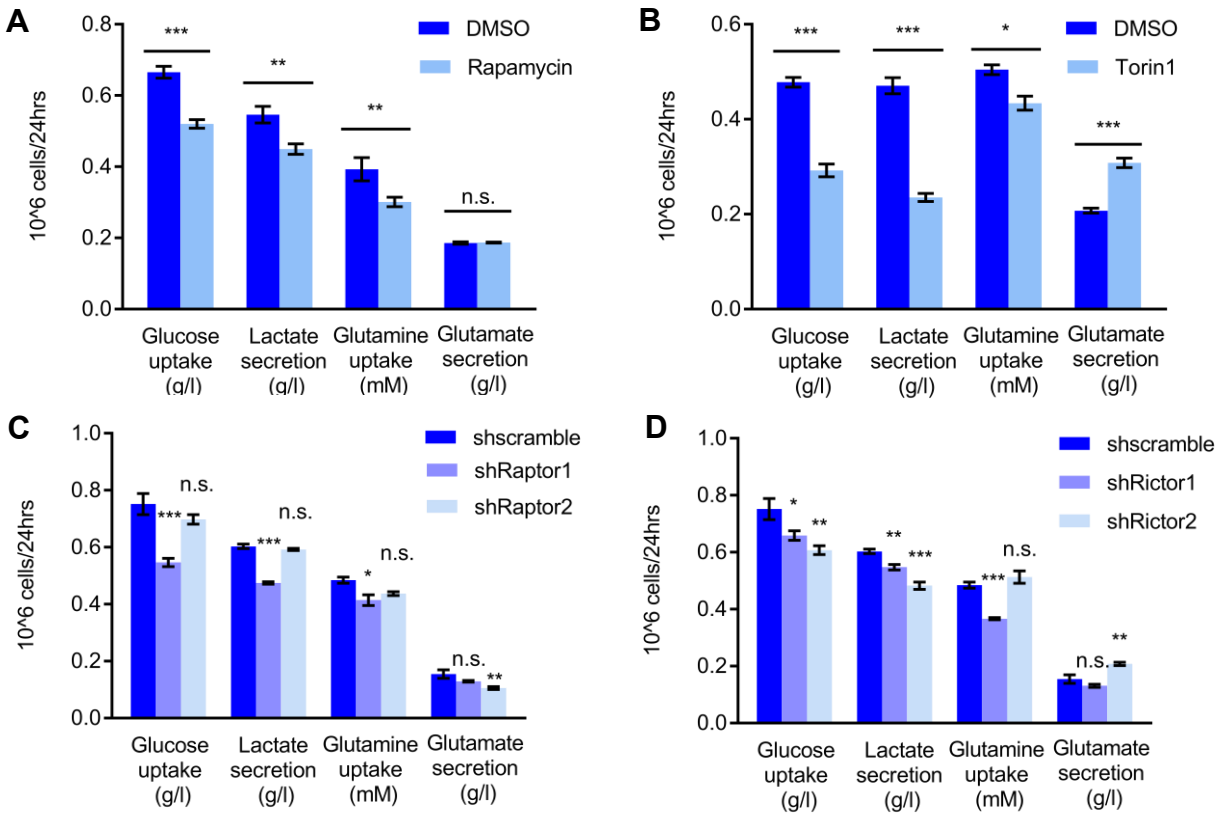

Fig. 3-4. mTOR Inhibition Suppresses Glycolysis and Glutamine Metabolism in GBM Cells.

Glucose, lactate, glutamine and glutamate levels in the media were measured using NOVA Bioprofile 400 analyzer after 24 h incubation with U87EGFRvIII cells together with Rapamycin (A), Torin1 (B), or stably transfected with two different shRNAs targeting Raptor (C) or Rictor (D). Results were obtained from three independent replicates and data are presented as mean ± SEM.

The Effect of mTOR Inhibition on Redox Metabolism in GBM

mTOR inhibition disrupts redox homeostasis in GBM cells

One important observation from our metabolomics studies was that mTOR inhibition resulted in significant reduction in total cellular glutathione levels (Fig. 3-5A and B), as well as suppression of major NADPH generating pathways, including the pentose phosphate pathway and de novo serine/glycine synthesis pathway, as well as reduction of the glutamine-derived pyruvate which indicates possible inhibition of the malic enzyme reaction (see Appendix II for complete labeling data) (Fan et al., 2014). These all suggest that mTOR inhibition might lower the redox capacity of GBM cells. To further determine whether mTOR inhibition disrupted the redox homeostasis in GBM cells, we also measured levels of different ROS species upon Torin1 treatment. Surprisingly, Torin1 significantly increased mitochondria ROS and lipid ROS in GBM cells (Fig. 3-6A and B), while the level of cytosolic ROS was lower in Torin1 treated cells compared to DMSO control (Fig. 3-6C). This suggests that in addition to suppressing glutathione and NADPH production, Torin1 might have also affected mitochondria properties. As we expected, mitochondria potential measured by JC-1 was significantly increased by Torin1 (Fig. 3-6D), which could potentially result from inhibition of the ATP synthase which prevented proton influx into the matrix. It will be interesting determine the detailed mechanism of how Torin1 resulted in increased mitochondria potential in future studies and whether this is also related to the increased mitochondria ROS and lipid ROS. These together suggested that mTOR inhibition could lead to disruption of the redox homeostasis in GBM cells by inhibiting synthesis of redox equivalents and affecting mitochondria function.

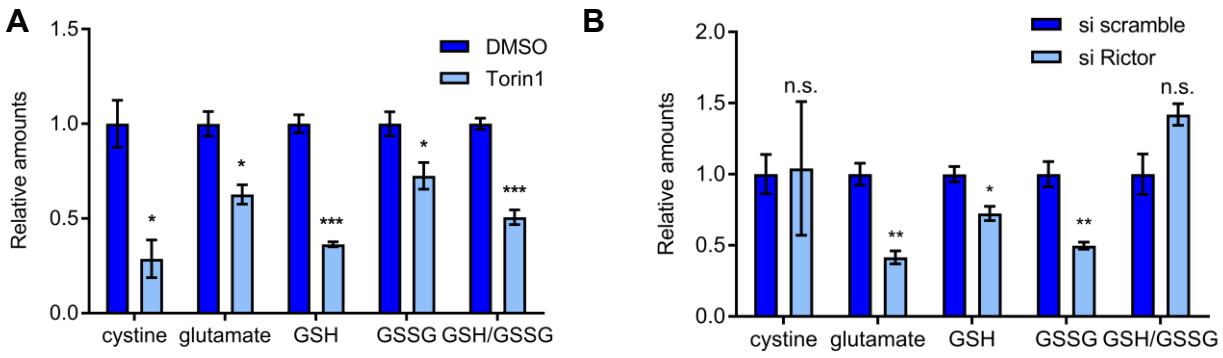

Fig. 3-5. mTORC2 Inhibition Resulted in Decreased Glutathione Levels in GBM Cells.

(A-B) LC-MS/MS metabolomics analysis of intracellular metabolites extracted from U87vIII cells treated with DMSO or Torin1 for 24 h(A), or after 72 h of transfection with scramble or Rictor siRNA(B).

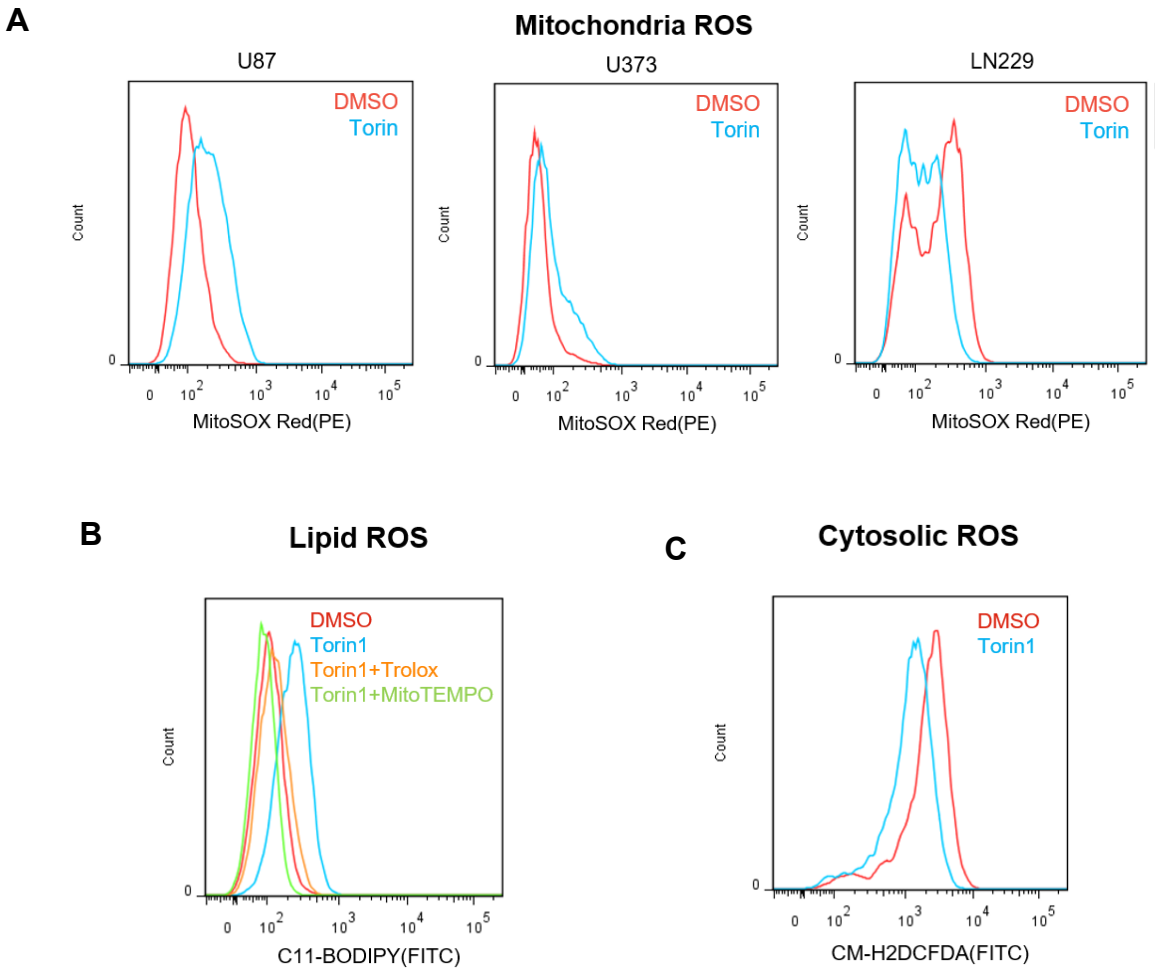

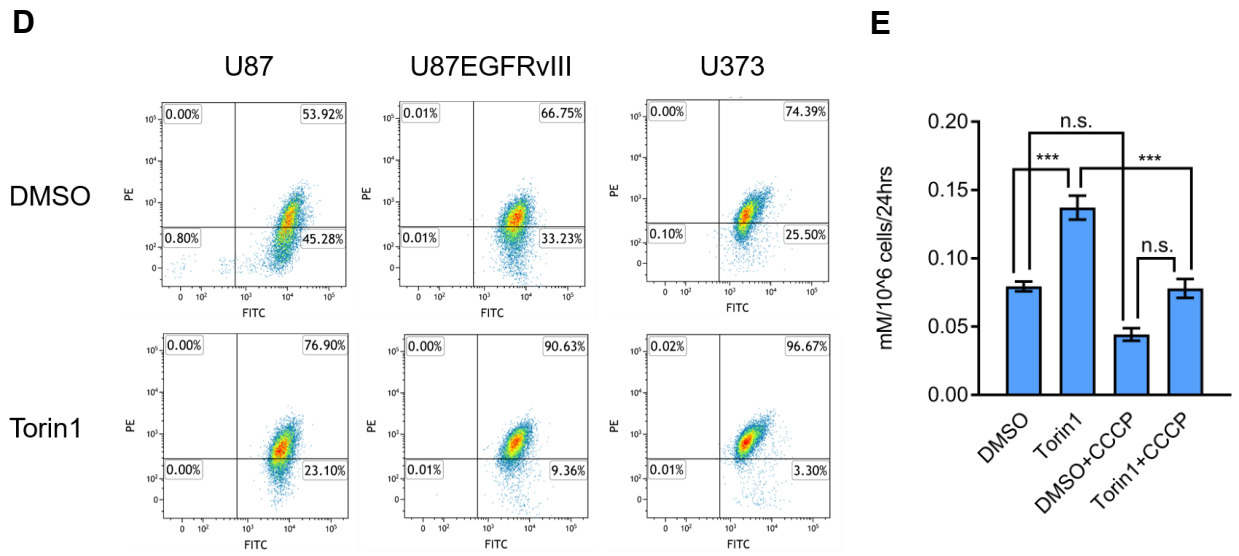

Fig. 3-6. Torin1 Induced Mitochondria ROS / Lipid ROS and Increased Mitochondria Potential in GBM Cells.

(A-C) Mitochondria ROS, lipid ROS and cytosolic ROS were analyzed by flow cytometry using MitoSOXRed, C11-BODIPY and CM-H2DCFDA. GBM cells were treated with indicated drugs or antioxidants for 24 h before cells were stained with different ROS probes for analysis.

(D) GBM cell lines U87, U87EGFRvIII and U373 were treated with DMSO or 250 nM Torin1for 24 h before mitochondria potential was measured by flow cytometry using the JC-1 dye.

(E) Glutamate secretion was measured by NOVA Bioprofile 400 analyzer using media collected from U87EGFRvIII cells treated with DMSO or 250 nM Torin1in the absence or presence of an mitochondria uncoupler CCCP (2.5 μM). Results were obtained from three replicate samples and data are presented as mean ± SEM. Statistical analysis was performed using two-way ANOVA. *** refers to p value < 0.001.

xCT is upregulated upon mTOR inhibition and contributes to glutathione synthesis in GBM cells

Previous studies have identified that xCT transcription is regulated by the ROS-responsive transcription factor Nrf2 to facilitate cystine uptake for glutathione synthesis upon oxidative stress (Ishii et al., 2000; Sasaki et al., 2002). Therefore we tested whether Torin1-induced glutathione reduction and mitochondria ROS could have also induced Nrf2-mediated xCT transcription. Indeed xCT mRNA as well as protein levels were both increased in Torin1 treated cells (Fig. 3-7A and B), and siRNA-mediated knockdown of Nrf2 significantly reduced both transcript and protein levels of xCT as well as GCLC, which is also an Nrf2 target gene and the rate-limiting enzyme for glutathione synthesis (Fig. 3-7A and B). Furthermore, Torin1 also increased nuclear Nrf2 levels as well as its binding onto the Electrophile Response Element (EpRE) within the xCT promoter (Fig. 3-7C and D). We also examined other known xCT transcription factors ATF4 and p53 (Jiang et al., 2015; Sato et al., 2004). Knockdown of ATF4 did not affect xCT transcription, and Torin1 on the contrary decreased nuclear ATF4 levels as well as binding of ATF4 onto the Amino Acid Response Element (AARE) in the xCT promoter (Fig. 3-7C, E and F). Interestingly, knockdown of p53 also suppressed xCT transcription in GBM cells, which is the opposite of its proposed role as an xCT transcription repressor reported recently, but this on the other hand suggest that p53 might also contribute to the Torin1-induced xCT transcription (Fig. 3-7 F).

Next, we performed rescue experiments to determine the exact underlying cause for the induction of Nrf2-mediated xCT transcription upon Torin1 treatment using cell-permeable glutathione GSHest as well as mitochondria and lipid ROS scavengers MitoTEMPO and Trolox.

RT-PCR showed that only the cell permeable glutathione GSHest was able to partially rescue the increased Nrf2-dependent transcription of xCT and GCLC, suggesting that it is the decreased glutathione rather than increased mitochondria or lipid ROS that induced Nrf2, which could be attributed to the different cellular compartmentalization of Nrf2 and mitochondria ROS (Fig. 3-8A and B). Consistent with this finding, Torin1-induced increase in glutamate secretion through xCT could also be rescued by GSHest, but not antioxidants such as Trolox or MnTBAP (Fig. 3-8C, D and E). And interestingly, the mitochondria uncoupler CCCP which counteracts the increased mitochondria potential by Torin1 also reduced glutamate secretion (Fig. 3-6E). But how changes in mitochondria potential is related to xCT-mediated glutamate transport is unclear. In addition to increased xCT transcription, we found that inhibition of mTORC2 but not mTORC1 resulted in increased xCT protein stability (Fig. 3-9A, B and C), but whether this is a consequence of decreased phosphorylation of xCT on serine 26 by mTORC2 still needs to be determined. Taken together, it is very likely that increased transcription, protein stability as well as decreased serine 26 phosphorylation of xCT all contributed to the consistent elevated xCT levels and function in GBM cells upon Torin1 treatment (Fig. 3-9D).

GBM cells are incapable of synthesizing cysteine from methionine (Chung et al., 2005) and heavily rely on uptake of extracellular cystine for glutathione synthesis through xCT. Therefore we wanted to determine whether induction of xCT contributed to glutathione synthesis, which could be important for cancer cells to survive upon mTOR inhibition. We performed metabolic tracer analysis using 13C-labeled cystine, to examine whether Torin1 increases exogenous cystine incorporation into glutathione (Fig. 3-10A). As predicted by our model, labeled-cystine incorporation into GSH and GSSG were both significantly increased over time with Torin1

treatment before steady state was reached with 100% labeling at 24h (Fig. 3-10B). In addition, xCT knockdown further decreased cellular glutathione levels in addition to Torin1 (Fig. 3-10C), indicating that increased cystine uptake through xCT and incorporation into glutathione could partially counteract glutathione loss upon mTOR inhibition. These data suggested that increased xCT transporter function is important for maintaining glutathione synthesis upon mTOR inhibition, which helps cancer cells to lower cellular ROS levels and avoid oxidative stress-induced cell death.

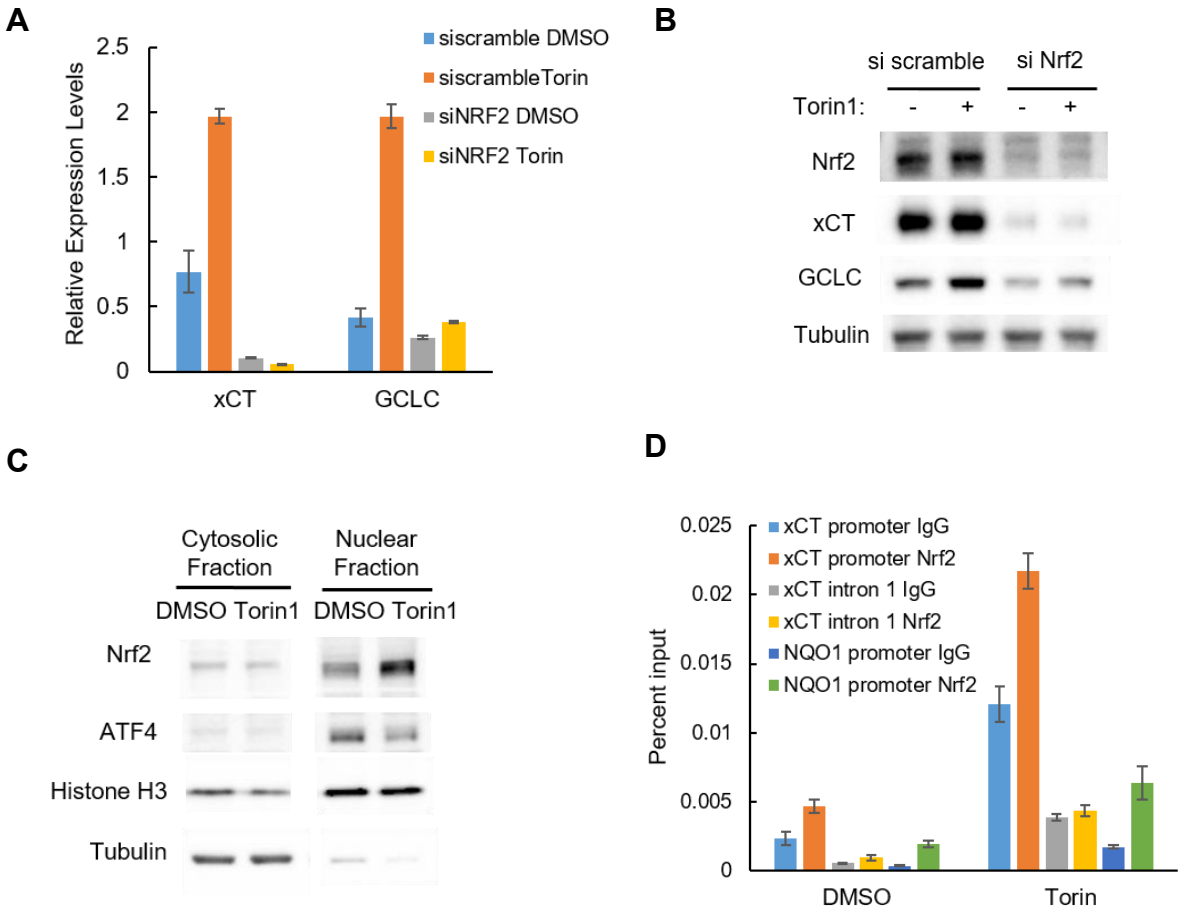

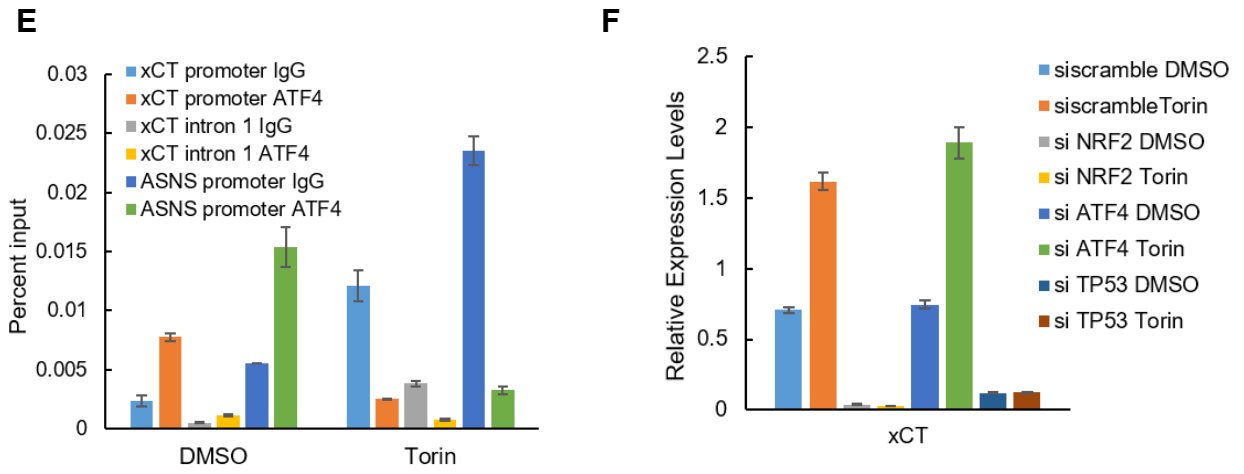

Fig. 3-7. mTORC2 Inhibition Induced Nrf-2 Mediated Transcription of xCT and Glutathione Synthesis Genes.

(A-B) RT-PCR (A) and western blot (B) showing xCT and GCLC mRNA and protein levels comparing cells transfected with a scramble or Nrf2 siRNA. Results were obtained from three replicates and data are presented as mean ± SEM.

(C) Western blot showing nuclear and cytosolic Nrf2 and ATF4 protein levels in U87EGFRvIII cells treated with DMSO or Torin1 for 24 h.

(D-E) ChIP-qPCR was performed to detect Nrf2 (C) or ATF4 (D) binding onto xCT promoter region in U87EGFRvIII cells treated with DMSO or Torin1 for 24 h. xCT intron1 was used as a negative control, NQO1 and ASNS were used as positive controls for Nrf2 and ATF4 respectively. Results were obtained from three replicates and data are presented as mean ± SEM.

(F) xCT expression levels was analyzed by RT-PCR in U87EGFRvIII cells after 72 h of transfection with siRNAs targeting Nrf2, ATF4 or TP53 and treated with DMSO or Torin1 for 24 h. Results were obtained from three replicates and data are presented as mean ± SEM.

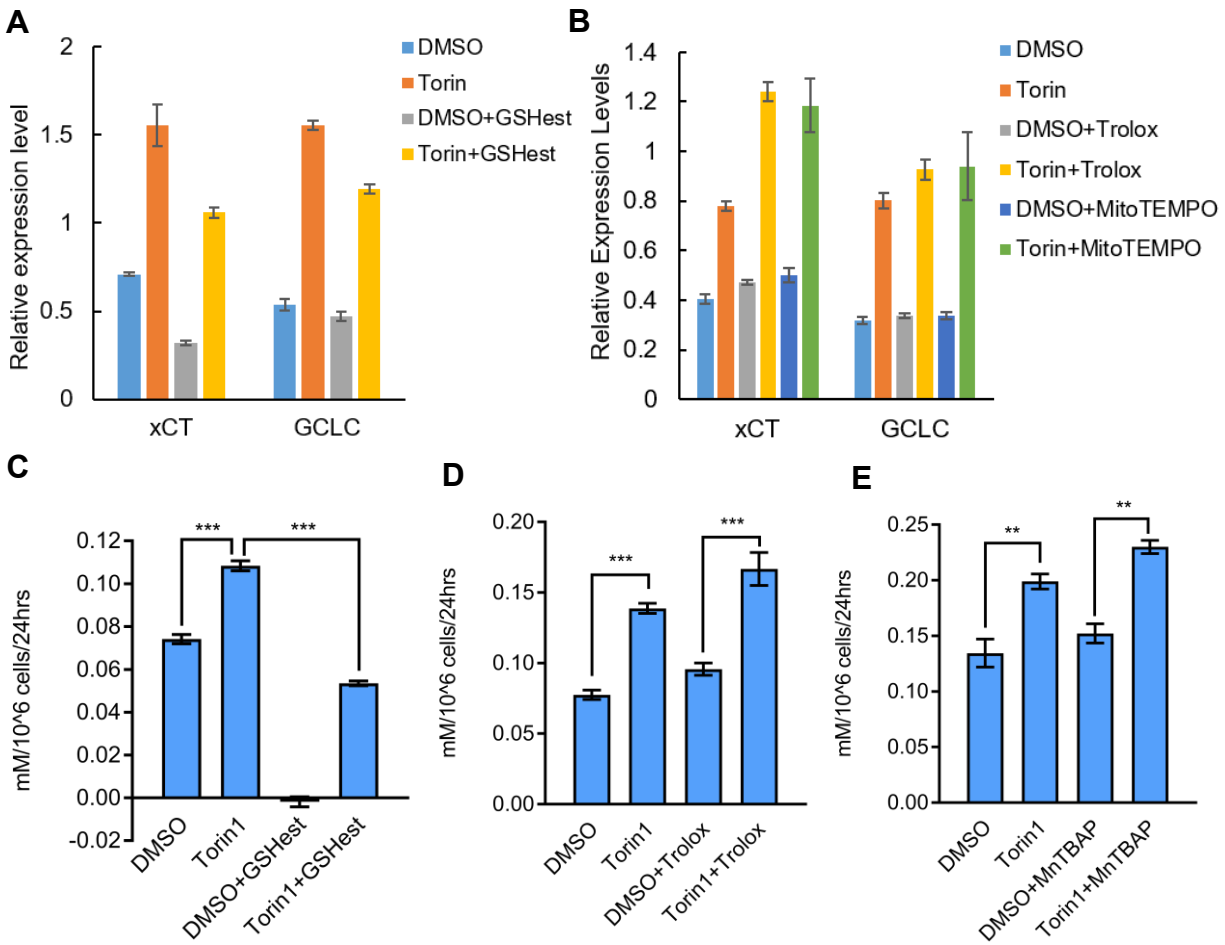

Fig. 3-8. Cell-permeable Glutathione but not Antioxidants Rescued Torin1-induced xCT Transcription and Glutamate Secretion.

(A-B) xCT expression levels were analyzed by RT-PCR in U87EGFRvIII cells treated with DMSO or Torin1 for 24 h together with 1.5 mM GSHest, 100 µM Trolox or 100 µM MnTBAP .. Results were obtained from three replicates and data are presented as mean ± SEM.

(C-E) Glutamate secretion was measured by NOVA Bioprofile 400 analyzer using media collected from U87EGFRvIII cells treated with DMSO or 250 nM Torin1 together with 1.5 mM GSHest, 100 µM Trolox or 100 µM MnTBAP. Results were obtained from three replicate samples and data are presented as mean ± SEM. Statistical analysis was performed using two-way ANOVA.

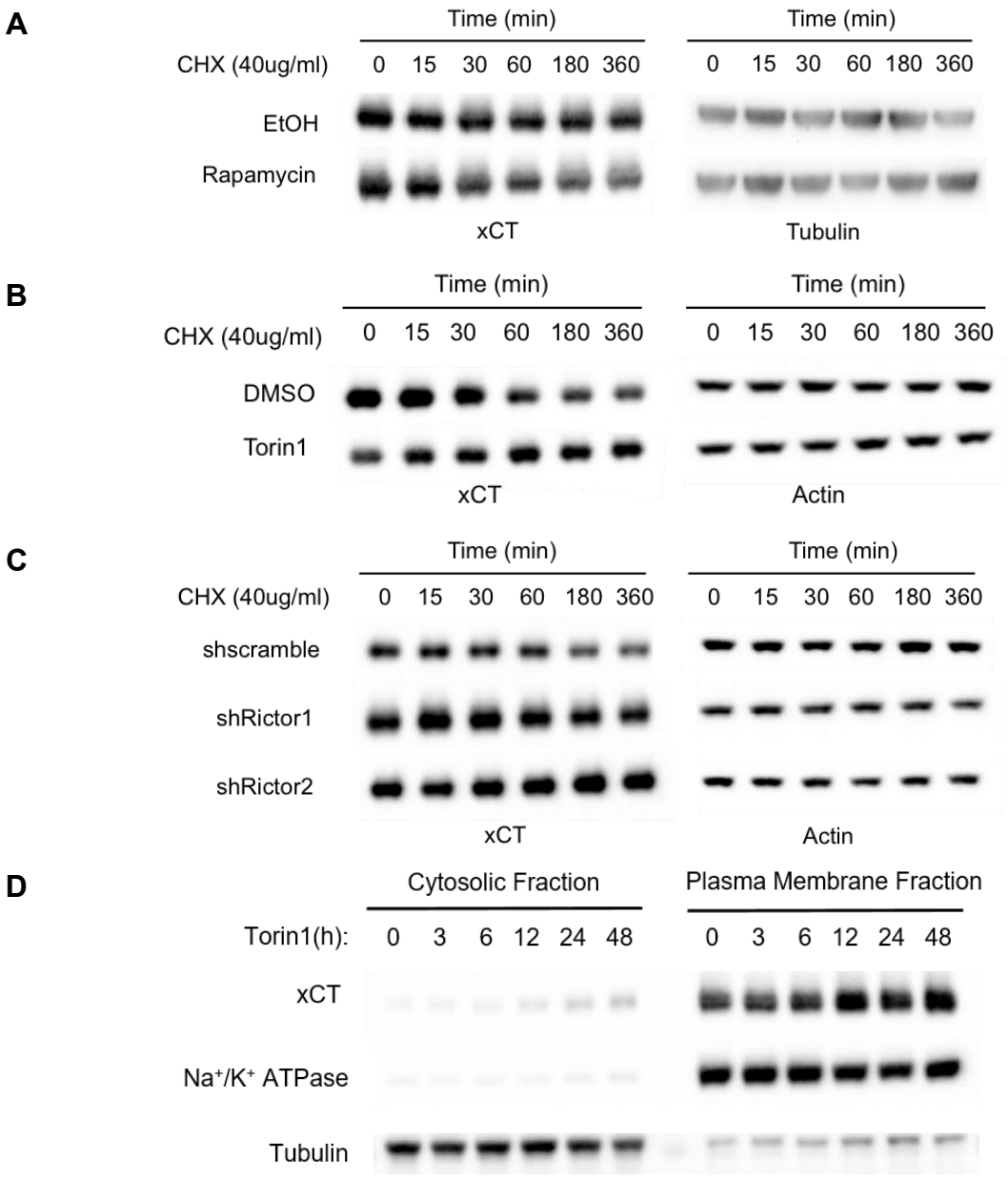

Fig. 3-9. mTORC2 Inhibition Increased xCT Stability and Surface Levels in GBM Cells.

(A-C) xCT protein stability was determined by time-course 40 μg/ml cycloheximide (CHX) treatment in U87vIII cells pre-treated with Rapamycin (A) or Torin1 (B) for 24 h, or with stable Rictor knockdown(C).

(D) Cell surface proteins was purified using the Pierce Cell Surface Protein Isolation Kit and levels of xCT on the plasma membrane was analyzed by western blot.

A

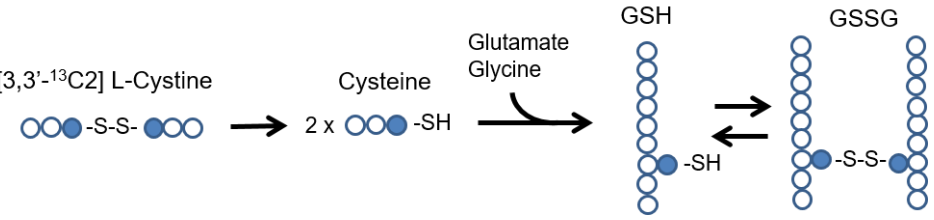
[3,3'-13C2] L-Cystine
-S-S-
Cysteine
2 x
-SH
Glutamate
Glycine
GSH
-SH
GSSG
-S-S-

B

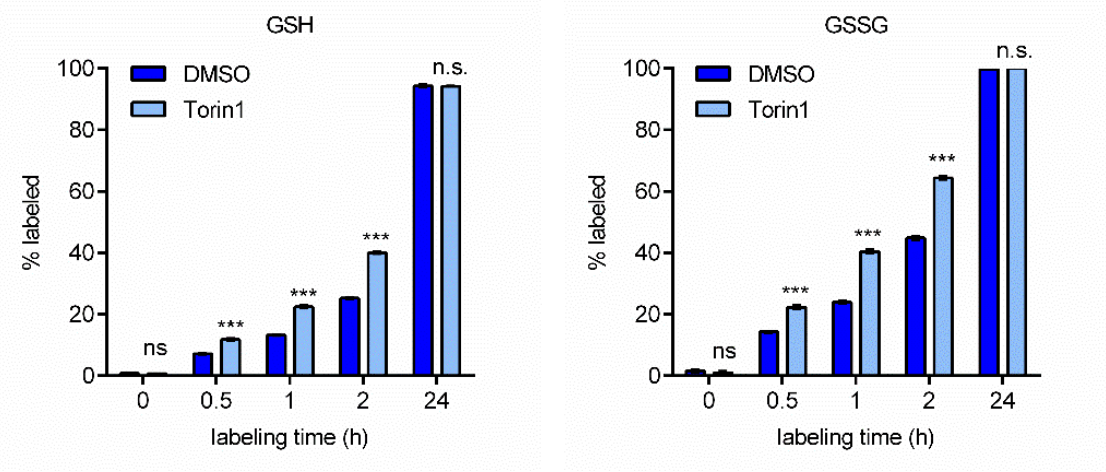
GSH
DMSO
Torin1
% labeled
labeling time (h)
ns
***
***
***
n.s.
0
0.5
1
2
24
GSSG
DMSO
Torin1
% labeled
labeling time (h)
ns
***
***
***
n.s.

C

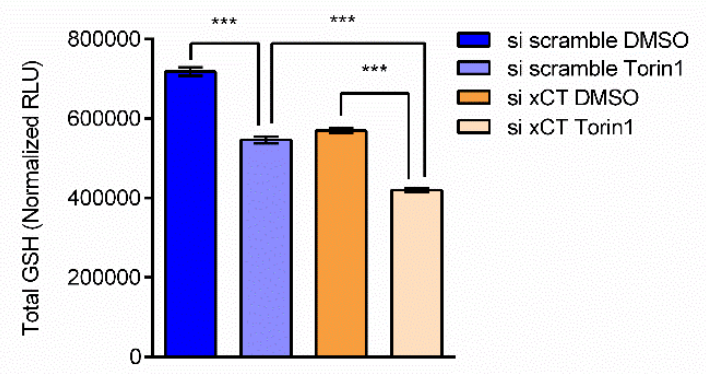
Total GSH (Normalized RLU)
si scramble DMSO
si scramble Torin1
si xCT DMSO
si xCT Torin1
***
***
***

Fig. 3-10. mTOR Inhibition Increased Cystine Uptake Through xCT and Incorporation into Glutathione in GBM Cells.

(A) A brief schematic showing the labeling process of GSH and GSSG with [3,3'-13C2] L-Cystine.

(B) Exogenous cystine incorporation into newly synthesized glutathione was determined by incubating cells with [3,3'-13C2] L-Cystine. Metabolites were extracted and analyzed by LC-MS/MS after 24h of DMSO or Torin1 treatment in DMEM supplemented with 5% dialyzed FBS. [3,3'-13C2] L-Cystine was added and incubated with the cells for indicated length of time of labeling. The percentage labeling of both GSH and GSSG by [3,3'-13C2] L-Cystine were calculated for both DMSO and Torin1 treated samples.

(C) Total cellular GSH levels were measured using the GSH/GSSG-Glo^{TM} Glutathione Assay Kit (Promega). U87EGFRvIII cells were treated with DMSO or 250 nM Torin1 for 24 h after being transfected with xCT siRNA for 48 h. Total cellular GSH levels were normalized to blank control and cell counts. Statistical analysis was performed using one-way ANOVA.

DISCUSSION

Metabolic plasticity in cancer not only ensures rapid adaptation to constantly changing environments, but also contributes to therapeutic resistance by enabling tumor cell survival and proliferation in unfavorable conditions. mTORC1 activation promotes tumor cell proliferation when amino acids are abundant, but restricts proliferation when amino acids are limiting (Palm et al., 2015). Thus, mTORC1 inhibitors currently used in the clinics such as rapalogs, which do not suppress mTORC2, may on the contrary stimulate tumor growth if nutrients are scarce by releasing tumor cells from mTORC1-dependent growth inhibition (Cloughesy et al., 2008; Palm et al., 2015). However, tumor cell's metabolic flexibility may also generate targetable vulnerabilities as shown here. xCT-dependent regulation of cystine-uptake may be important for preventing tumor cell death in response to cellular stress induced by mTOR inhibition (Jiang et al., 2015), likely through maintaining glutathione synthesis to buffer elevated mitochonrdrial ROS (Li et al., 2016). The data reported here indicate that inhibition of mTOR plays an important role in generating a targetable vulnerability in cancer cells by suppressing production reducing equivalents and inducing mitochondria and lipid ROS. mTOR kinase inhibitors are currently under clinical development although preliminary data suggest that it may be difficult to achieve therapeutic levels in the brain (Heffron, 2016; Heffron et al., 2016; Wander et al., 2011). Recently, a third generation of mTOR inhibitor RapaLink-1 was reported which combined the structure of first- and second-generation mTOR inhibitors with a linker designed based on the spatial distance between the drug docking sites on FKBP12 and mTOR kinase. RapaLink-1 was shown to reversed resistance due to FKBP12 and kinase domain mutations in xenograft tumors, and achieved much better brain penetrance compared to existing mTOR inhibitors (Rodrik-Outmezguine et al., 2016). Together with the mechanisms identified here, it will be interesting to

test combination approaches in future studies to determine whether targeting xCT or glutathione synthesis could further enhance the anti-tumor effect of mTOR inhibitors.

. `

EXPERIMENTAL PROCEDURES

Cell Culture

U87EGFRvIII isogenic cell lines were established as described previously (Wang et al., 2006). All cells were cultured in DMEM (CORNING, 10-013) supplemented with 10% FBS (Omega Scientific) in a humidified incubator with 5% CO2 at 37 °C unless specifically noted

Antibodies and Reagents

Antibodies used include: Actin (Sigma, A4700), Tubulin (Sigma, T6074), xCT/SLC7A11 (Cell Signaling, 13691), Nrf2 (Cell Signaling, 12721), ATF4 (Cell Signaling, 11815), GCLC (Thermo Scientific, PA519702), Histone H3 (Cell Signaling, 4499), Na^+/K^+ ATPase (Cell Signaling, 3010), anti-rabbit IgG (Cell Signaling, 7074), anti-mouse IgG (Cell Signaling, 7076).

Reagents and drugs used include: Torin1 (Tocris Bioscience, 4247), cycloheximide (CHX, Sigma, C4859), Rapamycin (Sigma, R0395), Glutathione reduced ethyl ester (GSHest, Sigma, G1404), Trolox (Sigma, 238813), MitoTEMPO (Sigma, SML0737), MnTBAP (Sigma, 475870), CCCP (Sigma, C2759).

Metabolite Extraction and LC-MS/MS Metabolomics Analysis

Cells were washed three times with 1 x PBS and incubated in Dulbecco's Modified Eagle's Medium (DMEM) supplemented with 5% dialyzed FBS for 24 h before sample extraction. Cells were rinsed quickly on ice with ice cold 150 mM ammonium acetate (NH_4AcO) and scraped off in 1 ml ice cold 80% methanol and collected into Eppendorf tubes. 5 nmol of norvaline was added to the cell suspension as internal control and the tubes were vortexed and spun down at

15,000 rpm for 5 min at 4 °C. Cell pellets were re-extracted with additional 200 µl of cold 80% methanol and supernatants were combined and transferred into glass vials and dried under vacuum. Metabolites were resuspended in 50 µl 70% acetonitrile (ACN) and 5 µl was used for analysis on a Q Exactive Orbitrap Mass Spectrometer (Thermo Scientific) in polarity-switching mode with positive voltage 3.0 kV and negative voltage 2.25 kV. The mass spectrometer was coupled to an UltiMate 3000RSLC (Thermo Scientific) UHPLC system. Mobile phase A was 5 mM NH4AcO, pH 9.9, B was ACN, and the separation achieved on a Luna 3 mm NH2 100 A (150 x 2.0 mm) (Phenomenex) column. The flow was 300 µl/min, and the gradient ran from 15% A to 95% A in 18 min, followed by an isocratic step for 9 minutes and re-equilibration for 7 minutes. Metabolites were detected and quantified as area under the curve (AUC) based on retention time and accurate mass (≤ 3 ppm) using the TraceFinder 3.3 (Thermo Scientific) software. Relative amounts of metabolites as well as percentage of labeling were calculated and normalized to control samples (DMSO treatment or si scramble knockdown) as well as total cell numbers.

Glutamate Secretion Assays

Glutamate secretion from cells were measured using a Nova BioProfile Basic Analyzer (Nova Biomedical), or with the Amplex® Red Glutamic Acid/Glutamate Oxidase Kit (ThermoFisher Scientific, A12221). Briefly cells were seeded in triplicates in 6-well plates at optimal density, and 24 h before measurement cells were washed three times with 1 x PBS and changed to 1 ml fresh DMEM media supplemented with 5% dialyzed FBS (Gibico), including three wells without cells as blank control. After incubation media were collected from each well and analyzed according to manufacturer's instructions. Cell numbers were determined using the TC20^{TM}

Automated Cell Counter (Bio-Rad). Glutamate secretion was calculated by subtracting the levels of glutamate in the blank control and normalized to cell counts for each sample. Cellular glucose uptake, lactate secretion and glutamine uptake was also measured by Nova BioProfile Basic Analyzer (Nova Biomedical) and calculated the same way as described for glutamate secretion.

Mitochondria ROS and Mitochondria Potential Measurement

Cells were seeded in 6 well plates and incubated with indicated drug or media. After treatment, media was removed and cells were washed with 1x PBS before incubated with the MitoSOX™ Red Mitochondria Superoxide Indicator (ThermoFisher Scientific, M36008) or the Mitochondria Membrane Potential Probe JC-1dye (ThermoFisher Scientific, T3168) according to manufacturer's protocol. After incubation cells were trypsinized and collect for flow cytometry analysis using the BD LSRII flow cytometer (BD Biosciences) and signals were recorded from 10,000 events in the PE channel for MitoSOX™, or FITC and PE channels for JC-1. Data analysis was performed using the Kaluza Analysis Software (Beckman Coulter).

Lipid ROS Measurement

Cells were seeded in 6 well plates and treated with indicated drugs. After treatment, media was removed and cells were washed with 1x PBS before incubated with the lipid peroxidation sensor BODIPY® 581/591 C11 (ThermoFisher Scientific, D3861) according to manufacturer's protocol. After incubation cells were trypsinized and collect for flow cytometry analysis using the BD LSRII flow cytometer (BD Biosciences) and signals were recorded from 10,000 events using the

FITC channel. And data analysis was performed using the Kaluza Analysis Software (Beckman Coulter).

Western Blotting

Cultured cells were lysed with RIPA lysis buffer containing 50 mM Tris-HCl, 150 mM NaCl, 1% NP-40, 0.5% sodium deoxycholate, and 0.1% SDS (Boston BioProducts, BP-115), and supplemented with protease and phosphatase inhibitor cocktail (ThermoFisher Scientific, 78842). Protein concentration of each sample was determined with Bradford Assay using the Protein Assay Dye Reagent Concentrate (Bio-Rad, 5000006). Equal amounts of protein extracts were mixed with 4 x Laemmli sample buffer (Bio-Rad, 161-0747) and separated by electrophoresis on 4-12% NuPAGE Bis-Tris Mini Gel (Invitrogen, NP0336), and then transferred using the Trans-Blot® Turbo™ Transfer System (Bio-Rad) onto nitrocellulose membranes (Bio-Rad, 1704159). Membranes were blocked with 5% bovine serum albumin (BSA) and incubated with corresponding primary antibodies and horseradish peroxidase-conjugated secondary antibodies. The immunoreactivity was detected with SuperSignal™ West Pico Chemiluminescent Substrate (ThermoFisher Scientific, 34080) or SuperSignal™ West Femto maximum Sensitivity Substrate (ThermoFisher Scientific, 34096). Signals were captured and analyzed using the Bio-Rad ChemiDoc™ MP Imaging system and the Image Lab™ Software (Bio-Rad).

Nuclear Protein Fractionation

Nuclear proteins were fractionated from total cell lysates using the NE-PER™ Nuclear and Cytoplasmic Extraction Reagents (ThermoFisher Scientific, 78833) according to the manufacturer's protocol. Cytosolic and nuclear fractions were analyzed by western blot and

Tubulin was used as the loading control for cytosolic proteins while Histone H3 was used as the loading control for nuclear proteins.

Chromatin Immunoprecipitation (ChIP) -qPCR

ChIP was performed using the SimpleChIP® Plus Enzymatic Chromatin IP Kit (Cell Signaling, 9004) according to the manufacturer's protocol. U87EGFRvIII cells were treated with DMSO or 250nM Torin1 for 24 h and fixed in 1% formaldehyde to crosslink proteins with DNA. Nuclear extracts were prepared with Micrococcal Nuclease digestion and following sonication in a water bath sonicator. Chromatin was immunoprecipitated with Nrf2 or ATF4 antibody at 1:50 dilution. Immunoprecipitated chromatin was washed and eluted, and purified DNA was used for RT-PCR using specific primers for xCT promoter, xCT intron 1 as negative control or NQO1 and ASNS promoter as positive control for Nrf2 and ATF4 to quantify transcription factor binding. Recoveries were calculated as percent of input.

Primer sequences used for RT-PCR are listed as follows:

xCT promoter forward: 5′-TGAGTAATGCTGGAGGCTTCTC-3′

xCT promoter reverse: 5′-TATTTAAGCGCCTGCCTGTC-3′

xCT intron1 forward: 5′-ATTGCAGGGAGTGTGCTCTT-3′

xCT intron1 reverse: 5′-TCAGATTTTGCTTTGCTTGC-3′

NQO1 promoter forward: 5′-CCCTTTTAGCCTTGGCACGAAA-3′

NQO1 promoter reverse: 5′-TGCACCCAGGGAAGTGTGTTGTAT-3′

ASNS promoter forward: 5'- GCAGGCATGATGAAACTTCC-3'

ASNS promoter reverse: 5'- AGGGATGTGGACAGCTTGAC-3'

siRNA, shRNA transfection and generation of stable cell lines

Transfection of siRNA into cells were performed using Lipofectamine® RNAiMAX Transfection Reagent (ThermoFisher Scientific, 13778150) in DMEM supplemented with 10% FBS. Media were changed after 24 h of transfection and cells were harvested 48 h post-transfection or with an additional 24 h of drug treatment. siRNA for Rictor was obtained from ThermoSCIENTIFIC (L-016984-00-0005), and siRNA for xCT was customed synthesized by ThermoSCIENTIFIC with the sequence: Sense: 5'-AGAAAUCUGGAGGUCAUUAdTdT-3', Antisense: 5'-UAAUGACCUCCAGAUUUCUdTdT-3'. Generation of stable cell lines was performed using the lentiviral delivering system. Lentivirus was packaged using 293T cells by co-transfecting cells with lentiviral packaging plasmid and DNA constructs containing gene of interest. Virus were collected and used to infect GBM cells in the presence of 12.5 μg/ml Polybrene Infection / Transfection Reagent (EMD Millipore, TR-1003-G). Media were changed after 24 h and cells were selected for one week before used for experiments and maintained cultured with 1 μg/ml puromycin. Raptor and Rictor shRNAs were obtained from Addgene.

Real-Time PCR (RT-PCR)

Total RNA was extracted using the RNeasy Mini Kit (Qiagen, 74106). RNA concentrations were measured and 1 μg of RNA was used from each sample for cDNA synthesis using the SuperScript® VILO™ cDNA Synthesis Kit (ThermoFisher Scientific, 11754050). RT-PCR was performed using the 2 x SYBR Green qPCR Master Mix (Bimake, B21202) on the CFX96 Real-Time PCR Detection System (Bio-Rad) following the manufacturer's instructions. Results were analyzed using the delta delta Ct method and TPB was used as the reference gene. Primer sequences used are:

xCT forward: 5’-CAGGAGAAAGTGCAGCTGAA-3’,

xCT reverse: 5’-CTCCAATGATGGTGCCAATG-3’,

TBP forward: 5’-GAGCTGTGATGTGAAGTTTCC-3’

TBP reverse: 5’-TCTGGGTTTGATCATTCTGTAG-3’.

Cell Surface Protein Purification

Cell Surface proteins were purified using the Pierce™ Cell Surface Protein Isolation Kit (ThermoFisher Scientific, 89881) according to manufacturer’s instructions. Briefly, cells were washed with cold PBS and incubated with Sulfo-NHS-SS-Biotin at 4°C for 30min to label cell surface proteins. After labeling the reaction was quenched and cells were collected and lysed. Protein concentrations of lysates were determined using Bradford assay and equal amount of proteins from each sample were incubated with NeutrAvidin Agarose gels at 4 °C overnight to purify labeled cell surface proteins. After incubation proteins were eluted and subject to electrophoresis and immunoblotting analysis.

Statistical Analysis

Data were all collected from at least three independent replicates and presented as mean ± SEM unless otherwise indicated. Statistical analysis was performed using unpaired Student’s t test unless otherwise indicated. Statistical significance was indicated as * $p < 0.05$, ** $p < 0.01$, *** $p < 0.001$, and n.s. as not statistically significant.

Complete Data Analysis of LC-MS/MS Metabolomics with [U-13C6]-D-Glucose and [U-13C5]-L-Glutamine Labeling

See Appendix II

REFERENCES

Alberghina, L., and Gaglio, D. (2014). Redox control of glutamine utilization in cancer. Cell death & disease *5*, e1561.

Altman, B.J., Stine, Z.E., and Dang, C.V. (2016). From Krebs to clinic: glutamine metabolism to cancer therapy. Nature reviews Cancer *16*, 619-634.

Babic, I., Anderson, E.S., Tanaka, K., Guo, D., Masui, K., Li, B., Zhu, S., Gu, Y., Villa, G.R., Akhavan, D., *et al.* (2013). EGFR mutation-induced alternative splicing of Max contributes to growth of glycolytic tumors in brain cancer. Cell metabolism *17*, 1000-1008.

Chung, W.J., Lyons, S.A., Nelson, G.M., Hamza, H., Gladson, C.L., Gillespie, G.Y., and Sontheimer, H. (2005). Inhibition of cystine uptake disrupts the growth of primary brain tumors. The Journal of neuroscience : the official journal of the Society for Neuroscience *25*, 7101-7110.

Cloughesy, T.F., Yoshimoto, K., Nghiemphu, P., Brown, K., Dang, J., Zhu, S., Hsueh, T., Chen, Y., Wang, W., Youngkin, D., *et al.* (2008). Antitumor activity of rapamycin in a Phase I trial for patients with recurrent PTEN-deficient glioblastoma. PLoS medicine *5*, e8.

Dienstmann, R., Rodon, J., Serra, V., and Tabernero, J. (2014). Picking the point of inhibition: a comparative review of PI3K/AKT/mTOR pathway inhibitors. Molecular cancer therapeutics *13*, 1021-1031.

Faivre, S., Kroemer, G., and Raymond, E. (2006). Current development of mTOR inhibitors as anticancer agents. Nature reviews Drug discovery *5*, 671-688.

Fan, J., Ye, J., Kamphorst, J.J., Shlomi, T., Thompson, C.B., and Rabinowitz, J.D. (2014). Quantitative flux analysis reveals folate-dependent NADPH production. Nature *510*, 298-302.

Fruman, D.A., and Rommel, C. (2014). PI3K and cancer: lessons, challenges and opportunities. Nature reviews Drug discovery *13*, 140-156.

Gini, B., Zanca, C., Guo, D., Matsutani, T., Masui, K., Ikegami, S., Yang, H., Nathanson, D., Villa, G.R., Shackelford, D., *et al.* (2013). The mTOR kinase inhibitors, CC214-1 and CC214-2, preferentially block the growth of EGFRvIII-activated glioblastomas. Clinical cancer research : an official journal of the American Association for Cancer Research *19*, 5722-5732.

Grabiner, B.C., Nardi, V., Birsoy, K., Possemato, R., Shen, K., Sinha, S., Jordan, A., Beck, A.H., and Sabatini, D.M. (2014). A diverse array of cancer-associated MTOR mutations are hyperactivating and can predict rapamycin sensitivity. Cancer discovery *4*, 554-563.

Heffron, T.P. (2016). Small Molecule Kinase Inhibitors for the Treatment of Brain Cancer. Journal of medicinal chemistry.

Heffron, T.P., Ndubaku, C.O., Salphati, L., Alicke, B., Cheong, J., Drobnick, J., Edgar, K., Gould, S.E., Lee, L.B., Lesnick, J.D., *et al.* (2016). Discovery of Clinical Development Candidate GDC-0084, a Brain Penetrant Inhibitor of PI3K and mTOR. ACS medicinal chemistry letters *7*, 351-356.

Hollander, M.C., Blumenthal, G.M., and Dennis, P.A. (2011). PTEN loss in the continuum of common cancers, rare syndromes and mouse models. Nature reviews Cancer *11*, 289-301.

Ishii, T., Itoh, K., Takahashi, S., Sato, H., Yanagawa, T., Katoh, Y., Bannai, S., and Yamamoto, M. (2000). Transcription factor Nrf2 coordinately regulates a group of oxidative stress-inducible genes in macrophages. The Journal of biological chemistry *275*, 16023-16029.

Iyer, G., Hanrahan, A.J., Milowsky, M.I., Al-Ahmadie, H., Scott, S.N., Janakiraman, M., Pirun, M., Sander, C., Socci, N.D., Ostrovnaya, I., *et al.* (2012). Genome sequencing identifies a basis for everolimus sensitivity. Science *338*, 221.

Jiang, L., Kon, N., Li, T., Wang, S.J., Su, T., Hibshoosh, H., Baer, R., and Gu, W. (2015). Ferroptosis as a p53-mediated activity during tumour suppression. Nature *520*, 57-62.

Li, J., Shin, S., Sun, Y., Yoon, S.O., Li, C., Zhang, E., Yu, J., Zhang, J., and Blenis, J. (2016). mTORC1-Driven Tumor Cells Are Highly Sensitive to Therapeutic Targeting by Antagonists of Oxidative Stress. Cancer research *76*, 4816-4827.

Lorenz, M.C., and Heitman, J. (1995). TOR mutations confer rapamycin resistance by preventing interaction with FKBP12-rapamycin. J Biol Chem *270*, 27531-27537.

Masui, K., Cavenee, W.K., and Mischel, P.S. (2015). mTORC2 and Metabolic Reprogramming in GBM: at the Interface of Genetics and Environment. Brain pathology *25*, 755-759.

Masui, K., Tanaka, K., Akhavan, D., Babic, I., Gini, B., Matsutani, T., Iwanami, A., Liu, F., Villa, G.R., Gu, Y., *et al.* (2013). mTOR complex 2 controls glycolytic metabolism in glioblastoma through FoxO acetylation and upregulation of c-Myc. Cell metabolism *18*, 726-739.

Palm, W., Park, Y., Wright, K., Pavlova, N.N., Tuveson, D.A., and Thompson, C.B. (2015). The Utilization of Extracellular Proteins as Nutrients Is Suppressed by mTORC1. Cell *162*, 259-270.

Rodrik-Outmezguine, V.S., Okaniwa, M., Yao, Z., Novotny, C.J., McWhirter, C., Banaji, A., Won, H., Wong, W., Berger, M., de Stanchina, E., *et al.* (2016). Overcoming mTOR resistance mutations with a new-generation mTOR inhibitor. Nature *534*, 272-276.

Sasaki, H., Sato, H., Kuriyama-Matsumura, K., Sato, K., Maebara, K., Wang, H., Tamba, M., Itoh, K., Yamamoto, M., and Bannai, S. (2002). Electrophile response element-mediated induction of the cystine/glutamate exchange transporter gene expression. The Journal of biological chemistry *277*, 44765-44771.

Sato, H., Nomura, S., Maebara, K., Sato, K., Tamba, M., and Bannai, S. (2004). Transcriptional control of cystine/glutamate transporter gene by amino acid deprivation. Biochemical and biophysical research communications *325*, 109-116.

Shackelford, D.B., and Shaw, R.J. (2009). The LKB1-AMPK pathway: metabolism and growth control in tumour suppression. Nature reviews Cancer *9*, 563-575.

Thoreen, C.C., Kang, S.A., Chang, J.W., Liu, Q., Zhang, J., Gao, Y., Reichling, L.J., Sim, T., Sabatini, D.M., and Gray, N.S. (2009). An ATP-competitive mammalian target of rapamycin inhibitor reveals rapamycin-resistant functions of mTORC1. J Biol Chem *284*, 8023-8032.

Vander Heiden, M.G., Cantley, L.C., and Thompson, C.B. (2009). Understanding the Warburg effect: the metabolic requirements of cell proliferation. Science *324*, 1029-1033.

Wagle, N., Grabiner, B.C., Van Allen, E.M., Amin-Mansour, A., Taylor-Weiner, A., Rosenberg, M., Gray, N., Barletta, J.A., Guo, Y., Swanson, S.J., *et al.* (2014). Response and acquired

resistance to everolimus in anaplastic thyroid cancer. The New England journal of medicine *371*, 1426-1433.

Wander, S.A., Hennessy, B.T., and Slingerland, J.M. (2011). Next-generation mTOR inhibitors in clinical oncology: how pathway complexity informs therapeutic strategy. The Journal of clinical investigation *121*, 1231-1241.

Wang, M.Y., Lu, K.V., Zhu, S., Dia, E.Q., Vivanco, I., Shackleford, G.M., Cavenee, W.K., Mellinghoff, I.K., Cloughesy, T.F., Sawyers, C.L., *et al.* (2006). Mammalian target of rapamycin inhibition promotes response to epidermal growth factor receptor kinase inhibitors in PTEN-deficient and PTEN-intact glioblastoma cells. Cancer research *66*, 7864-7869.

Wei, W., Shin, Y.S., Xue, M., Matsutani, T., Masui, K., Yang, H., Ikegami, S., Gu, Y., Herrmann, K., Johnson, D., *et al.* (2016). Single-Cell Phosphoproteomics Resolves Adaptive Signaling Dynamics and Informs Targeted Combination Therapy in Glioblastoma. Cancer cell *29*, 563-573.

Yang, M., and Vousden, K.H. (2016). Serine and one-carbon metabolism in cancer. Nature reviews Cancer *16*, 650-662.

Yuan, T.L., and Cantley, L.C. (2008). PI3K pathway alterations in cancer: variations on a theme. Oncogene *27*, 5497-5510.

Chapter 4

Targeting Metabolic Co-dependencies to Overcome Therapeutic Resistance in GBM

INTRODUCTION

Acquisition of oncogenic mutations or loss of tumor suppressors are commonly seen during tumorigenesis and are responsible for driving tumor cell proliferation as well as reprogramming of tumor cell metabolism. While granting a specific population of tumor cells with proliferative advantages, such oncogenic mutations also become indispensable for tumor cell survival as inhibition of oncogenes or reconstitution of tumor suppressors are usually lethal, as it is so-called the "oncogene addiction". This has set the foundation for modern cancer targeted therapies and achieved great success in certain cases, such as the use of Gleevec for chronic myeoloid lymphoma (CML) and EGFR inhibitors for non-small-cell lung cancer (NSCLC) (Luo et al., 2009). Studies in recently years have also uncovered that besides oncogene addiction, tumor cells also develop dependence on genes or pathways that are not intrinsically tumorigenic, and this is largely determined by elevated cellular stress levels, specific tumor-associated metabolic environments, as well as tumor-stromal interactions. These "non-oncogene addictions" have also become attractive targets in cancer (Galluzzi et al., 2013). For example, Piperlongumine was identified from a small molecule drug screen which targets the oxidative stress response pathway and showed profound anti-tumor effects in mouse xenograft tumors, while sparing both slow or fast dividing normal cells (Raj et al., 2011). In addition, previous study from our lab also discovered that the mutant oncogene EGFR drives a metabolic co-dependency on exogenous cholesterol in GBM, as these tumor cells reprogrammed cholesterol metabolism to take advantage of the ample cholesterol pool in the brain, which is a good example of non-oncogene addictions driven by both oncogenes and the tumor microenvironment (Villa et al., 2016). Other non-oncogene addictions include interactions between cancer and stromal cells (Sherman et al., 2014; Valencia et al., 2014; Zhang and Huang, 2011), as well as drug-induced co-dependencies

on specific signaling or metabolic pathways (Gini et al., 2013; Wei et al., 2016). Therefore, targeting these tumor-specific non-oncogene addictions might significantly improve the effect of existing oncogene-targeted therapies and prevent drug resistance.

mTOR kinase inhibitors are among the most promising drug candidates for cancer, but many cancers including GBM invariably developed drug resistance. Phosphoproteomic studies identified activation of the Src and Erk pathway as one mechanism mediating drug resistance in mTOR kinase inhibitor-resistant GBM tumors (Wei et al., 2016), while induction of autophagy as a consequence of mTORC1 inhibition serves as another resistance mechanism allowing tumor cells to survive when nutrient uptake and metabolism is suppressed (Gini et al., 2013) (see also Appendix III). While combined inhibition of Src and Erk or autophagy effectively reverted drug resistance to mTOR kinase inhibitors in GBM and prolonged tumor suppression, we also attempted to test whether targeting survival mechanisms during early phase of drug treatment could avoid development of drug resistance. Since previously it was identified from our metabolomics studies that mTOR inhibition significantly suppressed the redox capacity of GBM cells, resulting in decreased glutathione and increased mitochondria and lipid ROS, whereas xCT is upregulated to maintain glutathione synthesis, suggesting that xCT-mediated glutathione synthesis might be required for tumor cell survival upon mTOR kinase inhibition. Here we went on to determine whether inhibition of xCT or depletion of glutathione could create synthetic lethality in tumor cells when combined with mTOR kinase inhibitors. We discovered that GBM cells specifically rely on cystine uptake through xCT for glutathione synthesis and cell survival upon mTOR inhibition, and xCT or glutathione synthesis inhibitors significantly improved the anti-tumor effect and overcome drug resistance of mTOR kinase inhibitors in GBM.

RESULTS

xCT-dependent Glutathione Synthesis is Required for Maintaining Redox Homeostasis and Tumor Cell Survival upon mTOR Kinase Inhibition

To determine whether GBM cells become more dependent on glutathione synthesis for maintaining redox balance and cell survival upon mTOR kinase inhibition, we first examined whether combining glutathione depletion with mTOR kinase inhibitors affect ROS levels in GBM cells. Glutathione depletion was achieved by using cystine-free cell culture media or L-Buthionine Sulfoximine (BSO), an inhibitor of the rate-limiting enzyme GCLC in glutathione synthesis, which both significantly depleted total cellular glutathione (Fig. 4-1A). We then analyzed levels of different ROS species by flow cytometry (Fig. 4-1B, C and D) and observed that cystine-deprivation or BSO alone both increased cytosolic ROS and lipid ROS, while mitochondria ROS was unaffected. Whereas when combined with Torin1, cystine-deprivation and BSO both resulted in significant increase in all three ROS species, especially mitochondria ROS and lipid ROS. These imply that mTOR kinase inhibition sensitized GBM cells to glutathione depletion and vice versa.

To further test whether maintaining glutathione synthesis become essential for cell survival upon mTOR kinase inhibition, we quantified cell survival using Annexin V / PI staining (Fig. 4-2A and B) and observed that combining cystine-depletion or BSO with Torin1 both induced massive GBM cell death, while either alone is not sufficient. Meanwhile, cell-permeable glutathione GSHest (Fig. 4-3B), as well as antioxidants that specifically scavenges mitochondria or lipid ROS rescued cell death induced by cystine-depletion / BSO + Torin1 (Fig. 4-3C, D and E), which confirmed that the cell death is ROS-mediated. Furthermore, overexpression of xCT also

partially rescued cell death induced by BSO+Torin1 (Fig. 4-2D), supporting our hypothesis that xCT mediated-cystine uptake is crucial for maintaining glutathione synthesis and cell survival upon mTOR kinase inhibition.

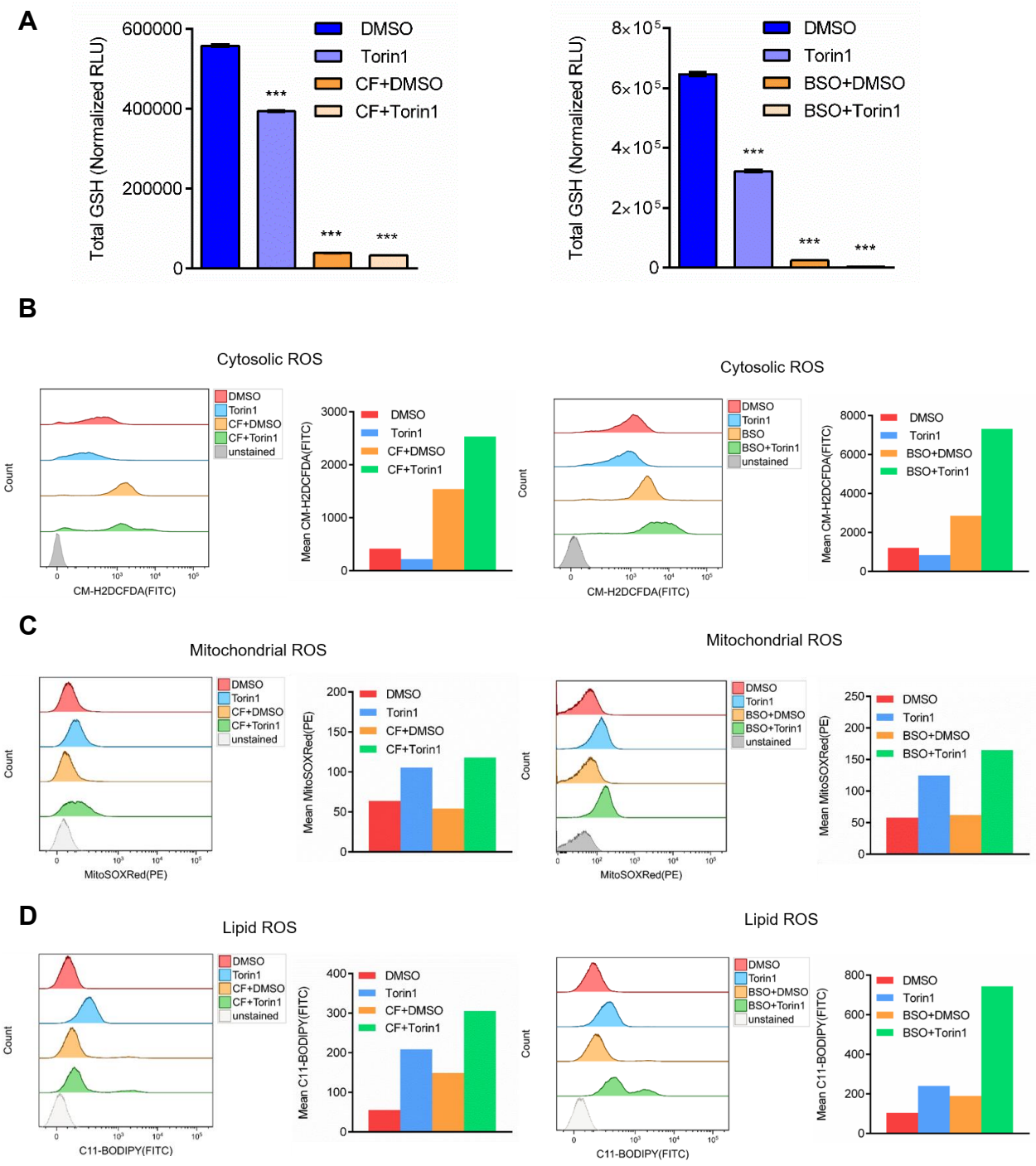

Fig. 4-1. Combining mTOR Kinase Inhibition with Glutathione Depletion Significantly Induced Mitochondria ROS and Lipid ROS in GBM Cells.

(A) Total cellular GSH levels were measured using the GSH/GSSG-GloTM Glutathione Assay Kit (Promega). U87EGFRvIII cells were treated with DMSO or 250 nM Torin1 in cystine-free media (left) or with 100 μM of BSO (right) for 24 h before total cellular GSH levels were measured and normalized to cell counts. Results were obtained from three replicate samples and data are presented as mean ± SEM. Statistical analysis was performed using one-way ANOVA. (B-D) Cytosolic ROS, mitochondria ROS and lipid ROS were analyzed by flow cytometry using CM-H2DCFDA, MitoSOXRed and C11-BODIPY. U87EGFRvIII cells were treated with DMSO or 250 nM Torin1 in cystine-free media (left) or with 100 μM of BSO (right) for 24 h before analysis.

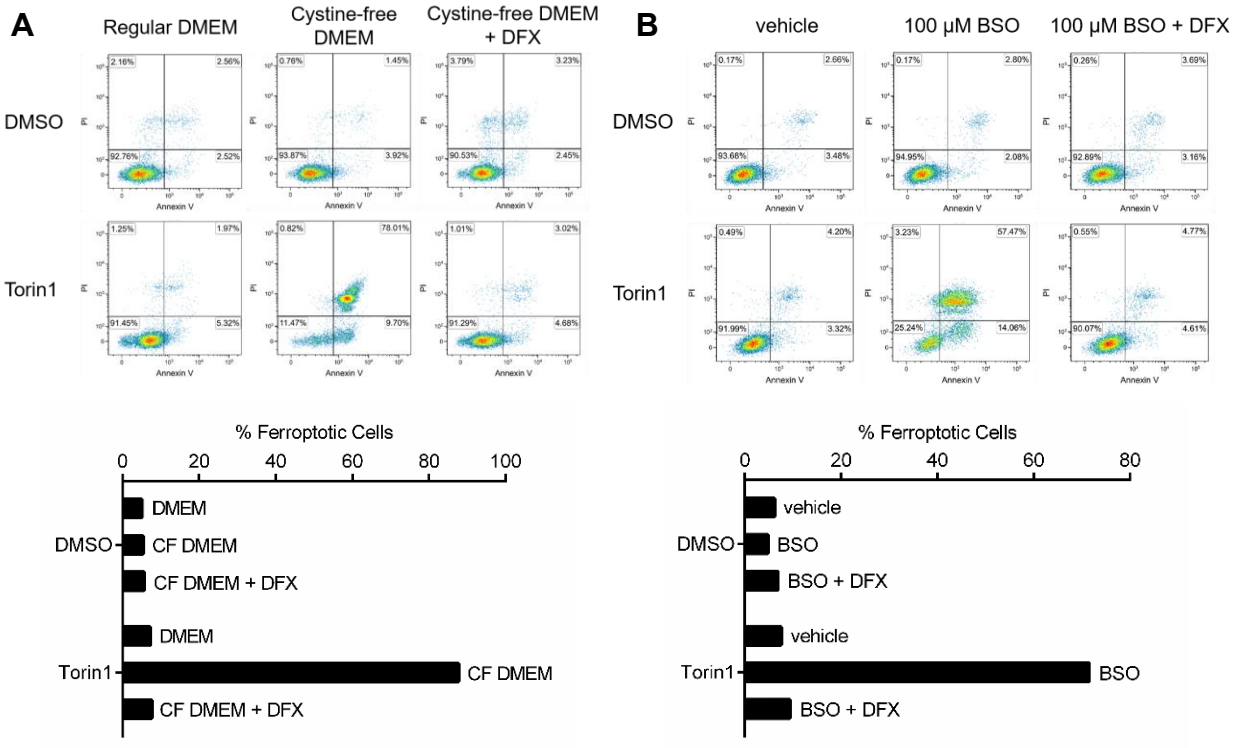
A
Regular DMEM
Cystine-free DMEM
Cystine-free DMEM + DFX
DMSO
Torin1
B
vehicle
100 μM BSO
100 μM BSO + DFX
DMSO
Torin1
% Ferroptotic Cells
0
20
40
60
80
100
DMEM
CF DMEM
CF DMEM + DFX
DMEM
CF DMEM
CF DMEM + DFX
% Ferroptotic Cells
0
20
40
60
80
vehicle
BSO
BSO + DFX
vehicle
BSO
BSO + DFX

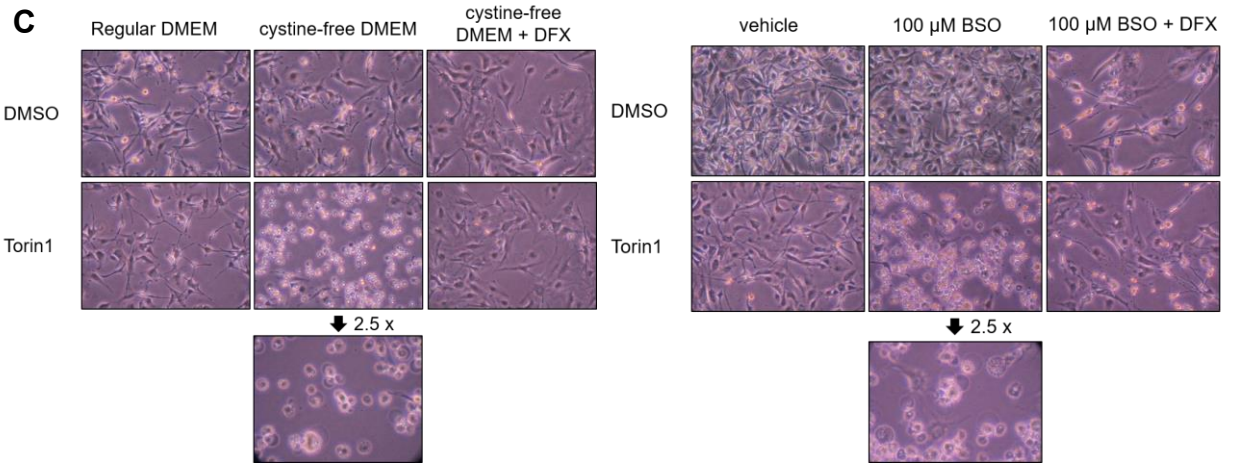
C
Regular DMEM
cystine-free DMEM
cystine-free DMEM + DFX
DMSO
Torin1
2.5 x
vehicle
100 μM BSO
100 μM BSO + DFX
DMSO
Torin1
2.5 x

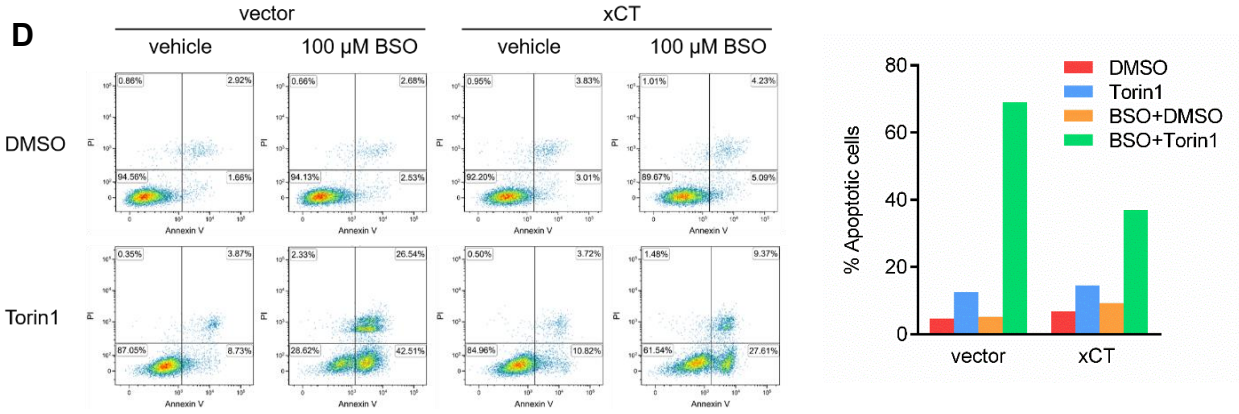
D
vector
xCT
vehicle
100 μM BSO
vehicle
100 μM BSO
DMSO
Torin1
% Apoptotic cells
80
60
40
20
0
DMSO
Torin1
BSO+DMSO
BSO+Torin1
vector
xCT

Fig. 4-2. xCT-dependent Glutathione Synthesis Protects Tumor Cells from Ferroptotic Cell Death in Response to mTOR Kinase Inhibition.

(A-B) Cell death was quantified by flow cytometry using FITC-Annexin V and propodium iodide (PI) assay. %Ferroptotic cells shown in the bar graph below was calculated by adding up the percentage of cells in the upper and lower right quadrant in each graph on the left.

(C) U87EGFRvIII cells were treated with indicated media conditions or drugs and pictures were taken at 24 h (left) or 48 h (right) when cell death was prominent. Cell death in the cystine-free DMEM + Torin1 and the BSO + Torin1 treated wells showed similar swelling and balloon-like morphology resembling ferroptotic cell death.

(D) U87EGFRvIII cells stably overexpressing xCT or vector control were treated with DMSO or 250 nM Torin1 in combination with 100 uM BSO for 48 h before cells were collected and analyzed. Cell death was quantified by flow cytometry using FITC-Annexin V and propodium iodide (PI) assay.

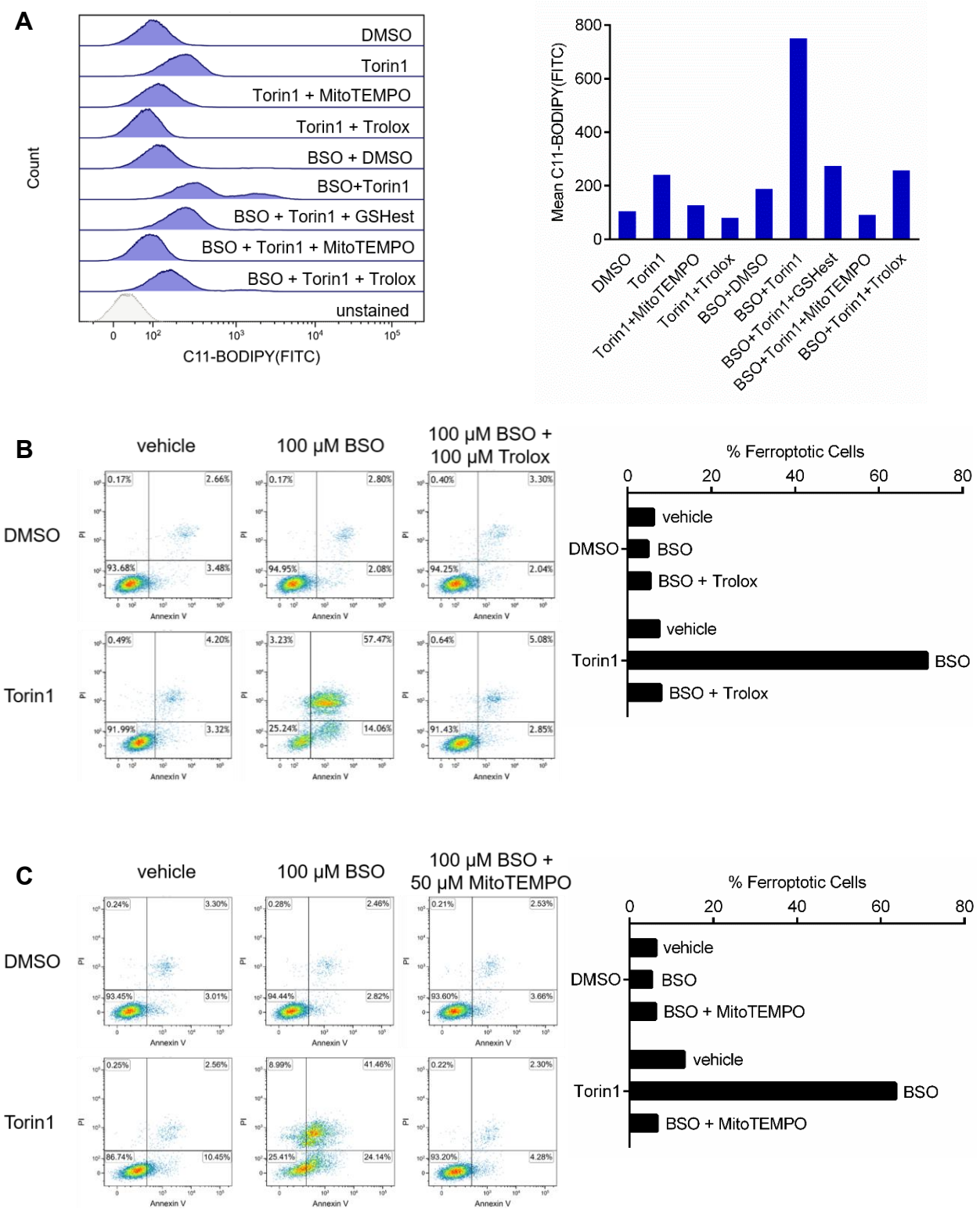
A
DMSO
Torin1
Torin1 + MitoTEMPO
Torin1 + Trolox
BSO + DMSO
BSO+Torin1
BSO + Torin1 + GSHest
BSO + Torin1 + MitoTEMPO
BSO + Torin1 + Trolox
unstained
Count
C11-BODIPY(FITC)
Mean C11-BODIPY(FITC)
B
vehicle
100 μM BSO
100 μM BSO + 100 μM Trolox
DMSO
Torin1
Annexin V
PI
% Ferroptotic Cells
vehicle
BSO
BSO + Trolox
C
100 μM BSO + 50 μM MitoTEMPO
BSO + MitoTEMPO

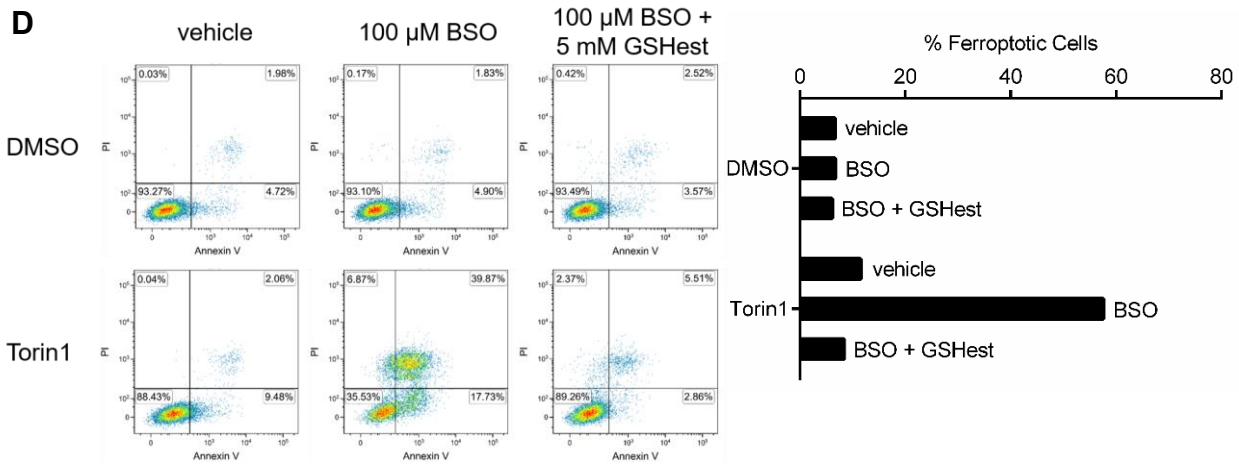
D
vehicle
100 μM BSO
100 μM BSO +
5 mM GSHest
DMSO
Torin1
0.03%
1.98%
93.27%
4.72%
0.17%
1.83%
93.10%
4.90%
0.42%
2.52%
93.49%
3.57%
0.04%
2.06%
88.43%
9.48%
6.87%
39.87%
35.53%
17.73%
2.37%
5.51%
89.26%
2.86%
PI
Annexin V
% Ferroptotic Cells
0
20
40
60
80
DMSO
vehicle
BSO
BSO + GSHest
Torin1
vehicle
BSO
BSO + GSHest

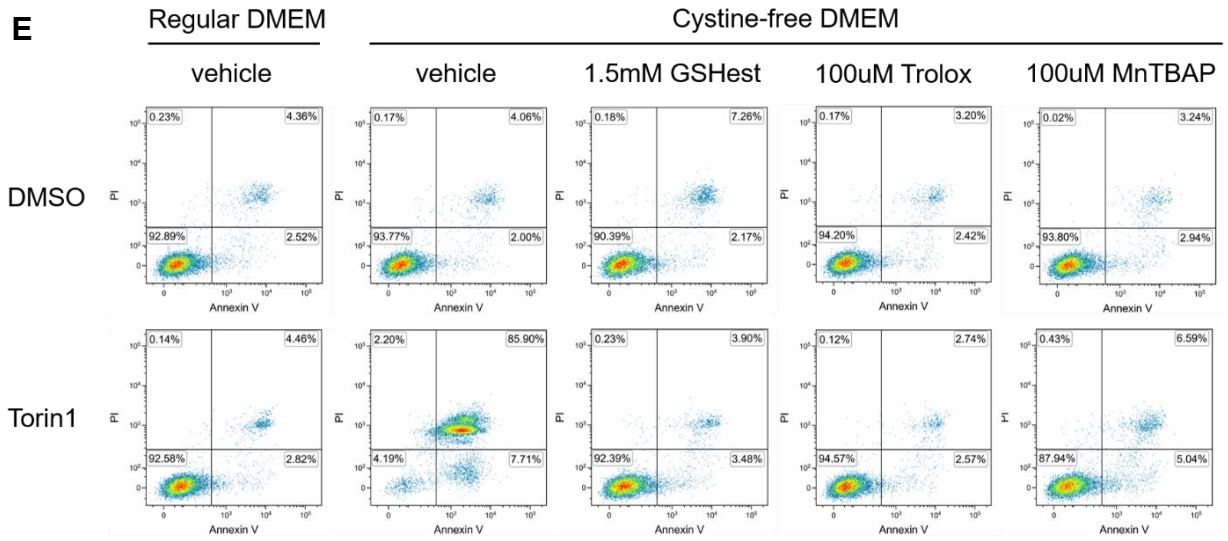
E
Regular DMEM
Cystine-free DMEM
vehicle
vehicle
1.5mM GSHest
100uM Trolox
100uM MnTBAP
DMSO
Torin1
0.23%
4.36%
92.89%
2.52%
0.17%
4.06%
93.77%
2.00%
0.18%
7.26%
90.39%
2.17%
0.17%
3.20%
94.20%
2.42%
0.02%
3.24%
93.80%
2.94%
0.14%
4.46%
92.58%
2.82%
2.20%
85.90%
4.19%
7.71%
0.23%
3.90%
92.39%
3.48%
0.12%
2.74%
94.57%
2.57%
0.43%
6.59%
87.94%
5.04%
PI
Annexin V

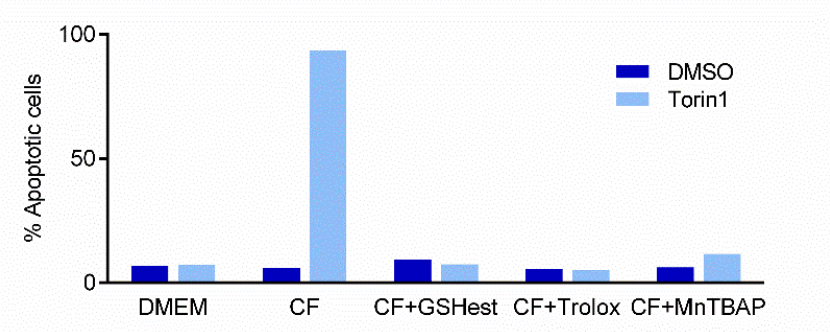
% Apoptotic cells
100
50
0
DMSO
Torin1
DMEM
CF
CF+GSHest
CF+Trolox
CF+MnTBAP

Fig. 4-3. Combined Inhibition of mTOR Kinase and Glutathione Synthesis Induced Lipid ROS-mediated Cell Death.

(A) U87EGFRvIII cells were treated with DMSO or 250 nM Torin1 in combination with 100 μM BSO and different antioxidants (5 mM GSHest: cell permeable glutathione ester; 100 μM Trolox: Vitamin E analog, cytosolic ROS and lipid ROS scavenger; 50 μM MitoTEMPO: mitochondria ROS scavenger) for 24h before cells were stained with C11-BODIPY and lipid ROS were analyzed using flow cytometry by recording the signal in the FITC channel. Histograms (left) and mean C11-BODIPY (FITC) signal (right) were shown for each treatment condition.

(B-D) U87EGFRvIII cells were treated with DMSO or 250 nM Torin1 in combination with 100 μM BSO and different antioxidants (5 mM GSHest (B): cell permeable glutathione ester; 100 μM Trolox (C): Vitamin E analog, cytosolic ROS and lipid ROS scavenger; 50 μM MitoTEMPO (D): mitochondria ROS scavenger) for 48 h before cells were collected and cell death was analyzed using flow cytometry after staining with FITC-Annexin V and PI.

(E) U87EGFRvIII cells were treated with DMSO or 250 nM Torin1 in regular DMEM or cystine-free DMEM supplemented with 5% FBS, together with different antioxidants (5 mM GSHest: cell permeable glutathione ester; 100 μM Trolox: Vitamine E analog, cytosolic ROS and lipid ROS scavenger; 100 μM MnTBAP: mitochondria ROS scavenger). Cell death was analyzed and quantified after 24 h of treatment by flow cytometry.

Combined Inhibition of mTOR Kinase and Glutathione Synthesis Triggered Ferroptotic Cell Death in GBM

Although we applied the conventional Annexin V / PI assay commonly used for apoptosis analysis to quantify cell death induced by combined inhibition of glutathione synthesis and mTOR kinase, it was observed that unlike normal apoptotic cells, the dying cells exhibit a distinct swollen, balloon-like feature under the microscope resembling that of ferroptosis (Fig. 4-2C), which has been linked to xCT regulation, glutathione depletion, lipid ROS, and can be rescued by iron-chelators such as deferoxamine (DFX) (Cao and Dixon, 2016; Dixon et al., 2012; Jiang et al., 2015). These evidence prompted us to test whether combined inhibition of glutathione synthesis and mTOR kinase induced cell death through ferroptosis in GBM. Ferroptosis inhibitors DFX, cycloheximide and the MEK inihibitor U0126 all rescued cell death induced by cystine-depletion + Torin1 (Fig. 4-2A-B and Fig. 4-4B), while other cell death modulators such as the apoptosis inhibitor z-VAD-fmk and the cell stress pathway p38 inhibitor SB239062 did not (Fig. 4-4A and B) (Dixon et al., 2012), which strongly support our hypothesis that the cell death is through ferroptosis. Consistent with this model, Erastin, which is a small molecule inhibitor of xCT and a strong ferroptosis inducer (Dixon et al., 2014; Dolma et al., 2003), caused tumor cell death in GBM cells only in the presence of Torin1 (Fig. 4-5B). In addition, while combining cystine-depletion or BSO with Torin1 induced massive cell death in multiple GBM cell lines as well as in patient-derived neurosphere lines (Fig. 4-5C), Rapamycin did not show the same effect (Fig. 4-5A). Taken together, these results demonstrate that inhibiting mTOR kinase concurrently with blocking glutathione synthesis results in massive cell death through ferroptosis in GBM.

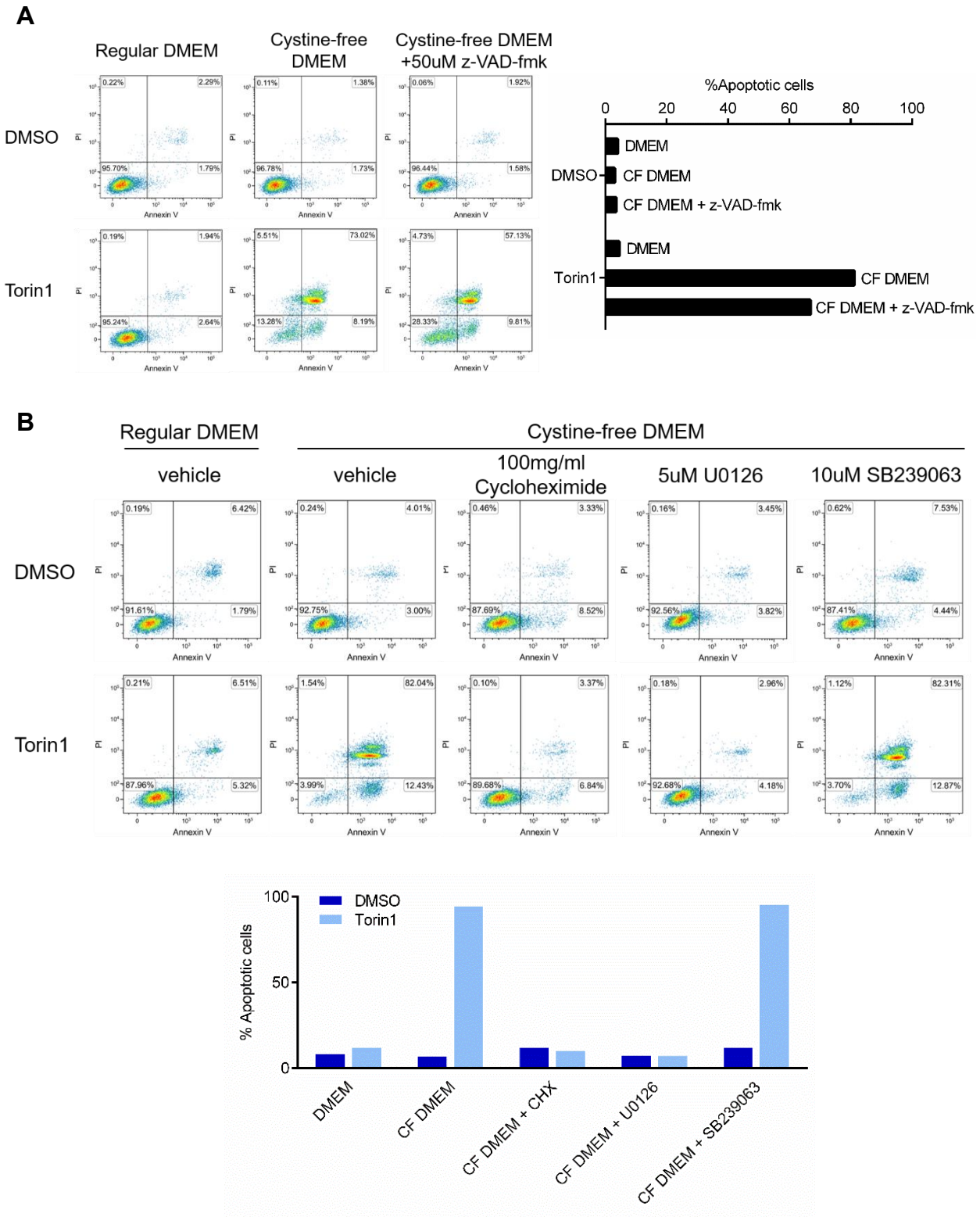
A
Regular DMEM
Cystine-free DMEM
Cystine-free DMEM +50uM z-VAD-fmk
DMSO
Torin1
0.22%
2.29%
95.70%
1.79%
0.11%
1.38%
96.78%
1.73%
0.06%
1.92%
96.44%
1.58%
0.19%
1.94%
95.24%
2.64%
5.51%
73.02%
13.28%
8.19%
4.73%
57.13%
28.33%
9.81%
Annexin V
PI
%Apoptotic cells
0
20
40
60
80
100
DMEM
CF DMEM
CF DMEM + z-VAD-fmk
DMEM
CF DMEM
CF DMEM + z-VAD-fmk
B
Regular DMEM
Cystine-free DMEM
vehicle
vehicle
100mg/ml Cycloheximide
5uM U0126
10uM SB239063
DMSO
Torin1
0.19%
6.42%
91.61%
1.79%
0.24%
4.01%
92.75%
3.00%
0.46%
3.33%
87.69%
8.52%
0.16%
3.45%
92.56%
3.82%
0.62%
7.53%
87.41%
4.44%
0.21%
6.51%
87.96%
5.32%
1.54%
82.04%
3.99%
12.43%
0.10%
3.37%
89.68%
6.84%
0.18%
2.96%
92.68%
4.18%
1.12%
82.31%
3.70%
12.87%
Annexin V
PI
100
50
0
% Apoptotic cells
DMSO
Torin1
DMEM
CF DMEM
CF DMEM + CHX
CF DMEM + U0126
CF DMEM + SB239063

Fig. 4-4. mTOR Kinase Inhibition Induces Cell Death through Ferroptosis when Combined with Cystine Depletion.

(A) U87EGFRvIII cells were treated in regular or cystine-free DMEM supplemented with 5% FBS with DMSO or 250 nM Torin1 with or without the apoptosis inhibitor z-VAD-fmk for 24 h. Cell death was quantified by flow cytometry using FITC-Annexin V / PI assay.

(B) U87EGFRvIII cells were treated with DMSO or 250 nM Torin1 in regular DMEM or cystine-free DMEM supplemented with 5% FBS with 100 mg/ml cycloheximide, 5 μM U0126, 10 μM SB239063 or vehicle control for 24 h. Cell death was analyzed by flow cytometry after FITC-Annexin V / PI staining and quantification was shown in the bar graph below.

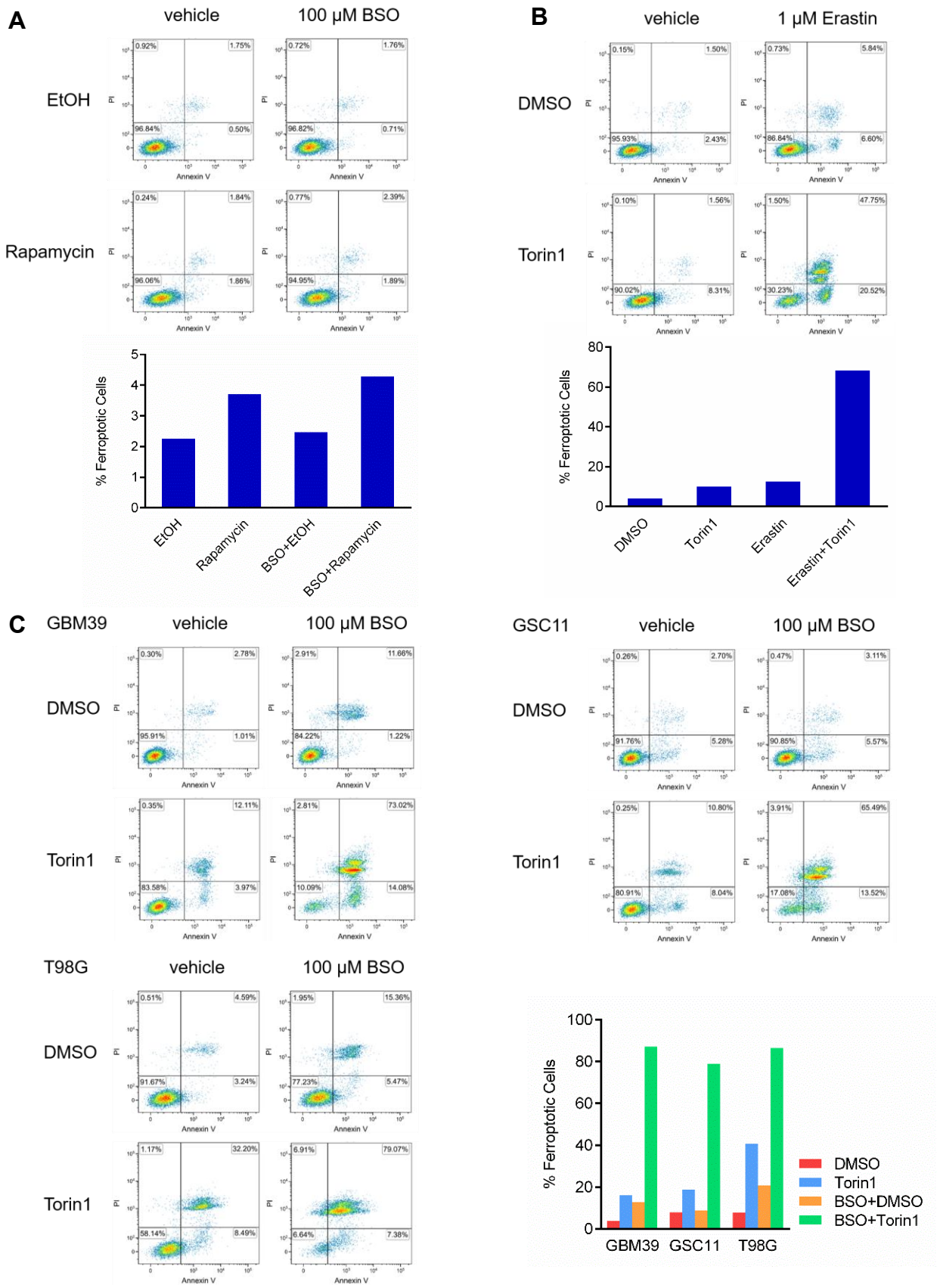
A
vehicle
100 μM BSO
EtOH
Rapamycin
Annexin V
PI
% Ferroptotic Cells
EtOH
Rapamycin
BSO+EtOH
BSO+Rapamycin
B
vehicle
1 μM Erastin
DMSO
Torin1
% Ferroptotic Cells
DMSO
Torin1
Erastin
Erastin+Torin1
C
GBM39
GSC11
T98G
vehicle
100 μM BSO
DMSO
Torin1
% Ferroptotic Cells
GBM39
GSC11
T98G
DMSO
Torin1
BSO+DMSO
BSO+Torin1

Fig. 4-5. Combined Inhibition of mTOR Kinase and Glutathione Metabolism Resulted in Massive Cell Death through Ferroptosis in GBM.

(A) U87EGFRvIII cells were treated with 10 nM rapamycin together with 100 μM BSO for 48 h and cell death was analyzed by flow cytometry after staining with FITC-Annexin V and PI and quantified as described previously.

(B) U87EGFRvIII cells were treated with DMSO or 250 nM Torin1 with or without 1 μM erastin. Cells were collected and stained with FITC-Annexin V and PI after 24 h of treatment and cell death was analyzed using flow cytometry and quantified as described previously.

(C) BSO + Torin1 treatment was tested in additional GBM cell line T98G and patient-derived neurosphere lines GBM39 and GSC11. Cell death was quantified by flow cytometry using FITC-Annexin V / PI assay as described in previous figures.

DISCUSSION

The metabolic flexibility of cancer cells allows them to rapidly adapt to the changing environment and respond to cellular stress, which also commonly mediates resistance to drug treatments. Here we took one step further and looked into whether GBM cells become dependent on xCT-mediated cystine uptake and glutathione synthesis for survival upon mTOR inhibition. We found that targeting this metabolic co-dependency by combining inhibition of mTOR kinase and glutathione depletion triggered massive GBM cell death through ferroptosis, which is a specific form of regulated necrosis recently identified. Ferroptosis is iron-dependent, lipid-ROS mediated, non-rescuable by apoptosis inhibitors, and can be induced by xCT inhibition, glutathione depletion as well as inhibition of the mitochondria glutathione peroxidase Gpx4 (Cao and Dixon, 2016; Dixon and Stockwell, 2014; Yang and Stockwell, 2016). GBM cells are in fact relatively resistant to ferroptosis, as cell survival was largely unaffected despite significant depletion of cellular glutathione by cystine deprivation or BSO, possibly due to upregulation of glutathione synthesis as well as the thioredoxin pathway (Harris et al., 2015). While glutathione depletion alone is not sufficient to induce lipid peroxidation and ferroptosis in GBM cells, the addition of mTOR kinase inhibition greatly synergized by increasing mitochondria ROS, especially as mitochondria membranes are composed of a higher ratio of unsaturated lipids and are more prone to oxidative damage (Valencak and Azzu, 2014). In fact, treating GBM cells with mTOR kinase inhibitors alone is already sufficient to increase lipid ROS, which is further enhanced by glutathione depletion. While the detailed mechanisms of how mTOR kinase inhibition induces mitochondria ROS and which mTOR complex is responsible for this effect still needs to be determined, a recent unbiased chemical screen revealed a similar finding that BSO can synergize with mTORC1 inhibition to induce cell death in Tsc2-/- cells, and suggested

that it's likely a consequence of the inability to buffer elevated mitochondrial ROS (Li et al., 2016). We also tested the combination of BSO with rapamycin but didn't observe any cytotoxic effect in GBM cells, suggesting that additional mTORC2-mediated mechanisms such as regulation of xCT might also contribute to the resistance of ferroptosis in GBM. Therefore it would require inhibition of both mTOR complexes to synergize with BSO in order to trigger ferroptotic cell death in GBM. As several mTOR kinase inhibitors are currently under clinical development with new generations of inhibitors being discovered with better efficacy and brain penetrance (Faivre et al., 2006; Rodrik-Outmezguine et al., 2016; Wander et al., 2011), while BSO have been tested in cancer patients including GBM in early phase clinical trials and showed specific accumulation in brain tumors (Fekete et al., 1990; Robe et al., 2006), it will be very exciting to see the combination approaches being tested in future studies, especially with next generation mTOR kinase inhibitors that have more favorable pharmacokinetic profiles.

EXPERIMENTAL PROCEDURES

Cell Culture

U87EGFRvIII isogenic cell lines were established as described previously (Wang et al., 2006). All cells were cultured in DMEM (CORNING, 10-013) supplemented with 10% FBS (Omega Scientific) in a humidified incubator with 5% CO2 at 37 °C unless specifically noted. GBM39, and GSC11 patient-derived neurosphere lines were cultured in NeuroCult medium (STEMCELL Technologies, 05751) supplemented with epidermal growth factor (Sigma, E9644), fibroblast growth factor (Sigma, F0291), and heparin (Sigma, H3149).

Reagents and Drugs

Reagents and drugs used include: Torin1 (Tocris Bioscience, 4247), L-Buthionine-sulfoximine (BSO, Sigma, 2515), Deferoxamine mesylate salt (DFX, Sigma, D9533), Rapamycin (Sigma, R0395), Glutathione reduced ethyl ester (GSHest, Sigma, G1404), Trolox (Sigma, 238813), MitoTEMPO (Sigma, SML0737), MnTBAP (Sigma, 475870), z-VAD-fmk (Selleckchem, S7023), cycloheximide (CHX, Sigma, C4859), U0126 (EMD Millipore, 19-147), SB239063 (Tocris Bioscience, 1962), Erastin (Sigma, E7781).

Total Glutathione Measurement

Total cellular glutathione was measured using the GSH/GSSG-GloTM Assay Kit (Promega, V6611). Briefly, cells were seeded at 1000 cells/well in 96 well plates and treated with indicated drug or incubated with specific media conditions. For cystine depletion experiments cells were incubated with cystine-free DMEM (CORNING, 17-204-CI) supplemented with L-methionine

(MP BIOMEDICALS, 02194707) and L-glutamine (CORNING, 61-030). After treatment media was removed and cells were lysed on a plate shaker for 5min with Total Glutathione Reagent provided by the kit and transferred to a white 96 well plate. Subsequent reagents were added following manufacturer's protocol and luminescence was measured using a Tecan Infinite M1000 microplate reader (Tecan) and normalized to cell counts from parallel wells for each treatment condition.

Cytosolic ROS and Mitochondria ROS Measurement

Cells were seeded in 6 well plates and incubated with indicated drug or media. After treatment, media was removed and cells were washed with 1x PBS before incubated with the CM-H2DCFDA (ThermoFisher Scientific, C6827) or the MitoSOX^{TM} Red Mitochondria Superoxide Indicator (ThermoFisher Scientific, M36008) according to manufacturer's protocol. After incubation cells were trypsinized and collect for flow cytometry analysis using the BD LSRII flow cytometer (BD Biosciences) and signals were recorded from 10,000 events using the FITC channel for CM-H2DCFDA and PE channel for MitoSOXRed. And data analysis was performed using the Kaluza Analysis Software (Beckman Coulter).

Lipid ROS Measurement

Cells were seeded in 6 well plates and treated with indicated drugs. After treatment, media was removed and cells were washed with 1x PBS before incubated with the lipid peroxidation sensor BODIPY® 581/591 C11 (ThermoFisher Scientific, D3861) according to manufacturer's protocol. After incubation cells were trypsinized and collect for flow cytometry analysis using the BD LSRII flow cytometer (BD Biosciences) and signals were recorded from 10,000 events using the

FITC channel. And data analysis was performed using the Kaluza Analysis Software (Beckman Coulter).

DNA Constructs and Generation of xCT mutants

myc-FLAG-tagged xCT plasmid were obtained from Origene (RC204136) and the myc-FLAG-tagged xCT ORF was cloned into the lentiviral expression vector pLVX-Puro (Clontech, 632164) for generation of xCT stable overexpression cell lines.

DNA plasmid, siRNA, shRNA transfection and Generation of stable cell lines

Generation of stable cell lines was performed using the lentiviral delivering system. Lentivirus was packaged using 293T cells by co-transfecting cells with lentiviral packaging plasmid and DNA constructs containing gene of interest. Transfection of DNA plasmids were performed using X-tremeGENE HP (Roche, 06366236001) in DMEM supplemented with 10% FBS. Media were changed after 24 h of transfection and virus were collected from supernatant after another 48 h of incubation and used to infect GBM cells in the presence of 12.5 μg/ml Polybrene Infection / Transfection Reagent (EMD Millipore, TR-1003-G). Media were changed after 24 h and cells were selected for one week before used for experiments and maintained cultured with 1 μg/ml puromycin.

FITC-Annexin V / PI Apoptosis Assay

Cells were seeded in 6-well plates at optimal density. Next day media was changed to regular DMEM or cystine-free DMEM supplemented with 5% FBS (Gemini bio-products) together with

indicated drug treatment for experiments with established cancer cell lines. For patient-derived neurosphere lines, cells were grown adherent on laminin-coated 6-well plates and treated with drugs in DMEM F12 media supplemented with B27, EGF, FGF heparin and Glutamax. Cells were trypsinized, collected and combined with media supernatant to ensure collection of the dead cells. Cell death analysis was performed using the FITC Annexin V Apoptosis Detection Kit I (BD Biosciences) according to the manufacturer's protocol. Samples were analyzed by flow cytometry using the BD LSRII flow cytometer (BD Biosciences). Data analysis was performed using the Kaluza Analysis Software (Beckman Coulter).

Additional Mechanisms Mediating mTOR inhibitor Resistance in GBM

See Appendix III

REFERENCES

Cao, J.Y., and Dixon, S.J. (2016). Mechanisms of ferroptosis. Cellular and molecular life sciences : CMLS *73*, 2195-2209.

Dixon, S.J., Lemberg, K.M., Lamprecht, M.R., Skouta, R., Zaitsev, E.M., Gleason, C.E., Patel, D.N., Bauer, A.J., Cantley, A.M., Yang, W.S., *et al.* (2012). Ferroptosis: an iron-dependent form of nonapoptotic cell death. Cell *149*, 1060-1072.

Dixon, S.J., Patel, D.N., Welsch, M., Skouta, R., Lee, E.D., Hayano, M., Thomas, A.G., Gleason, C.E., Tatonetti, N.P., Slusher, B.S., *et al.* (2014). Pharmacological inhibition of cystine-glutamate exchange induces endoplasmic reticulum stress and ferroptosis. eLife *3*, e02523.

Dixon, S.J., and Stockwell, B.R. (2014). The role of iron and reactive oxygen species in cell death. Nature chemical biology *10*, 9-17.

Dolma, S., Lessnick, S.L., Hahn, W.C., and Stockwell, B.R. (2003). Identification of genotype-selective antitumor agents using synthetic lethal chemical screening in engineered human tumor cells. Cancer cell *3*, 285-296.

Faivre, S., Kroemer, G., and Raymond, E. (2006). Current development of mTOR inhibitors as anticancer agents. Nature reviews Drug discovery *5*, 671-688.

Fekete, I., Griffith, O.W., Schlageter, K.E., Bigner, D.D., Friedman, H.S., and Groothuis, D.R. (1990). Rate of buthionine sulfoximine entry into brain and xenotransplanted human gliomas. Cancer research *50*, 1251-1256.

Galluzzi, L., Kepp, O., Vander Heiden, M.G., and Kroemer, G. (2013). Metabolic targets for cancer therapy. Nature reviews Drug discovery *12*, 829-846.

Gini, B., Zanca, C., Guo, D., Matsutani, T., Masui, K., Ikegami, S., Yang, H., Nathanson, D., Villa, G.R., Shackelford, D., *et al.* (2013). The mTOR kinase inhibitors, CC214-1 and CC214-2,

preferentially block the growth of EGFRvIII-activated glioblastomas. Clinical cancer research : an official journal of the American Association for Cancer Research *19*, 5722-5732.

Harris, I.S., Treloar, A.E., Inoue, S., Sasaki, M., Gorrini, C., Lee, K.C., Yung, K.Y., Brenner, D., Knobbe-Thomsen, C.B., Cox, M.A., *et al.* (2015). Glutathione and thioredoxin antioxidant pathways synergize to drive cancer initiation and progression. Cancer cell *27*, 211-222.

Jiang, L., Kon, N., Li, T., Wang, S.J., Su, T., Hibshoosh, H., Baer, R., and Gu, W. (2015). Ferroptosis as a p53-mediated activity during tumour suppression. Nature *520*, 57-62.

Li, J., Shin, S., Sun, Y., Yoon, S.O., Li, C., Zhang, E., Yu, J., Zhang, J., and Blenis, J. (2016). mTORC1-Driven Tumor Cells Are Highly Sensitive to Therapeutic Targeting by Antagonists of Oxidative Stress. Cancer research *76*, 4816-4827.

Luo, J., Solimini, N.L., and Elledge, S.J. (2009). Principles of cancer therapy: oncogene and non-oncogene addiction. Cell *136*, 823-837.

Raj, L., Ide, T., Gurkar, A.U., Foley, M., Schenone, M., Li, X., Tolliday, N.J., Golub, T.R., Carr, S.A., Shamji, A.F., *et al.* (2011). Selective killing of cancer cells by a small molecule targeting the stress response to ROS. Nature *475*, 231-234.

Robe, P.A., Martin, D., Albert, A., Deprez, M., Chariot, A., and Bours, V. (2006). A phase 1-2, prospective, double blind, randomized study of the safety and efficacy of Sulfasalazine for the treatment of progressing malignant gliomas: study protocol of [ISRCTN45828668]. BMC cancer *6*, 29.

Rodrik-Outmezguine, V.S., Okaniwa, M., Yao, Z., Novotny, C.J., McWhirter, C., Banaji, A., Won, H., Wong, W., Berger, M., de Stanchina, E., *et al.* (2016). Overcoming mTOR resistance mutations with a new-generation mTOR inhibitor. Nature *534*, 272-276.

Sherman, M.H., Yu, R.T., Engle, D.D., Ding, N., Atkins, A.R., Tiriac, H., Collisson, E.A., Connor, F., Van Dyke, T., Kozlov, S., *et al.* (2014). Vitamin D receptor-mediated stromal reprogramming suppresses pancreatitis and enhances pancreatic cancer therapy. Cell *159*, 80-93.

Valencak, T.G., and Azzu, V. (2014). Making heads or tails of mitochondrial membranes in longevity and aging: a role for comparative studies. Longevity & healthspan *3*, 3.

Valencia, T., Kim, J.Y., Abu-Baker, S., Moscat-Pardos, J., Ahn, C.S., Reina-Campos, M., Duran, A., Castilla, E.A., Metallo, C.M., Diaz-Meco, M.T., *et al.* (2014). Metabolic reprogramming of stromal fibroblasts through p62-mTORC1 signaling promotes inflammation and tumorigenesis. Cancer cell *26*, 121-135.

Villa, G.R., Hulce, J.J., Zanca, C., Bi, J., Ikegami, S., Cahill, G.L., Gu, Y., Lum, K.M., Masui, K., Yang, H., *et al.* (2016). An LXR-Cholesterol Axis Creates a Metabolic Co-Dependency for Brain Cancers. Cancer cell *30*, 683-693.

Wander, S.A., Hennessy, B.T., and Slingerland, J.M. (2011). Next-generation mTOR inhibitors in clinical oncology: how pathway complexity informs therapeutic strategy. The Journal of clinical investigation *121*, 1231-1241.

Wang, M.Y., Lu, K.V., Zhu, S., Dia, E.Q., Vivanco, I., Shackleford, G.M., Cavenee, W.K., Mellinghoff, I.K., Cloughesy, T.F., Sawyers, C.L., *et al.* (2006). Mammalian target of rapamycin inhibition promotes response to epidermal growth factor receptor kinase inhibitors in PTEN-deficient and PTEN-intact glioblastoma cells. Cancer research *66*, 7864-7869.

Wei, W., Shin, Y.S., Xue, M., Matsutani, T., Masui, K., Yang, H., Ikegami, S., Gu, Y., Herrmann, K., Johnson, D., *et al.* (2016). Single-Cell Phosphoproteomics Resolves Adaptive Signaling Dynamics and Informs Targeted Combination Therapy in Glioblastoma. Cancer cell *29*, 563-573.

Yang, W.S., and Stockwell, B.R. (2016). Ferroptosis: Death by Lipid Peroxidation. Trends in cell biology *26*, 165-176.

Zhang, W., and Huang, P. (2011). Cancer-stromal interactions: role in cell survival, metabolism and drug sensitivity. Cancer biology & therapy *11*, 150-156.

Chapter 5

Concluding Remarks and Future Directions

SUMMARY

Targeting xCT in Cancer and its Therapeutic Implications

In conclusion, our studies uncovered an irreplaceable role of xCT in coupling glutamine and glutathione metabolism in cancer, as well as mechanisms regulating xCT by nutrient availability and oxidative stress. When nutrients are abundant, activated mTORC2 phosphorylates xCT on serine 26 and inhibits glutamate secretion, reserving glutamine-derived glutamate for biosynthesis. Whereas when nutrients are limited, such as upon glucose starvation, inactivated mTORC2 and ROS-mediated Nrf2 activation upregulate xCT activity and gene transcription, increasing cystine uptake for glutathione synthesis. The unique dependency on xCT-mediated cystine uptake and glutathione synthesis in GBM cells, especially upon mTOR inhibition, provided us the opportunity to induce tumor cell death through ferroptosis by combining glutathione synthesis and mTOR kinase inhibitors (Fig. 5-1). Future studies will be needed to test this combination in in vivo GBM mouse models and if successful, may advance to clinical trials on GBM patients. It will also be interesting to look into other cancers that also express high levels of xCT, such as triple-negative breast cancer, as our studies indicate that the mTORC2-mediated regulation of xCT could be a common mechanism across different cancer types.

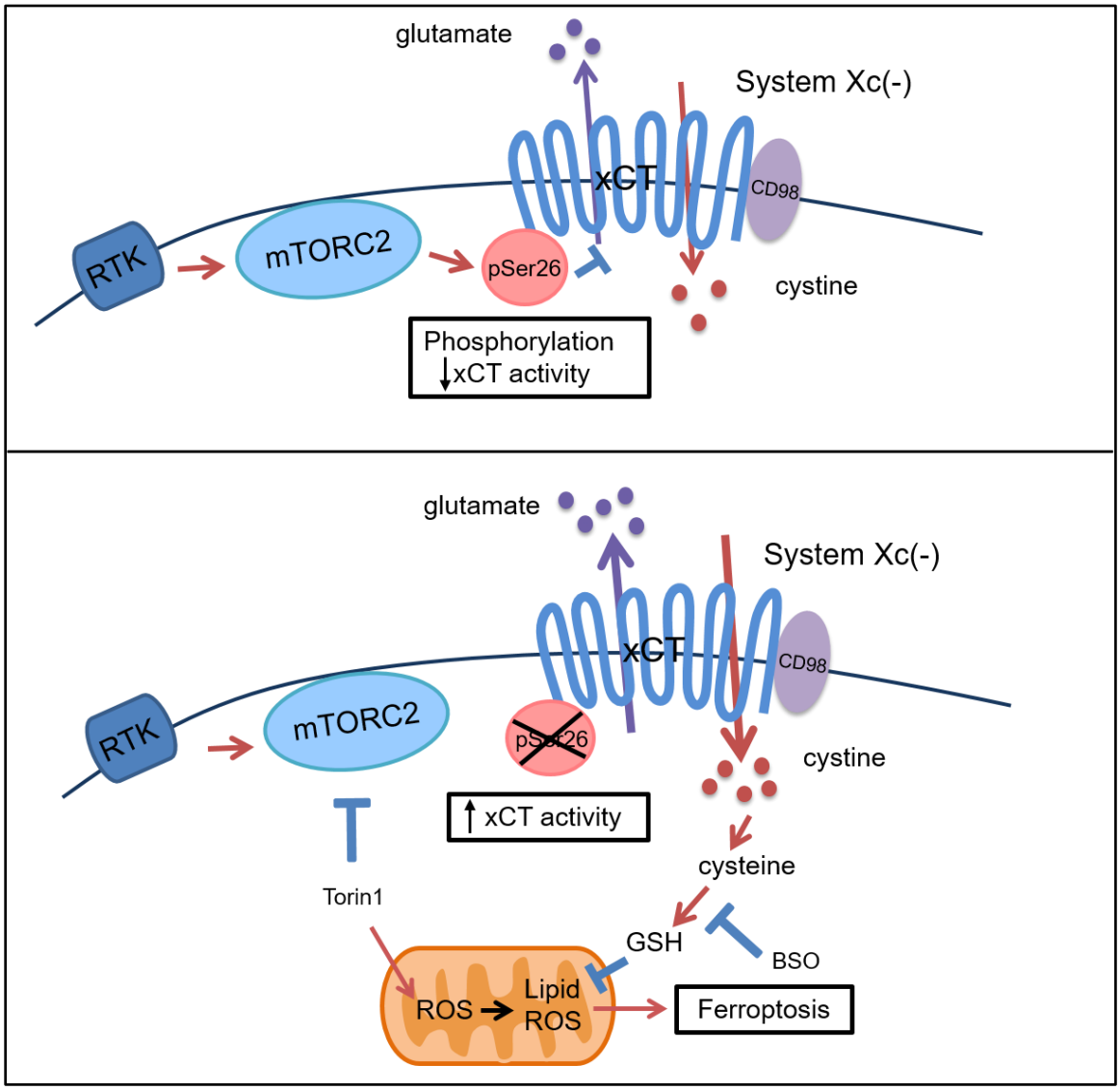

Fig. 5-1. The Model of xCT Regulation in GBM and Its Therapeutic Implications.

(Top) Hyperactivation of mTORC2 downstream of growth factor signaling regulates xCT through inhibitory phosphorylation and prevents glutamate export when nutrient is abundant to maximize the use of glutamine-derived glutamate for biosynthesis. (Bottom) On the contrary, upregulation of xCT is required upon nutrient limitation or mTOR kinase inhibition to facilitate uptake of cystine for glutathione synthesis to reduce oxidative stress, creating a targetable co-dependency in GBM.

DISCUSSIONS AND FUTURE DIRECTIONS

The Multifaceted Roles of xCT in Cancer

Additional roles of xCT have been suggested in cancer besides its primary function to take up cystine for glutathione synthesis as an oxidative stress defense mechanism (Huang et al., 2005; Lewerenz et al., 2012; Sasaki et al., 2002). Recently Briggs and colleagues reported an interesting paracrine mechanism of xCT regulation in triple negative breast cancer (Briggs et al., 2016), showing that high extracellular glutamate levels as a consequence of xCT upregulation feedback inhibited xCT function and depleted tumor cells of intracellular cysteine. Intracellular cysteine depletion resulted in oxidation of specific cysteine residues of the prolyl hydroxylase EglN1, which led to elevated intra-tumoral HIF1α levels to drive tumor growth due to suppression of EglN1-dependent HIF1α degradations (Briggs et al., 2016). The mechanism of mTORC2-mediated inhibitory post-translational modification of xCT to conserve glutamate for biosynthesis in nutrient-replete conditions discovered in our study nicely complemented Briggs and colleagues' finding. These mechanisms suggest that growth factor signaling-mediated regulation of xCT contributes to metabolic adaptations in different cancers to maximize nutrient utilization and cell growth. Future studies will be needed to determine whether there is any cooperation between these complementary post-translational regulatory mechanisms regulating xCT and their importance in context-dependent manners.

Metabolic Reprogramming Generates Targetable Co-dependencies in Cancer

Several studies from our lab and others have shown that oncogene-driven metabolic co-dependencies in cancer are promising drug targets (Luo et al., 2009; Raj et al., 2011; Villa et al., 2016). Apart from being major drivers of aberrant and uncontrolled proliferation of cancer cells, activating mutations in oncogenes and loss of tumor suppressor genes also play very important roles in metabolic reprogramming to satisfy the increasing demand of biosynthesis of macromolecules and capacity to reduce cellular stress (Koppenol et al., 2011; Pavlova and Thompson, 2016), creating targetable metabolic co-dependencies in cancer. To maximize nutrient utilization, the tumor-specific metabolic co-dependencies are also determined by nutrient abundance and tumor-stromal cell interactions in the microenvironment (Luo et al., 2009; Zhang and Huang, 2011). Metabolic co-dependencies could also be induced by drug treatments as survival and resistance mechanisms (Gini et al., 2013). Albeit tumor cells still maintain certain metabolic flexibility, they are invariably more susceptible to inhibition of the oncogene or drug induced metabolic co-dependencies compared to normal cells (Villa et al., 2016). Therefore identifying tumor-specific metabolic vulnerabilities would reveal a much broader category of drug targets in addition to the existing targeted therapies, which can potentially lead to better tumor-killing effects and help overcome drug resistance in cancer.

Cancer is an Adaptive and Evolving Disease

To date, therapeutic resistance still remained a major problem for most targeted therapies in cancer, despite that various survival and escape mechanisms mediating drug resistance have been identified. While understanding the dynamic tumor cell response to different drug treatment is important, overcoming therapeutic resistance might require a deeper understanding of the fundamental principles behind tumor adaptation and evolution, which leads to one of the important hallmark of cancer - genome instability (Hanahan and Weinberg, 2011). The unstable cancer genome has been suggested as a consequence of mutations in DNA repair genes or oncogene-induced DNA replication damages (Curtin, 2012; Negrini et al., 2010). Although it seems counterintuitive that tumor cells could survive and even gain proliferative advantage with such damaged genome, one explanation could have come from studies of cancer evolution. From the view of Darwinian evolution, increased genome instability could generate much more diversified and heterogeneous tumor cell populations, within which cells that acquired the fitness-enhancing mutations would be selected and survive the changing environment or drug treatment (Furnari et al., 2015; Nathanson et al., 2014). The increased heterogeneity is in fact tightly correlated with the fitness as well as aggressiveness of tumors, driving cancer progression and therapeutic resistance (Durrett et al., 2011; Koren and Bentires-Alj, 2015; Merlo et al., 2006; Polyak et al., 2009). These suggest that to successfully achieve tumor inhibition, it would require the treatment strategies to co-evolve with the tumor, thus identifying the immediate genetic signatures as well as the signaling and metabolic states of the tumor will be crucial to pinpoint the most deleterious target. Another promising alternative being pursued heavily is to take advantage of our own immune system, as it is inherently equipped with the ability to recognize and target foreign antigens on the evolving cancer cells (Blankenstein et al., 2012; Khalil et al., 2016). This is also supported by recent clinical

trials and approvals of checkpoint inhibitors in cancer, in which successful reactivation of the immune system has been shown to specifically target and suppress tumor progression, and in some cases even witnessed complete tumor remission in patients (Byun et al., 2017; Pardoll, 2012).

In summary, our discovery of the mTORC2 mediated-regulation of xCT and its role as a metabolic co-dependency upon mTOR kinase inhibition only revealed a tip of the iceberg in the comprehensive picture of metabolic reprogramming and adaptation in cancer. The fact that cancer is a complex disease driven by genetic, epigenetic and metabolic alterations with the ability to rapidly adapt and evolve with the environment and drug treatments suggest that besides dissecting the detailed molecular mechanisms driving oncogenesis, understanding the rudimentary principles of cancer is equally important to explain the complexity behind the disease and eventually translate into better cures for patients in the clinic.

REFERENCES

Blankenstein, T., Coulie, P.G., Gilboa, E., and Jaffee, E.M. (2012). The determinants of tumour immunogenicity. Nature reviews Cancer *12*, 307-313.

Briggs, K.J., Koivunen, P., Cao, S., Backus, K.M., Olenchock, B.A., Patel, H., Zhang, Q., Signoretti, S., Gerfen, G.J., Richardson, A.L., *et al.* (2016). Paracrine Induction of HIF by Glutamate in Breast Cancer: EglN1 Senses Cysteine. Cell *166*, 126-139.

Byun, D.J., Wolchok, J.D., Rosenberg, L.M., and Girotra, M. (2017). Cancer immunotherapy - immune checkpoint blockade and associated endocrinopathies. Nature reviews Endocrinology.

Curtin, N.J. (2012). DNA repair dysregulation from cancer driver to therapeutic target. Nature reviews Cancer *12*, 801-817.

Durrett, R., Foo, J., Leder, K., Mayberry, J., and Michor, F. (2011). Intratumor heterogeneity in evolutionary models of tumor progression. Genetics *188*, 461-477.

Furnari, F.B., Cloughesy, T.F., Cavenee, W.K., and Mischel, P.S. (2015). Heterogeneity of epidermal growth factor receptor signalling networks in glioblastoma. Nature reviews Cancer *15*, 302-310.

Gini, B., Zanca, C., Guo, D., Matsutani, T., Masui, K., Ikegami, S., Yang, H., Nathanson, D., Villa, G.R., Shackelford, D., *et al.* (2013). The mTOR kinase inhibitors, CC214-1 and CC214-2, preferentially block the growth of EGFRvIII-activated glioblastomas. Clinical cancer research : an official journal of the American Association for Cancer Research *19*, 5722-5732.

Hanahan, D., and Weinberg, R.A. (2011). Hallmarks of cancer: the next generation. Cell *144*, 646-674.

Huang, Y., Dai, Z., Barbacioru, C., and Sadee, W. (2005). Cystine-glutamate transporter SLC7A11 in cancer chemosensitivity and chemoresistance. Cancer research *65*, 7446-7454.

Khalil, D.N., Smith, E.L., Brentjens, R.J., and Wolchok, J.D. (2016). The future of cancer treatment: immunomodulation, CARs and combination immunotherapy. Nature reviews Clinical oncology *13*, 394.

Koppenol, W.H., Bounds, P.L., and Dang, C.V. (2011). Otto Warburg's contributions to current concepts of cancer metabolism. Nature reviews Cancer *11*, 325-337.

Koren, S., and Bentires-Alj, M. (2015). Breast Tumor Heterogeneity: Source of Fitness, Hurdle for Therapy. Molecular cell *60*, 537-546.

Lewerenz, J., Hewett, S.J., Huang, Y., Lambros, M., Gout, P.W., Kalivas, P.W., Massie, A., Smolders, I., Methner, A., Pergande, M., *et al.* (2012). The Cystine/Glutamate Antiporter System x(c)(-) in Health and Disease: From Molecular Mechanisms to Novel Therapeutic Opportunities. Antioxidants & redox signaling.

Luo, J., Solimini, N.L., and Elledge, S.J. (2009). Principles of cancer therapy: oncogene and non-oncogene addiction. Cell *136*, 823-837.

Merlo, L.M., Pepper, J.W., Reid, B.J., and Maley, C.C. (2006). Cancer as an evolutionary and ecological process. Nature reviews Cancer *6*, 924-935.

Nathanson, D.A., Gini, B., Mottahedeh, J., Visnyei, K., Koga, T., Gomez, G., Eskin, A., Hwang, K., Wang, J., Masui, K., *et al.* (2014). Targeted therapy resistance mediated by dynamic regulation of extrachromosomal mutant EGFR DNA. Science *343*, 72-76.

Negrini, S., Gorgoulis, V.G., and Halazonetis, T.D. (2010). Genomic instability--an evolving hallmark of cancer. Nature reviews Molecular cell biology *11*, 220-228.

Pardoll, D.M. (2012). The blockade of immune checkpoints in cancer immunotherapy. Nature reviews Cancer *12*, 252-264.

Pavlova, N.N., and Thompson, C.B. (2016). The Emerging Hallmarks of Cancer Metabolism. Cell metabolism *23*, 27-47.

Polyak, K., Haviv, I., and Campbell, I.G. (2009). Co-evolution of tumor cells and their microenvironment. Trends in genetics : TIG *25*, 30-38.

Raj, L., Ide, T., Gurkar, A.U., Foley, M., Schenone, M., Li, X., Tolliday, N.J., Golub, T.R., Carr, S.A., Shamji, A.F., *et al.* (2011). Selective killing of cancer cells by a small molecule targeting the stress response to ROS. Nature *475*, 231-234.

Sasaki, H., Sato, H., Kuriyama-Matsumura, K., Sato, K., Maebara, K., Wang, H., Tamba, M., Itoh, K., Yamamoto, M., and Bannai, S. (2002). Electrophile response element-mediated induction of the cystine/glutamate exchange transporter gene expression. The Journal of biological chemistry *277*, 44765-44771.

Villa, G.R., Hulce, J.J., Zanca, C., Bi, J., Ikegami, S., Cahill, G.L., Gu, Y., Lum, K.M., Masui, K., Yang, H., *et al.* (2016). An LXR-Cholesterol Axis Creates a Metabolic Co-Dependency for Brain Cancers. Cancer cell *30*, 683-693.

Zhang, W., and Huang, P. (2011). Cancer-stromal interactions: role in cell survival, metabolism and drug sensitivity. Cancer biology & therapy *11*, 150-156.

APPENDIX I - Related to Chapter 2

Growth Factor Signaling Reprograms Glucose and Lipid Metabolism in GBM

INTRODUCTION

In Chapter 2, we presented an example of how mTORC2 reprograms amino acid metabolism downstream of EGFR through phosphorylation of xCT in cancer, providing cancer cells the flexibility to repurpose nutrients for distinct metabolic needs under different nutrient and stress conditions. Besides amino acid metabolism, aberrant activation of growth factor signaling pathways such as EGFR also drives reprogramming of glucose and lipid metabolism to fulfill the anabolic and energetic demands to support tumor cell growth and proliferation. Interestingly, we also start seeing evidence about how tumor microenvironment, such as nutrient and oxygen availability, also contributes to selecting for the specific metabolic phenotypes in different cancers, or is even required for activation of downstream kinases upon growth factor stimulation. Therefore understanding the intricate crosstalk between signaling and metabolic pathways in caner will be crucial for us to identify potential novel therapeutic targets as well as to predict and overcome drug resistance of existing kinase and metabolic enzyme inhibitors. Here I presented several studies resulted from collaborative efforts with other members from the lab which significantly advanced our understandings of how growth factor signaling and environment together drive metabolic reprogramming in GBM and other cancers.

RESULTS

mTORC1 upregulates glycolysis downstream of mutant EGFR in GBM through inducing alternative splicing of the c-Myc binding partner Max

Through an unbiased screen of alternative splicing events in GBM xenografts derived from parental and mutant EGFRvIII-expressing U87 cells (Fig. A1-1A), we discovered that the mutant receptor EGFRvIII specifically upregulates the splicing factor heterogeneous nuclear ribonucleoprotein A1 (hnRNPA1) through mTOR (Fig. A1-1C and E). Further studies identified that hnRNPA1 induces alternative splicing of the c-Myc binding protein Max, and resulted in significant increase in c-Myc activity and a c-Myc related gene signature in GBM (Fig. A1-1B and D). HnRNPA1 was found to physically interact with the intronic region upstream of exon 5 of the Max mRNA, resulting in inclusion of exon 5 and generates a truncated Max protein referred to as Delta Max (Fig. A1-1G and H). The expression of Delta Max in GBM cells significantly augmented c-Myc-dependent transcription of glycolytic genes and is required for maintaining the EGFRvIII-driven glycolytic phenotype and tumor growth (Fig. A1-1I, J and K). In addition, activation of c-Myc downstream of EGFR and mTOR was found to be required for upregulating hnRNPA1 expression (Fig. A1-1F), creating an auto-activation loop to sustain high levels and activity of c-myc in GBM cells. (Babic et al., 2013)

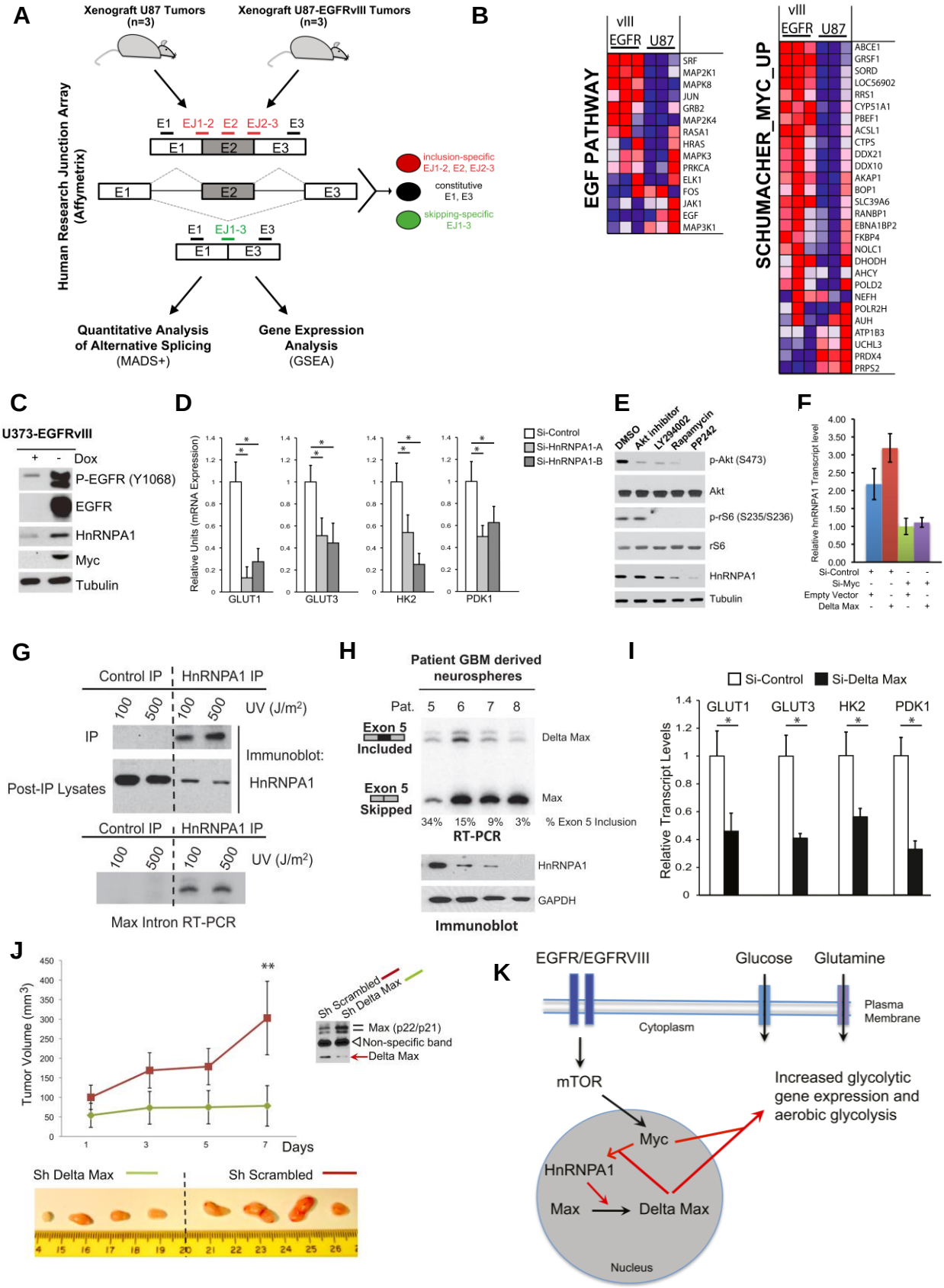
A
Xenograft U87 Tumors (n=3)
Xenograft U87-EGFRvIII Tumors (n=3)
Human Research Junction Array (Affymetrix)
E1 EJ1-2 E2 EJ2-3 E3
E1 E2 E3
E1 EJ1-3 E3
E1 E3
inclusion-specific EJ1-2, E2, EJ2-3
constitutive E1, E3
skipping-specific EJ1-3
Quantitative Analysis of Alternative Splicing (MADS+)
Gene Expression Analysis (GSEA)
B
vIII EGFR U87
EGF PATHWAY
SRF
MAP2K1
MAPK8
JUN
GRB2
MAP2K4
RASA1
HRAS
MAPK3
PRKCA
ELK1
FOS
JAK1
EGF
MAP3K1
SCHUMACHER_MYC_UP
ABCE1
GRSF1
SORD
LOC56902
RRS1
CYP51A1
PBEF1
ACSL1
CTPS
DDX21
DDX10
AKAP1
BOP1
SLC39A6
RANBP1
EBNA1BP2
FKBP4
NOLC1
DHODH
AHCY
POLD2
NEFH
POLR2H
AUH
ATP1B3
UCHL3
PRDX4
PRPS2
C
U373-EGFRvIII
Dox
P-EGFR (Y1068)
EGFR
HnRNPA1
Myc
Tubulin
D
Relative Units (mRNA Expression)
GLUT1
GLUT3
HK2
PDK1
Si-Control
Si-HnRNPA1-A
Si-HnRNPA1-B
E
DMSO
Akt inhibitor
LY294002
Rapamycin
PP242
p-Akt (S473)
Akt
p-rS6 (S235/S236)
rS6
HnRNPA1
Tubulin
F
Relative hnRNPA1 Transcript level
Si-Control
Si-Myc
Empty Vector
Delta Max
G
Control IP
HnRNPA1 IP
UV (J/m2)
IP
Post-IP Lysates
Immunoblot:
HnRNPA1
Max Intron RT-PCR
H
Patient GBM derived neurospheres
Pat. 5 6 7 8
Exon 5 Included
Exon 5 Skipped
Delta Max
Max
34% 15% 9% 3% % Exon 5 Inclusion
RT-PCR
HnRNPA1
GAPDH
Immunoblot
I
Si-Control
Si-Delta Max
GLUT1
GLUT3
HK2
PDK1
Relative Transcript Levels
J
Tumor Volume (mm3)
Days
Sh Scrambled
Sh Delta Max
Max (p22/p21)
Non-specific band
Delta Max
Sh Delta Max
Sh Scrambled
K
EGFR/EGFRVIII
Glucose
Glutamine
Cytoplasm
Plasma Membrane
mTOR
Increased glycolytic gene expression and aerobic glycolysis
Myc
HnRNPA1
Max
Delta Max
Nucleus

Fig. A1-1. Mutant EGFR Induced Alternative Splicing of Max and Drives Glycolysis and Tumor Growth in GBM.

(A) A brief scheme of the experimental design to concordantly identify alternative splicing events and gene expression comparing GBM xenograft tumors derived from parental and EGFRvIII U87 cells.

(B) Gene expression analysis was performed in U87 and U87-EGFRvIII tumors from three mice. Heatmap showing upregulation of EGF Pathway and Myc related genes in U87-EGFRvIII tumors.

(C) Immunoblot analysis of lysates from U373 showing doxycycline-induced EGFRvIII expression correlates with higher HnRNPA1 level.

(D) Real-time qPCR was performed to analyze expression levels of glycolytic enzymes in U87-EGFRvIII cells upon hnRNPA1 knockdowns (n = 3; results were shown as mean + SD; *$p < 0.05$).

(E) Pharmacological inhibition of mTOR in U87-EGFRvIII cells inhibits expression of hnRNPA1.

(F) Real-time qPCR analyzing hnRNPA1 expression level upon siRNA-mediated Myc knockdown or Delta Max overexpression. (n = 3; results were shown as mean ± SD).

(G) Real-time PCR was performed using primers targeting the Max intron upstream of exon 5 using RNA extracted from hnRNPA1 immunoprecipitants from U87-EGFRvIII cells after UV crosslinking (CLIP).

(H) Real-time PCR splicing analysis for Max exon 5 and immunoblot analysis for hnRNPA1 in GBM neurospheres established from patient biopsies.

(I) Real-time qPCR analysis of glycolytic gene expression in Delta Max knockdown U87-EGFRvIII cells (n = 3; results were shown as mean + SD; *p < 0.05).

(J) Xenograft tumors from U87-EGFRvIII cells with stable knockdown of Delta Max grew slower than control (Sh Scrambled) cells as measured by tumor size (n = 4; results were shown as mean ± SD; **p < 0.01).

(K) A brief diagram illustrating that EGFRvIII activation of mTOR upregulates Myc, which stimulates hnRNPA1 expression and promotes alternative splicing of Max, generating Delta Max and in turn augments Myc activity and increases aerobic glycolysis in GBM.

Figure was modified and originally published by Babic *et al* (Babic et al., 2013). For detailed experimental procedures please refer to Babic *et al* (Babic et al., 2013).

mTORC2 controls glycolysis through FOXO acetylation and upregulation of c-Myc in GBM

mTOR is an essential regulator of cellular metabolism in cancer, mediating metabolic reprogramming upon activation by growth factor signaling such as EGFR. mTORC1 has been shown to promote glycolysis and lipid metabolism in different cancers through regulating transcription factors such as c-Myc, Hif-1a and SREBP1 (Duvel et al., 2010). But less is known about the role of mTORC2 in regulating metabolism in cancer. mTORC2, like mTORC1, is also activated downstream of EGFR, albeit the detailed mechanism is still unclear. We first sought to determine whether mTORC2 is required for EGFR-driven GBM cell growth and discovered that mTORC2 is specifically required for GBM cell growth in the presence of glucose and for maintaining the c-Myc-driven glycolytic phenotype in GBM cells (Fig. A1-2A and B). This suggests that c-Myc is also regulated by mTORC2 besides mTORC1. Further studies revealed that mTORC2 mediates inhibitory phosphorylation of Class IIa HDACs, including HDAC4/5/7, in an Akt-independent manner (Fig. A1-2C), resulting in suppression of FoxO acetylation, which relieves c-Myc suppression by miR-34c (Fig. A1-2D, E, F and G). Previous studies have identified that PI3K/Akt directly phosphorylates and inhibits FoxO to upregulate c-Myc, suggesting that PI3K/Akt inhibitors should suppress c-Myc in cancer cells (Fig. A1-2J) (Kress et al., 2011). Our findings uncovered an additional bypass pathway through which mTORC2 activates c-Myc independent of PI3K and Akt, indicating that it would require inhibition of both PI3K and mTORC2 to achieve complete suppression of c-Myc in GBM cells (Fig. A1-2H, I and J) (Masui et al., 2013).

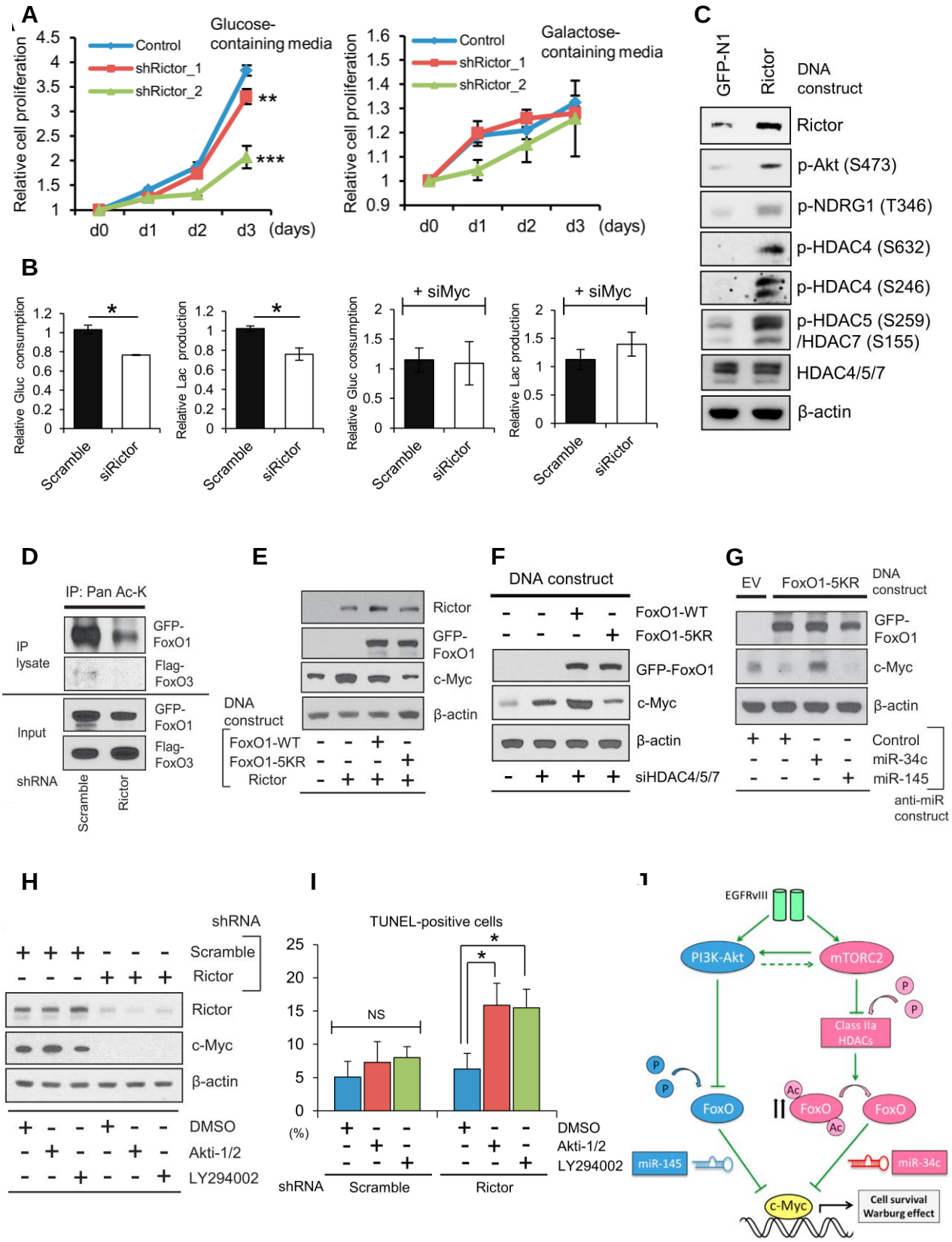
A
Glucose-containing media
Galactose-containing media
Control
shRictor_1
shRictor_2
Relative cell proliferation
d0 d1 d2 d3 (days)
**
***
B
Relative Gluc consumption
Relative Lac production
+ siMyc
Scramble
siRictor
C
GFP-N1
Rictor
DNA construct
Rictor
p-Akt (S473)
p-NDRG1 (T346)
p-HDAC4 (S632)
p-HDAC4 (S246)
p-HDAC5 (S259) /HDAC7 (S155)
HDAC4/5/7
β-actin
D
IP: Pan Ac-K
IP lysate
Input
GFP-FoxO1
Flag-FoxO3
shRNA
Scramble
Rictor
E
DNA construct
FoxO1-WT
FoxO1-5KR
Rictor
GFP-FoxO1
c-Myc
β-actin
F
DNA construct
FoxO1-WT
FoxO1-5KR
GFP-FoxO1
c-Myc
β-actin
siHDAC4/5/7
G
EV
FoxO1-5KR
DNA construct
GFP-FoxO1
c-Myc
β-actin
Control
miR-34c
miR-145
anti-miR construct
H
shRNA
Scramble
Rictor
Rictor
c-Myc
β-actin
DMSO
Akti-1/2
LY294002
I
TUNEL-positive cells
NS
*
(%)
shRNA
Scramble
Rictor
DMSO
Akti-1/2
LY294002
J
EGFRvIII
PI3K-Akt
mTORC2
Class IIa HDACs
FoxO
miR-145
miR-34c
c-Myc
Cell survival
Warburg effect

Fig. A1-2. mTORC2 Promotes c-Myc-dependent Glycolytic Phenotype in GBM through Inhibitory Phosphorylation of Class IIa HDACs and Acetylation of FoxO.

(A) Cell growth was quantified in U87EGFRvIII cells with si scramble control or si Rictor knockdown and cultured in media containing glucose or galactose. Results were presented as mean ± SD.

(B) Relative glucose consumption and lactate production was measured in control versus Rictor knockdown U87EGFRvIII cells with or without c-Myc knockdown.

(C) Immunoblot showing change in phosphorylated Class IIa HDACs from U87 cells overexpressing GFP or Rictor DNA plasmids.

(D) IP analysis of acetyl-lysine (Ac-K) levels on overexpressed GFP-FoxO1 and Flag-FoxO3 in U87EGFRvIII cells with shscramble control or shRictor stable knockdown.

(E) Immunoblot assessment of c-Myc in U87 cells co-transfected with Rictor and wild-type or acetylation resistant mutant FoxO plasmids.

(F) Immunoblot showing c-Myc levels in U87 cells with siRNA knockdowns against Class IIa HDACs, combined with overexpression of wild-type or acetylation resistant mutant FoxOs.

(G) Inhibition of miR-34c, but not miR-145 with anti-miR constructs reverted 5KR-FoxO1-mediated downregulation of c-Myc in U87EGFRvIII cells.

(H) Immunoblot comparing the effect of PI3K/Akt inhibitors combined with or without Rictor KD in suppressing c-Myc levels in U87EGFRvIII cells.

(I) Quantification of TUNEL-positive U87EGFRvIII cells treated with PI3K/Akt inhibitors combined with or without Rictor knockdown.

(J) EGFRvIII activates mTORC2 which inhibits FoxO activity via acetylation, bypassing PI3K/Akt inhibitor mediated suppression and sustained upregulation of c-Myc in GBM.

Figure was modified and originally published by Masui *et al* (Masui et al., 2013). For detailed experimental procedures please also refer to Masui *et al* (Masui et al., 2013).

Activation of mTORC2 downstream of EGFR requires glucose-dependent acetylation of Rictor

Activating mutations in growth factor signaling drive metabolic reprogramming in cancer cells through downstream kinases such as Akt and mTOR. But whether nutrient status affects signaling pathways is largely unknown. Coordination between growth factor signals with nutrient availability is very important for both normal cells as well as cancer cells, as proliferation under lack of nutrient could have devastating consequences such as inducing cellular stress and even apoptosis. mTORC1 was recently depicted as part of a complex and highly coordinated amino acid sensing machinery on the lysosome, adding to its multifaceted roles integrating nutrient availability with growth signals and metabolism to coordinate tumor cell proliferation and survival (Goberdhan et al., 2016; Shimobayashi and Hall, 2016). When examining how signaling pathways respond to depletion of different nutrients in GBM cells, we made the surprising finding that mTORC2 activity tightly correlates with the availability of glucose, suggesting that mTORC2 might act as a glucose sensor in tumor cells (Fig. A1-3A). It appeared that glucose or acetate is required for activation of mTORC2 upon growth factor stimulation, by providing a consistent supply of acetyl-CoA through PDH and ACSS2 for Rictor acetylation (Fig. A1-3B). Activation of mTORC2 downstream kinase PKCα phosphorylates and inhibits Class IIa HDACs, which prevents deacetylation of Rictor (Fig. A1-3E), and creates an auto-activation loop to sustain mTORC2 activation even after the initial growth factor signal is withdrawn (Fig. A1-3C, D and F). This suggests that elevated systemic levels of glucose and acetate could potentially contribute to drug resistance to EGFR, PI3K and Akt inhibitors in GBM by maintaining the activity of mTORC2 (Fig. A1-3G and H) (Masui et al., 2015).

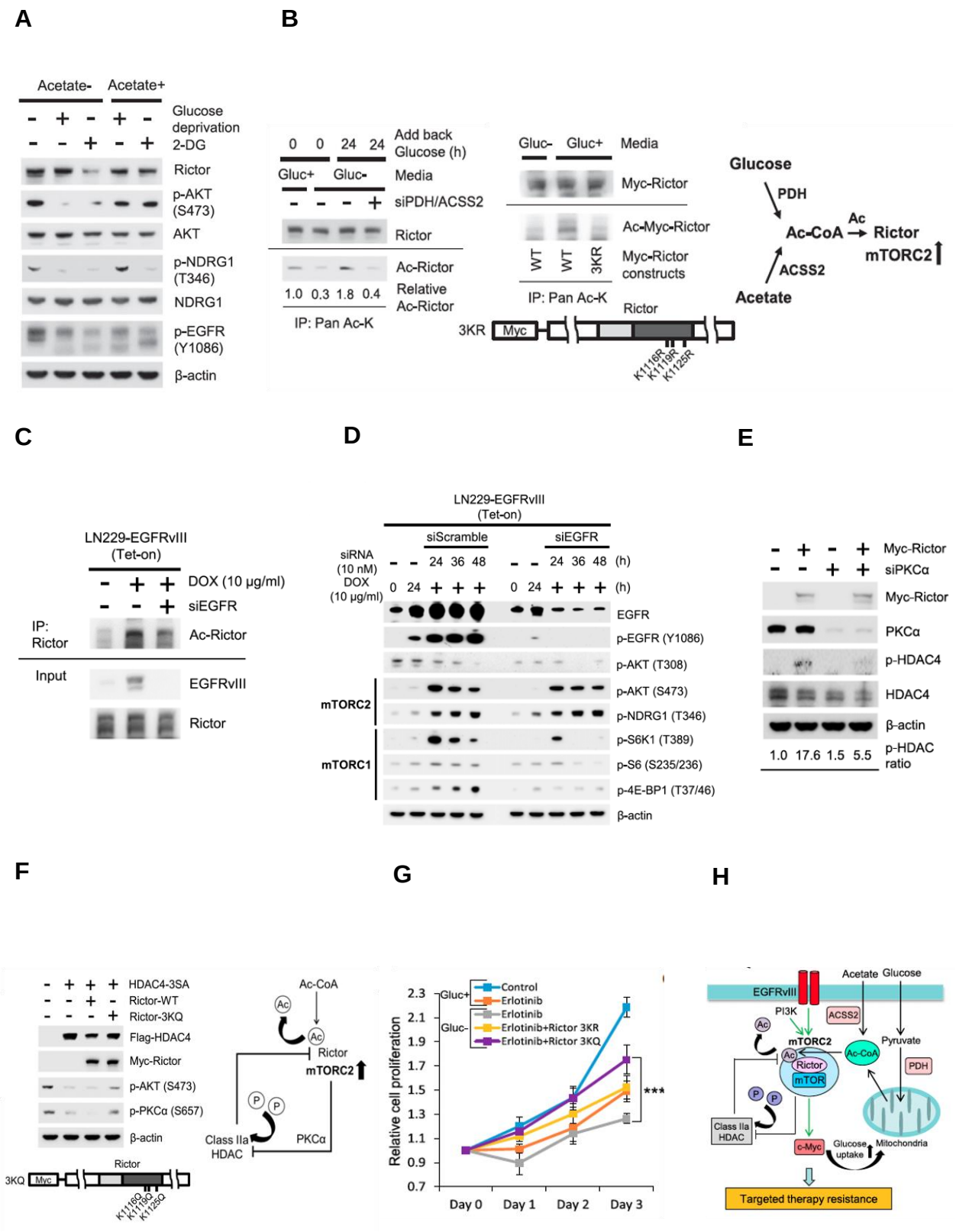
A
Acetate-
Acetate+
Glucose deprivation
2-DG
Rictor
p-AKT (S473)
AKT
p-NDRG1 (T346)
NDRG1
p-EGFR (Y1086)
β-actin
B
Add back Glucose (h)
Media
siPDH/ACSS2
Rictor
Ac-Rictor
Relative Ac-Rictor
IP: Pan Ac-K
Myc-Rictor
Ac-Myc-Rictor
Myc-Rictor constructs
3KR
K1116R
K1119R
K1125R
Glucose
PDH
Ac-CoA
Ac
Rictor
mTORC2
ACSS2
Acetate
C
LN229-EGFRvIII (Tet-on)
DOX (10 μg/ml)
siEGFR
IP: Rictor
Ac-Rictor
Input
EGFRvIII
Rictor
D
LN229-EGFRvIII (Tet-on)
siScramble
siEGFR
siRNA (10 nM)
DOX (10 μg/ml)
EGFR
p-EGFR (Y1086)
p-AKT (T308)
p-AKT (S473)
p-NDRG1 (T346)
p-S6K1 (T389)
p-S6 (S235/236)
p-4E-BP1 (T37/46)
β-actin
mTORC2
mTORC1
E
Myc-Rictor
siPKCα
PKCα
p-HDAC4
HDAC4
β-actin
p-HDAC ratio
F
HDAC4-3SA
Rictor-WT
Rictor-3KQ
Flag-HDAC4
Myc-Rictor
p-AKT (S473)
p-PKCα (S657)
β-actin
Ac-CoA
Rictor
mTORC2
Class IIa HDAC
PKCα
3KQ
K1116Q
K1119Q
K1125Q
G
Control
Erlotinib
Erlotinib
Erlotinib+Rictor 3KR
Erlotinib+Rictor 3KQ
Gluc+
Gluc-
Relative cell proliferation
Day 0
Day 1
Day 2
Day 3
***
H
Acetate
Glucose
EGFRvIII
PI3K
ACSS2
mTORC2
Rictor
mTOR
Ac-CoA
Pyruvate
PDH
Class IIa HDAC
c-Myc
Glucose uptake
Mitochondria
Targeted therapy resistance

Fig. A1-3. Glucose-dependent Acetylation of Rictor Sustains Activation of mTORC2 Downstream of EGFR.

(A) Immunoblot analysis of mTORC2 activity in U87EGFRvIII cells with 24 h of glucose deprivation or treatment with the glycolytic inhibitor 2-DG (10 mM) combined with or without addition of exogenous acetate (50 mM).

(B) Glucose and acetate provides acetyl-CoA for Rictor acetylation through PDH and ACSS2. Immunoblot analysis of Rictor acetylation in U87-EGFRvIII cells with or without 24 h of glucose deprivation combined with siRNA-mediated knockdown of PDH and ACSS2 for an additional 24 h (left). IP analysis of acetylation status of wildtype or 3KR acetylation-resistant mutant Rictor in U87 cells in the presence or absence of glucose, with a schematic below indicating the three acetylation sites mutated in the 3KR mutant of Rictor (middle). A schematic illustrating glucose and acetate activates mTORC2 by providing acetyl-CoA for Rictor acetylation through PDH and ACSS2.

(C) IP assessment of Rictor acetylation status in LN229 GBM cells with doxycycline-inducible (Tet-on) EGFRvIII showing ablation of EGFR signaling by siRNA does not affect Rictor acetylation once it's been activated.

(D) Immunoblot assessment of mTORC2 and mTORC1 downstream pathway activation in LN229 cells with doxycycline-inducible (Tet-on) EGFRvIII, combined with time-course inhibition of EGFR by siRNAs showing that mTORC2 downstream pathway still remained active even after withdrawal of upstream EGFR signaling.

(E) Immunoblot analysis and quantification of HDAC4 phosphorylation upon siRNA mediated PKCα knockdown in U87 cells expressing Myc-Rictor.

(F) Immunoblot showing that PKCα mediated inhibitory phosphorylation of Class IIa HDACs sustains Rictor acetylation in U87EGFRvIII cells.

(G) Cell proliferation was quantified in U87EGFRvIII cells treated with a combination of Erlotinib, glucose deprivation, and upon overexpression of Rictor-3KR or 3KQ mutants. Results were presented as mean ±SD, and *** refers to $P < 0.01$.

(H) mTORC2 forms an auto-activation loop in GBM tumor cells by promoting glucose uptake and acetyl-CoA production through c-Myc and by PKCα-mediated inactivating phosphorylation of Class IIa HDACs, which together sustains Rictor acetylation and activation of mTORC2. These mechanisms suggest that GBM cells with activated mTORC2 are resistant to targeted therapies against mTORC2 upstream kinases including EGFR and PI3K.

Figure was modified and originally published by Masui *et al* (Masui et al., 2015). For detailed experimental procedures please also refer to Masui *et al* (Masui et al., 2015).

EGFR creates a targetable metabolic co-dependency on exogenous cholesterol and sensitize tumor cells to LXR agonists in GBM.

Many targeted therapies for GBM such as small molecule kinase inhibitors encountered the problem of low penetrance across the blood brain barrier, and without being able to achieve sufficient dose in the brain, most of them failed to show anti-tumor efficacy in patients. Oncogene-driven metabolic co-dependencies in cancer on the other hand provide us with a brand new range of drug targets and the opportunity to explore potential small molecule compounds with better brain penetrance as alternative GBM therapy. Previous studies from our lab discovered that activating mutations in EGFR results in the metabolic dependency on uptake of exogenous cholesterol through LDLR in GBM cells (Guo et al., 2009), while de novo cholesterol synthesis is largely suppressed possibly due to the demand of a large amount of ATP and reducing equivalents (Fig. A1-4A and B). This EGFR-driven cholesterol dependency specifically sensitizes GBM cells to LXR agonists while sparing normal cells in the brain (Fig. A1-4C). The compound LXR-623 was initially developed as a potent LXR agonist for atherosclerosis but failed in clinical trials as it caused central nervous system side effects due to brain penetrance (Katz et al., 2009). Re-purposing LXR-623 for GBM showed great efficacy in inducing tumor cell death through significant depletion of cholesterol from tumor cells by suppressing LDLR-mediated cholesterol uptake and promoting cholesterol efflux through ABCA1 (Fig. A1-4D, E and F). The efficacy of LXR-623 successfully extended to an intracranial patient-derived GBM xenograft model. LXR-623 was able to specifically accumulate in the brain, significantly suppressed GBM tumor growth and prolonged survival, suggesting that it would be a very promising drug candidate for the treatment of GBM in the clinic (Fig. A1-4G, H and I) (Villa et al., 2016).

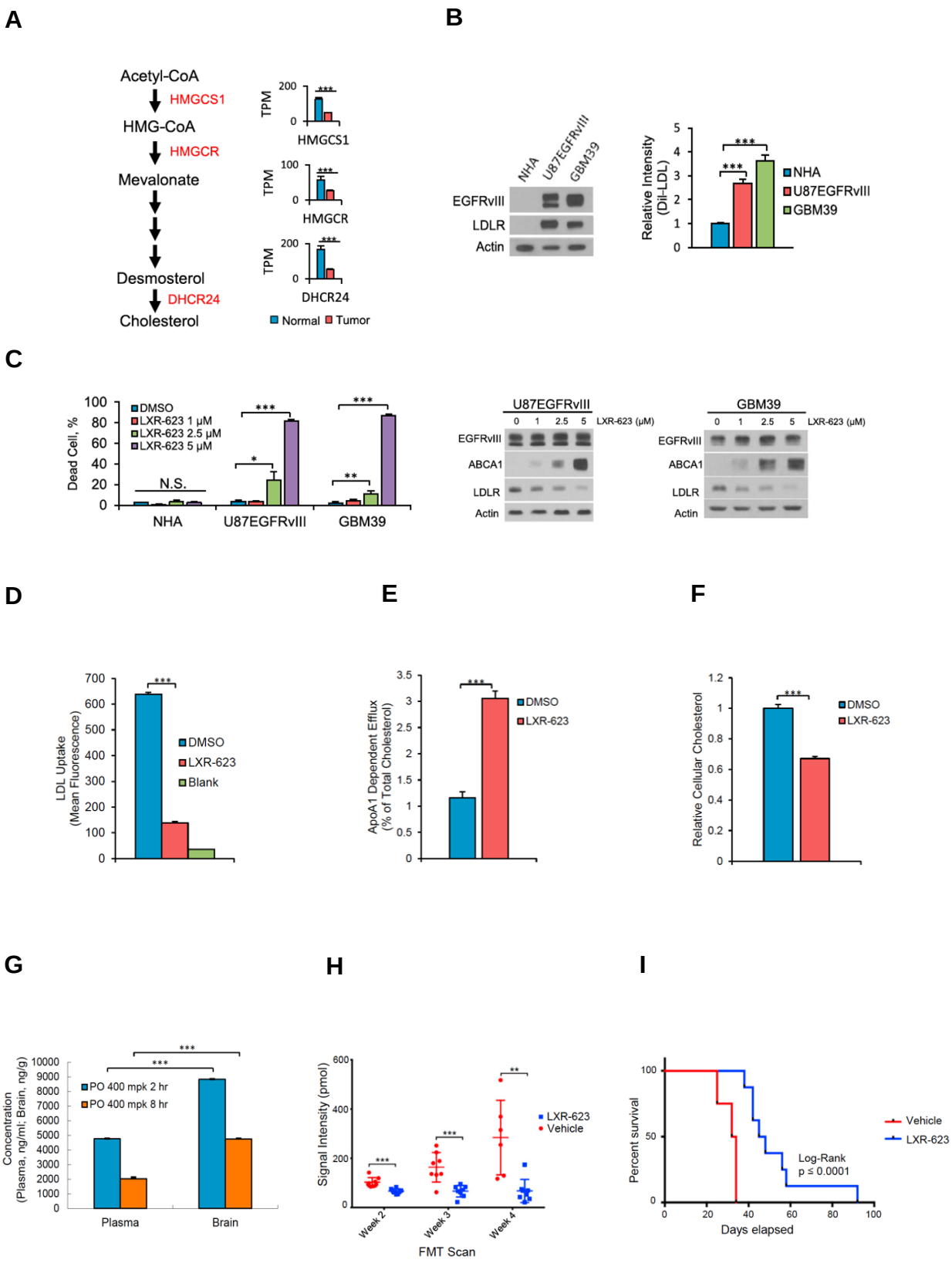
A
Acetyl-CoA
HMGCS1
HMG-CoA
HMGCR
Mevalonate
Desmosterol
DHCR24
Cholesterol
TPM
HMGCS1
HMGCR
DHCR24
Normal
Tumor
B
NHA
U87EGFRvIII
GBM39
EGFRvIII
LDLR
Actin
Relative Intensity (Dil-LDL)
C
Dead Cell, %
DMSO
LXR-623 1 μM
LXR-623 2.5 μM
LXR-623 5 μM
N.S.
U87EGFRvIII
GBM39
LXR-623 (μM)
ABCA1
D
LDL Uptake (Mean Fluorescence)
Blank
E
ApoA1 Dependent Efflux (% of Total Cholesterol)
F
Relative Cellular Cholesterol
G
Concentration (Plasma, ng/ml; Brain, ng/g)
PO 400 mpk 2 hr
PO 400 mpk 8 hr
Plasma
Brain
H
Signal Intensity (pmol)
LXR-623
Vehicle
Week 2
Week 3
Week 4
FMT Scan
I
Percent survival
Log-Rank
p ≤ 0.0001
Days elapsed

Fig. A1-4. Targeting EGFR-driven Cholesterol Dependency with LXR-623 Significantly Suppressed Tumor Growth, Induced Tumor Cell Death and Prolonged Survival in Intracranial GBM Mouse Xenograft Models.

(A) Analysis of de novo cholesterol synthesis genes in GBMs versus normal brain from TCGA gene expression data. Data are presented as mean ± SEM.

(B) Immunoblotting comparing EGFR and LDLR protein levels in NHA, U87EGFRvIII, and GBM39 cells (left). And FACS quantification of LDL uptake in U87EGFRvIII and GBM39 cells (right).

(C) Quantification of cell death in response to LXR-623 at day 5 of treatment in NHA, U87EGFRvIII, and GBM39 cells. As well as immunoblot analysis of suppression of LDLR and induction of ABCA1 by LXR-623 treatment.

(D) Flow cytometry analysis of LDL uptake was performed in U87EGFRvIII cells treated with LXR-623 for a total of 48 h and by incubated with a fluorescent-labeled LDL probe for 4 h.

(E) Cholesterol efflux was determined by scintillation counting by incubating U87EGFRvIII cells with ^{3}H-cholesterol after treated with 5 μM of LXR-623.

(F) U87EGFRvIII cells were treated with LXR-623 for a total of 48 h and total cellular cholesterol levels were measured by LC/MS.

(G) Mice were treated with a single dose of 400 mg/kg LXR-623 by oral gavage. Plasma and brain were extracted from mice at 2 or 8 h after treatment and LXR-623 concentration was measured (n = 5 for each time point).

(H) GBM39 patient-derived neurosphere cells engineered to stably express the infrared fluorescent protein 720 were orthotopically injected into 5-week-old nu/nu mice. Mice were

treated with vehicle or LXR-623 400 mg/kg PO daily (n = 8 for each group). Tumor size was assessed via FMT weekly.

(I) Kaplan-Meier curves were plotted assessing overall survival of mice treatment with vehicle control or LXR-623 400 mg/kg PO daily. Log rank (Mantel-Cox) test: p =0.0001, Gehan-Breslow-Wilcoxon test: p = 0.0002.

Figure was modified and originally published by Villa *et al* (Villa et al., 2016). For detailed experimental procedures please also refer to Villa *et al* (Villa et al., 2016).

DISCUSSION

Previously, metabolic reprogramming in cancer was perceived as a response towards the decreased cellular ATP:ADP ratio when energies are over-consumed by rapid cell proliferation, also known as the traditional “demand model”. But accumulating evidence have emerged from recent studies suggesting that constitutively activated growth factor signaling is in fact directly driving biosynthesis and anabolic metabolism in proliferating cancer cells, which has been better described as the new “supply model” (Bar-Peled et al., 2013). Concordant metabolic reprogramming provides cancer cells a head start to catch up with the biosynthetic demand to maintain an ample supply of nucleotides, proteins and lipids, which are all essential for cell replication.

We can see from the examples described above that growth factor signaling was not only able to reprogram metabolism through regulating transcription factors such as c-Myc, which controls a wide range of target genes involved in glucose and glutamine metabolism, but pathways downstream of growth factor signaling is also responsive to nutrient status through nutrient “sensors” such as mTOR. Most cancers maintain at least part of their ability to sense nutrient status, which enables the coordination between growth signals with nutrient availability to avoid potential catastrophic energy collapse. But loss of certain nutrient or energy sensing pathways is also commonly seen in cancer, which is assumed to provide cancer cells a proliferative advantage through increasing the threshold of nutrient limitation on cell growth. For example, loss-of-function mutations or deletion of LKB1 underlies the cause of the Puetz-Jegher’s syndrome and is also commonly seen in non-small cell lung cancer, which leads to inactivation of the energy sensor AMPK and hyperactivation of mTORC1 (Shackelford and Shaw, 2009).

Loss-of-function mutations are also found in the GATOR complex, which is required for amino acid depletion-induced mTORC1 inhibition on the lysosome (Bar-Peled et al., 2013; Menon and Manning, 2013). These indicate that nutrient-sensing mechanisms might be playing distinct roles under different circumstances in cancer and future studies are needed to better understand its contribution in the course of cancer development.

In addition, we observed that the metabolic environment also plays an important role in growth factor signaling-driven metabolic reprogramming in cancer, such as the specific dependence on cholesterol uptake in EGFR-driven GBM cells is largely determined by the steady cholesterol pool in the brain. These together suggest that nutrient availability is no longer only a limiting factor for the passive selection of cancer cells during its course of evolution, but plays a rather active role in driving metabolic reprogramming together with hyperactivated growth factor signaling. Therefore it is very important to fully understand the specific metabolic environment cancer cells reside in before we could capture a complete view of how metabolism is differentially reprogrammed in cancer, so that we could identify the correct targetable metabolic dependencies as potential alternative treatment strategies when targeted therapies fail.

REFERENCES

Babic, I., Anderson, E.S., Tanaka, K., Guo, D., Masui, K., Li, B., Zhu, S., Gu, Y., Villa, G.R., Akhavan, D., *et al.* (2013). EGFR mutation-induced alternative splicing of Max contributes to growth of glycolytic tumors in brain cancer. Cell metabolism *17*, 1000-1008.

Bar-Peled, L., Chantranupong, L., Cherniack, A.D., Chen, W.W., Ottina, K.A., Grabiner, B.C., Spear, E.D., Carter, S.L., Meyerson, M., and Sabatini, D.M. (2013). A Tumor suppressor complex with GAP activity for the Rag GTPases that signal amino acid sufficiency to mTORC1. Science *340*, 1100-1106.

Duvel, K., Yecies, J.L., Menon, S., Raman, P., Lipovsky, A.I., Souza, A.L., Triantafellow, E., Ma, Q., Gorski, R., Cleaver, S., *et al.* (2010). Activation of a metabolic gene regulatory network downstream of mTOR complex 1. Molecular cell *39*, 171-183.

Goberdhan, D.C., Wilson, C., and Harris, A.L. (2016). Amino Acid Sensing by mTORC1: Intracellular Transporters Mark the Spot. Cell metabolism *23*, 580-589.

Guo, D., Prins, R.M., Dang, J., Kuga, D., Iwanami, A., Soto, H., Lin, K.Y., Huang, T.T., Akhavan, D., Hock, M.B., *et al.* (2009). EGFR signaling through an Akt-SREBP-1-dependent, rapamycin-resistant pathway sensitizes glioblastomas to antilipogenic therapy. Science signaling *2*, ra82.

Katz, A., Udata, C., Ott, E., Hickey, L., Burczynski, M.E., Burghart, P., Vesterqvist, O., and Meng, X. (2009). Safety, pharmacokinetics, and pharmacodynamics of single doses of LXR-623, a novel liver X-receptor agonist, in healthy participants. Journal of clinical pharmacology *49*, 643-649.

Kress, T.R., Cannell, I.G., Brenkman, A.B., Samans, B., Gaestel, M., Roepman, P., Burgering, B.M., Bushell, M., Rosenwald, A., and Eilers, M. (2011). The MK5/PRAK kinase and Myc form a negative feedback loop that is disrupted during colorectal tumorigenesis. Molecular cell *41*, 445-457.

Masui, K., Tanaka, K., Akhavan, D., Babic, I., Gini, B., Matsutani, T., Iwanami, A., Liu, F., Villa, G.R., Gu, Y., *et al.* (2013). mTOR complex 2 controls glycolytic metabolism in glioblastoma through FoxO acetylation and upregulation of c-Myc. Cell metabolism *18*, 726-739.

Masui, K., Tanaka, K., Ikegami, S., Villa, G.R., Yang, H., Yong, W.H., Cloughesy, T.F., Yamagata, K., Arai, N., Cavenee, W.K., *et al.* (2015). Glucose-dependent acetylation of Rictor

promotes targeted cancer therapy resistance. Proceedings of the National Academy of Sciences of the United States of America *112*, 9406-9411.

Menon, S., and Manning, B.D. (2013). Cell signalling: nutrient sensing lost in cancer. Nature *498*, 444-445.

Shackelford, D.B., and Shaw, R.J. (2009). The LKB1-AMPK pathway: metabolism and growth control in tumour suppression. Nature reviews Cancer *9*, 563-575.

Shimobayashi, M., and Hall, M.N. (2016). Multiple amino acid sensing inputs to mTORC1. Cell Res *26*, 7-20.

Villa, G.R., Hulce, J.J., Zanca, C., Bi, J., Ikegami, S., Cahill, G.L., Gu, Y., Lum, K.M., Masui, K., Yang, H., *et al.* (2016). An LXR-Cholesterol Axis Creates a Metabolic Co-Dependency for Brain Cancers. Cancer cell *30*, 683-693.

APPENDIX II - Related to Chapter 3

Complete Data Analysis of LC-MS/MS Metabolomics with [U-13C6]-D-Glucose and [U-13C5]-L-Glutamine Labeling

LC-MS/MS Metabolomics Analysis with [U-13C6]-D-Glucose Labeling

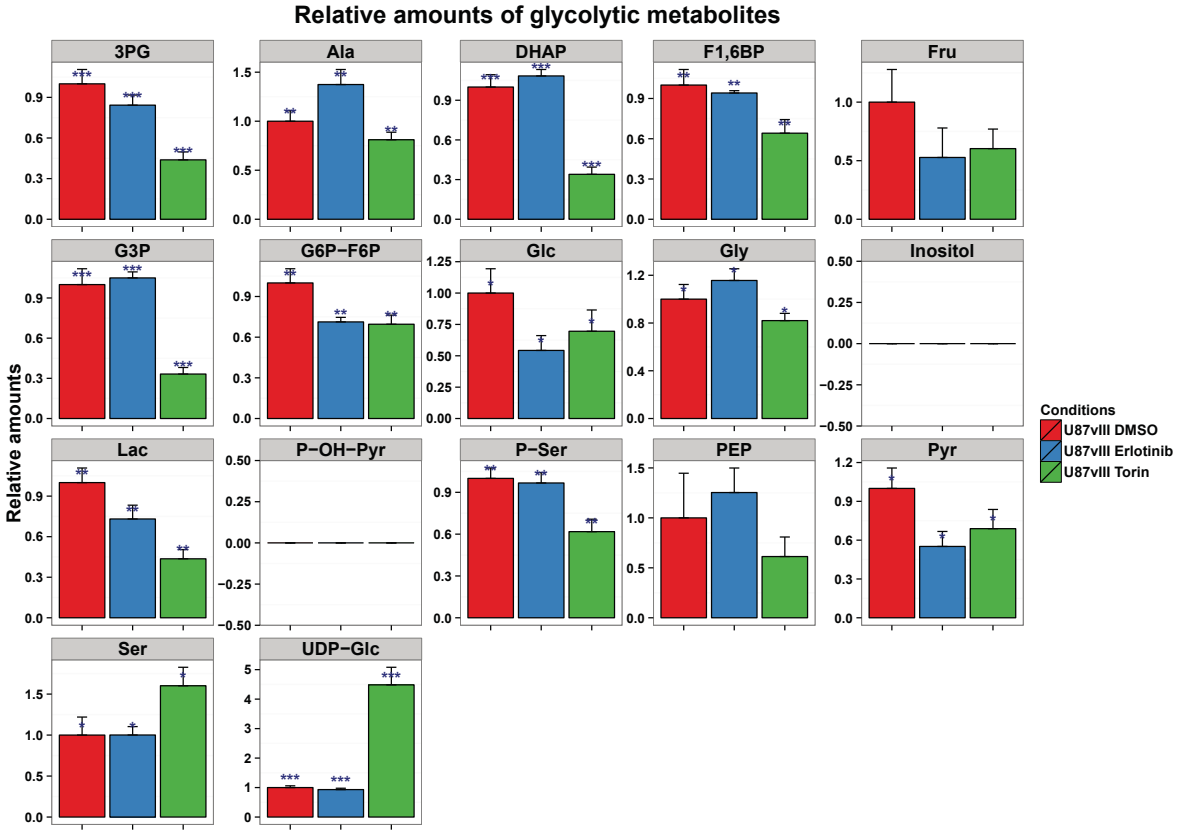
Relative amounts of glycolytic metabolites
3PG
Ala
DHAP
F1,6BP
Fru
G3P
G6P−F6P
Glc
Gly
Inositol
Lac
P−OH−Pyr
P−Ser
PEP
Pyr
Ser
UDP−Glc
Relative amounts
Conditions
U87vIII DMSO
U87vIII Erlotinib
U87vIII Torin

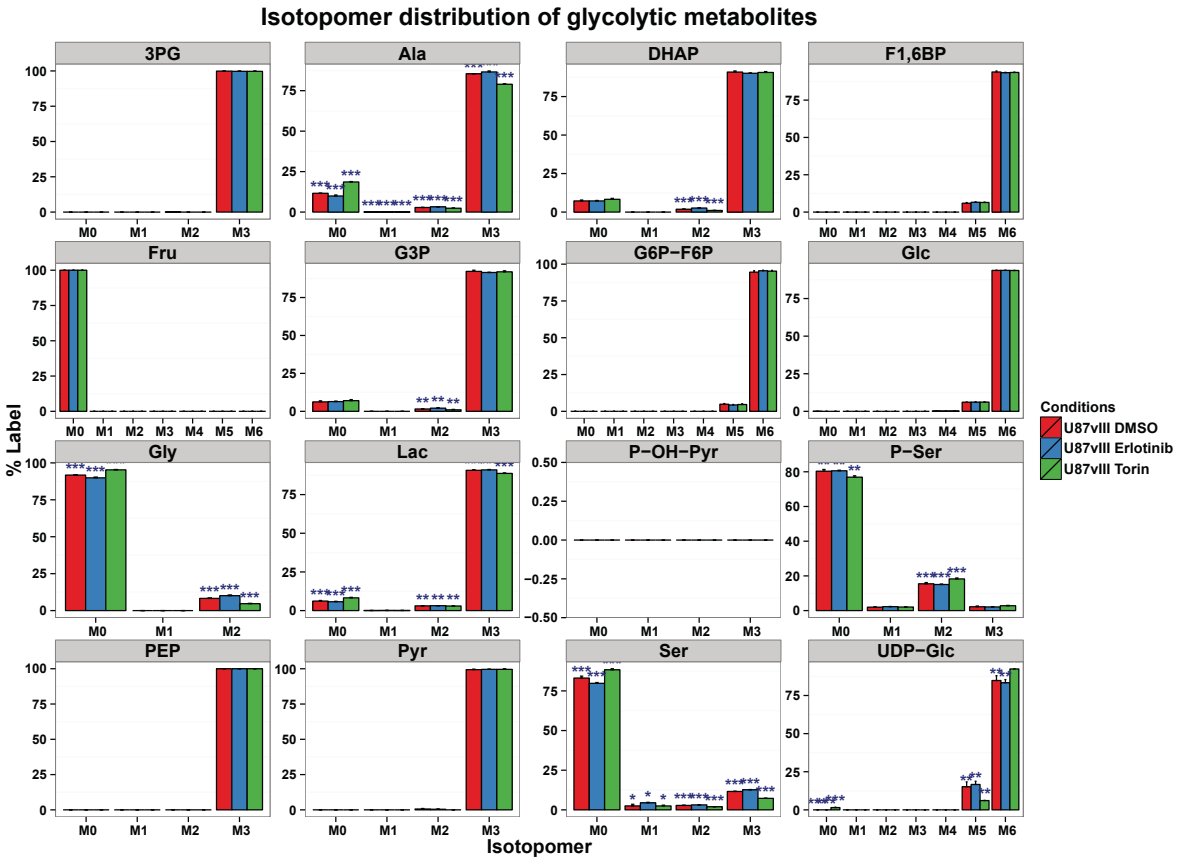
Isotopomer distribution of glycolytic metabolites
3PG
Ala
DHAP
F1,6BP
Fru
G3P
G6P−F6P
Glc
Gly
Lac
P−OH−Pyr
P−Ser
PEP
Pyr
Ser
UDP−Glc
% Label
Isotopomer
Conditions
U87vIII DMSO
U87vIII Erlotinib
U87vIII Torin

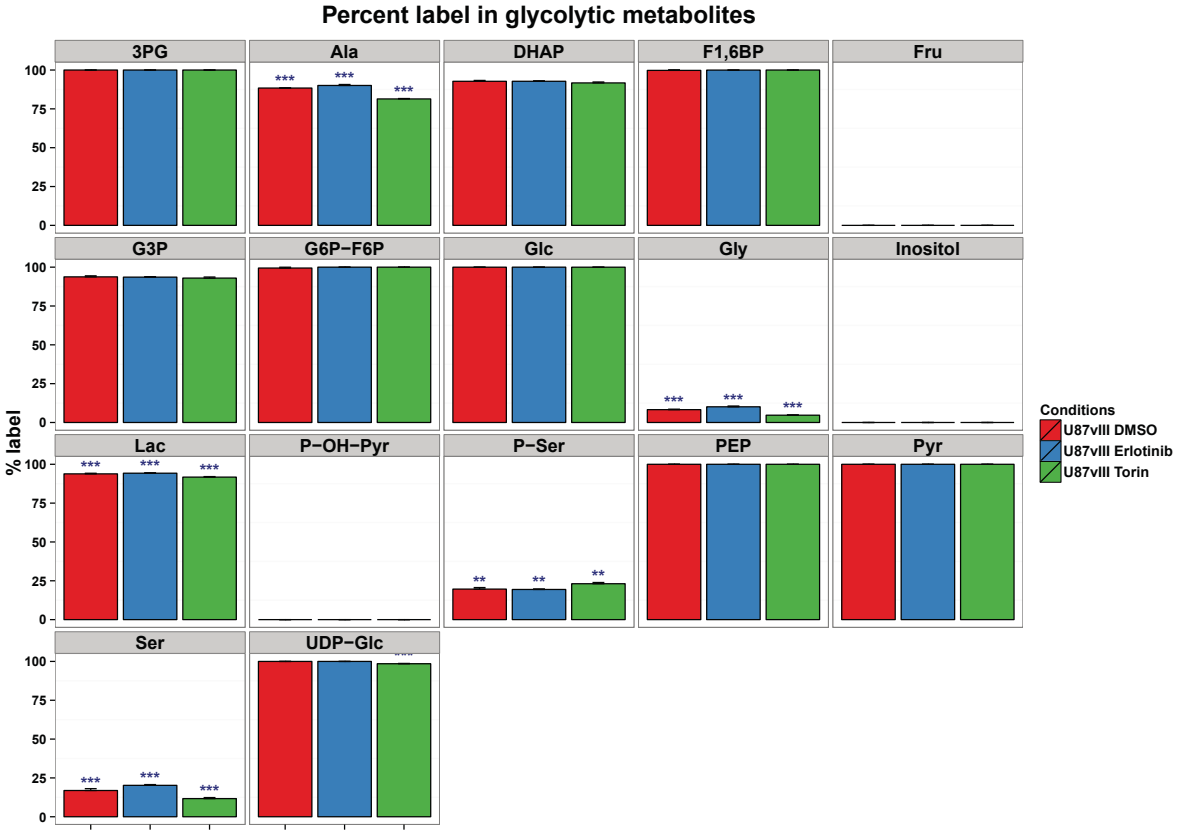
Percent label in glycolytic metabolites
3PG
Ala
DHAP
F1,6BP
Fru
G3P
G6P−F6P
Glc
Gly
Inositol
Lac
P−OH−Pyr
P−Ser
PEP
Pyr
Ser
UDP−Glc
% label
Conditions
U87vIII DMSO
U87vIII Erlotinib
U87vIII Torin

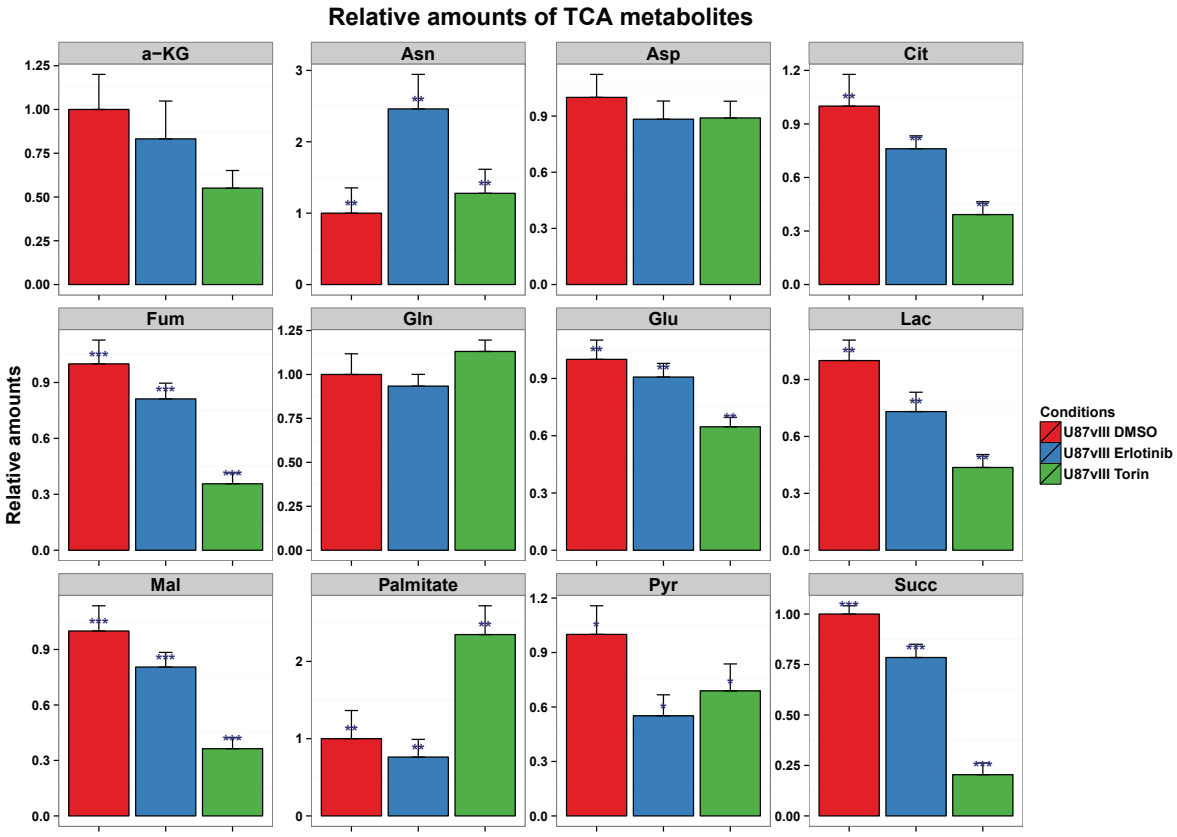
Relative amounts of TCA metabolites
a−KG
Asn
Asp
Cit
Fum
Gln
Glu
Lac
Mal
Palmitate
Pyr
Succ
Relative amounts
Conditions
U87vIII DMSO
U87vIII Erlotinib
U87vIII Torin

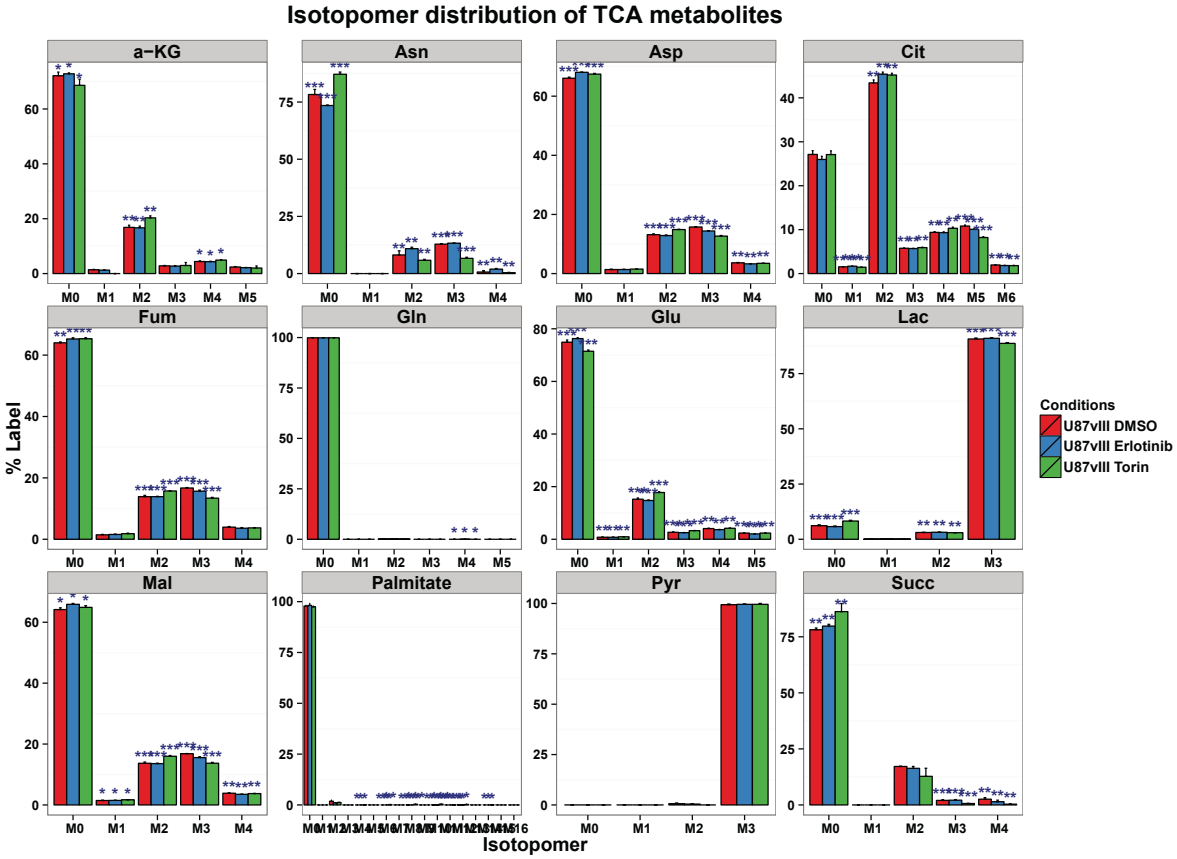
Isotopomer distribution of TCA metabolites
a−KG
Asn
Asp
Cit
Fum
Gln
Glu
Lac
Mal
Palmitate
Pyr
Succ
% Label
Isotopomer
Conditions
U87vIII DMSO
U87vIII Erlotinib
U87vIII Torin

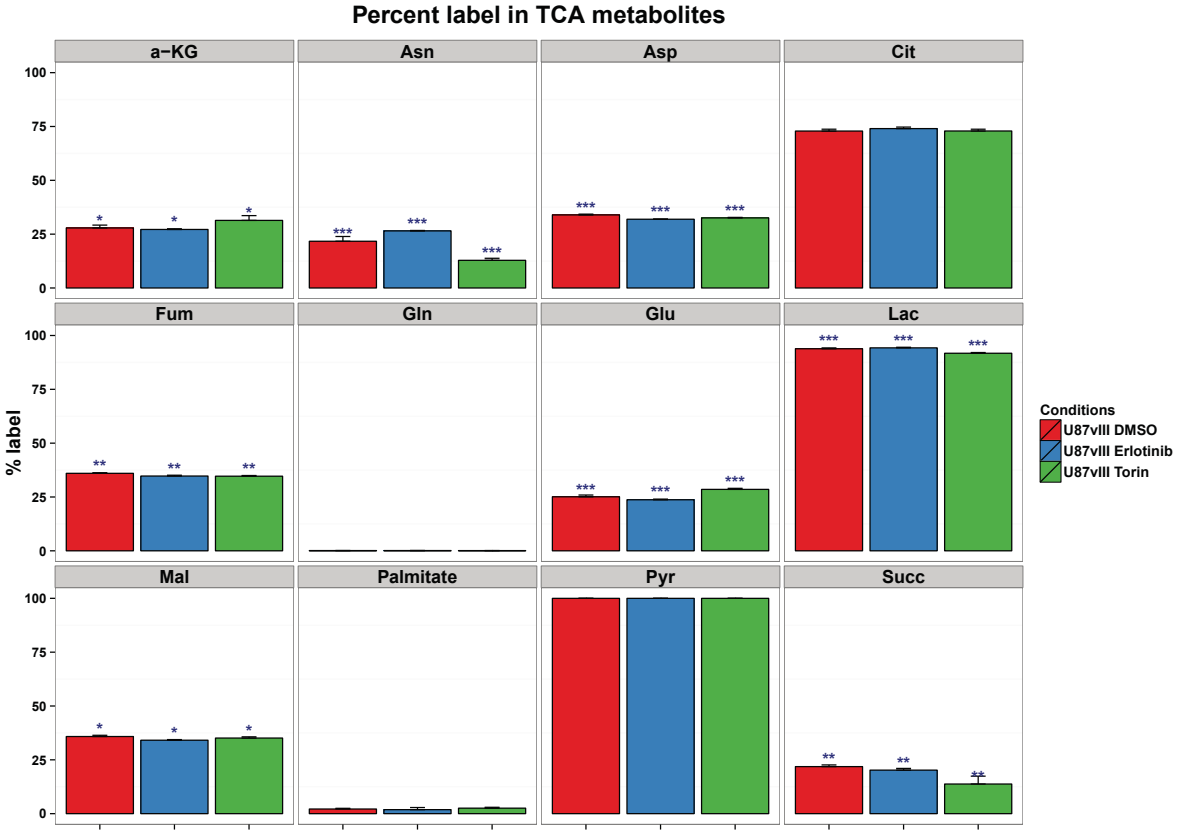
Percent label in TCA metabolites
a−KG
Asn
Asp
Cit
Fum
Gln
Glu
Lac
Mal
Palmitate
Pyr
Succ
% label
Conditions
U87vIII DMSO
U87vIII Erlotinib
U87vIII Torin

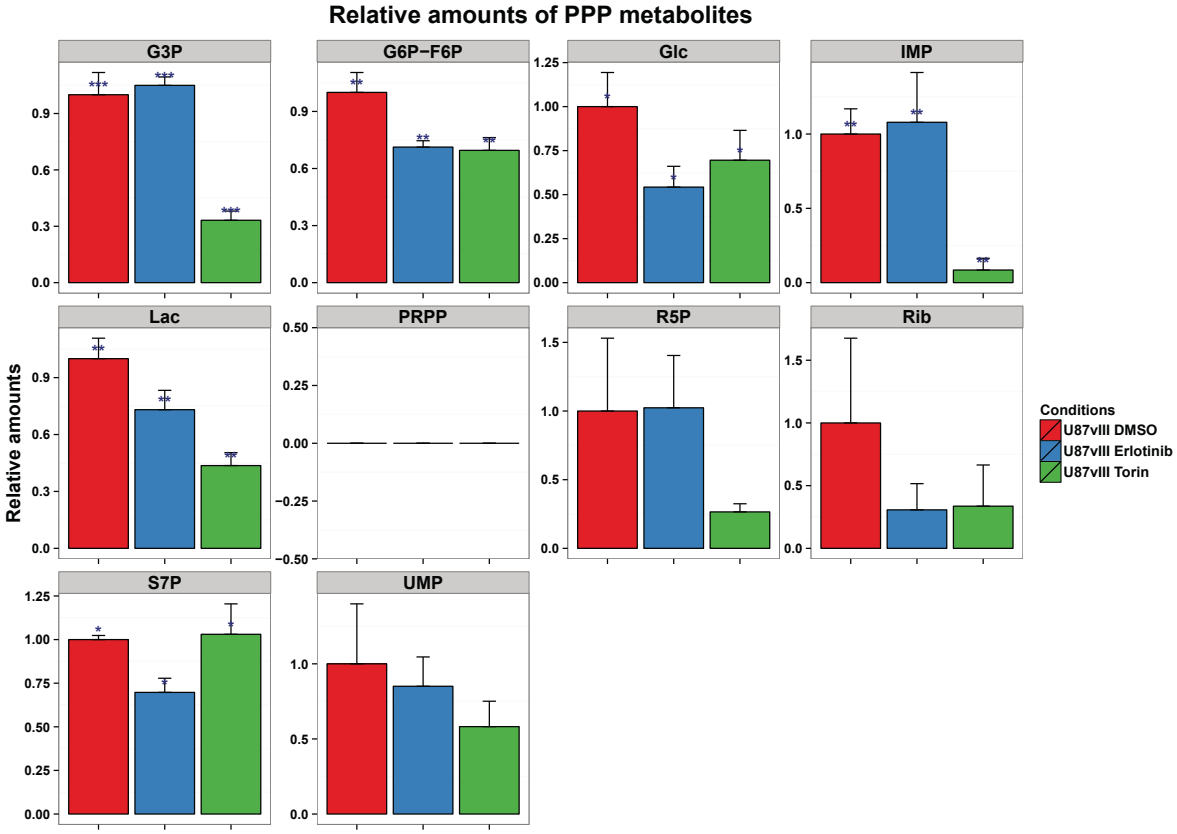
Relative amounts of PPP metabolites
G3P
G6P−F6P
Glc
IMP
Lac
PRPP
R5P
Rib
S7P
UMP
Relative amounts
Conditions
U87vIII DMSO
U87vIII Erlotinib
U87vIII Torin

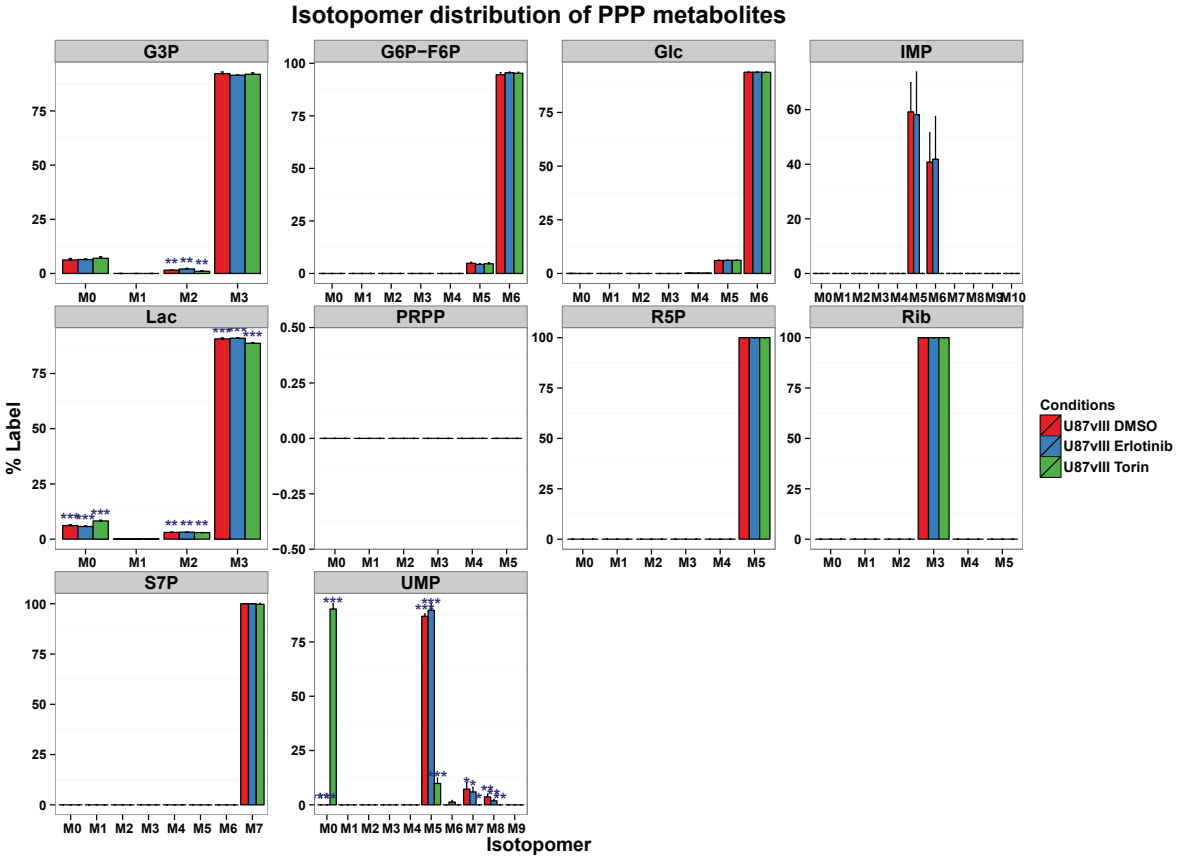
Isotopomer distribution of PPP metabolites
G3P
G6P−F6P
Glc
IMP
Lac
PRPP
R5P
Rib
S7P
UMP
% Label
Isotopomer
Conditions
U87vIII DMSO
U87vIII Erlotinib
U87vIII Torin

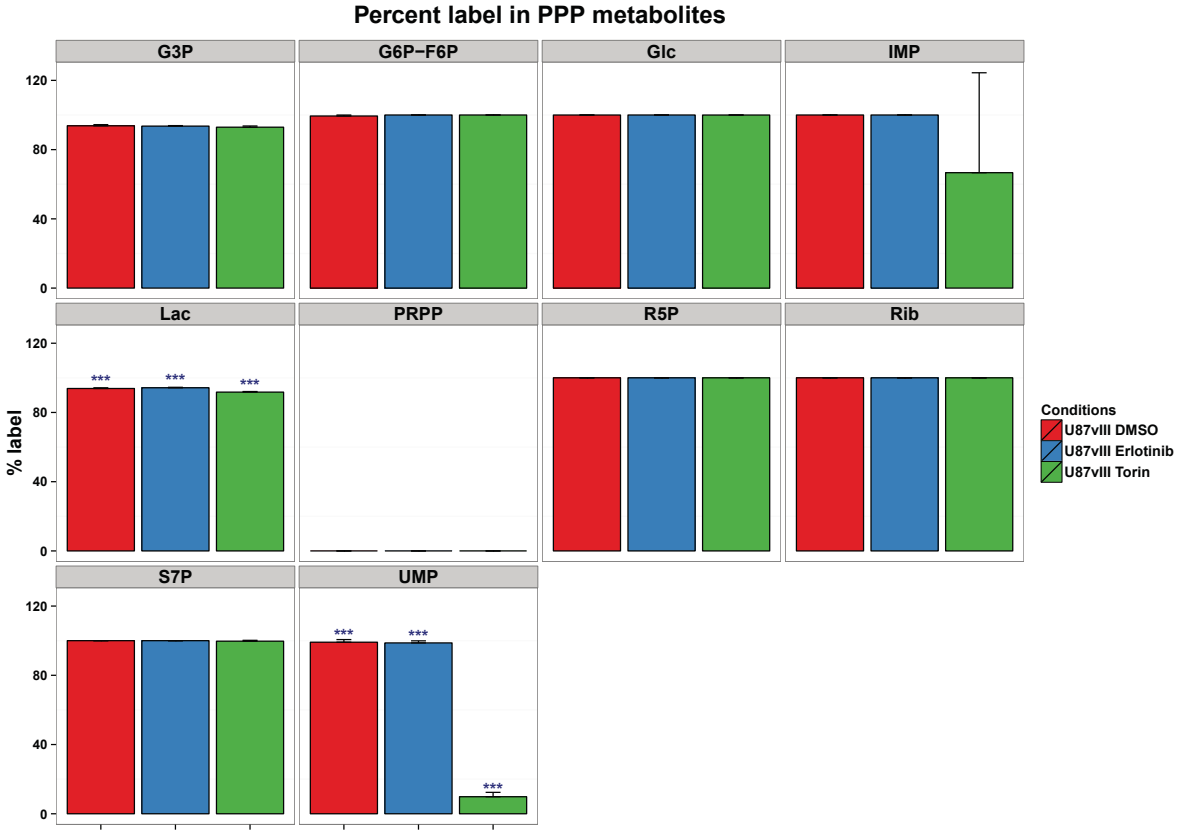
Percent label in PPP metabolites
G3P
G6P−F6P
Glc
IMP
Lac
PRPP
R5P
Rib
S7P
UMP
% label
Conditions
U87vIII DMSO
U87vIII Erlotinib
U87vIII Torin

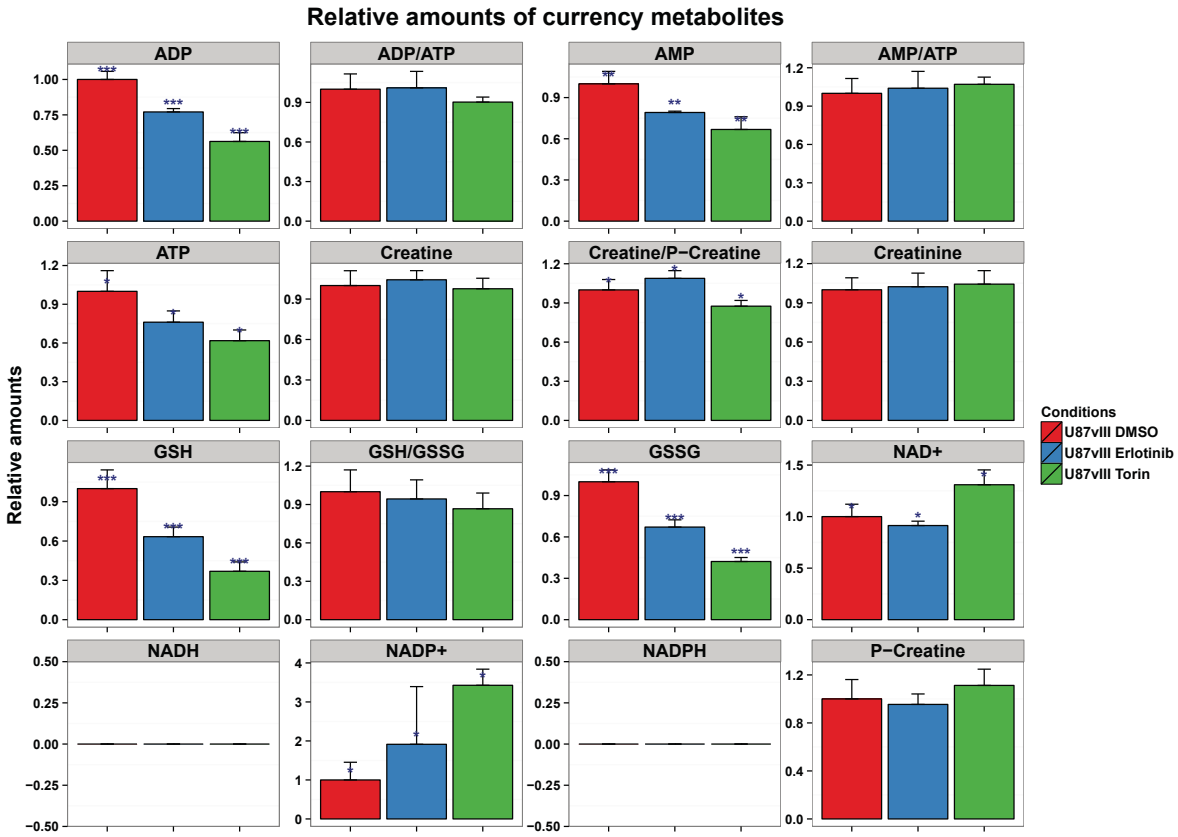
Relative amounts of currency metabolites
ADP
ADP/ATP
AMP
AMP/ATP
ATP
Creatine
Creatine/P−Creatine
Creatinine
GSH
GSH/GSSG
GSSG
NAD+
NADH
NADP+
NADPH
P−Creatine
Relative amounts
Conditions
U87vIII DMSO
U87vIII Erlotinib
U87vIII Torin

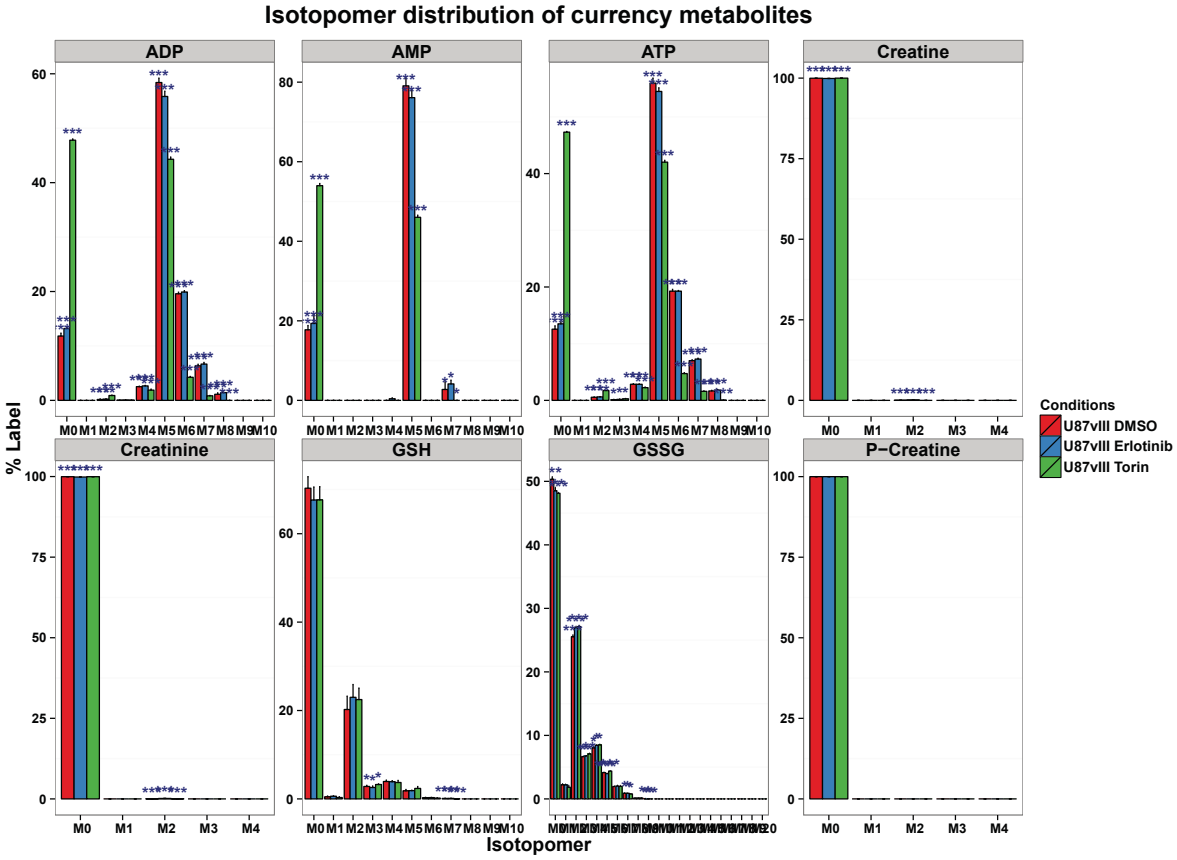
Isotopomer distribution of currency metabolites
ADP
AMP
ATP
Creatine
Creatinine
GSH
GSSG
P−Creatine
% Label
Isotopomer
Conditions
U87vIII DMSO
U87vIII Erlotinib
U87vIII Torin

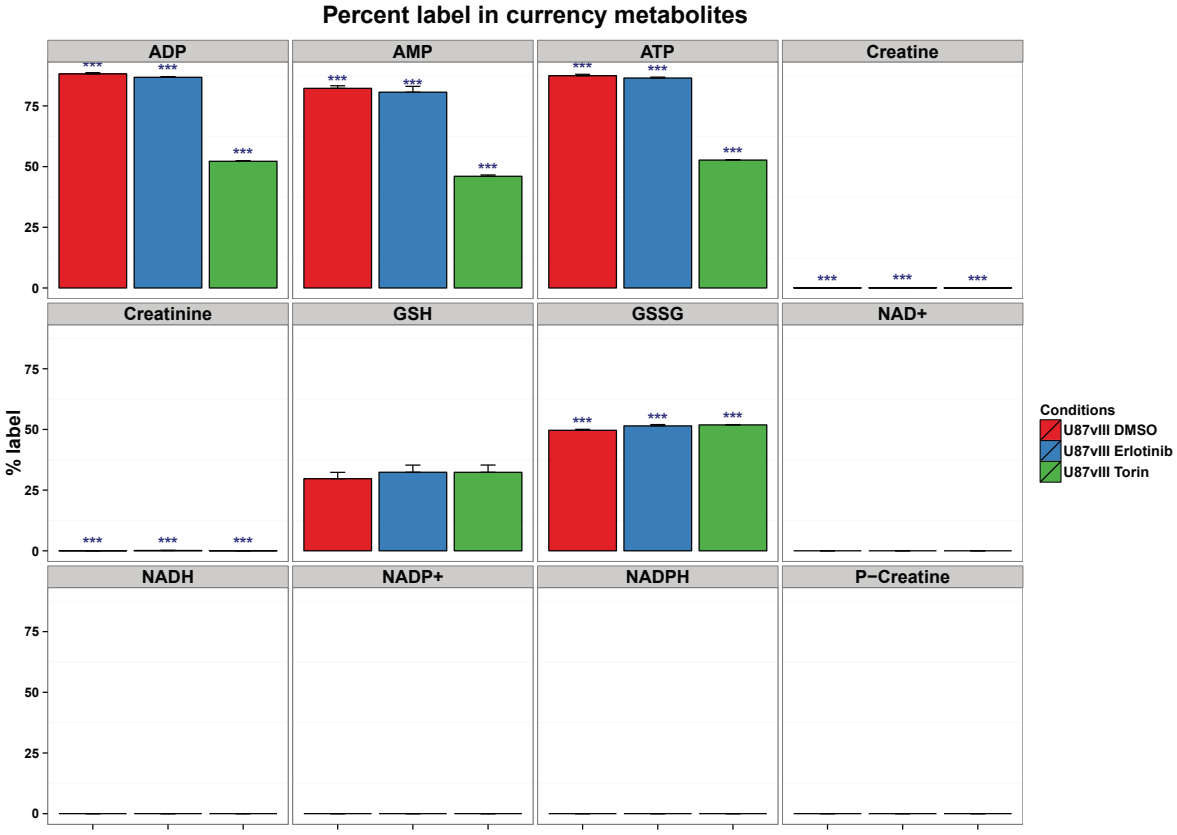
Percent label in currency metabolites
ADP
AMP
ATP
Creatine
Creatinine
GSH
GSSG
NAD+
NADH
NADP+
NADPH
P−Creatine
% label
Conditions
U87vIII DMSO
U87vIII Erlotinib
U87vIII Torin

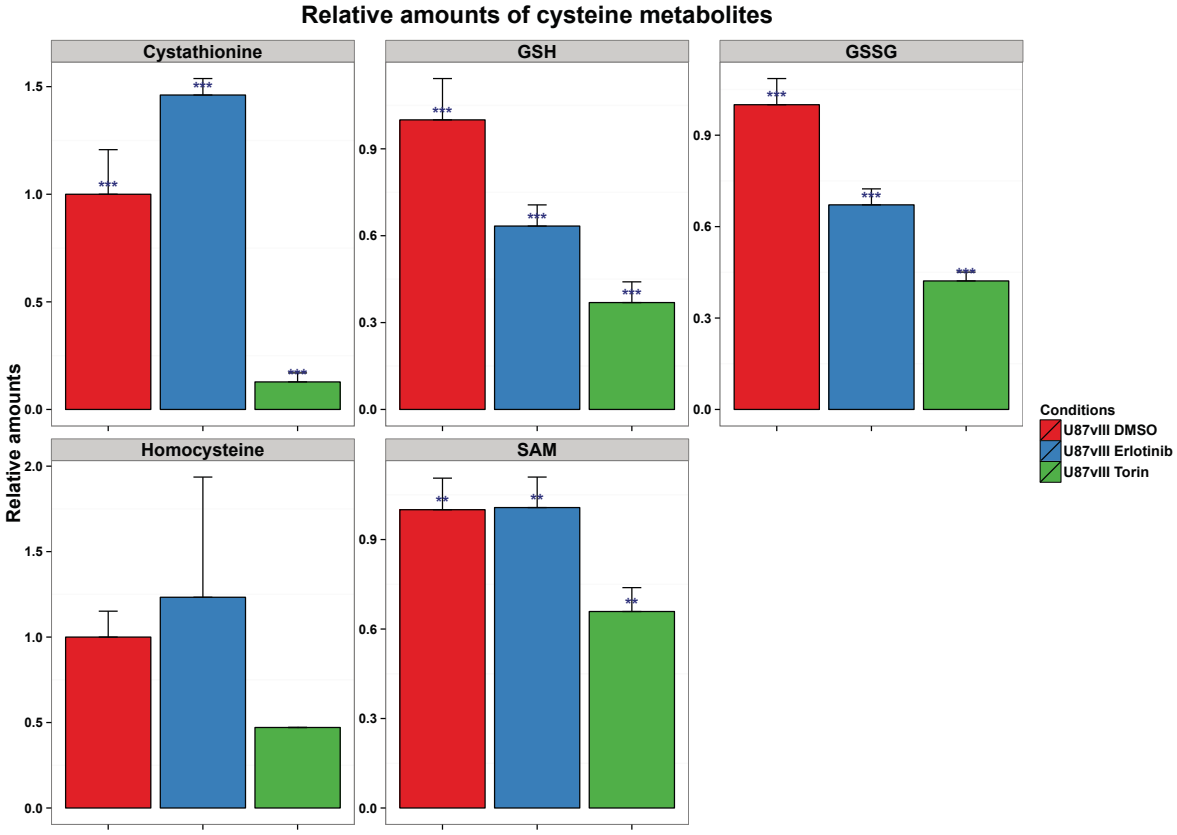
Relative amounts of cysteine metabolites
Cystathionine
GSH
GSSG
Homocysteine
SAM
Relative amounts
Conditions
U87vIII DMSO
U87vIII Erlotinib
U87vIII Torin

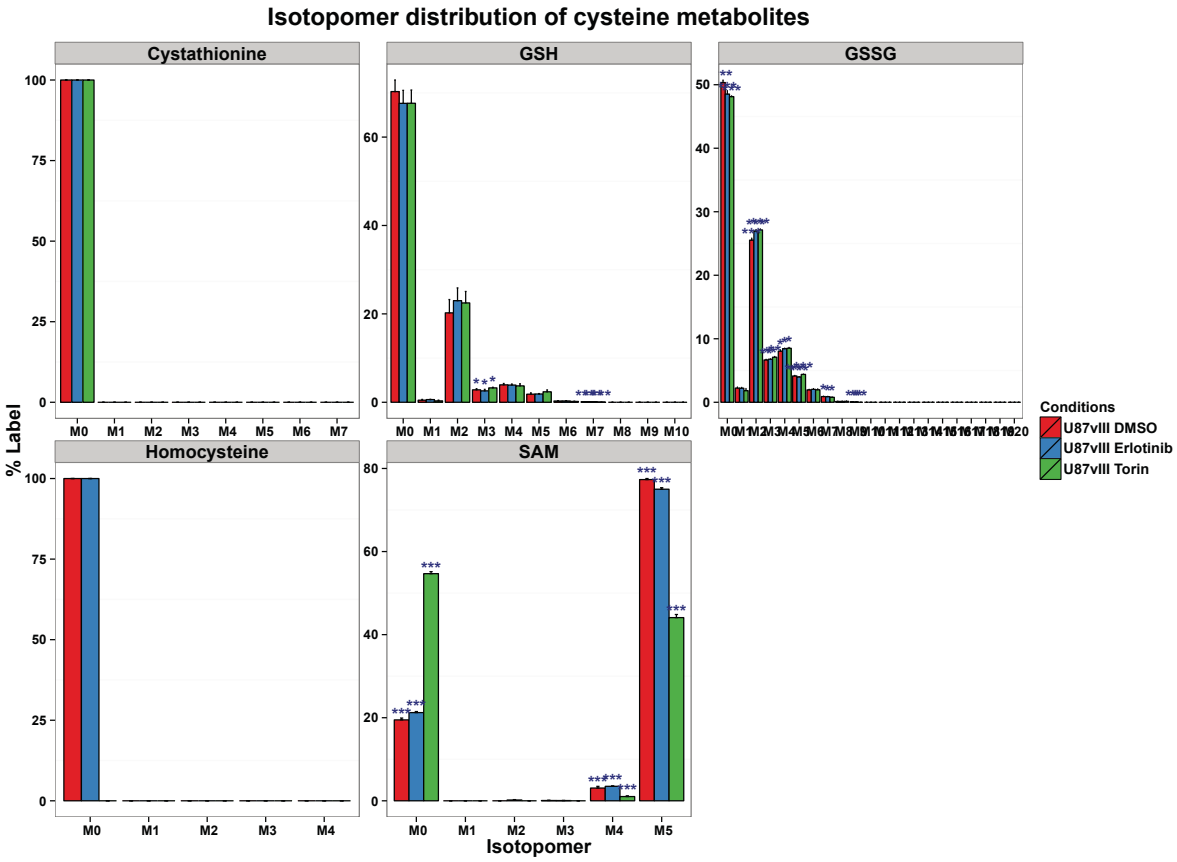
Isotopomer distribution of cysteine metabolites
Cystathionine
GSH
GSSG
Homocysteine
SAM
% Label
Isotopomer
Conditions
U87vIII DMSO
U87vIII Erlotinib
U87vIII Torin

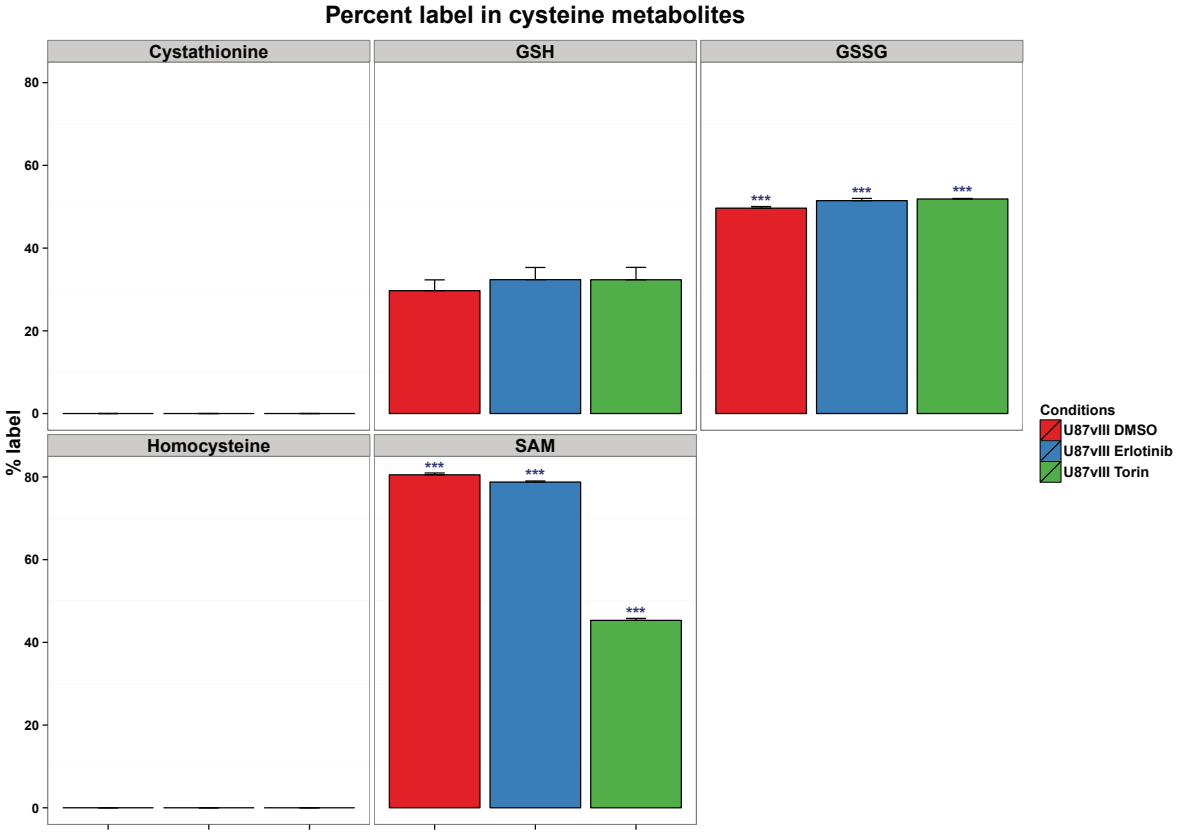
Percent label in cysteine metabolites
Cystathionine
GSH
GSSG
Homocysteine
SAM
% label
Conditions
U87vIII DMSO
U87vIII Erlotinib
U87vIII Torin

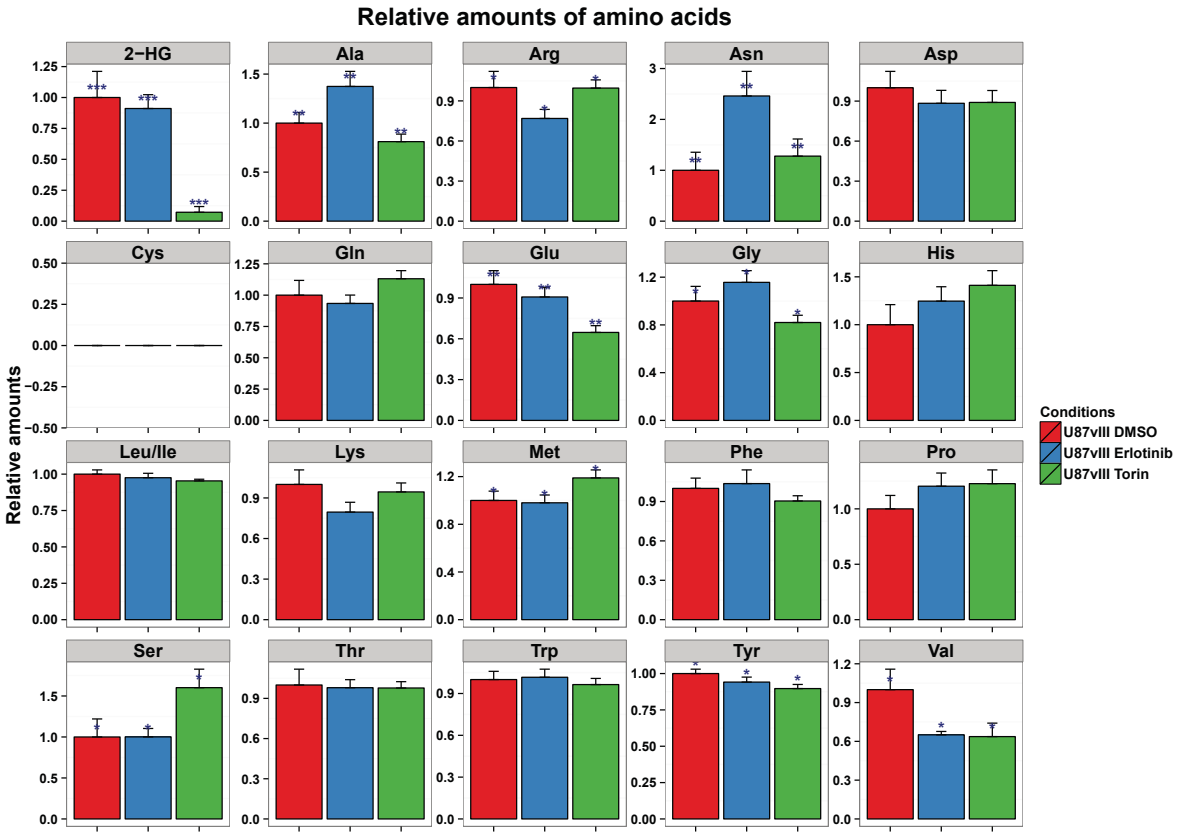
Relative amounts of amino acids
2−HG
Ala
Arg
Asn
Asp
Cys
Gln
Glu
Gly
His
Leu/Ile
Lys
Met
Phe
Pro
Ser
Thr
Trp
Tyr
Val
Relative amounts
Conditions
U87vIII DMSO
U87vIII Erlotinib
U87vIII Torin

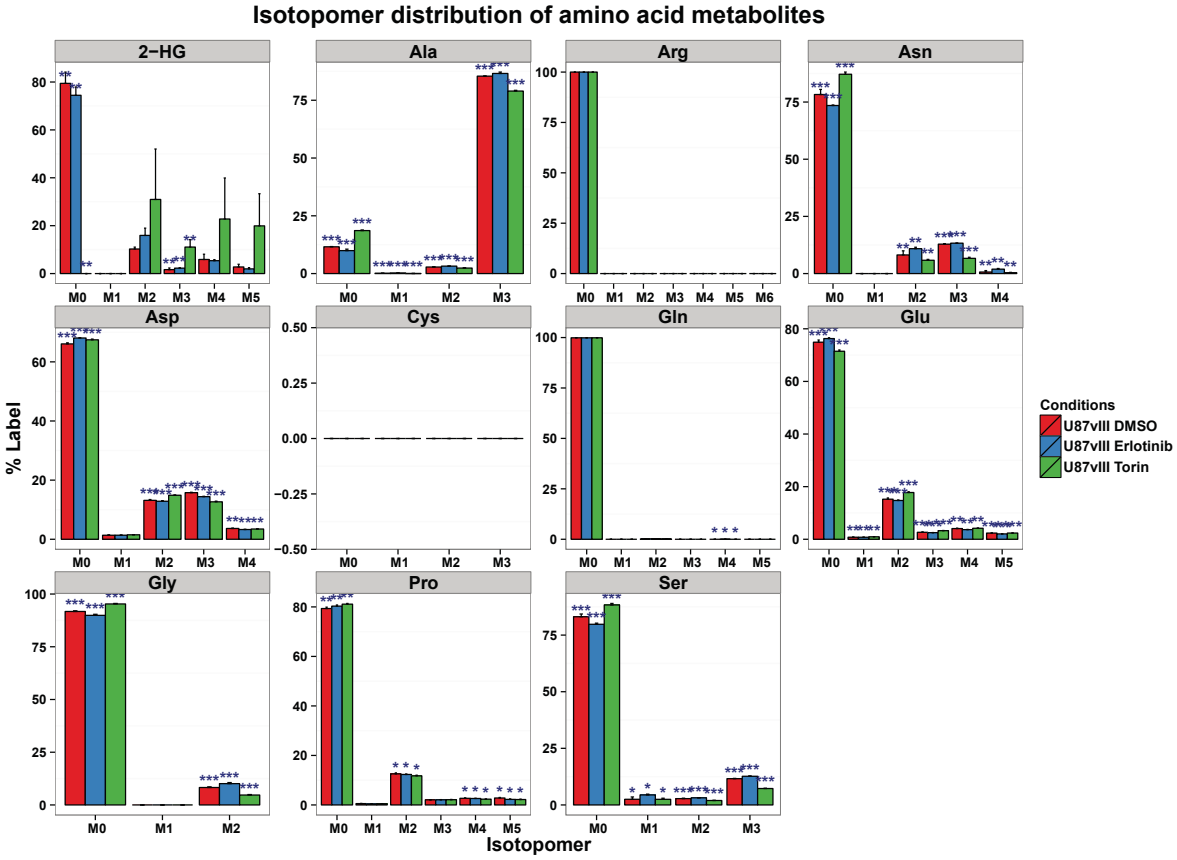
Isotopomer distribution of amino acid metabolites
2−HG
Ala
Arg
Asn
Asp
Cys
Gln
Glu
Gly
Pro
Ser
% Label
Isotopomer
Conditions
U87vIII DMSO
U87vIII Erlotinib
U87vIII Torin

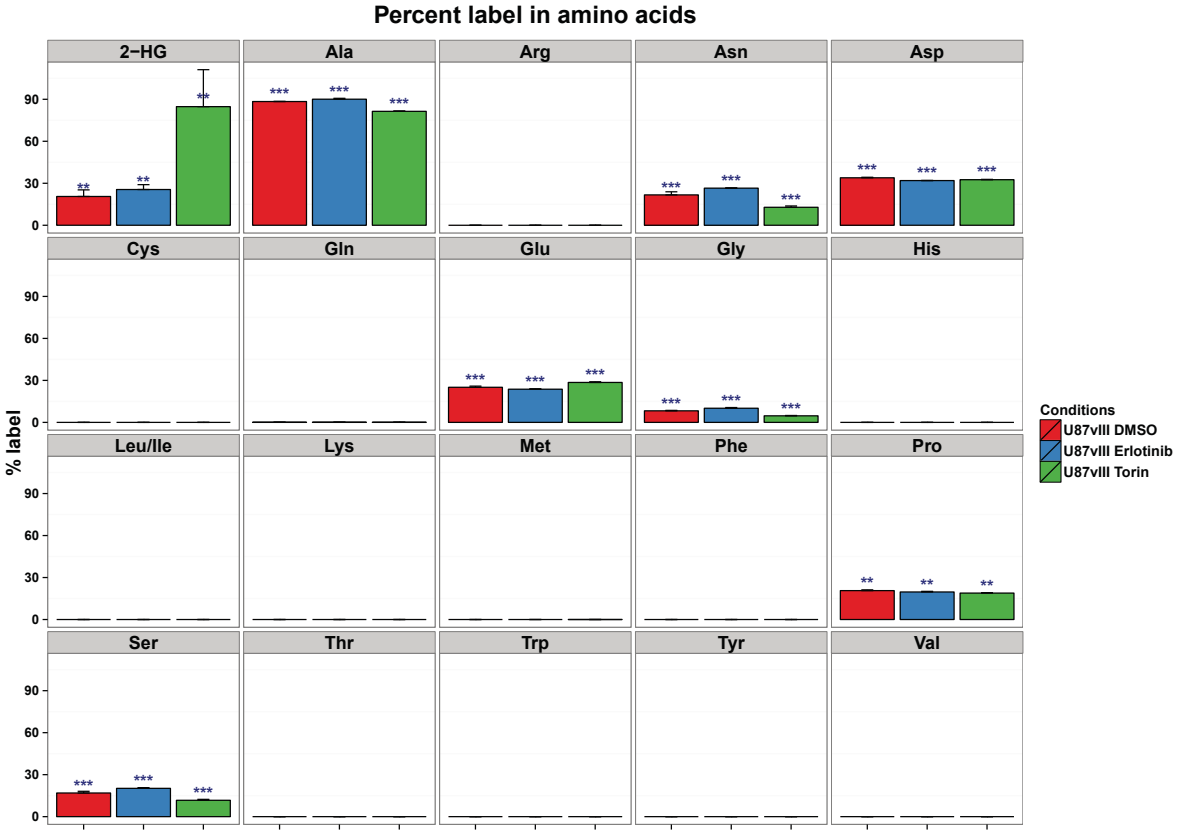
Percent label in amino acids
2−HG
Ala
Arg
Asn
Asp
Cys
Gln
Glu
Gly
His
Leu/Ile
Lys
Met
Phe
Pro
Ser
Thr
Trp
Tyr
Val
% label
Conditions
U87vIII DMSO
U87vIII Erlotinib
U87vIII Torin

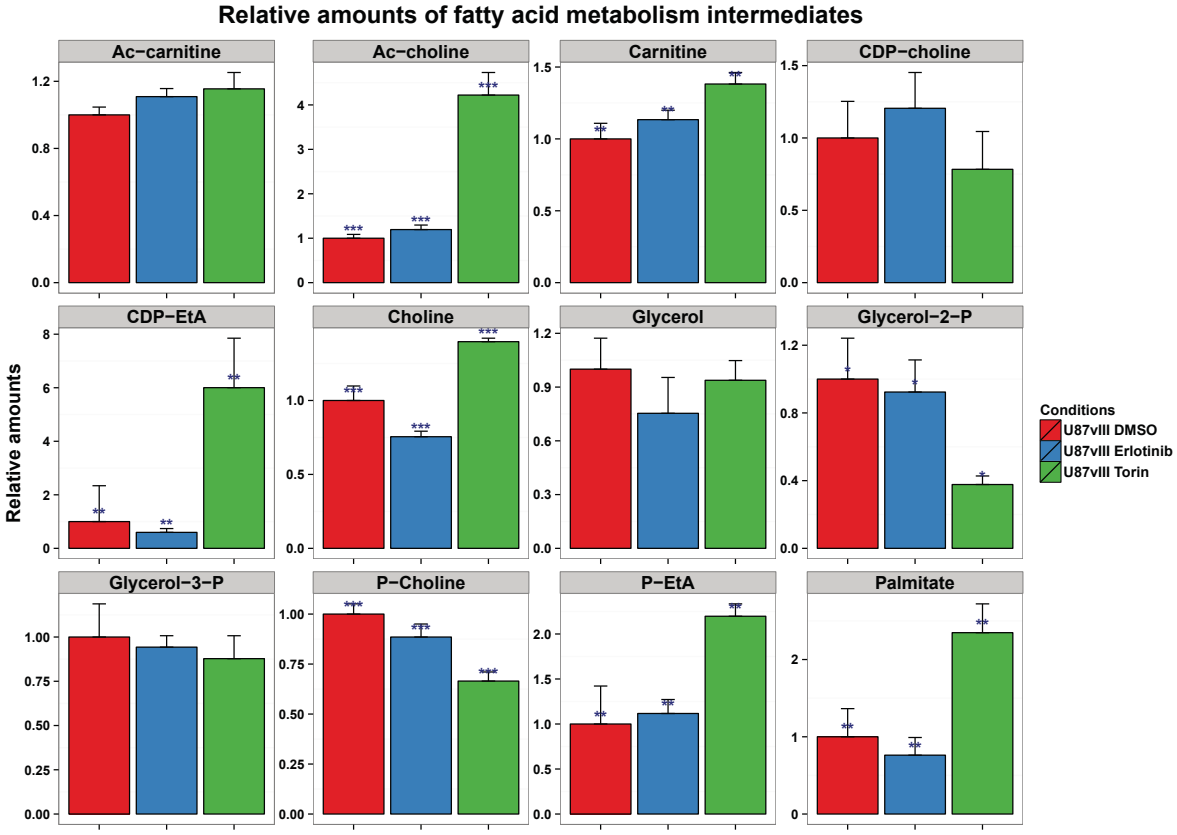
Relative amounts of fatty acid metabolism intermediates
Ac−carnitine
Ac−choline
Carnitine
CDP−choline
CDP−EtA
Choline
Glycerol
Glycerol−2−P
Glycerol−3−P
P−Choline
P−EtA
Palmitate
Relative amounts
Conditions
U87vIII DMSO
U87vIII Erlotinib
U87vIII Torin

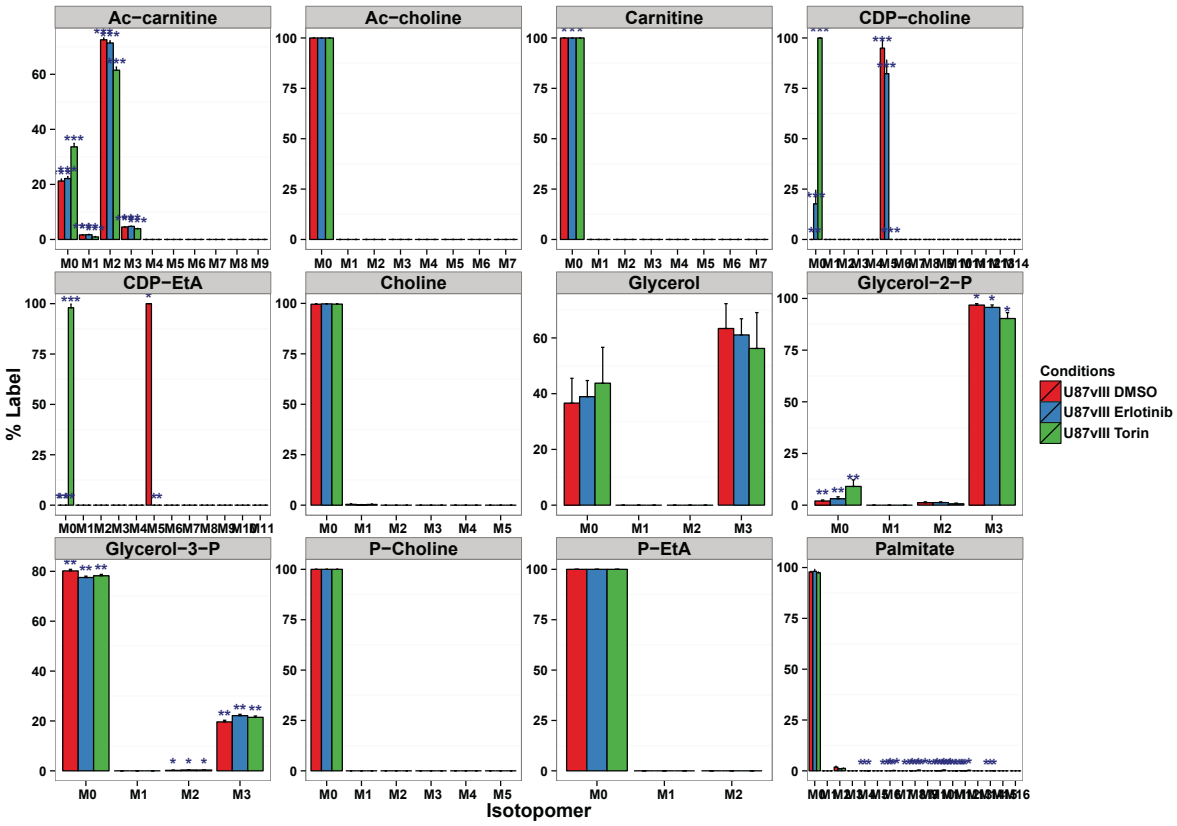
Isotopomer distribution of fatty acid metabolism intermediates
Ac−carnitine
Ac−choline
Carnitine
CDP−choline
CDP−EtA
Choline
Glycerol
Glycerol−2−P
Glycerol−3−P
P−Choline
P−EtA
Palmitate
% Label
Isotopomer
Conditions
U87vIII DMSO
U87vIII Erlotinib
U87vIII Torin

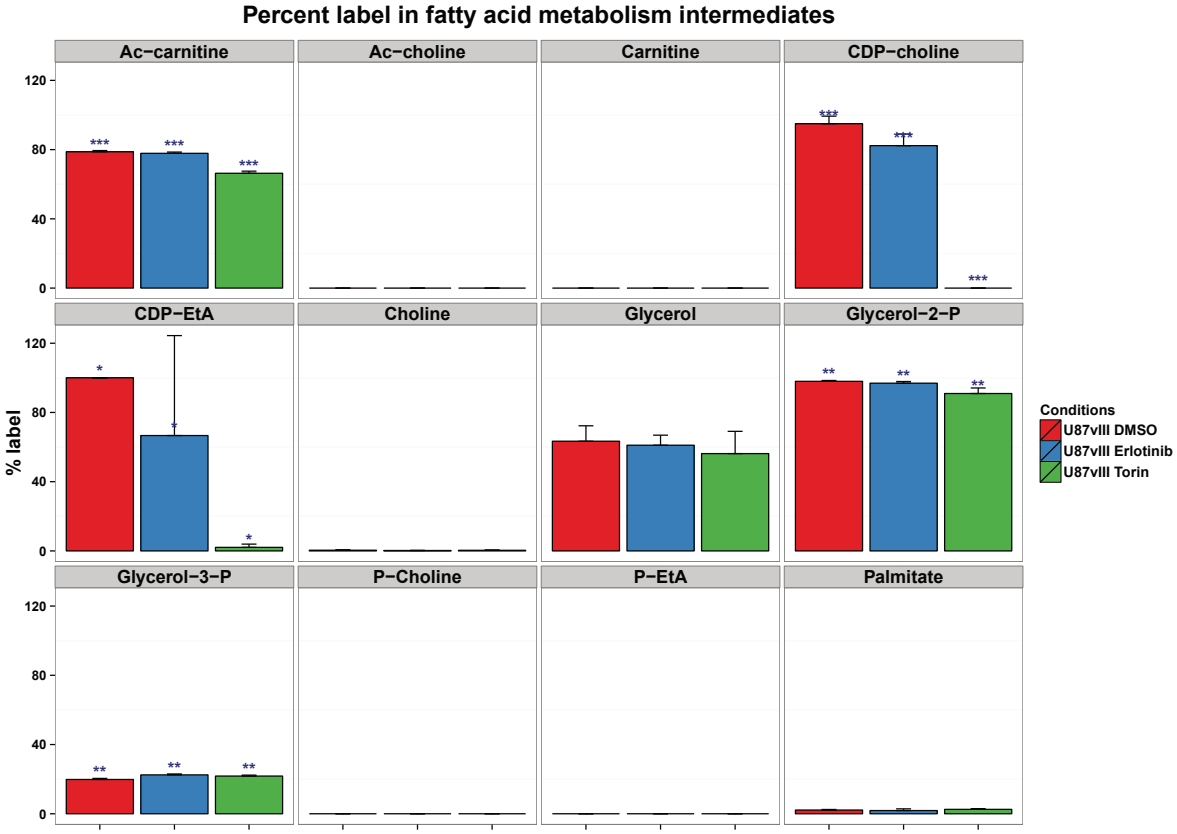
Percent label in fatty acid metabolism intermediates
Ac−carnitine
Ac−choline
Carnitine
CDP−choline
CDP−EtA
Choline
Glycerol
Glycerol−2−P
Glycerol−3−P
P−Choline
P−EtA
Palmitate
% label
Conditions
U87vIII DMSO
U87vIII Erlotinib
U87vIII Torin

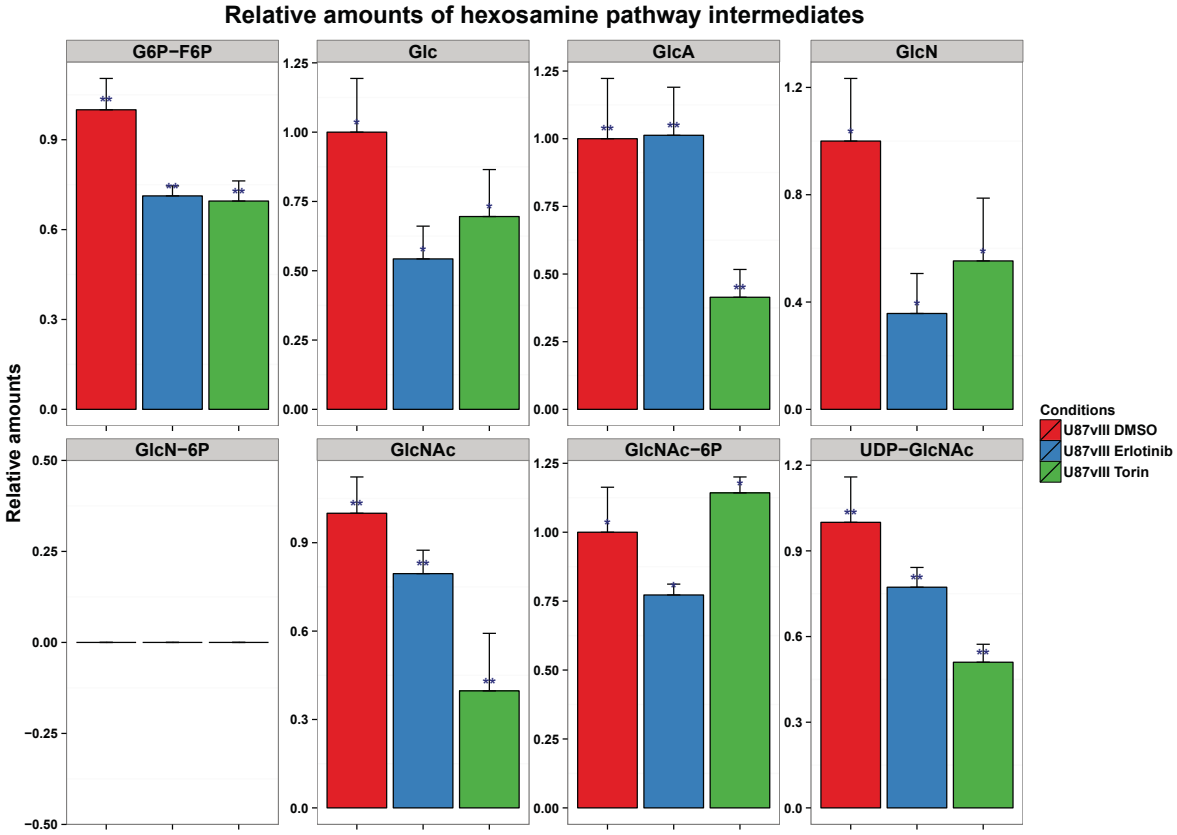
Relative amounts of hexosamine pathway intermediates
G6P−F6P
Glc
GlcA
GlcN
GlcN−6P
GlcNAc
GlcNAc−6P
UDP−GlcNAc
Relative amounts
Conditions
U87vIII DMSO
U87vIII Erlotinib
U87vIII Torin

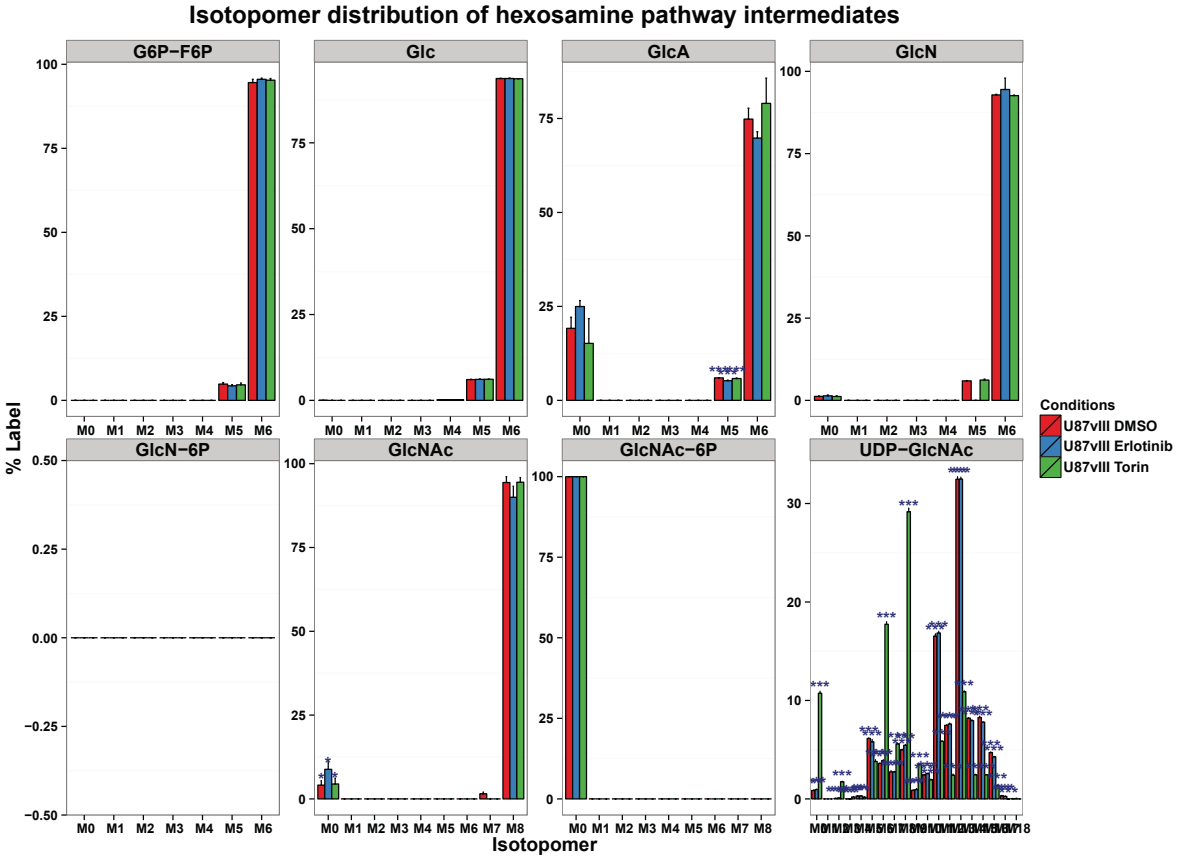
Isotopomer distribution of hexosamine pathway intermediates
G6P−F6P
Glc
GlcA
GlcN
GlcN−6P
GlcNAc
GlcNAc−6P
UDP−GlcNAc
% Label
Isotopomer
Conditions
U87vIII DMSO
U87vIII Erlotinib
U87vIII Torin

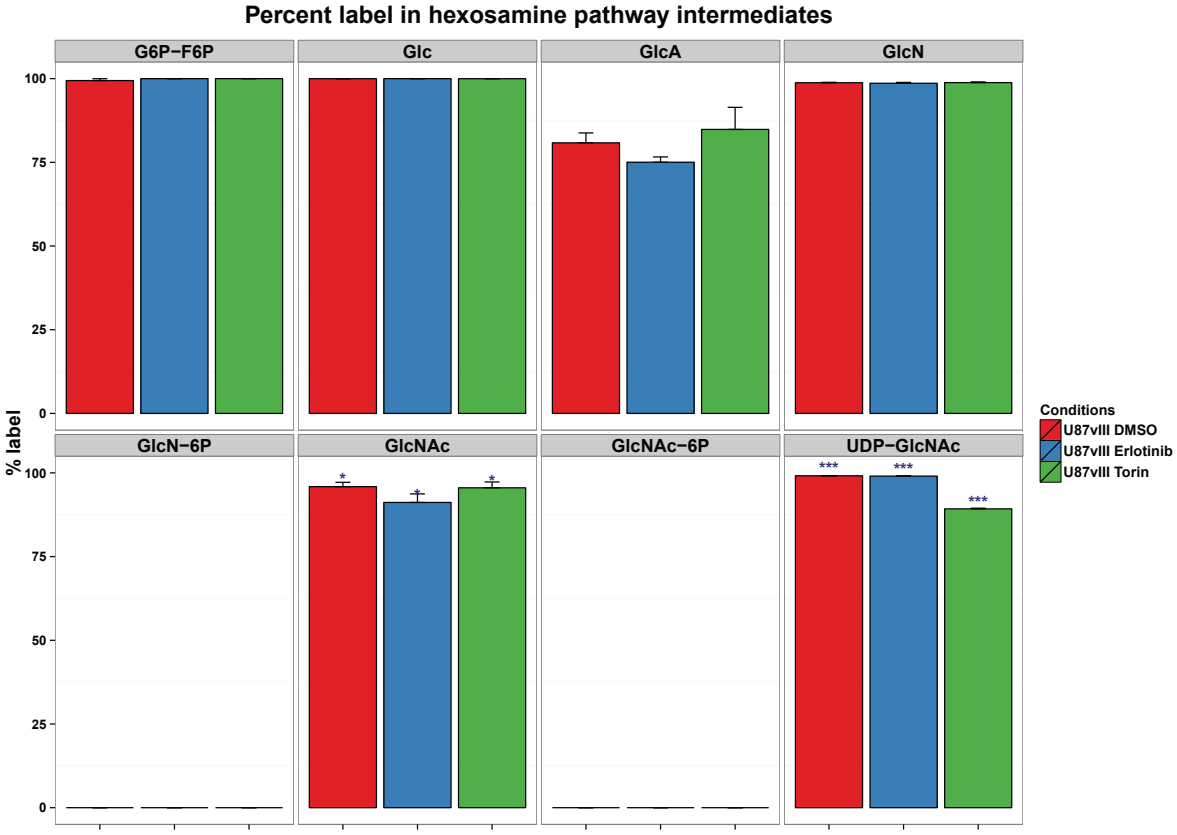
Percent label in hexosamine pathway intermediates
G6P−F6P
Glc
GlcA
GlcN
GlcN−6P
GlcNAc
GlcNAc−6P
UDP−GlcNAc
% label
Conditions
U87vIII DMSO
U87vIII Erlotinib
U87vIII Torin

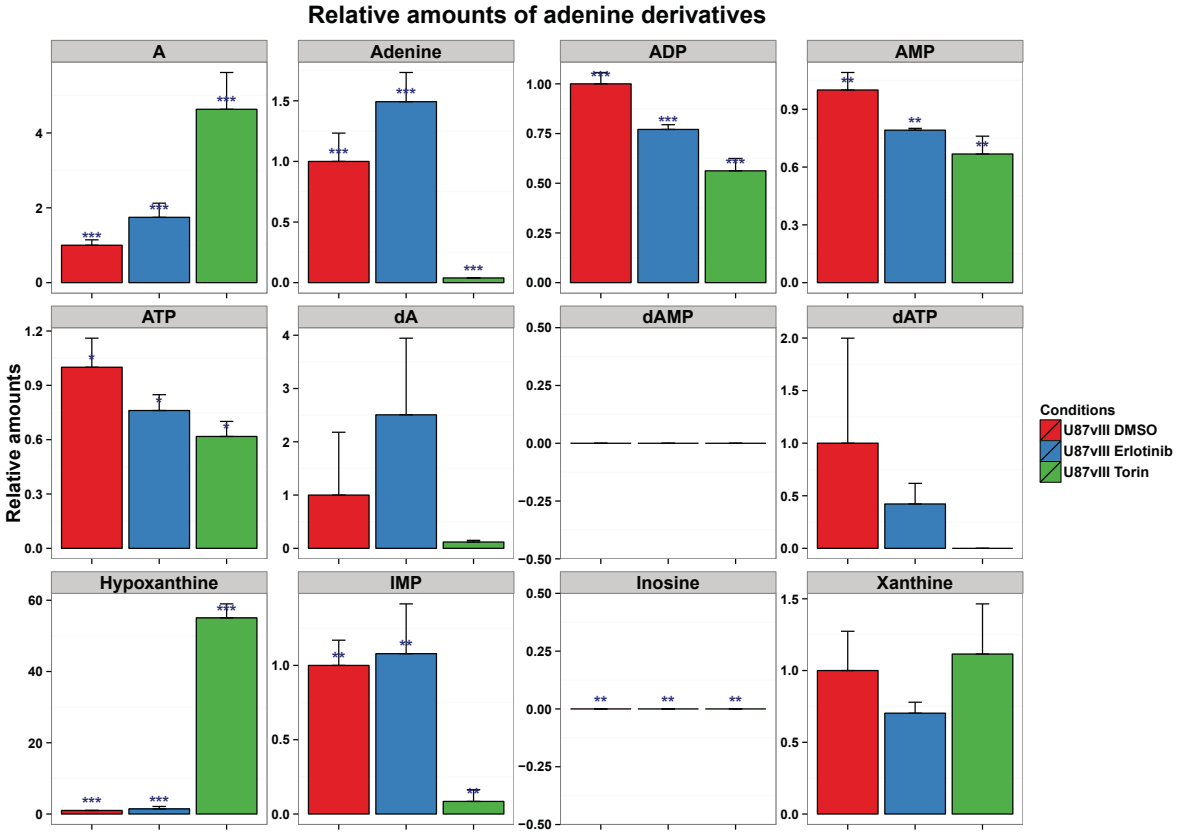
Relative amounts of adenine derivatives
A
Adenine
ADP
AMP
ATP
dA
dAMP
dATP
Hypoxanthine
IMP
Inosine
Xanthine
Relative amounts
Conditions
U87vIII DMSO
U87vIII Erlotinib
U87vIII Torin

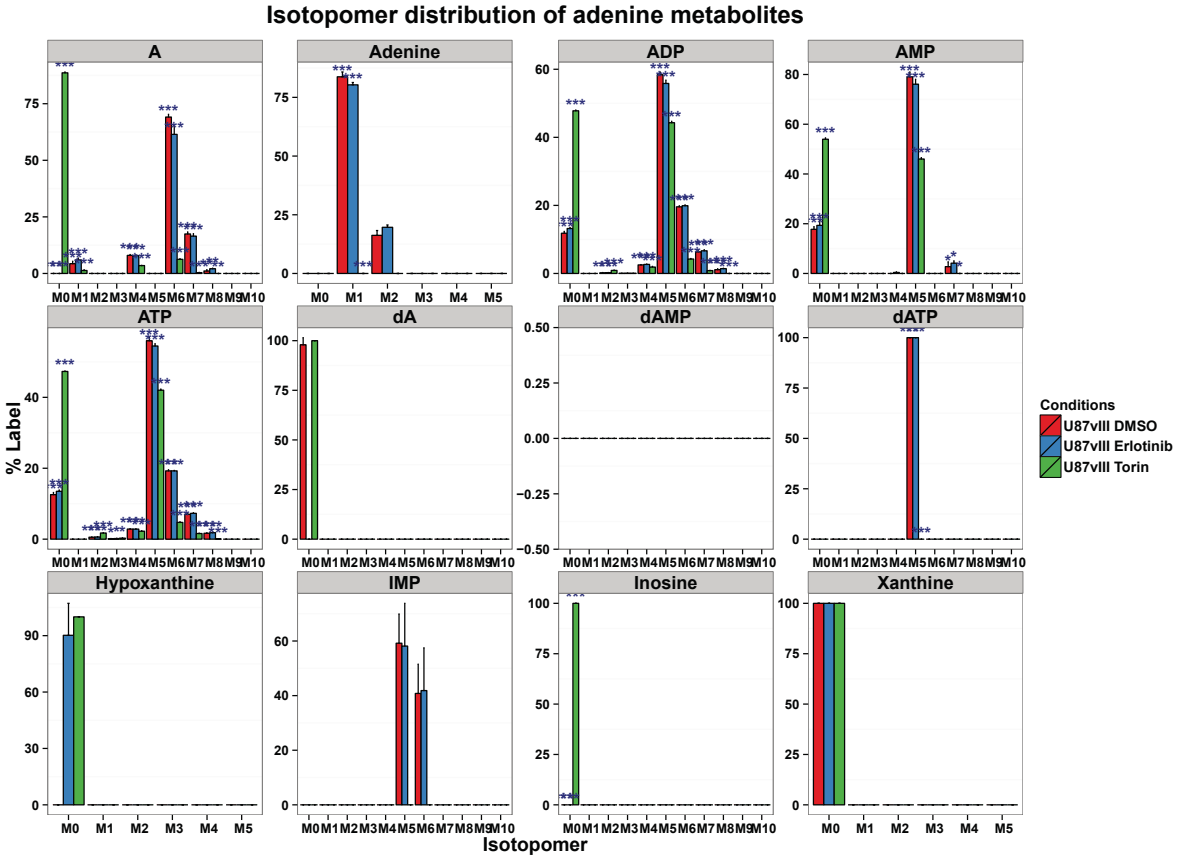
Isotopomer distribution of adenine metabolites
A
Adenine
ADP
AMP
ATP
dA
dAMP
dATP
Hypoxanthine
IMP
Inosine
Xanthine
% Label
Isotopomer
Conditions
U87vIII DMSO
U87vIII Erlotinib
U87vIII Torin

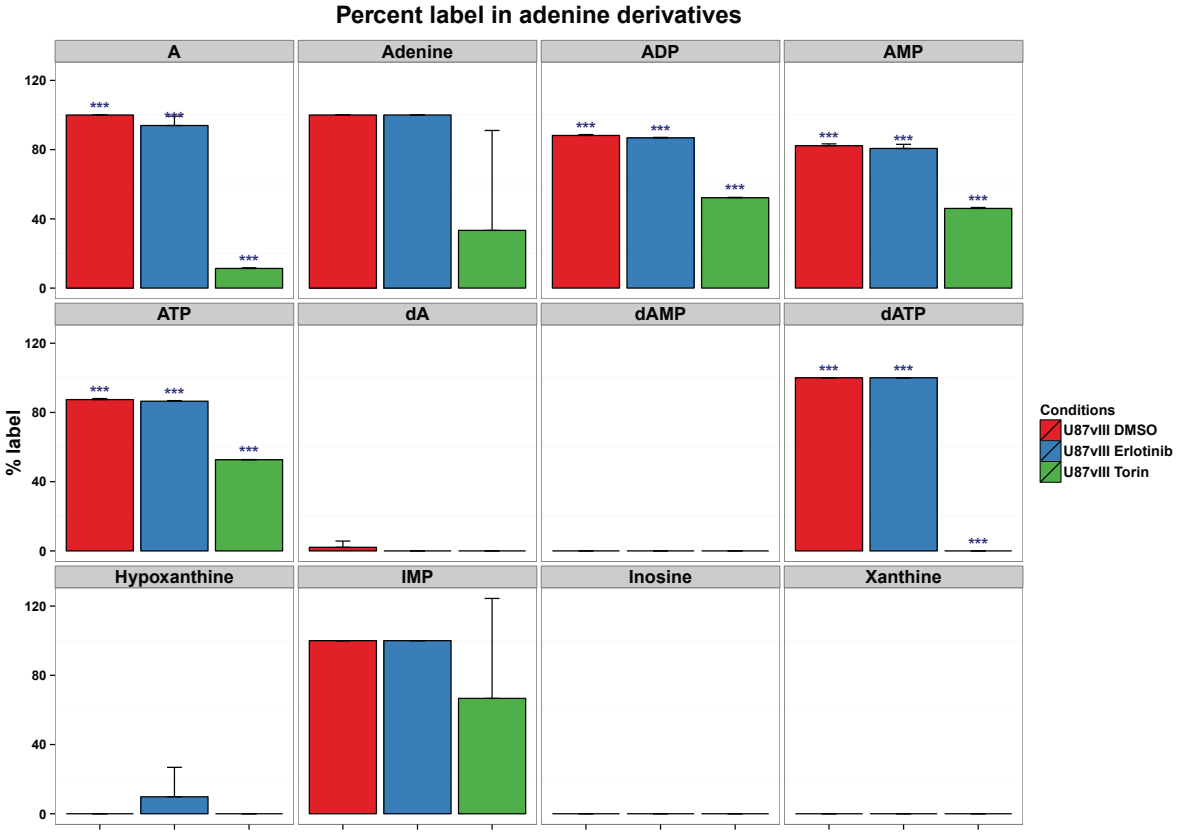
Percent label in adenine derivatives
A
Adenine
ADP
AMP
ATP
dA
dAMP
dATP
Hypoxanthine
IMP
Inosine
Xanthine
% label
Conditions
U87vIII DMSO
U87vIII Erlotinib
U87vIII Torin

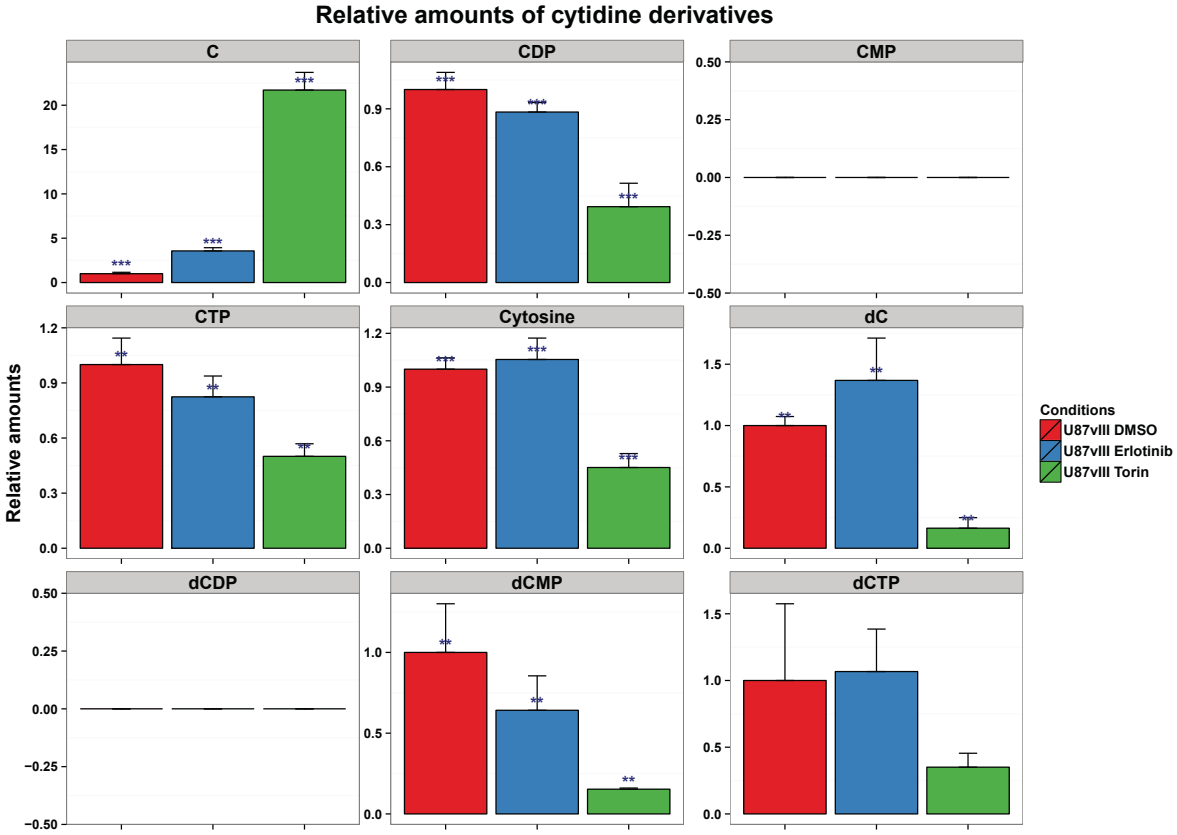
Relative amounts of cytidine derivatives
C
CDP
CMP
CTP
Cytosine
dC
dCDP
dCMP
dCTP
Relative amounts
Conditions
U87vIII DMSO
U87vIII Erlotinib
U87vIII Torin

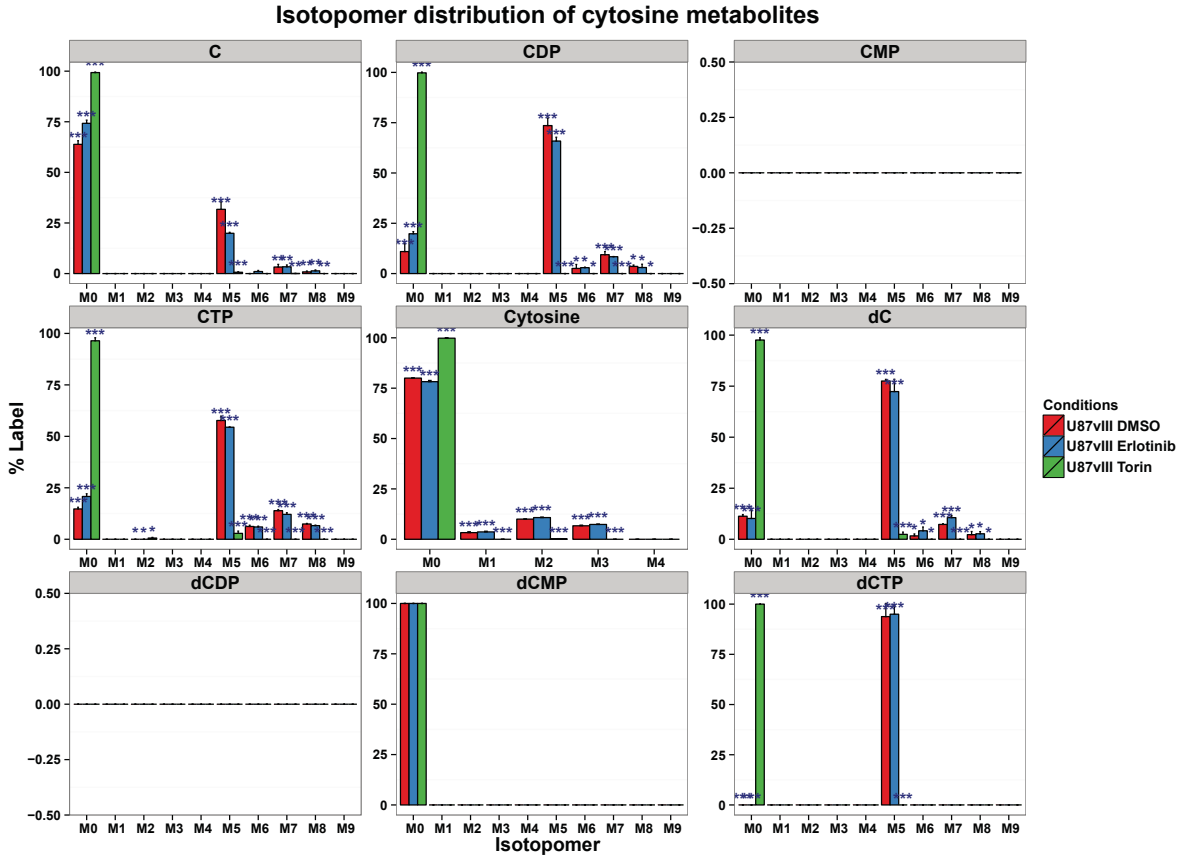
Isotopomer distribution of cytosine metabolites
C
CDP
CMP
CTP
Cytosine
dC
dCDP
dCMP
dCTP
% Label
Isotopomer
Conditions
U87vIII DMSO
U87vIII Erlotinib
U87vIII Torin

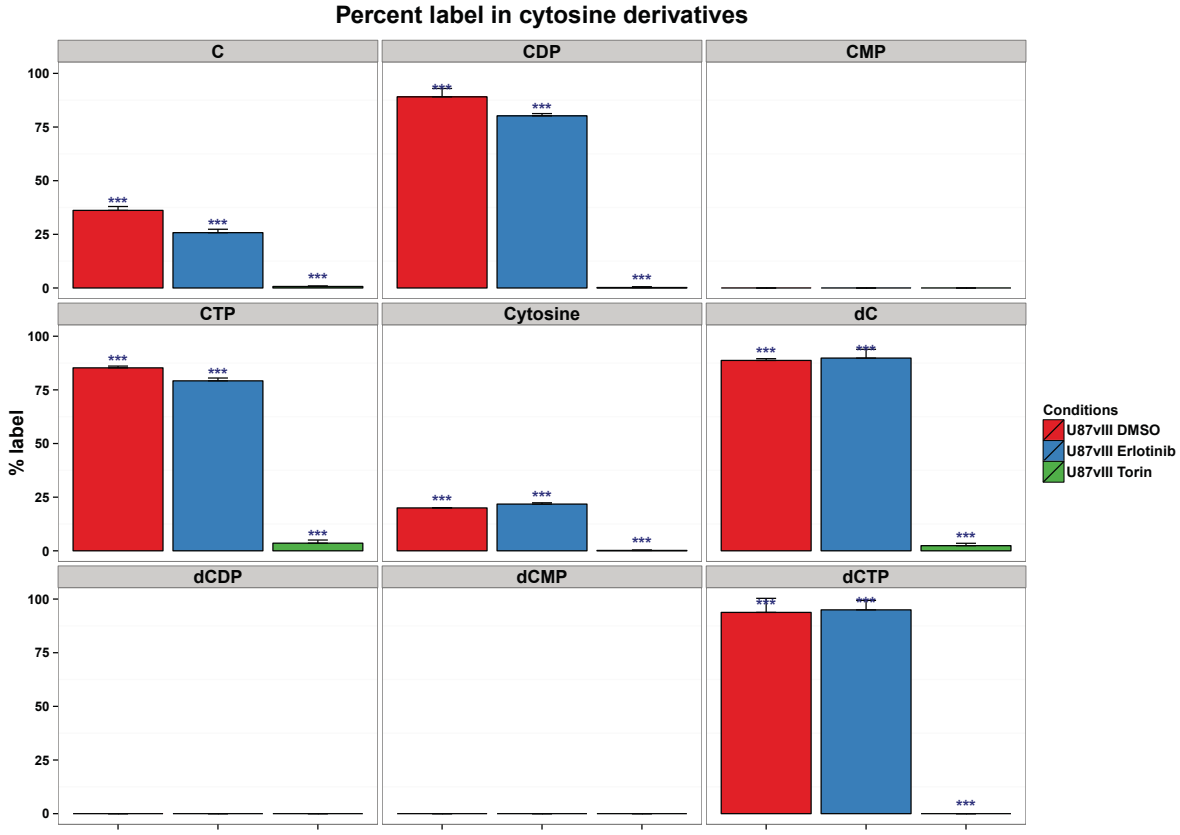
Percent label in cytosine derivatives
C
CDP
CMP
CTP
Cytosine
dC
dCDP
dCMP
dCTP
% label
Conditions
U87vIII DMSO
U87vIII Erlotinib
U87vIII Torin

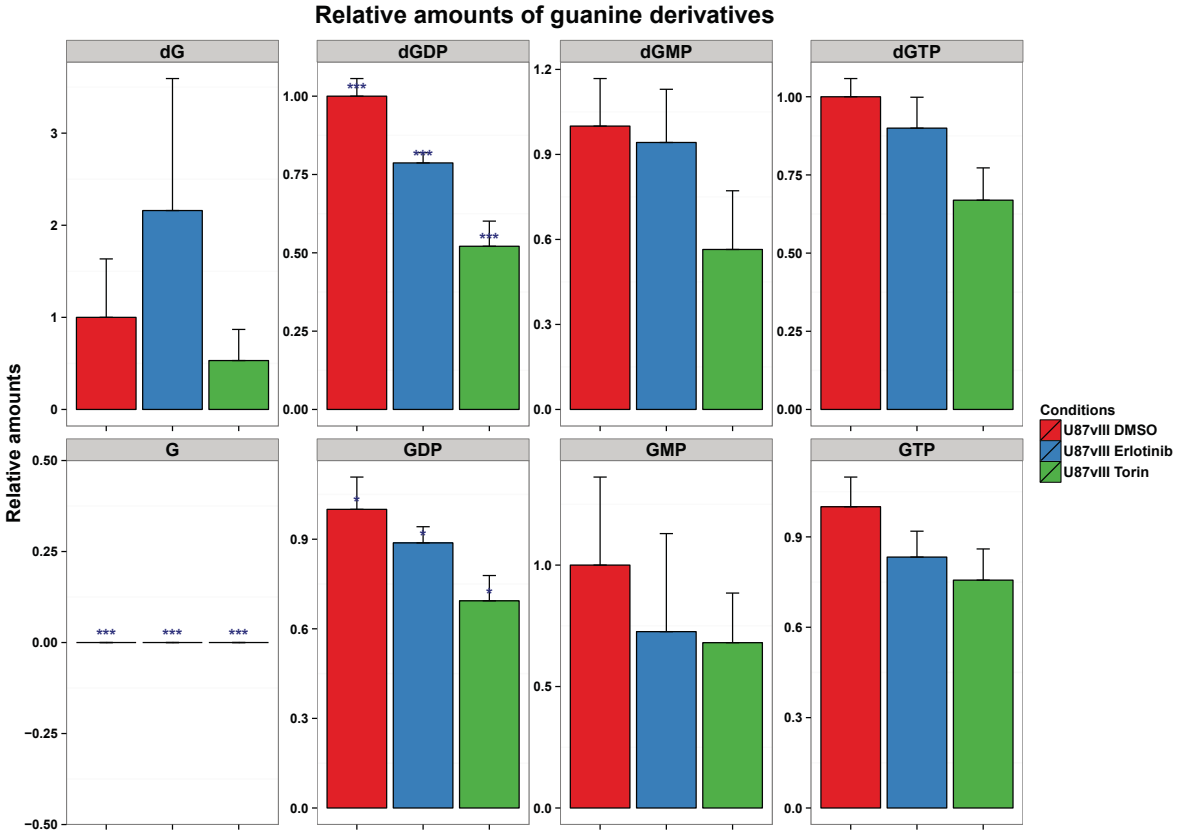
Relative amounts of guanine derivatives
dG
dGDP
dGMP
dGTP
G
GDP
GMP
GTP
Relative amounts
Conditions
U87vIII DMSO
U87vIII Erlotinib
U87vIII Torin

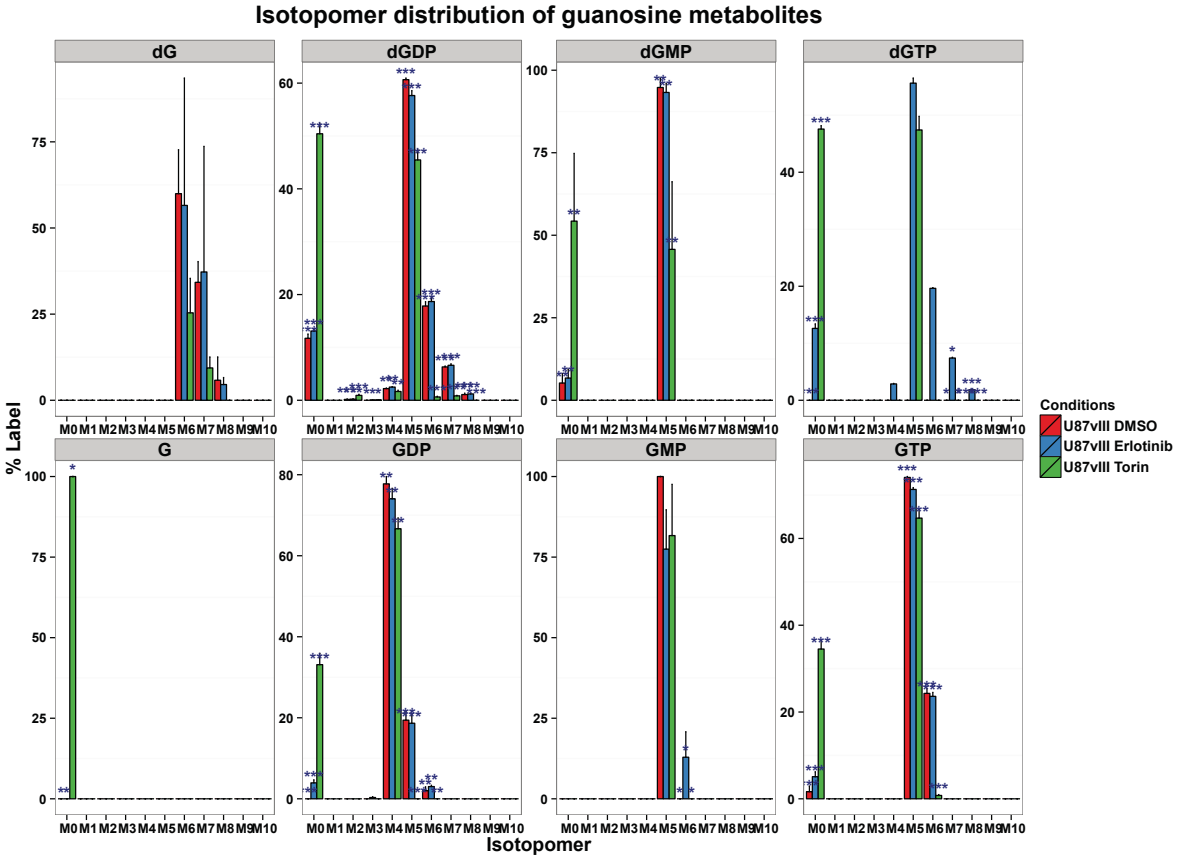
Isotopomer distribution of guanosine metabolites
dG
dGDP
dGMP
dGTP
G
GDP
GMP
GTP
% Label
Isotopomer
M0 M1 M2 M3 M4 M5 M6 M7 M8 M9 M10
Conditions
U87vIII DMSO
U87vIII Erlotinib
U87vIII Torin

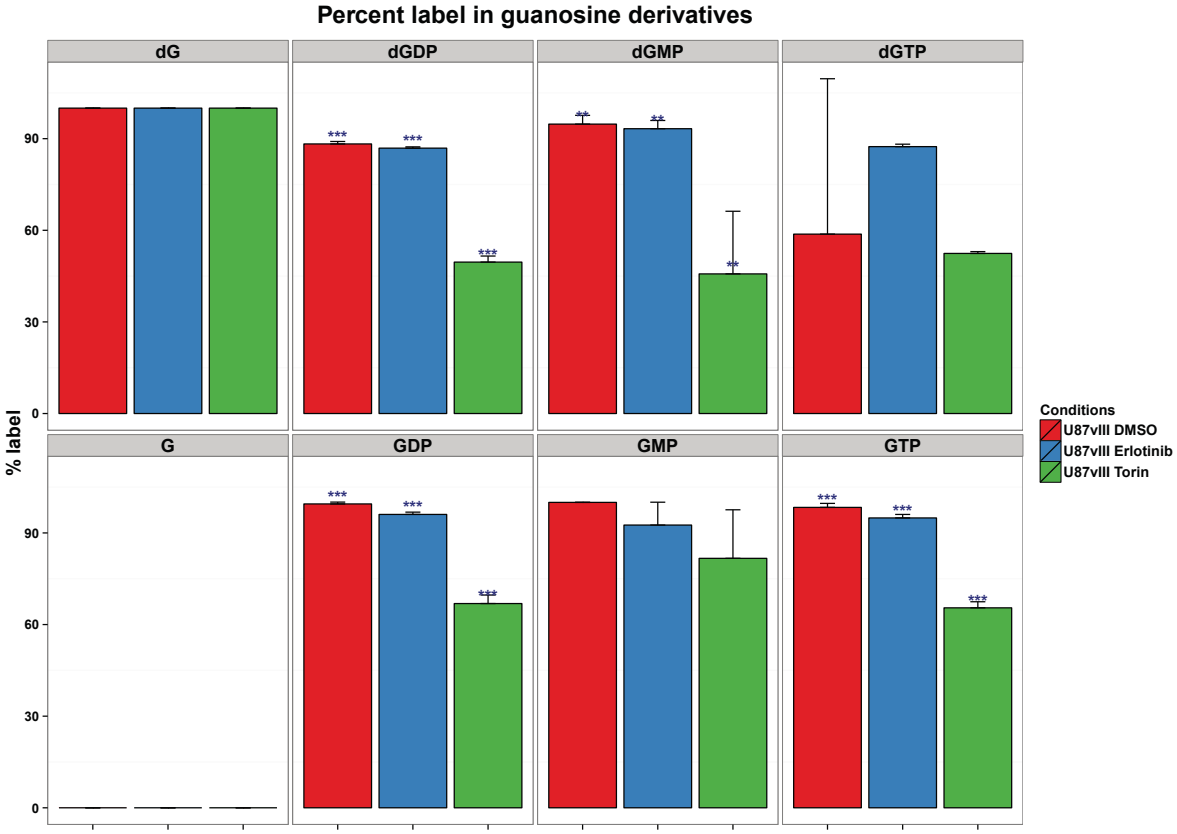
Percent label in guanosine derivatives
dG
dGDP
dGMP
dGTP
G
GDP
GMP
GTP
% label
0
30
60
90
***
**
Conditions
U87vIII DMSO
U87vIII Erlotinib
U87vIII Torin

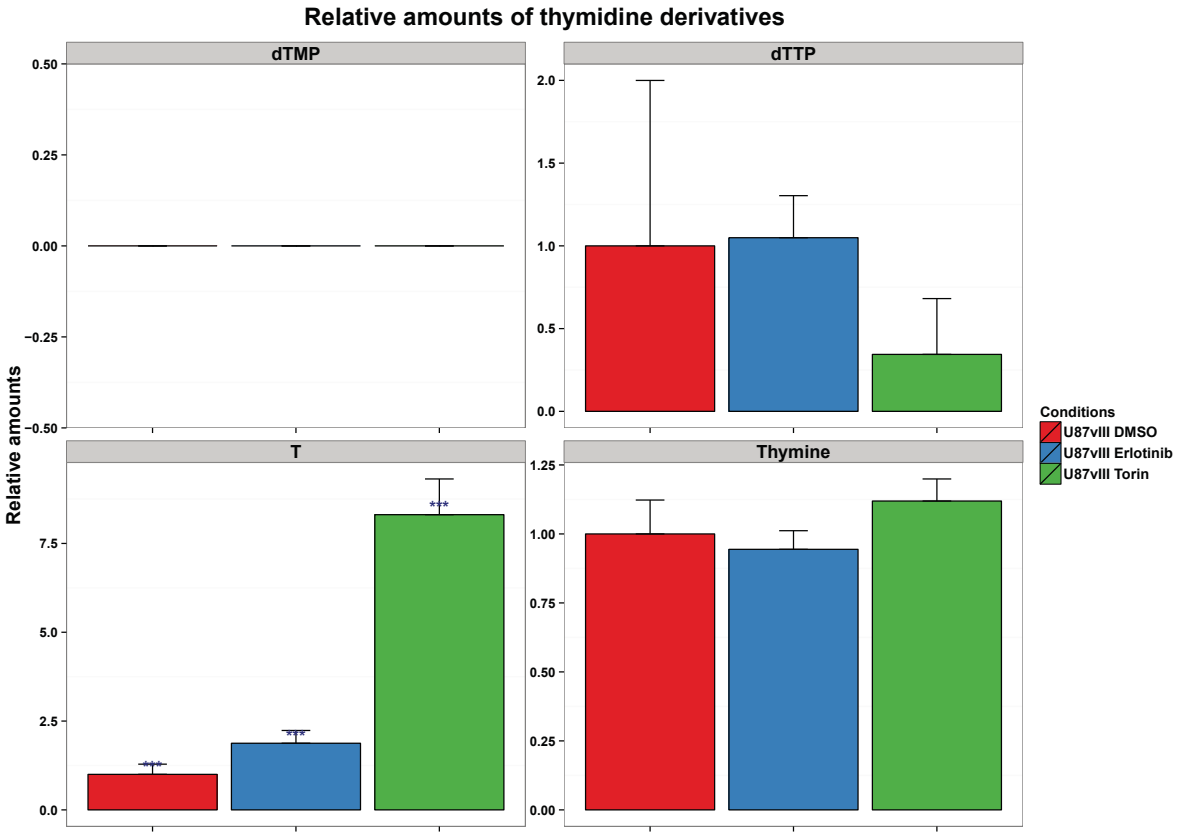
Relative amounts of thymidine derivatives
dTMP
dTTP
T
Thymine
Relative amounts
0.50
0.25
0.00
−0.25
−0.50
2.0
1.5
1.0
0.5
0.0
7.5
5.0
2.5
1.25
1.00
0.75
0.50
0.25
0.00
***
Conditions
U87vIII DMSO
U87vIII Erlotinib
U87vIII Torin

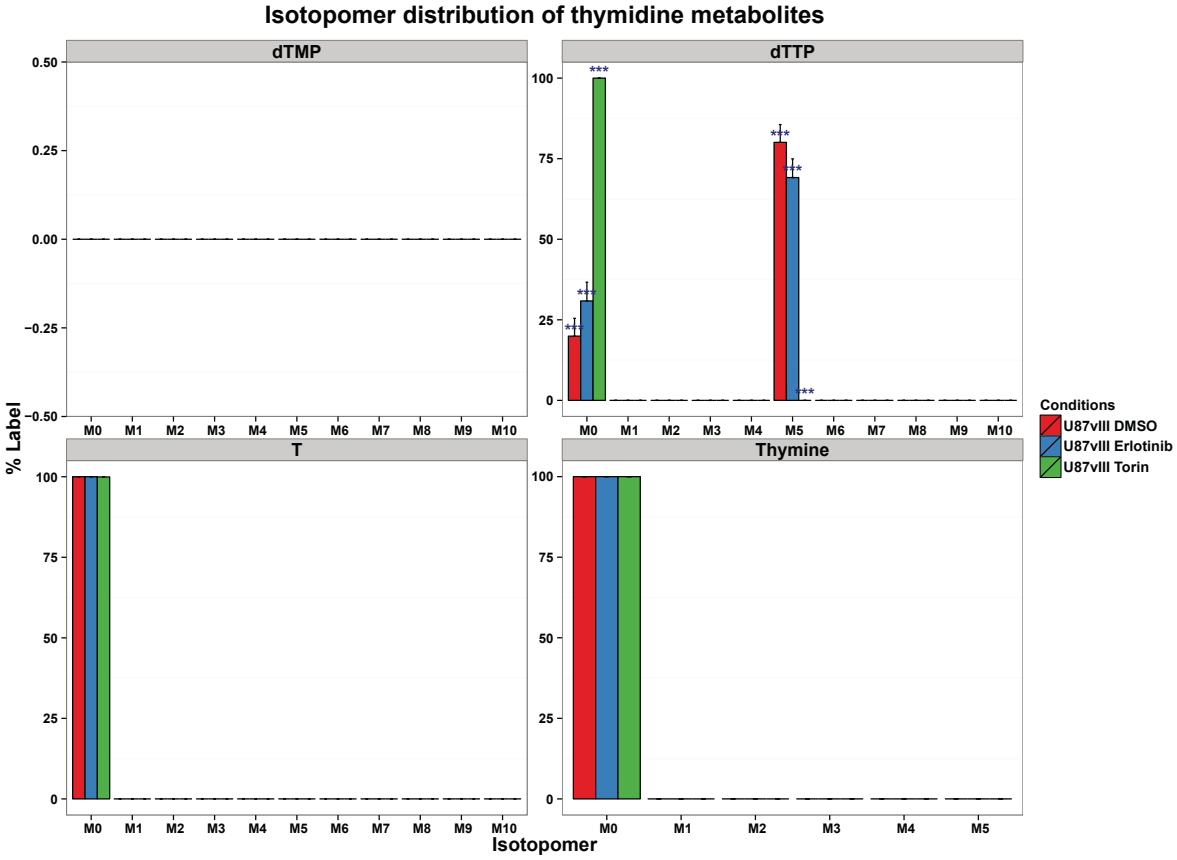
Isotopomer distribution of thymidine metabolites
dTMP
dTTP
T
Thymine
% Label
Isotopomer
M0
M1
M2
M3
M4
M5
M6
M7
M8
M9
M10
Conditions
U87vIII DMSO
U87vIII Erlotinib
U87vIII Torin

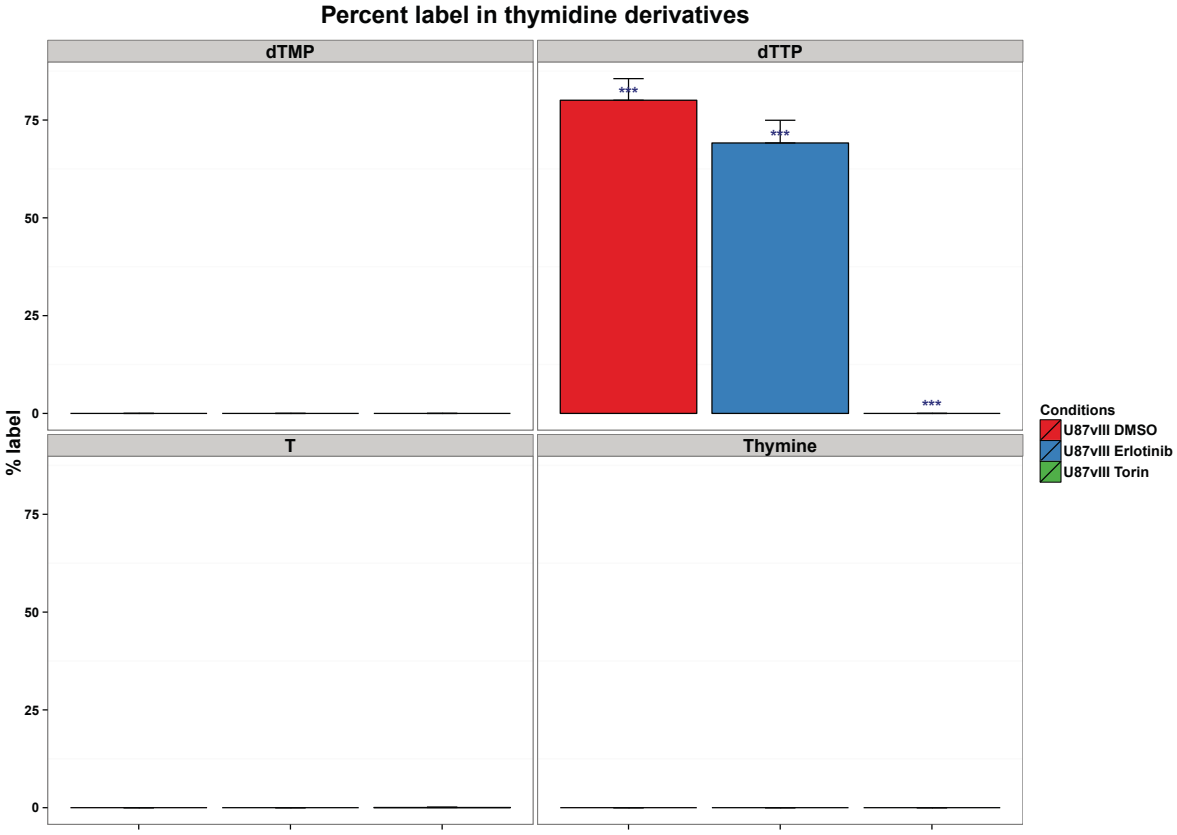
Percent label in thymidine derivatives
dTMP
dTTP
T
Thymine
% label
Conditions
U87vIII DMSO
U87vIII Erlotinib
U87vIII Torin

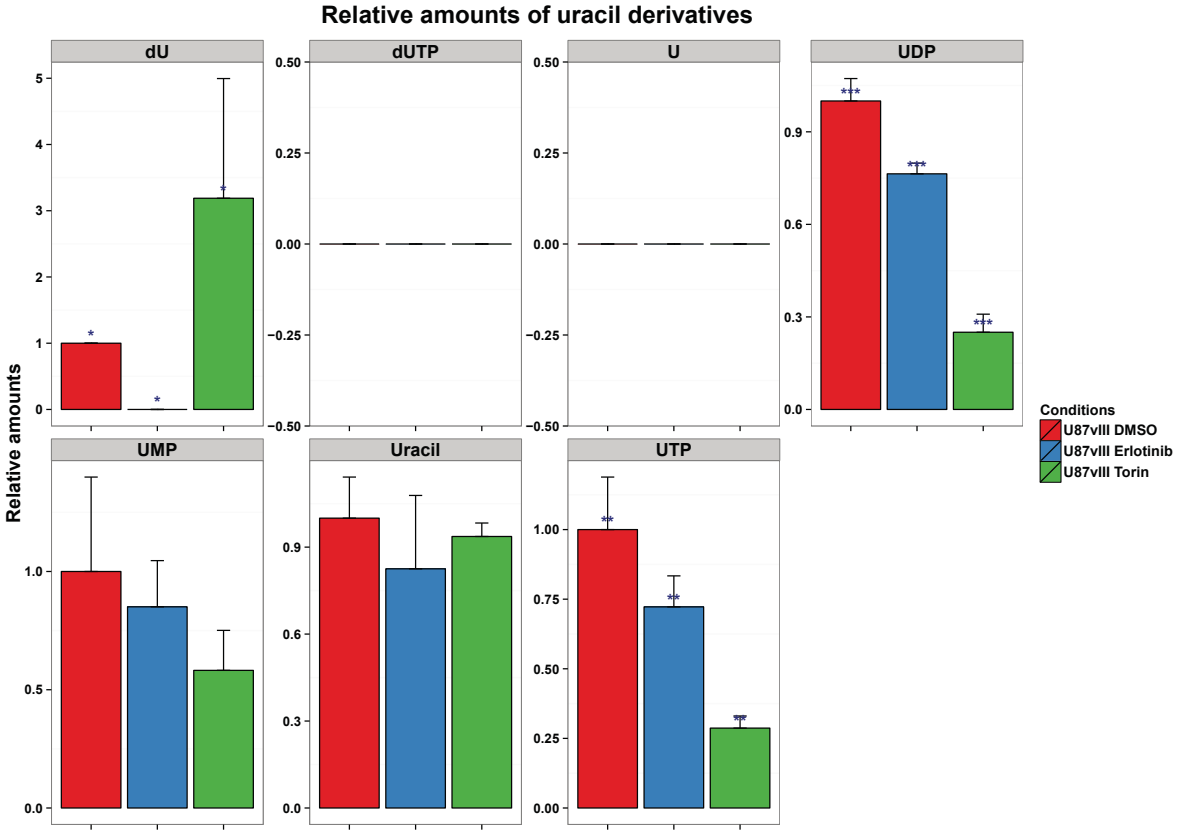
Relative amounts of uracil derivatives
dU
dUTP
U
UDP
UMP
Uracil
UTP
Relative amounts
Conditions
U87vIII DMSO
U87vIII Erlotinib
U87vIII Torin

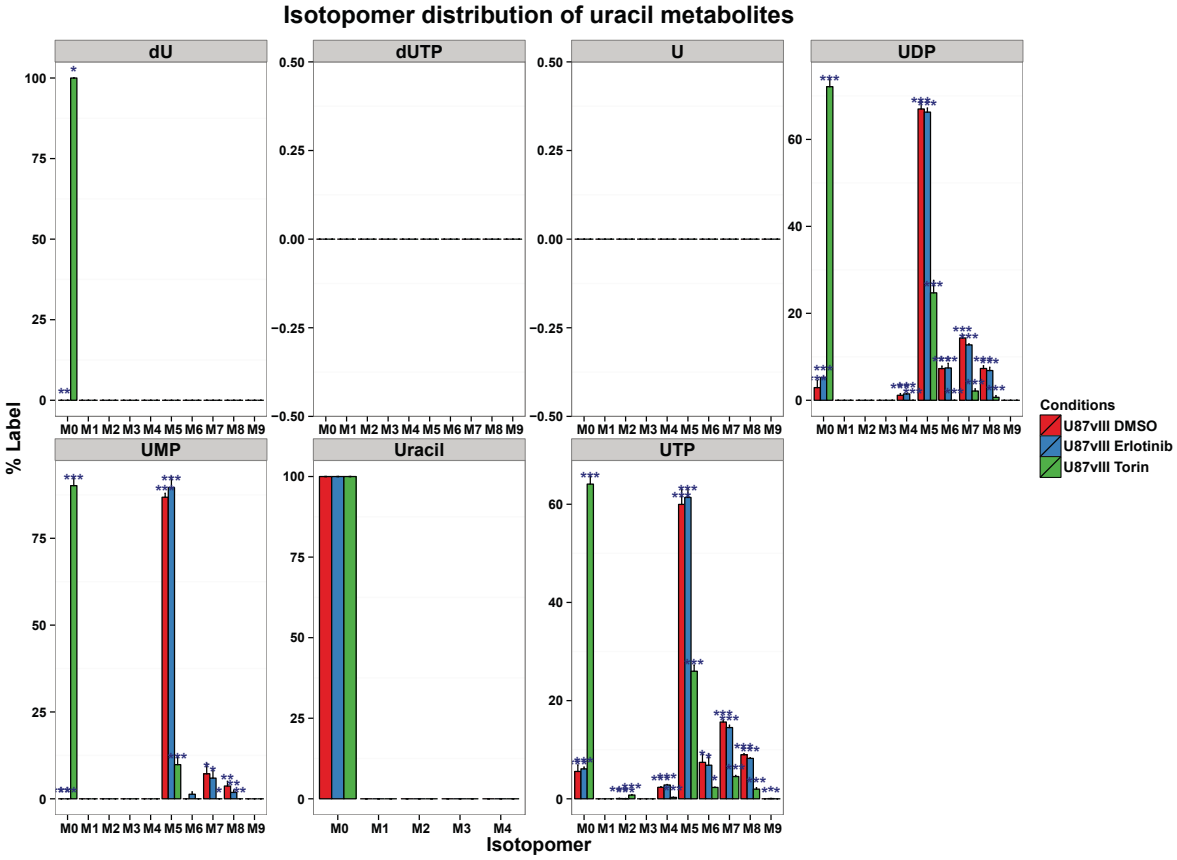
Isotopomer distribution of uracil metabolites
dU
dUTP
U
UDP
UMP
Uracil
UTP
% Label
Isotopomer
M0 M1 M2 M3 M4 M5 M6 M7 M8 M9
Conditions
U87vIII DMSO
U87vIII Erlotinib
U87vIII Torin

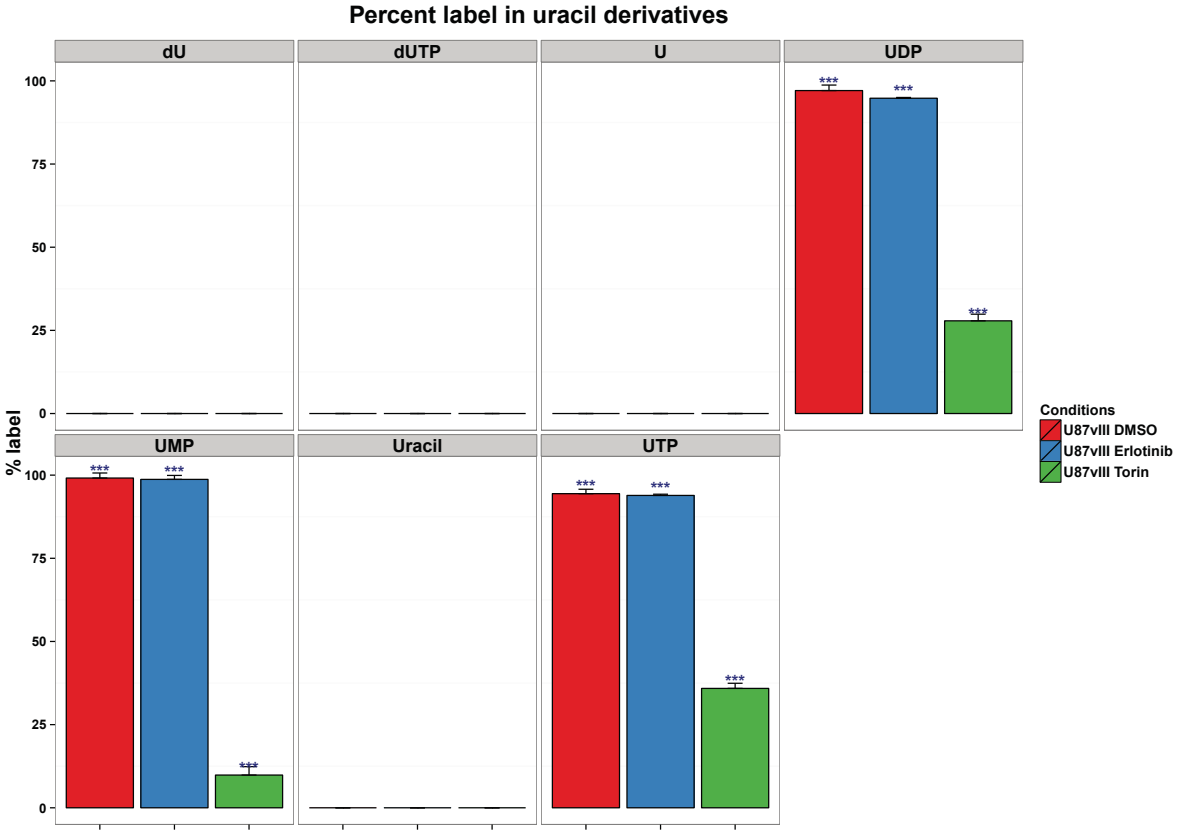
Percent label in uracil derivatives
dU
dUTP
U
UDP
UMP
Uracil
UTP
% label
100
75
50
25
0
***
Conditions
U87vIII DMSO
U87vIII Erlotinib
U87vIII Torin

LC-MS/MS Metabolomics Analysis with [U-13C5]-L-Glutamine Labeling

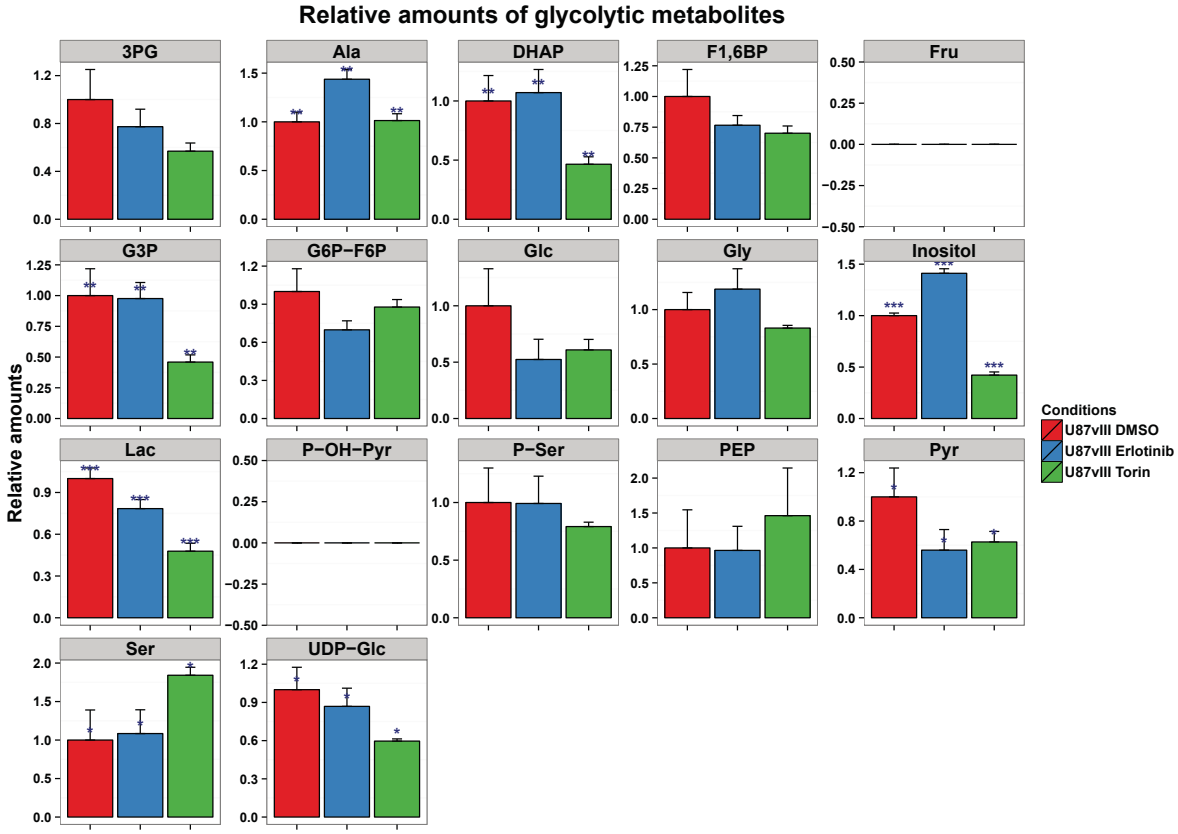
Relative amounts of glycolytic metabolites
3PG
Ala
DHAP
F1,6BP
Fru
G3P
G6P−F6P
Glc
Gly
Inositol
Lac
P−OH−Pyr
P−Ser
PEP
Pyr
Ser
UDP−Glc
Relative amounts
Conditions
U87vIII DMSO
U87vIII Erlotinib
U87vIII Torin

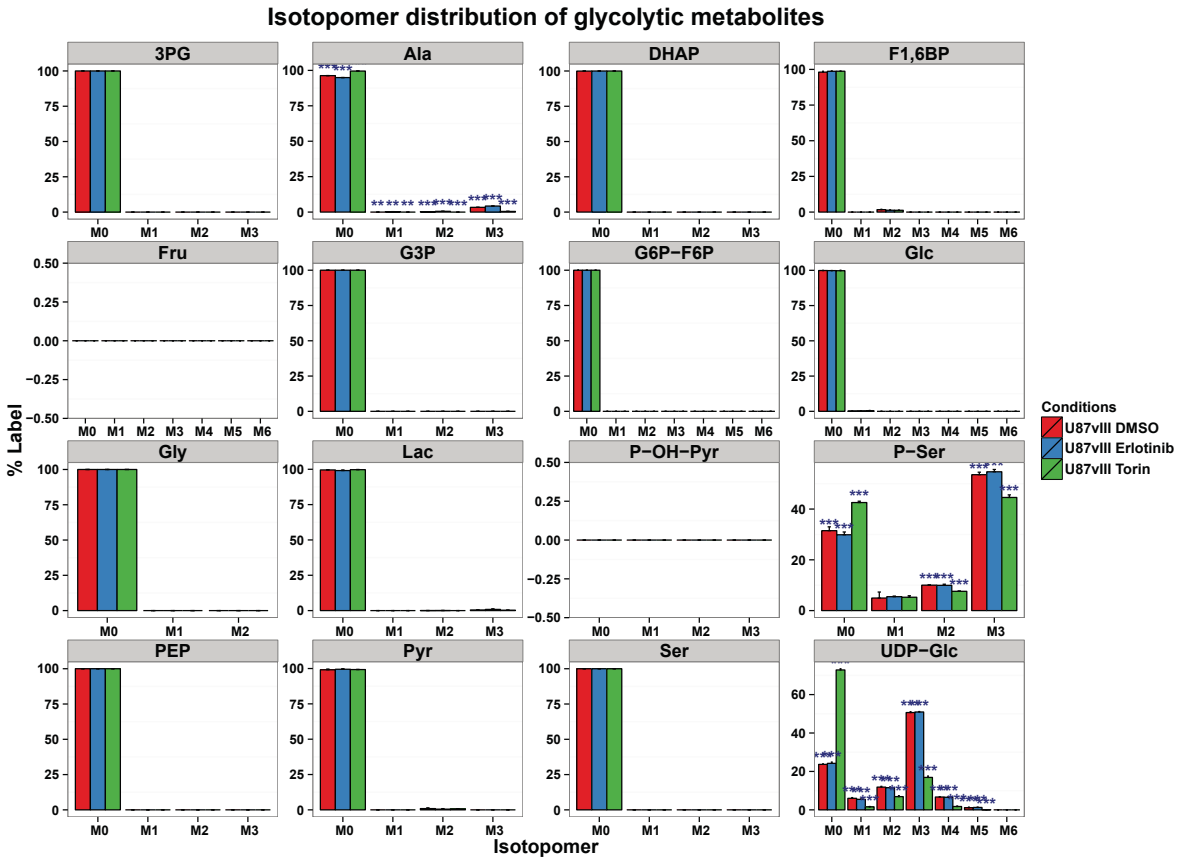
Isotopomer distribution of glycolytic metabolites
3PG
Ala
DHAP
F1,6BP
Fru
G3P
G6P−F6P
Glc
Gly
Lac
P−OH−Pyr
P−Ser
PEP
Pyr
Ser
UDP−Glc
% Label
Isotopomer
Conditions
U87vIII DMSO
U87vIII Erlotinib
U87vIII Torin

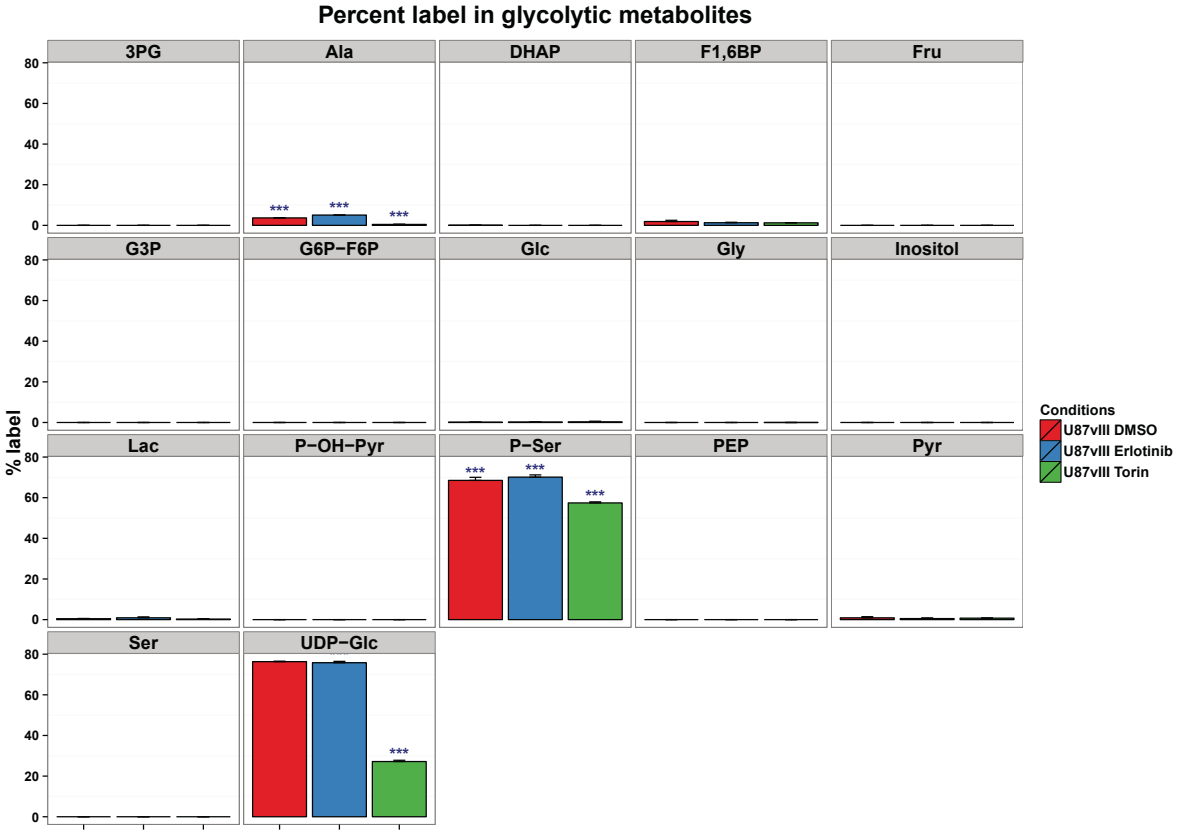
Percent label in glycolytic metabolites
3PG
Ala
DHAP
F1,6BP
Fru
G3P
G6P−F6P
Glc
Gly
Inositol
Lac
P−OH−Pyr
P−Ser
PEP
Pyr
Ser
UDP−Glc
% label
Conditions
U87vIII DMSO
U87vIII Erlotinib
U87vIII Torin

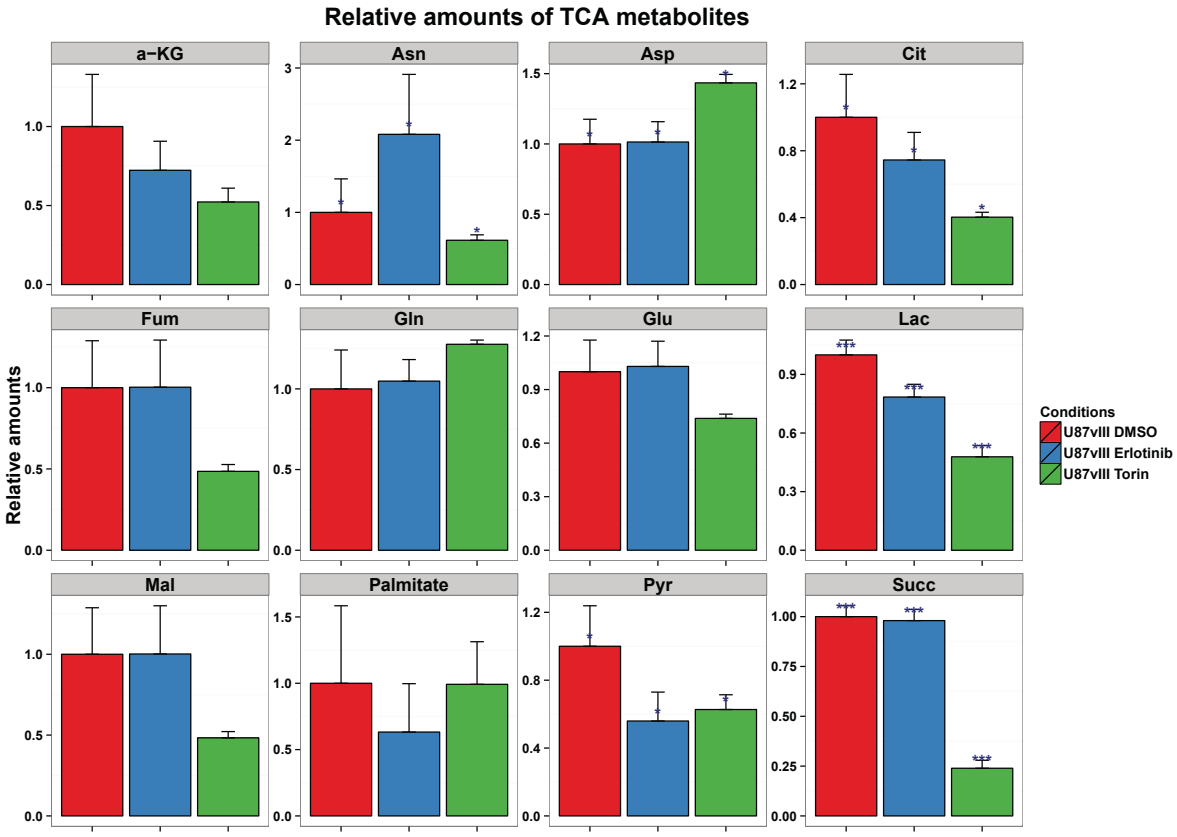
Relative amounts of TCA metabolites
a−KG
Asn
Asp
Cit
Fum
Gln
Glu
Lac
Mal
Palmitate
Pyr
Succ
Relative amounts
Conditions
U87vIII DMSO
U87vIII Erlotinib
U87vIII Torin

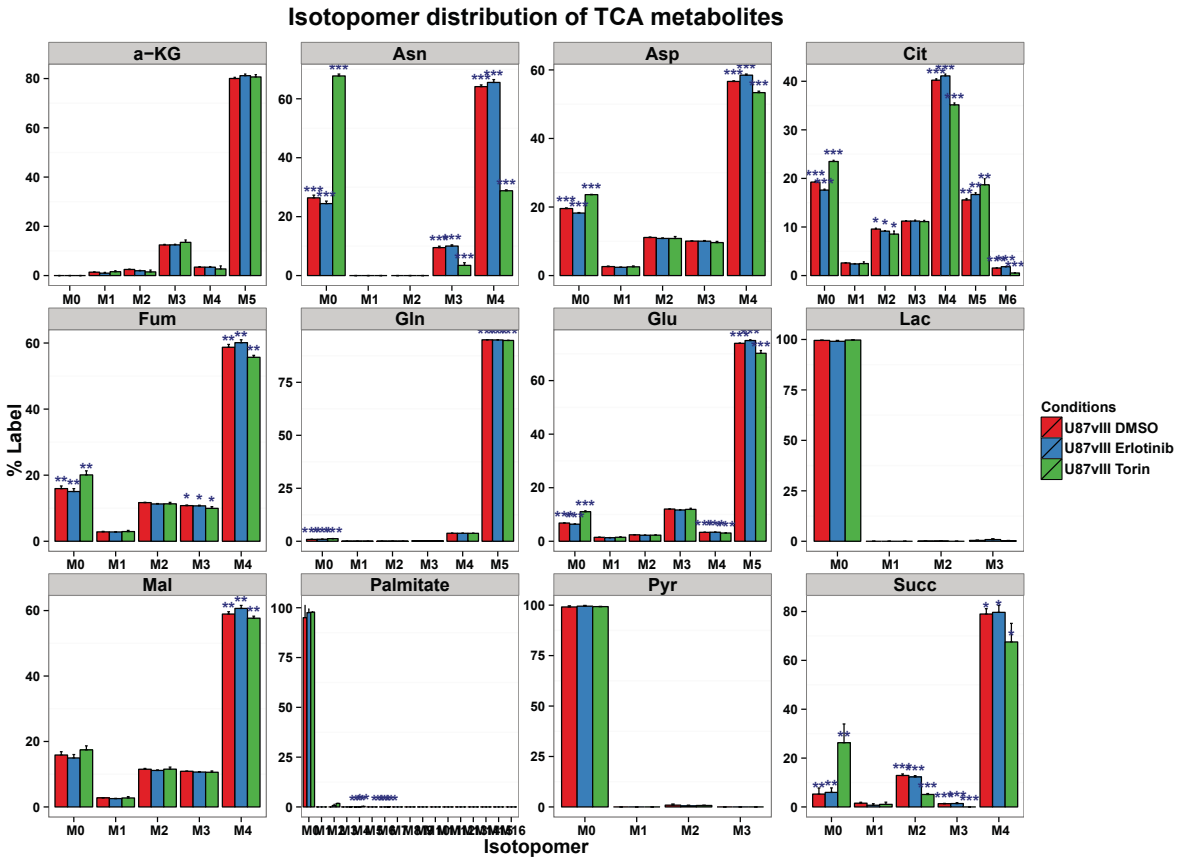
Isotopomer distribution of TCA metabolites
a−KG
Asn
Asp
Cit
Fum
Gln
Glu
Lac
Mal
Palmitate
Pyr
Succ
% Label
Isotopomer
Conditions
U87vIII DMSO
U87vIII Erlotinib
U87vIII Torin

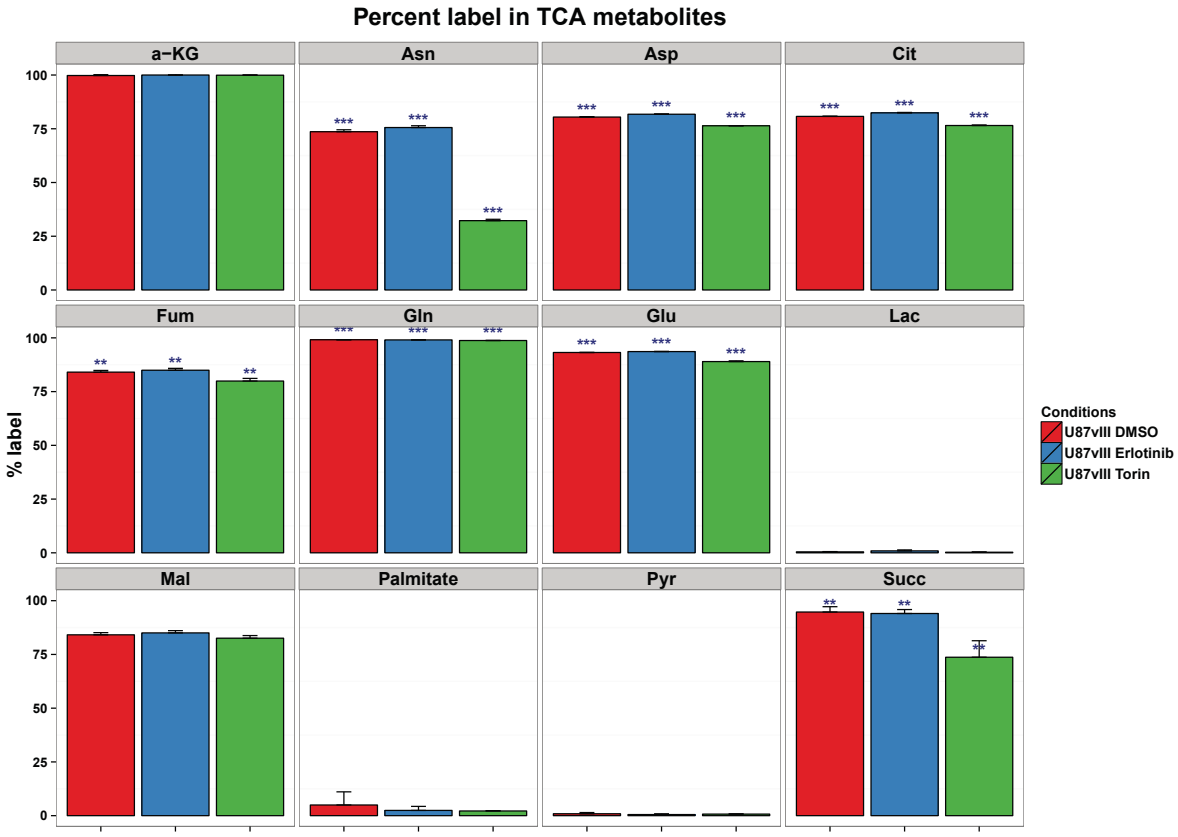
Percent label in TCA metabolites
a−KG
Asn
Asp
Cit
Fum
Gln
Glu
Lac
Mal
Palmitate
Pyr
Succ
% label
Conditions
U87vIII DMSO
U87vIII Erlotinib
U87vIII Torin

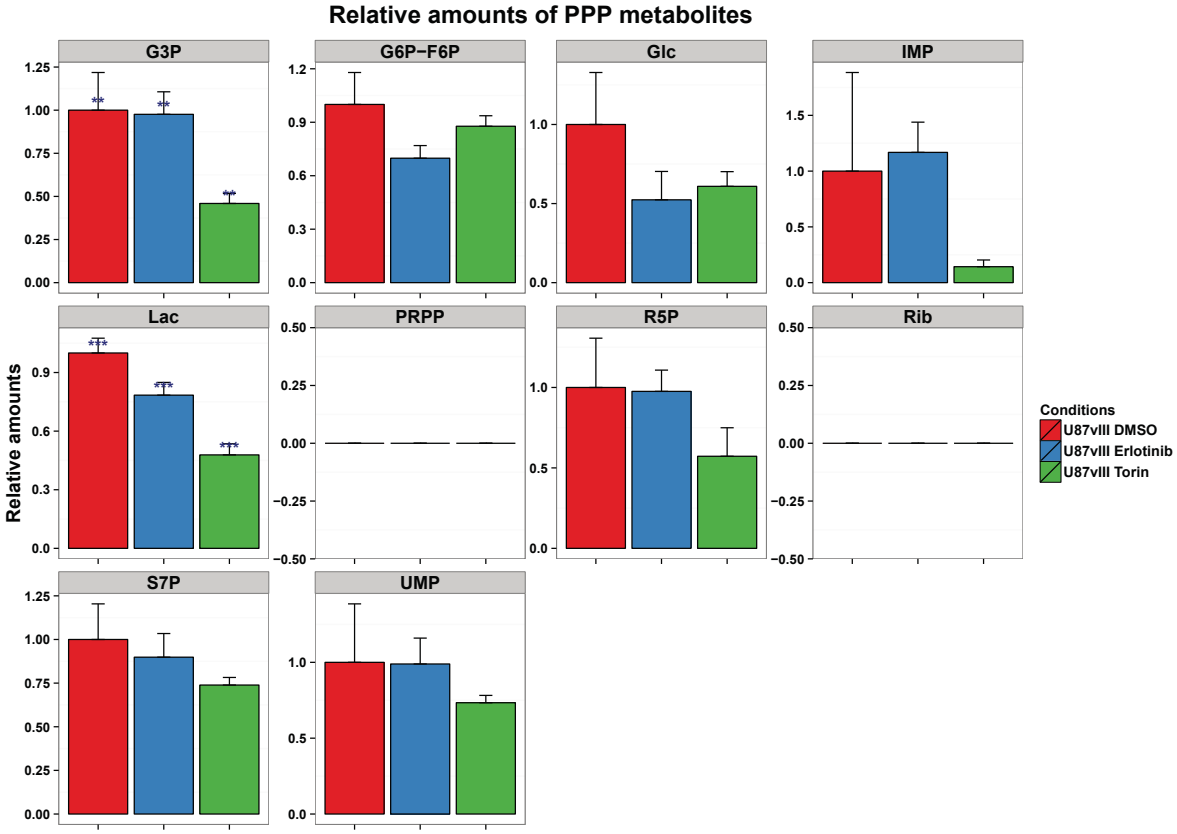
Relative amounts of PPP metabolites
G3P
G6P−F6P
Glc
IMP
Lac
PRPP
R5P
Rib
S7P
UMP
Relative amounts
Conditions
U87vIII DMSO
U87vIII Erlotinib
U87vIII Torin

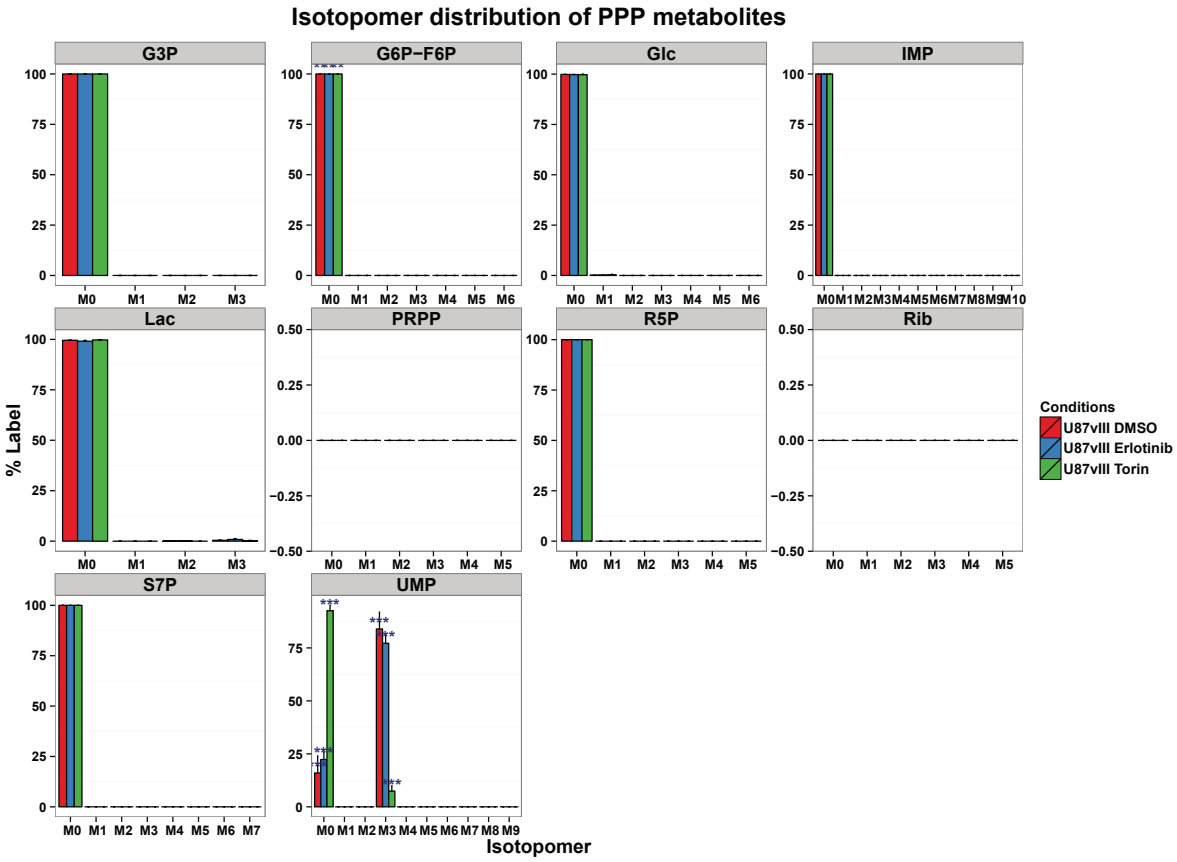
Isotopomer distribution of PPP metabolites
G3P
G6P−F6P
Glc
IMP
Lac
PRPP
R5P
Rib
S7P
UMP
% Label
Isotopomer
Conditions
U87vIII DMSO
U87vIII Erlotinib
U87vIII Torin

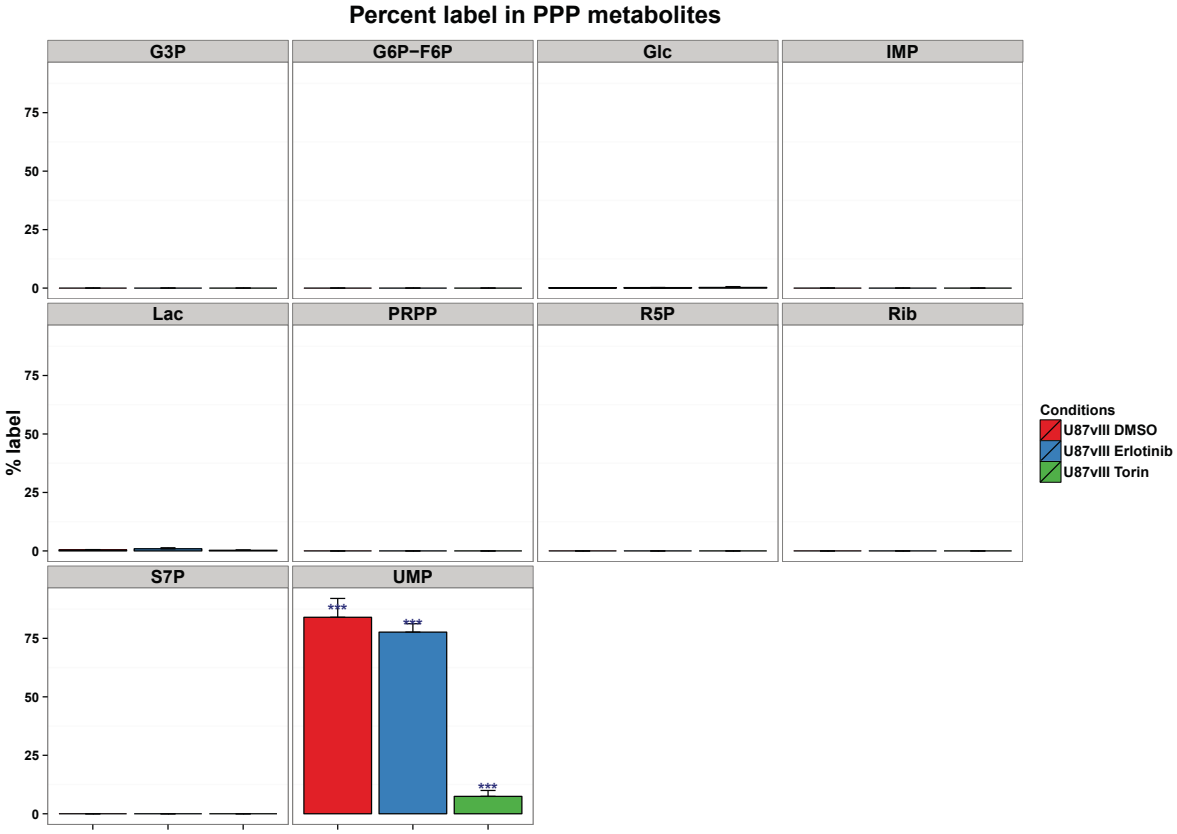
Percent label in PPP metabolites
G3P
G6P−F6P
Glc
IMP
Lac
PRPP
R5P
Rib
S7P
UMP
% label
Conditions
U87vIII DMSO
U87vIII Erlotinib
U87vIII Torin

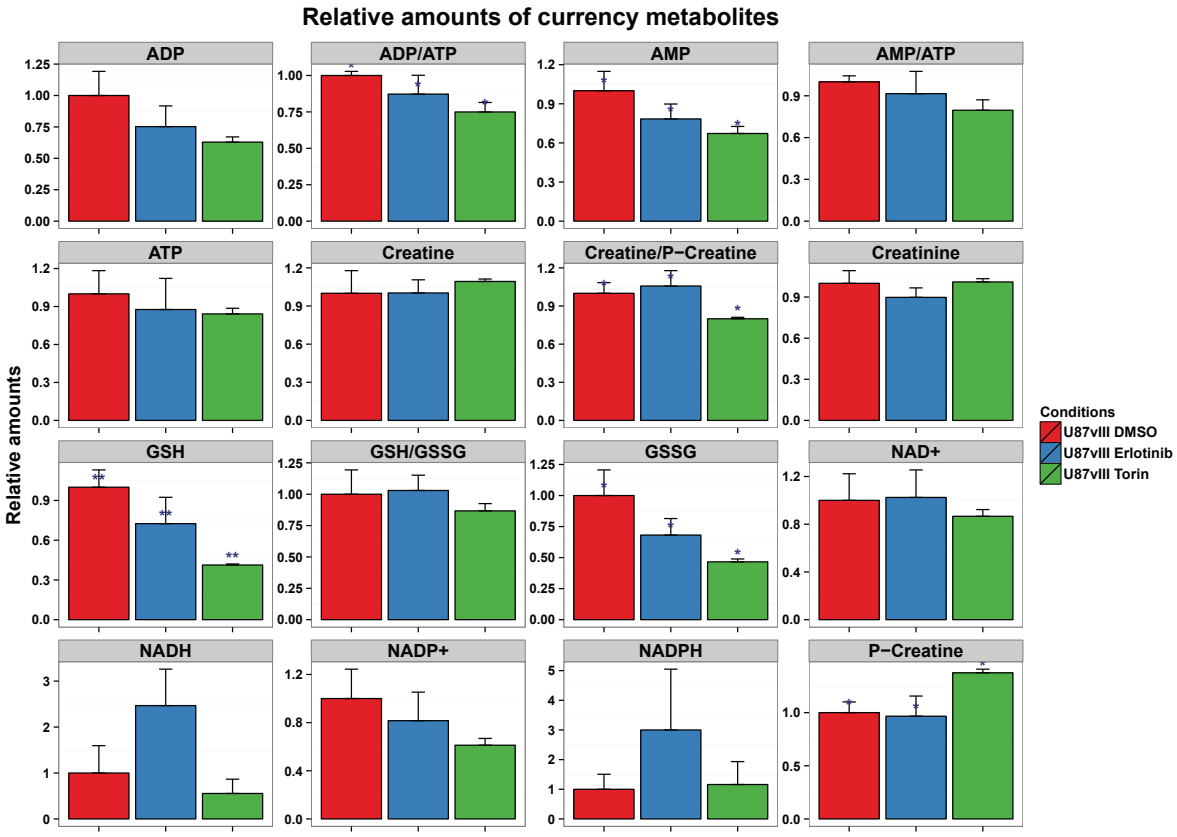
Relative amounts of currency metabolites
ADP
ADP/ATP
AMP
AMP/ATP
ATP
Creatine
Creatine/P−Creatine
Creatinine
GSH
GSH/GSSG
GSSG
NAD+
NADH
NADP+
NADPH
P−Creatine
Relative amounts
Conditions
U87vIII DMSO
U87vIII Erlotinib
U87vIII Torin

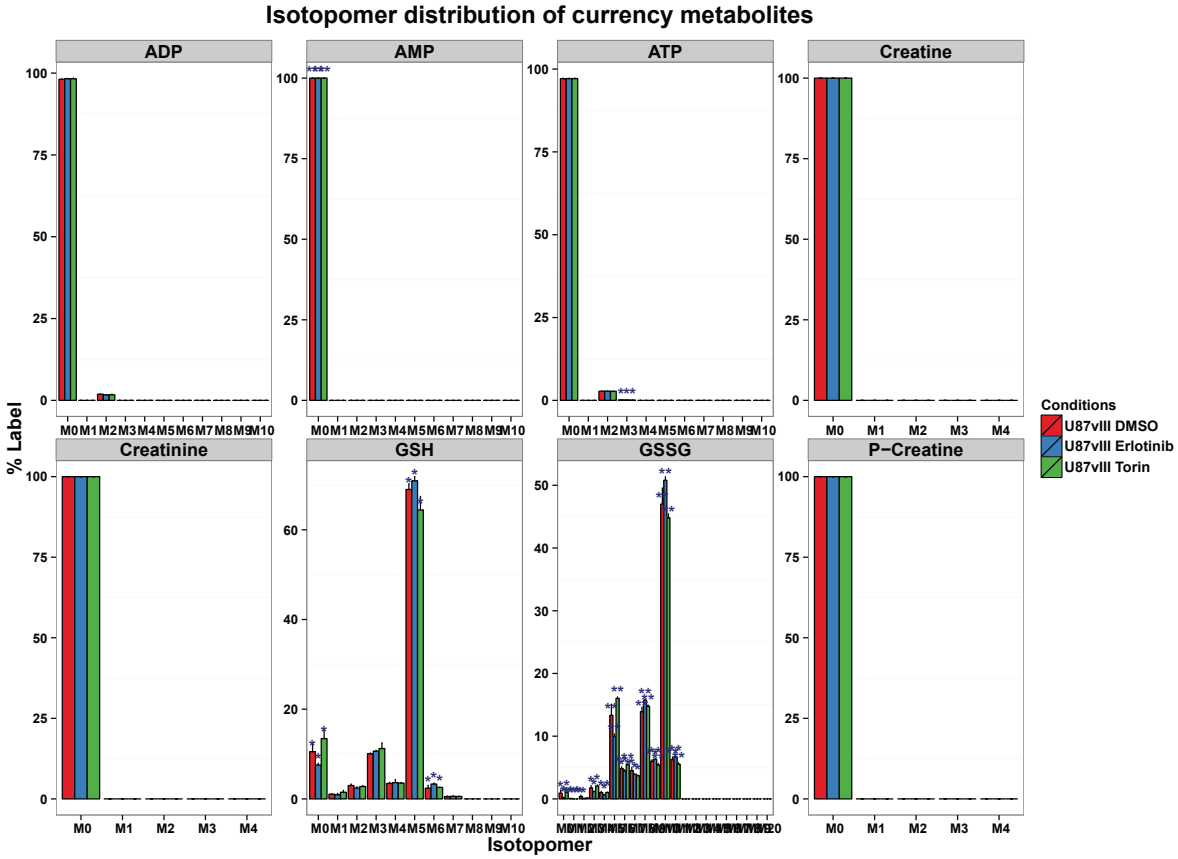
Isotopomer distribution of currency metabolites
ADP
AMP
ATP
Creatine
Creatinine
GSH
GSSG
P−Creatine
% Label
Isotopomer
Conditions
U87vIII DMSO
U87vIII Erlotinib
U87vIII Torin

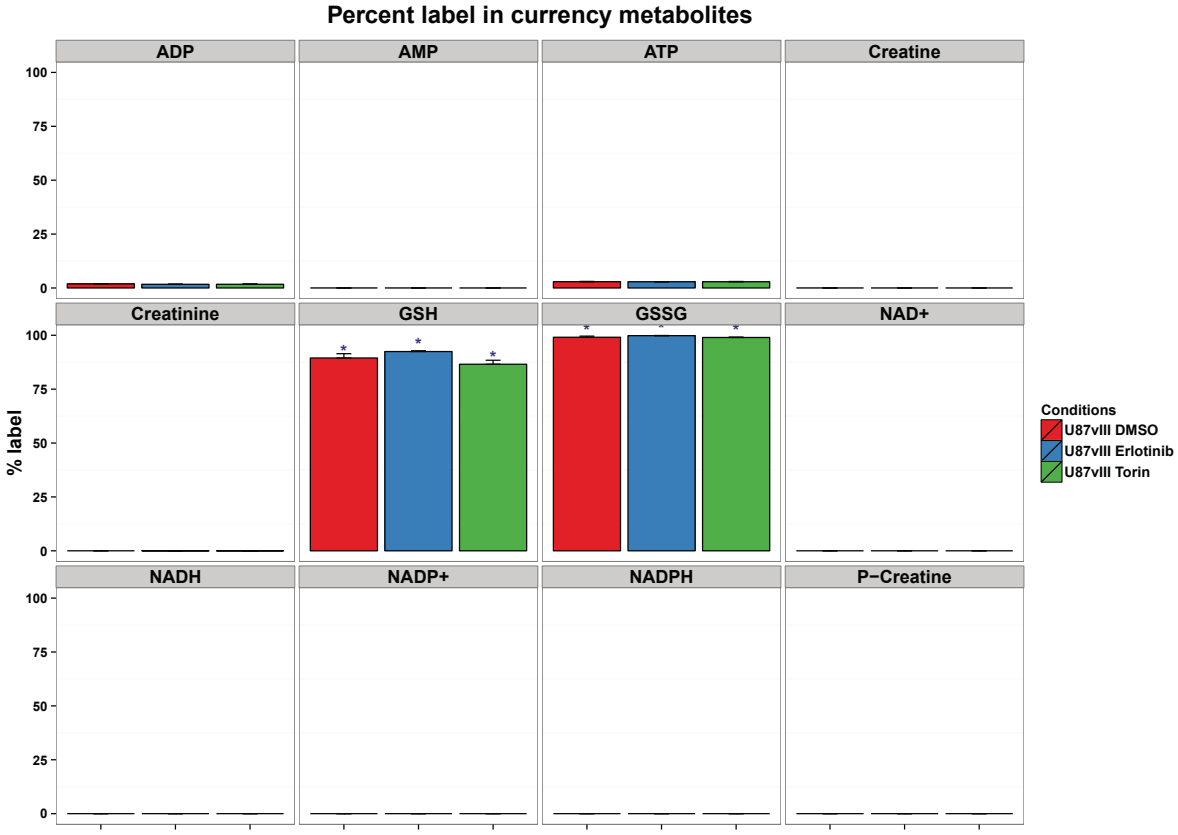
Percent label in currency metabolites
ADP
AMP
ATP
Creatine
Creatinine
GSH
GSSG
NAD+
NADH
NADP+
NADPH
P−Creatine
% label
Conditions
U87vIII DMSO
U87vIII Erlotinib
U87vIII Torin

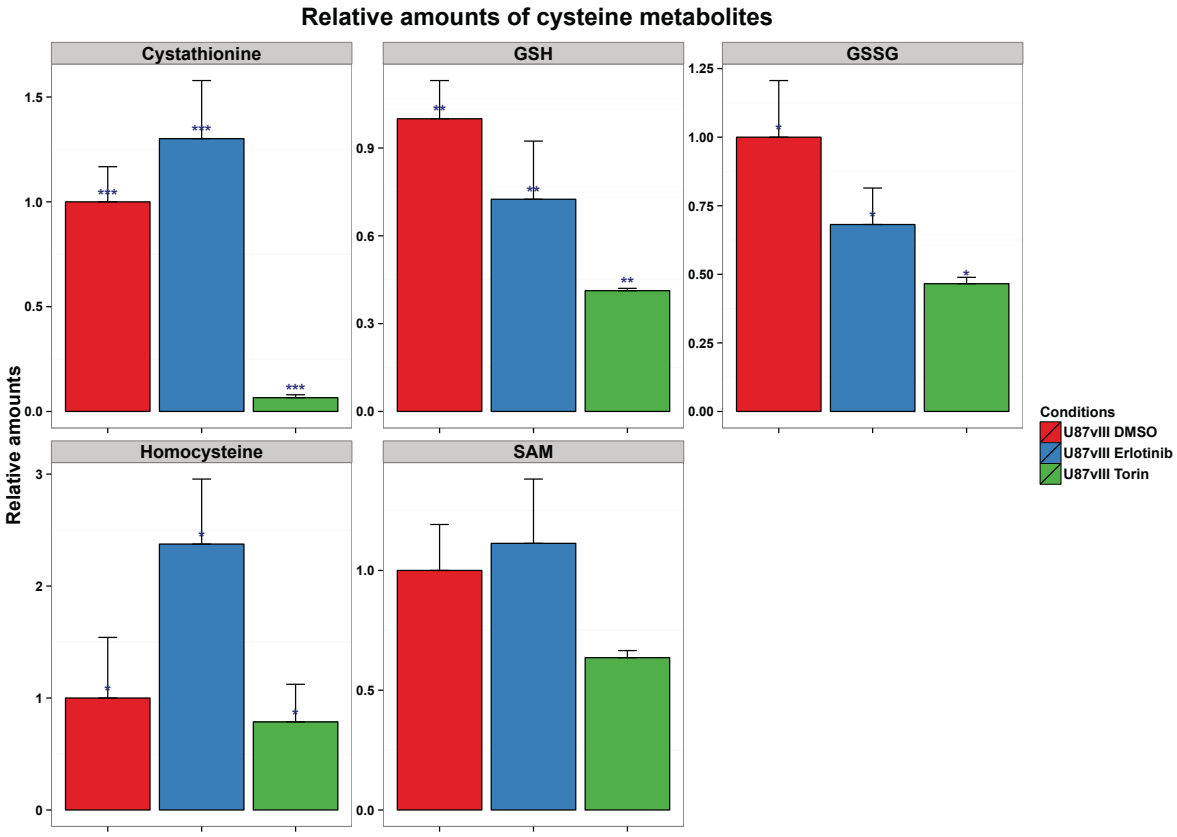
Relative amounts of cysteine metabolites
Cystathionine
GSH
GSSG
Homocysteine
SAM
Relative amounts
Conditions
U87vIII DMSO
U87vIII Erlotinib
U87vIII Torin

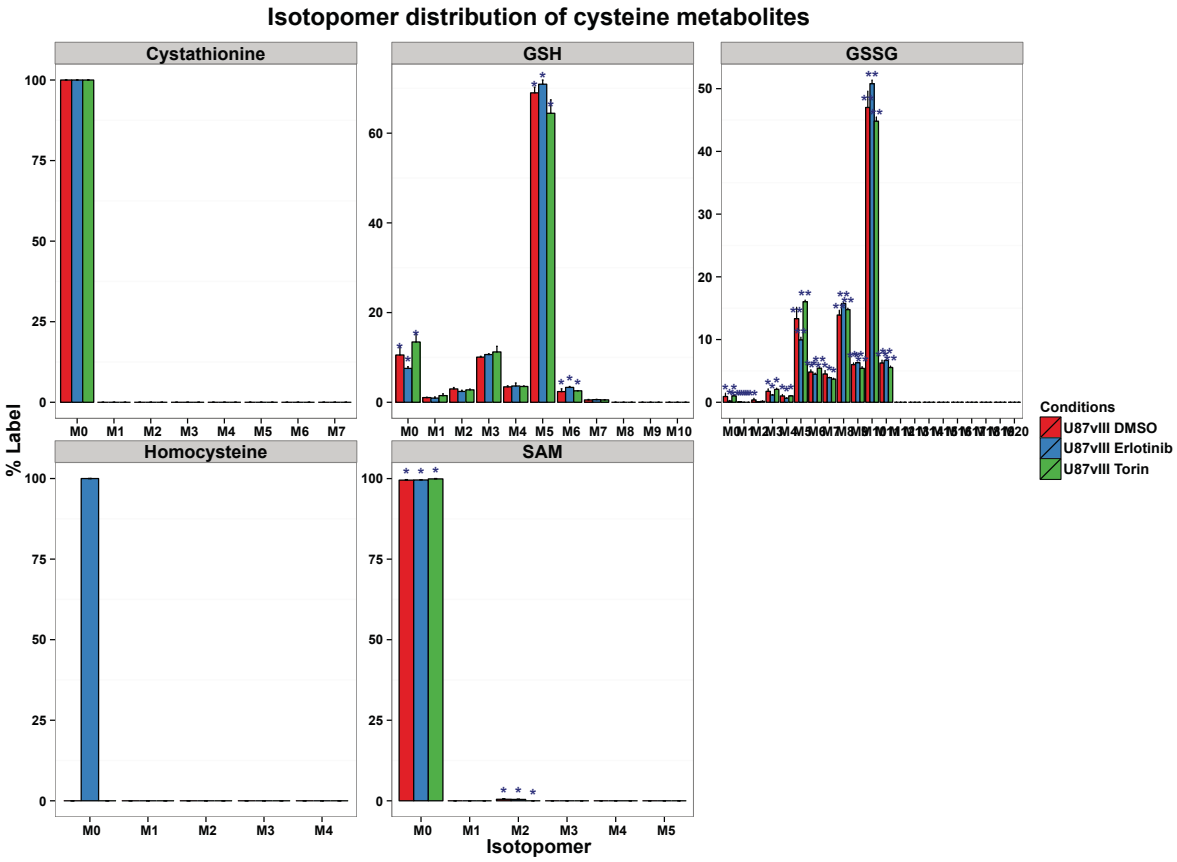
Isotopomer distribution of cysteine metabolites
Cystathionine
GSH
GSSG
Homocysteine
SAM
% Label
Isotopomer
Conditions
U87vIII DMSO
U87vIII Erlotinib
U87vIII Torin

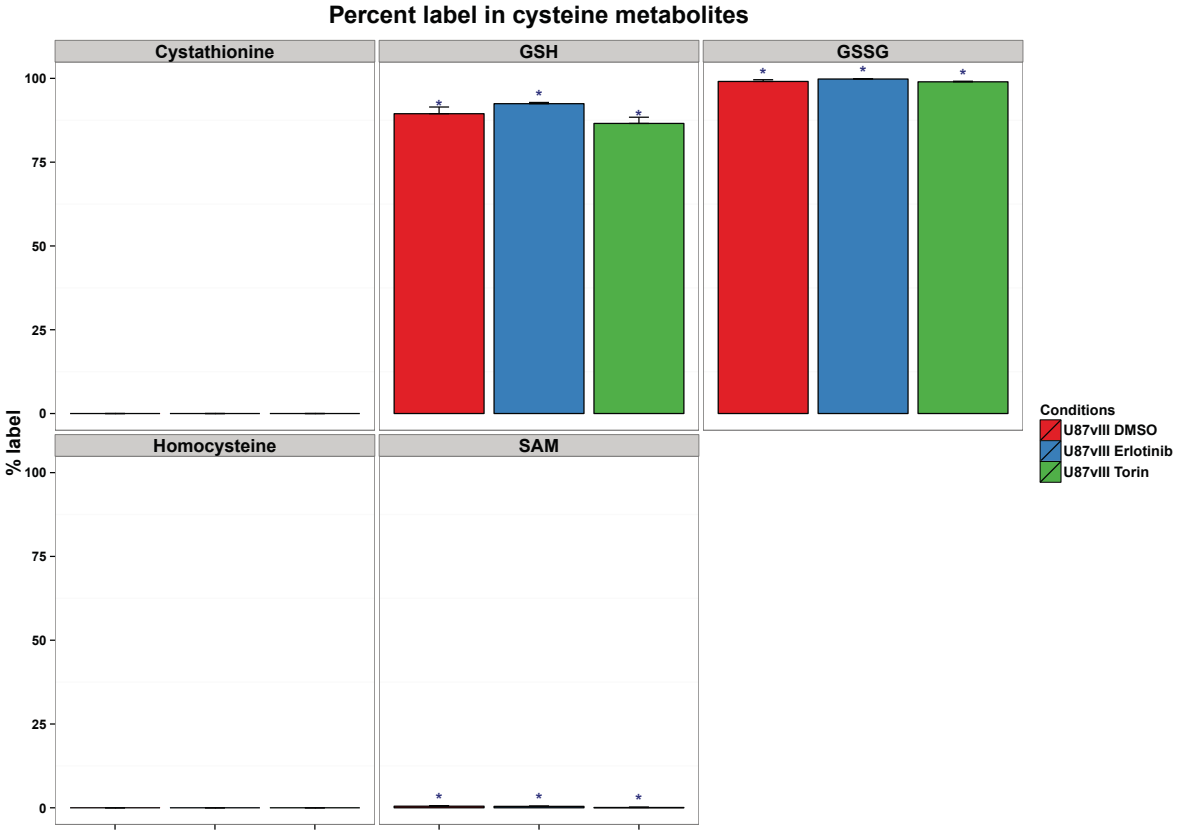
Percent label in cysteine metabolites
Cystathionine
GSH
GSSG
Homocysteine
SAM
% label
Conditions
U87vIII DMSO
U87vIII Erlotinib
U87vIII Torin

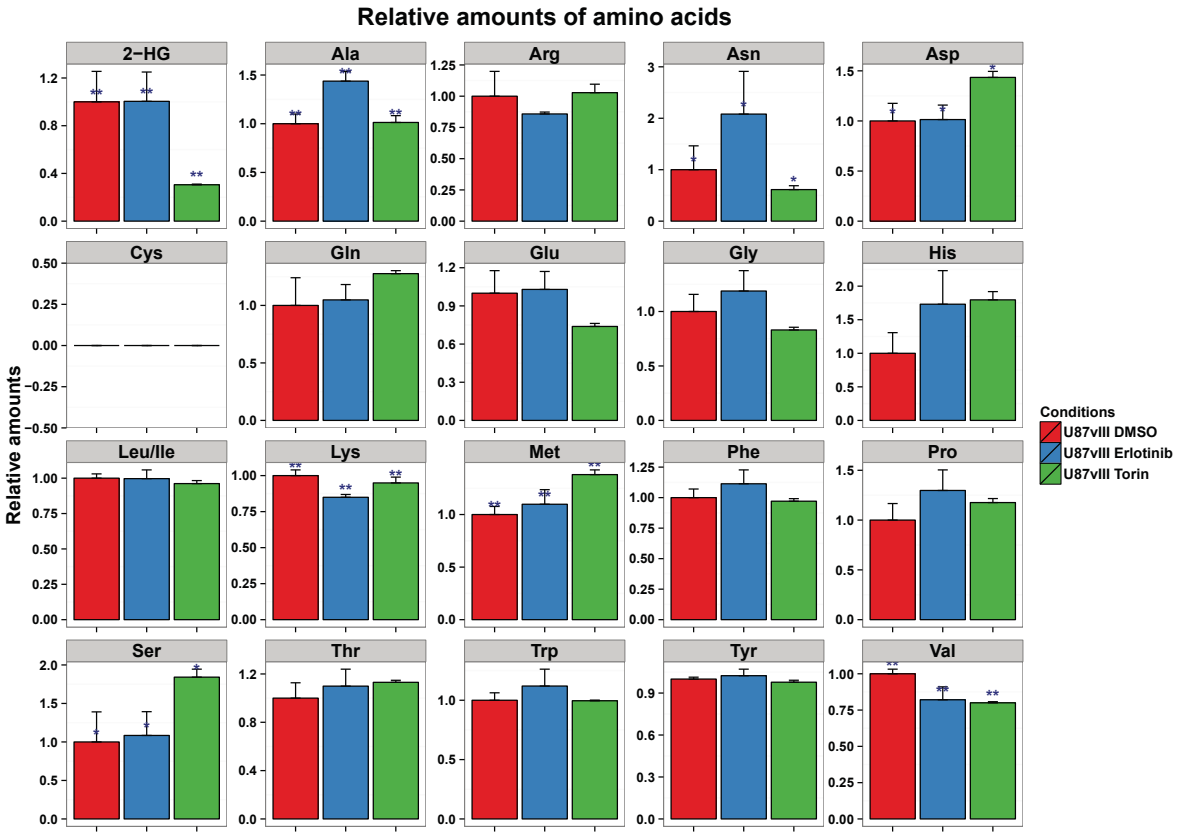
Relative amounts of amino acids
2−HG
Ala
Arg
Asn
Asp
Cys
Gln
Glu
Gly
His
Leu/Ile
Lys
Met
Phe
Pro
Ser
Thr
Trp
Tyr
Val
Relative amounts
Conditions
U87vIII DMSO
U87vIII Erlotinib
U87vIII Torin

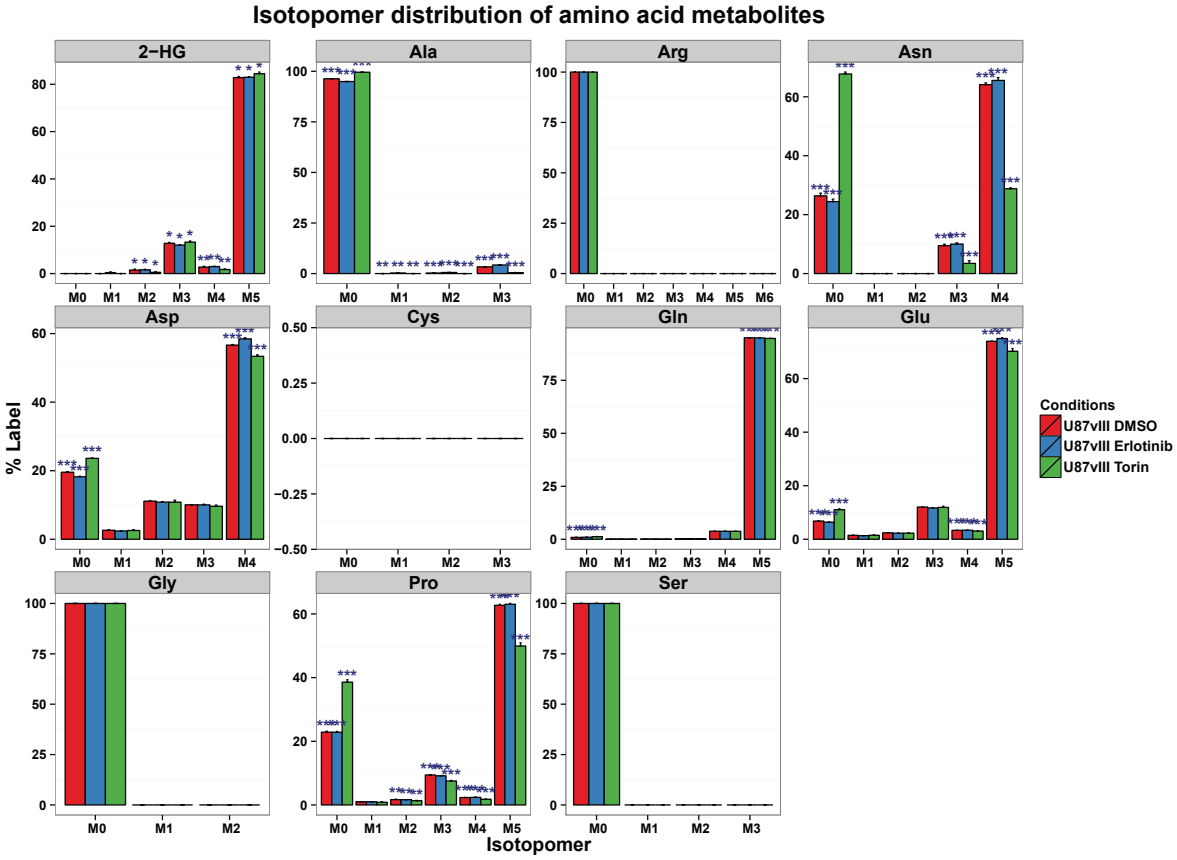
Isotopomer distribution of amino acid metabolites
2−HG
Ala
Arg
Asn
Asp
Cys
Gln
Glu
Gly
Pro
Ser
% Label
Isotopomer
Conditions
U87vIII DMSO
U87vIII Erlotinib
U87vIII Torin

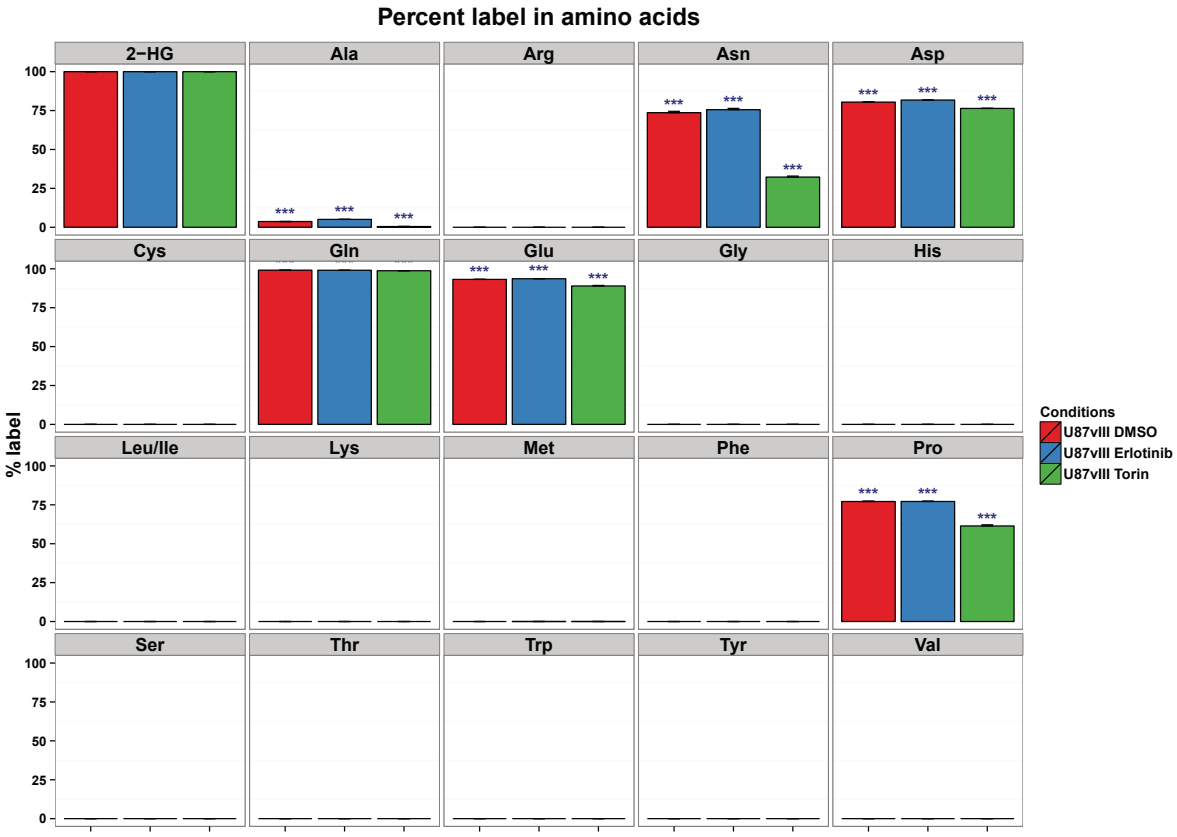
Percent label in amino acids
2−HG
Ala
Arg
Asn
Asp
Cys
Gln
Glu
Gly
His
Leu/Ile
Lys
Met
Phe
Pro
Ser
Thr
Trp
Tyr
Val
% label
Conditions
U87vIII DMSO
U87vIII Erlotinib
U87vIII Torin

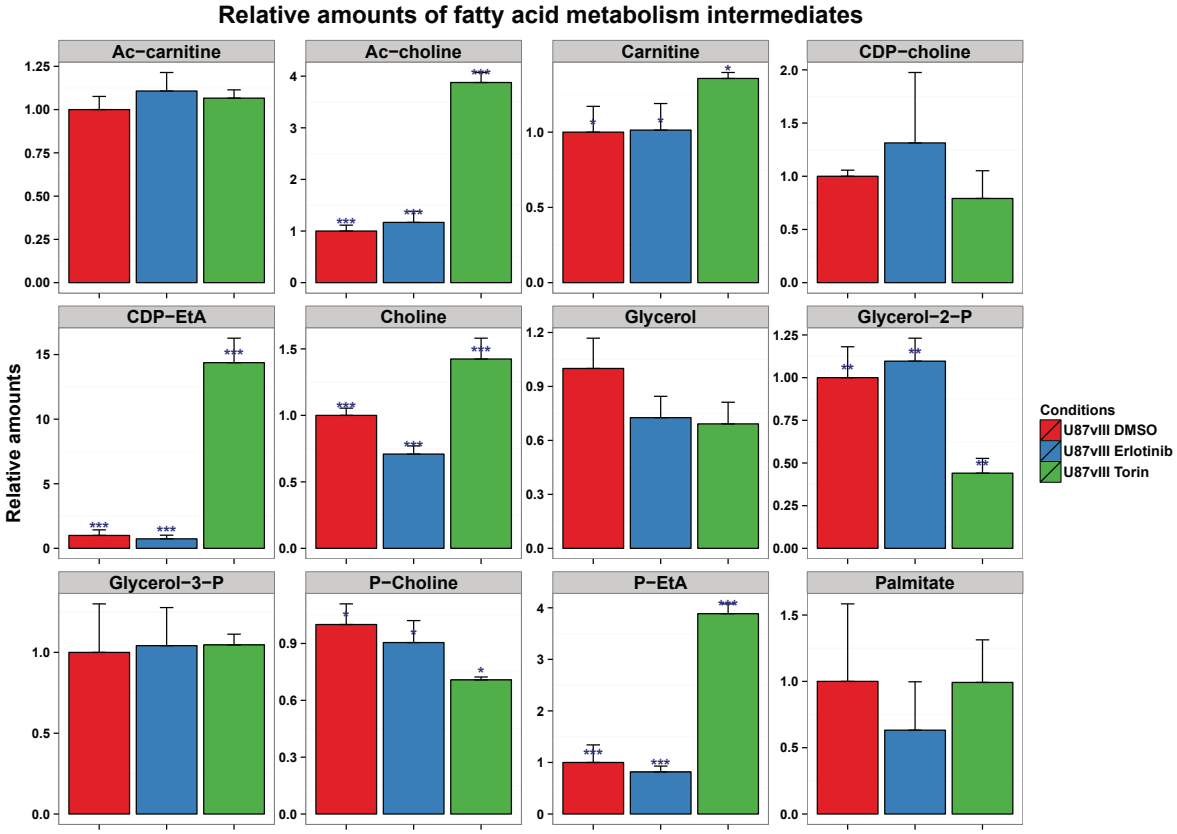
Relative amounts of fatty acid metabolism intermediates
Ac−carnitine
Ac−choline
Carnitine
CDP−choline
CDP−EtA
Choline
Glycerol
Glycerol−2−P
Glycerol−3−P
P−Choline
P−EtA
Palmitate
Relative amounts
Conditions
U87vIII DMSO
U87vIII Erlotinib
U87vIII Torin

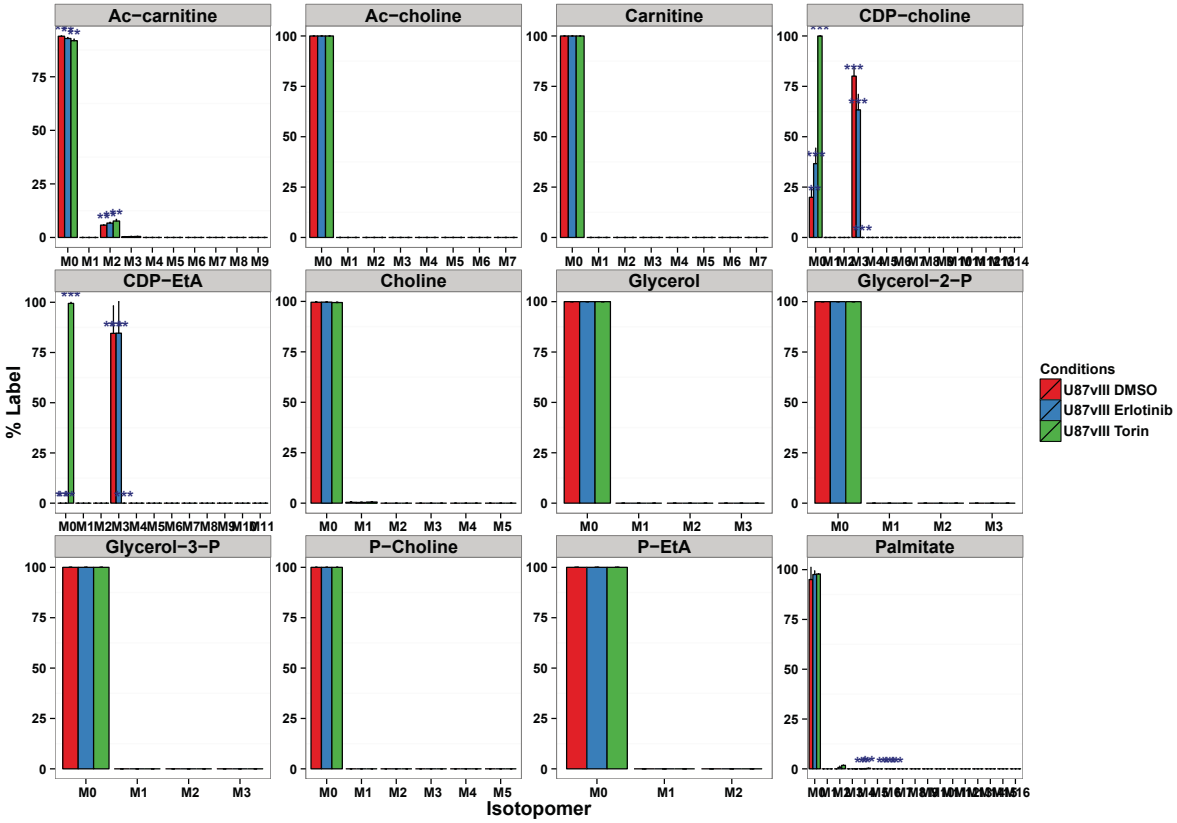
Isotopomer distribution of fatty acid metabolism intermediates
Ac−carnitine
Ac−choline
Carnitine
CDP−choline
CDP−EtA
Choline
Glycerol
Glycerol−2−P
Glycerol−3−P
P−Choline
P−EtA
Palmitate
% Label
Isotopomer
Conditions
U87vIII DMSO
U87vIII Erlotinib
U87vIII Torin

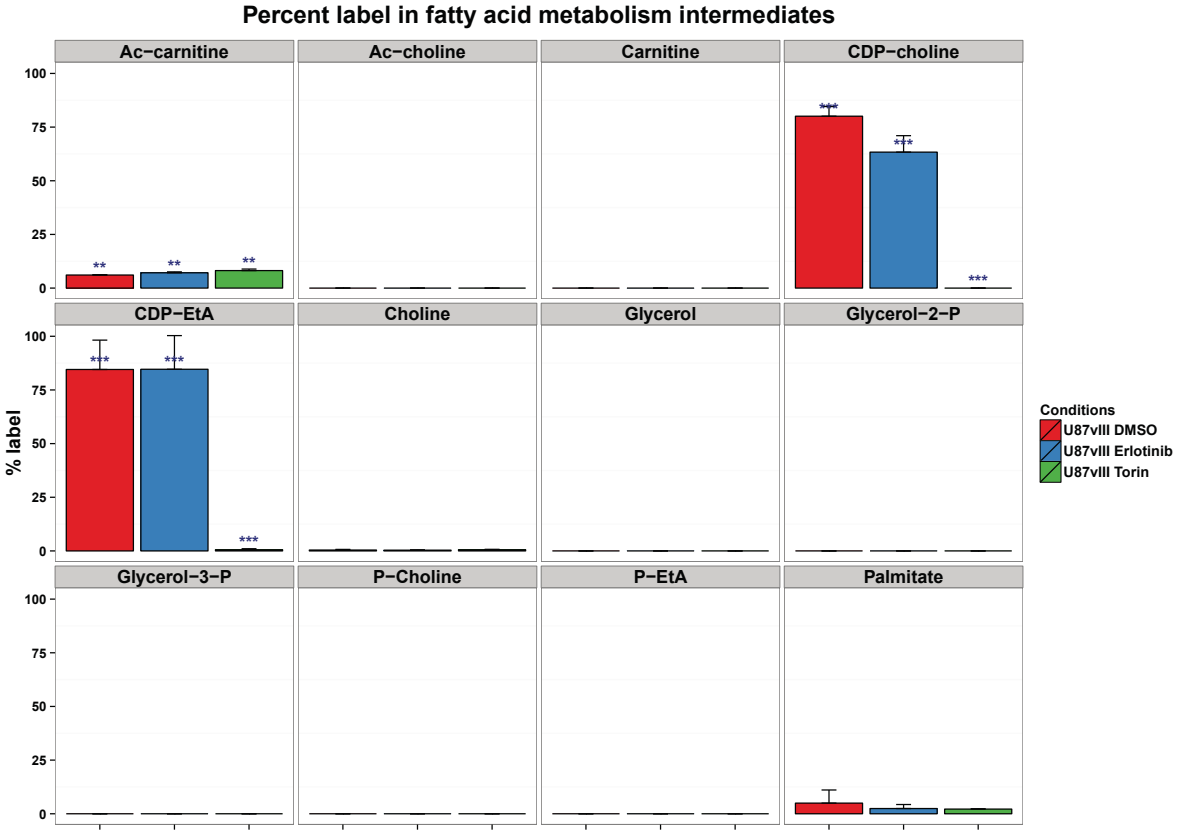
Percent label in fatty acid metabolism intermediates
Ac−carnitine
Ac−choline
Carnitine
CDP−choline
CDP−EtA
Choline
Glycerol
Glycerol−2−P
Glycerol−3−P
P−Choline
P−EtA
Palmitate
% label
Conditions
U87vIII DMSO
U87vIII Erlotinib
U87vIII Torin

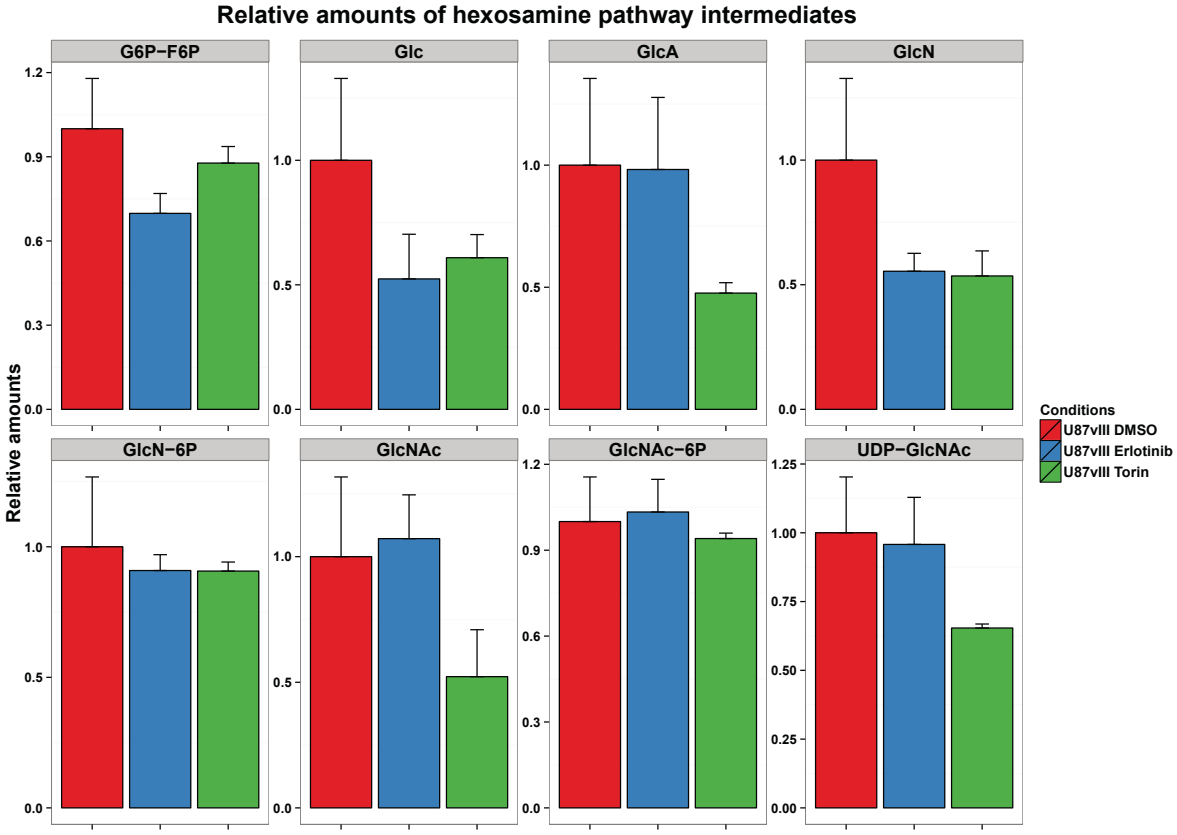
Relative amounts of hexosamine pathway intermediates
G6P−F6P
Glc
GlcA
GlcN
GlcN−6P
GlcNAc
GlcNAc−6P
UDP−GlcNAc
Relative amounts
Conditions
U87vIII DMSO
U87vIII Erlotinib
U87vIII Torin

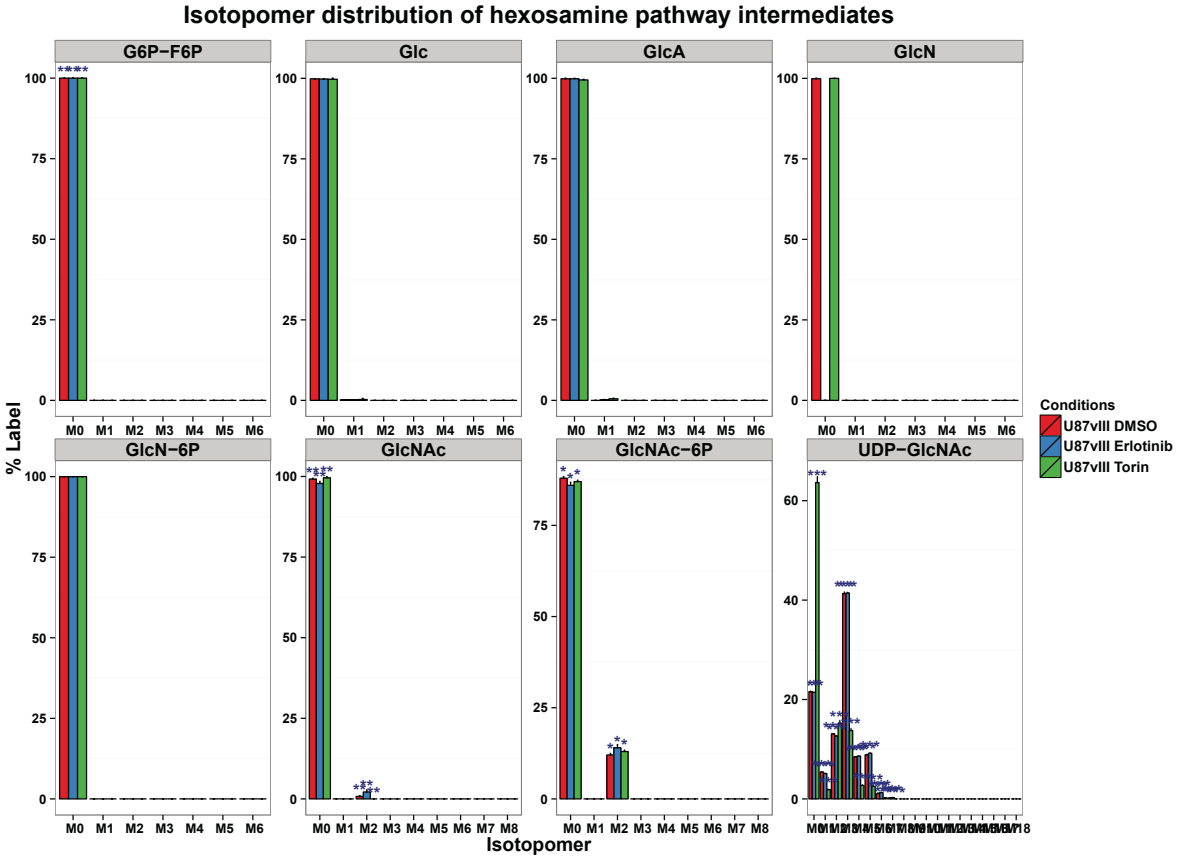
Isotopomer distribution of hexosamine pathway intermediates
G6P−F6P
Glc
GlcA
GlcN
GlcN−6P
GlcNAc
GlcNAc−6P
UDP−GlcNAc
% Label
Isotopomer
Conditions
U87vIII DMSO
U87vIII Erlotinib
U87vIII Torin

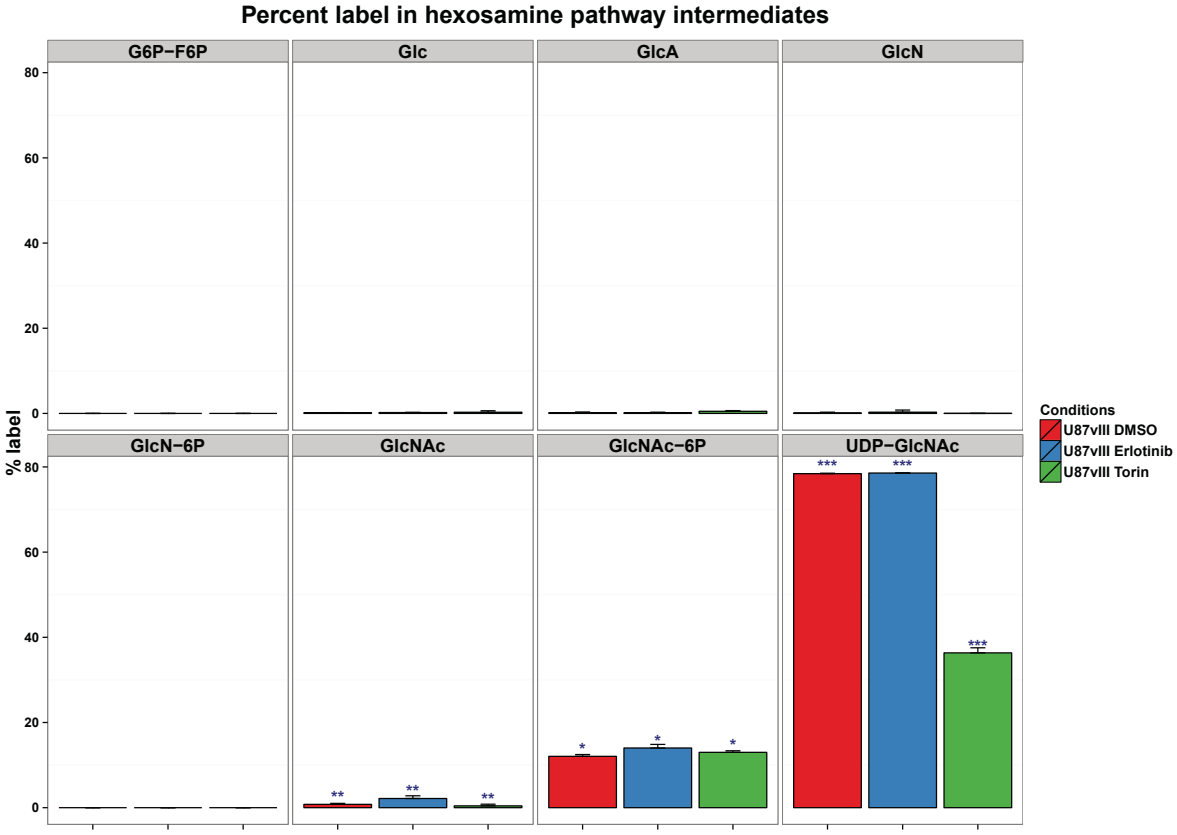
Percent label in hexosamine pathway intermediates
G6P−F6P
Glc
GlcA
GlcN
GlcN−6P
GlcNAc
GlcNAc−6P
UDP−GlcNAc
% label
Conditions
U87vIII DMSO
U87vIII Erlotinib
U87vIII Torin

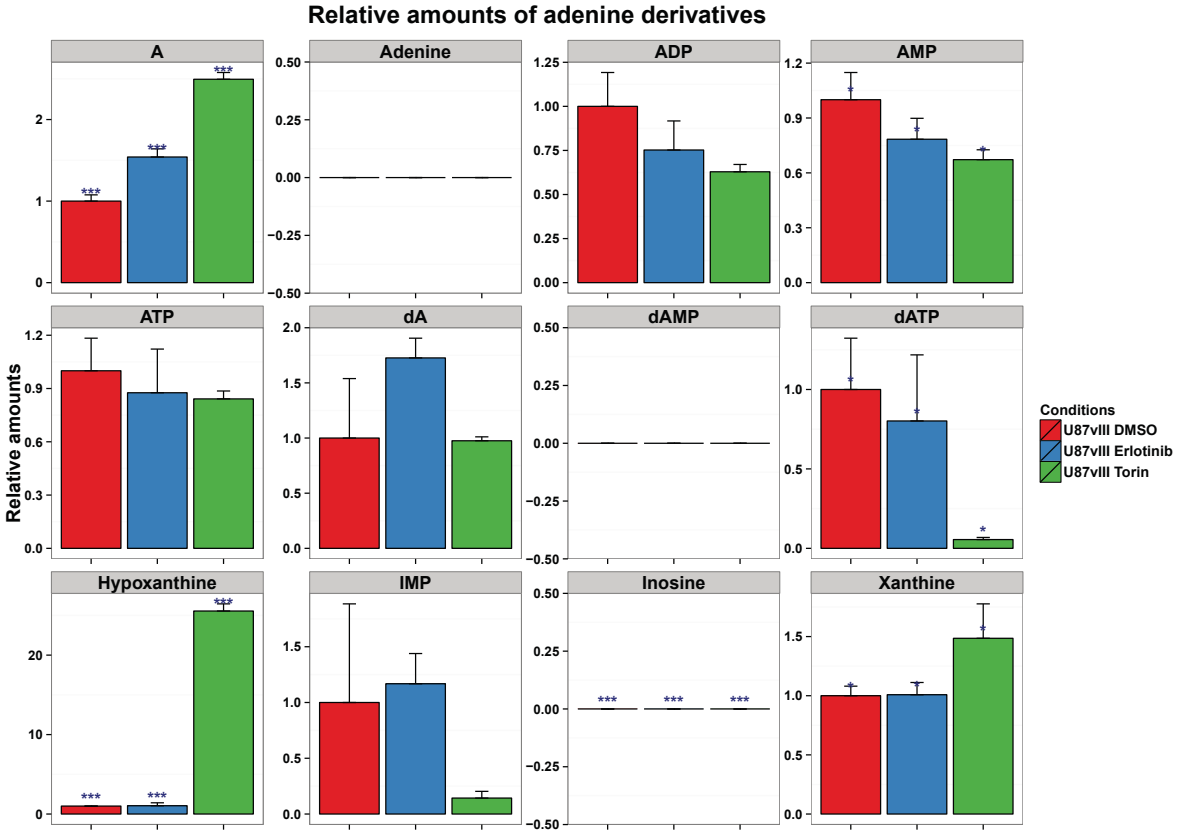
Relative amounts of adenine derivatives
A
Adenine
ADP
AMP
ATP
dA
dAMP
dATP
Hypoxanthine
IMP
Inosine
Xanthine
Relative amounts
Conditions
U87vIII DMSO
U87vIII Erlotinib
U87vIII Torin

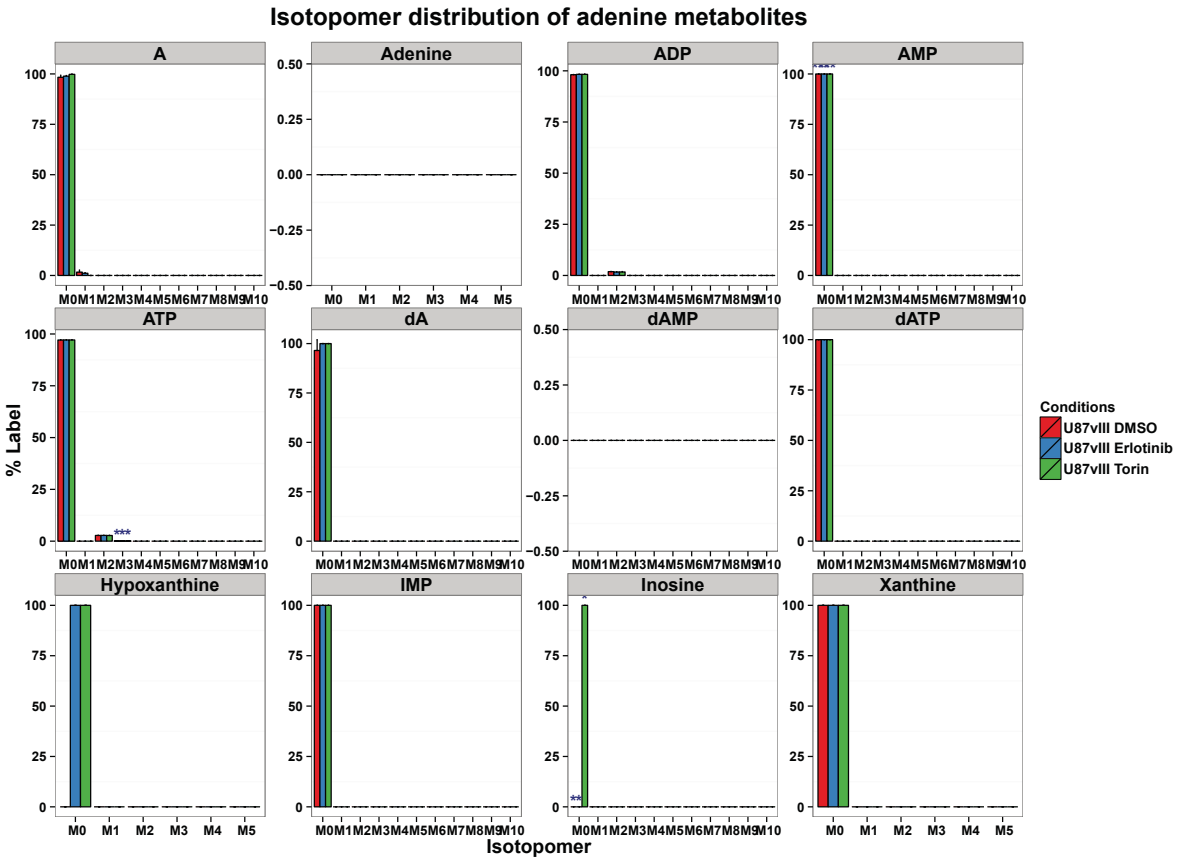
Isotopomer distribution of adenine metabolites
A
Adenine
ADP
AMP
ATP
dA
dAMP
dATP
Hypoxanthine
IMP
Inosine
Xanthine
% Label
Isotopomer
Conditions
U87vIII DMSO
U87vIII Erlotinib
U87vIII Torin

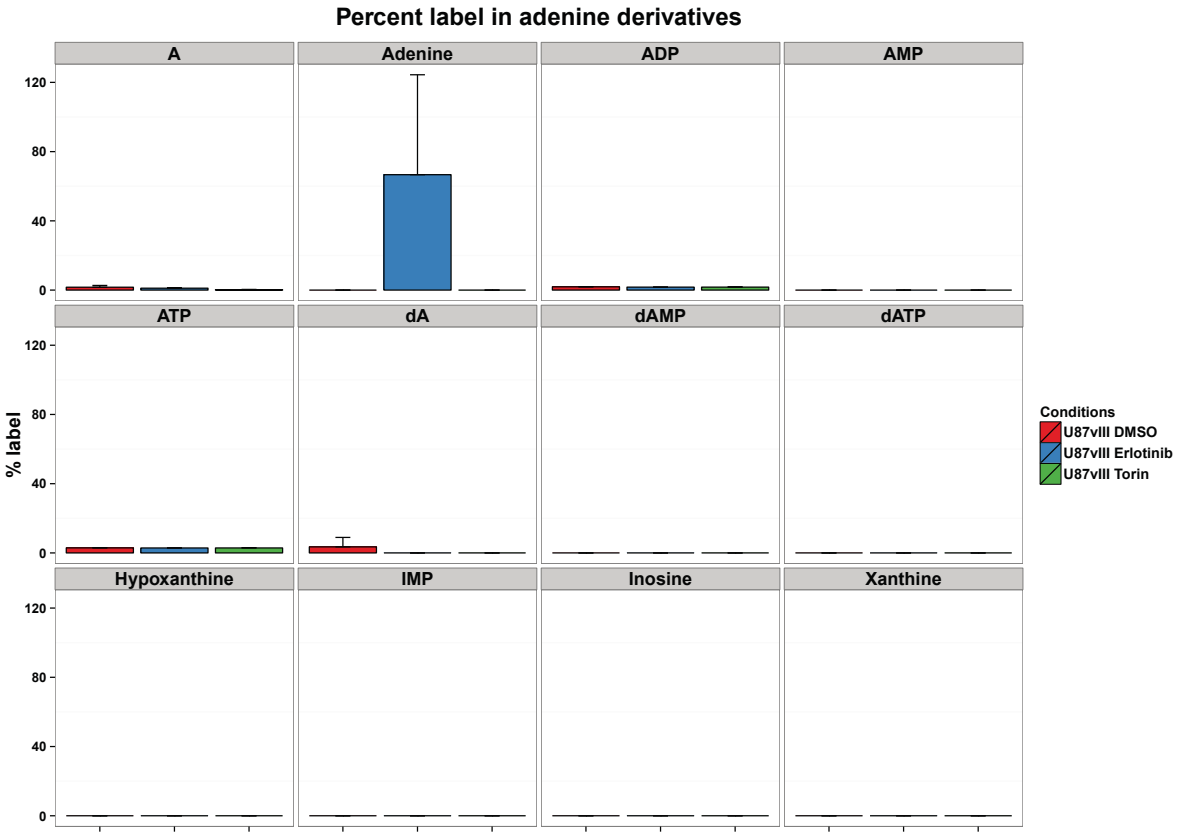
Percent label in adenine derivatives
A
Adenine
ADP
AMP
ATP
dA
dAMP
dATP
Hypoxanthine
IMP
Inosine
Xanthine
% label
Conditions
U87vIII DMSO
U87vIII Erlotinib
U87vIII Torin

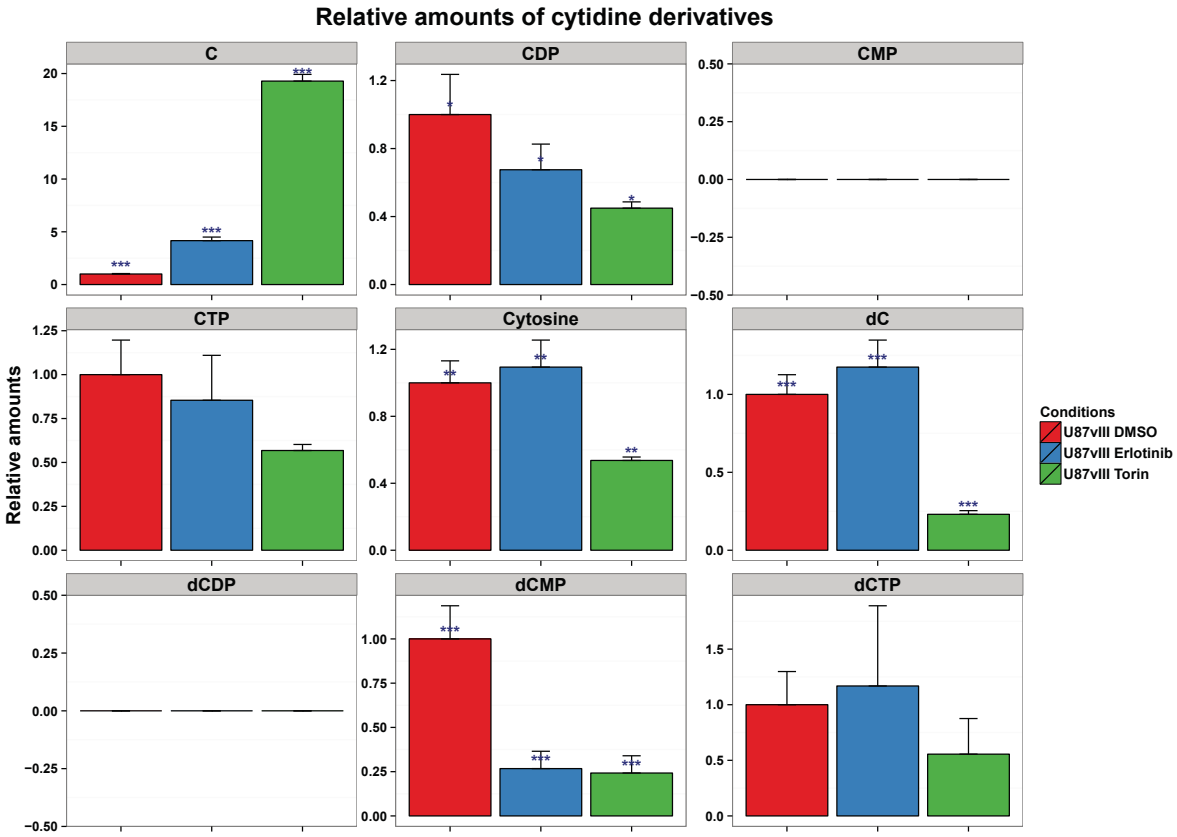
Relative amounts of cytidine derivatives
C
CDP
CMP
CTP
Cytosine
dC
dCDP
dCMP
dCTP
Relative amounts
Conditions
U87vIII DMSO
U87vIII Erlotinib
U87vIII Torin

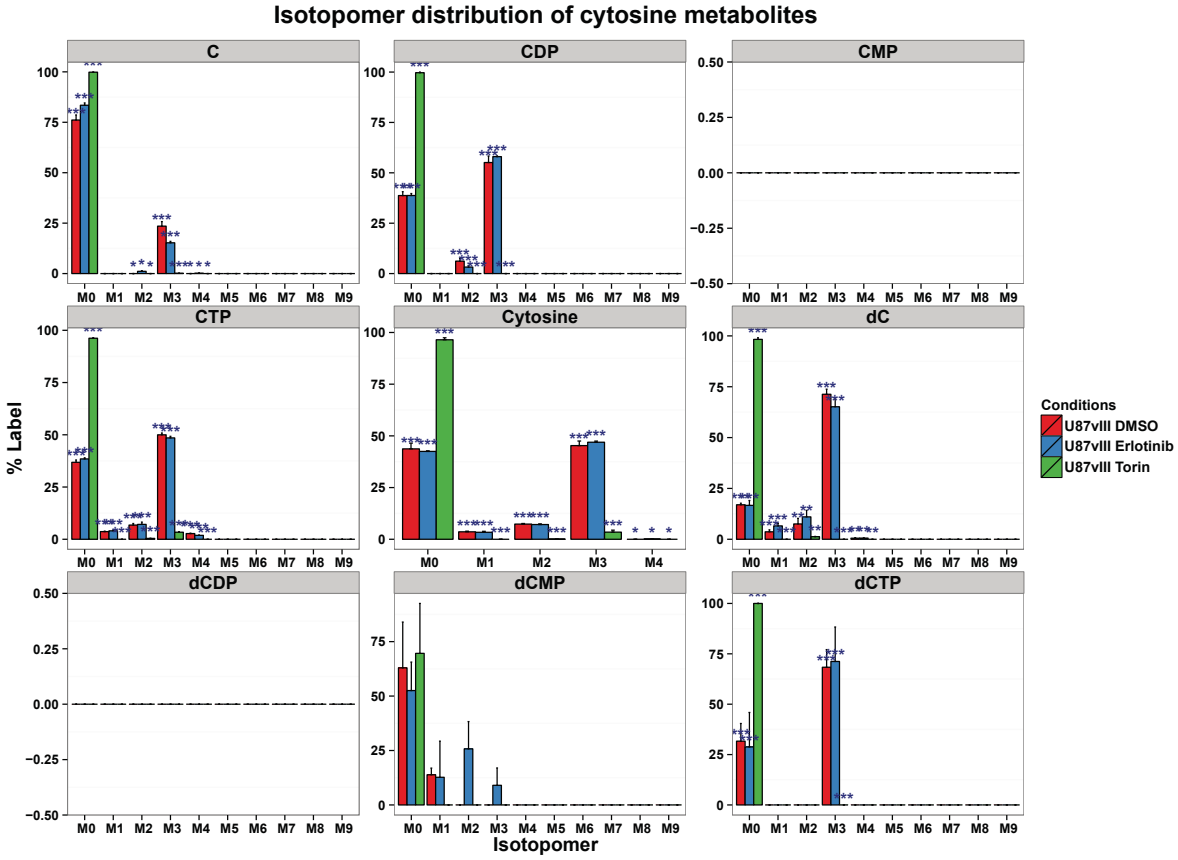
Isotopomer distribution of cytosine metabolites
C
CDP
CMP
CTP
Cytosine
dC
dCDP
dCMP
dCTP
% Label
Isotopomer
M0 M1 M2 M3 M4 M5 M6 M7 M8 M9
Conditions
U87vIII DMSO
U87vIII Erlotinib
U87vIII Torin

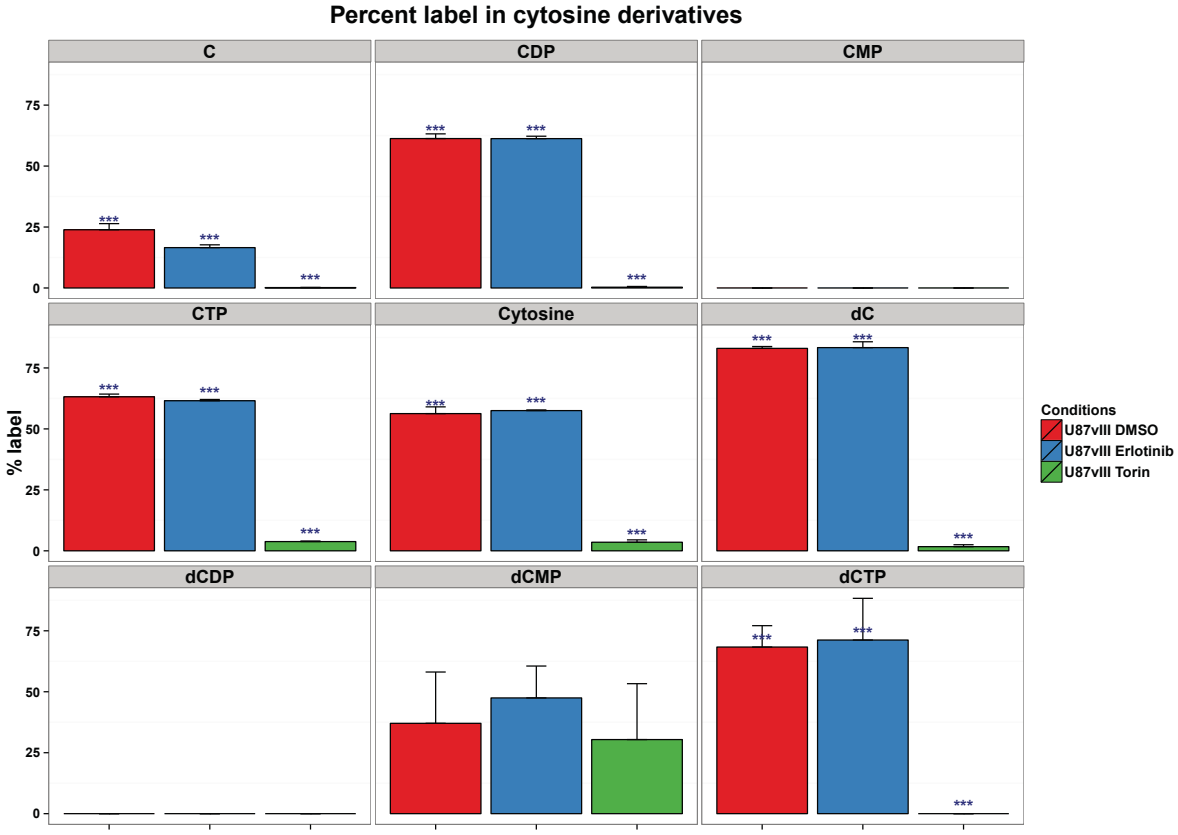
Percent label in cytosine derivatives
C
CDP
CMP
CTP
Cytosine
dC
dCDP
dCMP
dCTP
% label
Conditions
U87vIII DMSO
U87vIII Erlotinib
U87vIII Torin

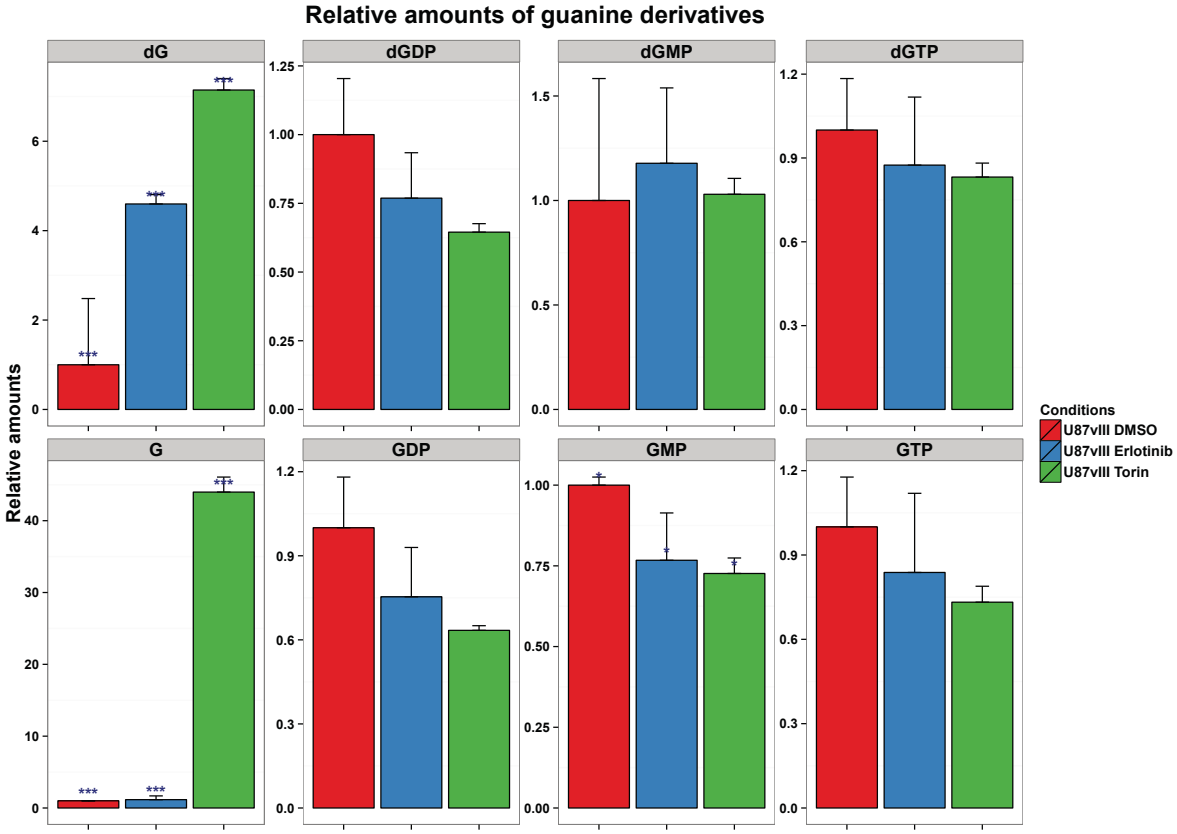
Relative amounts of guanine derivatives
dG
dGDP
dGMP
dGTP
G
GDP
GMP
GTP
Relative amounts
Conditions
U87vIII DMSO
U87vIII Erlotinib
U87vIII Torin

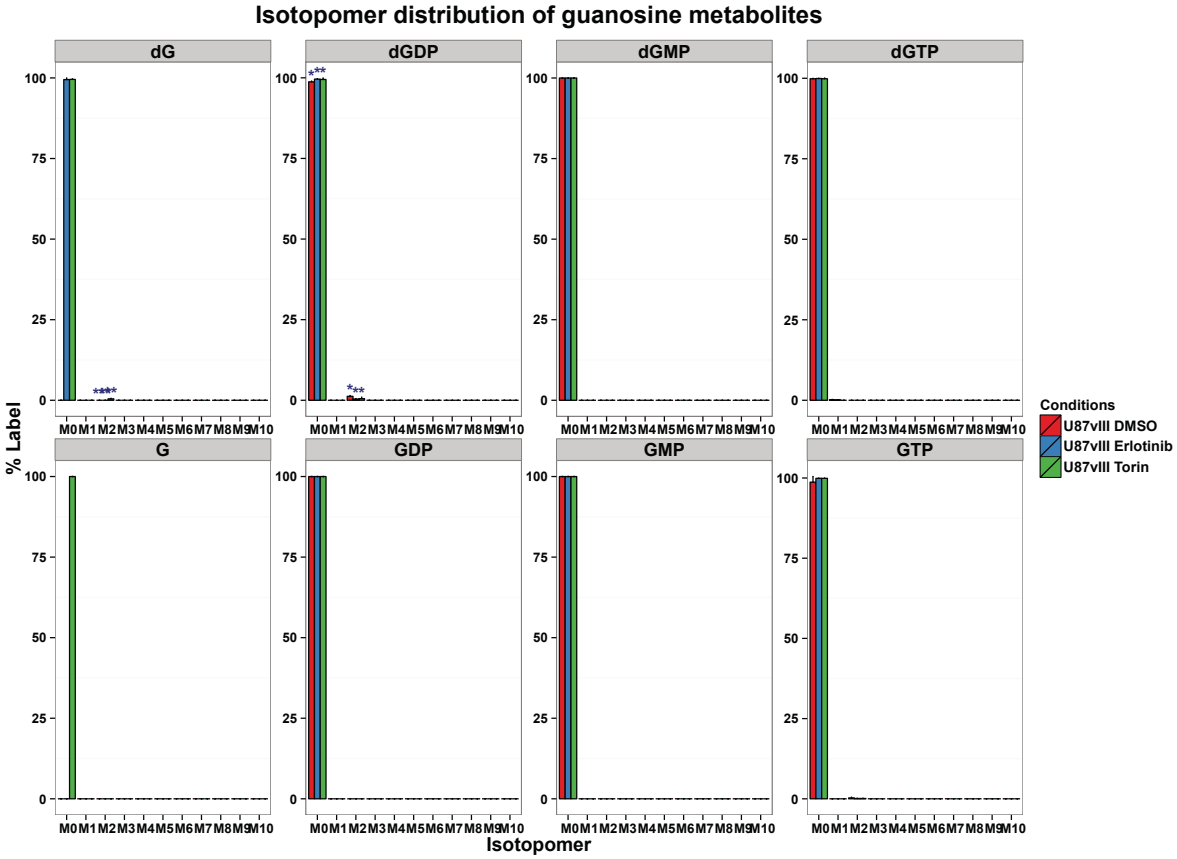
Isotopomer distribution of guanosine metabolites
dG
dGDP
dGMP
dGTP
G
GDP
GMP
GTP
% Label
Isotopomer
M0 M1 M2 M3 M4 M5 M6 M7 M8 M9 M10
Conditions
U87vIII DMSO
U87vIII Erlotinib
U87vIII Torin

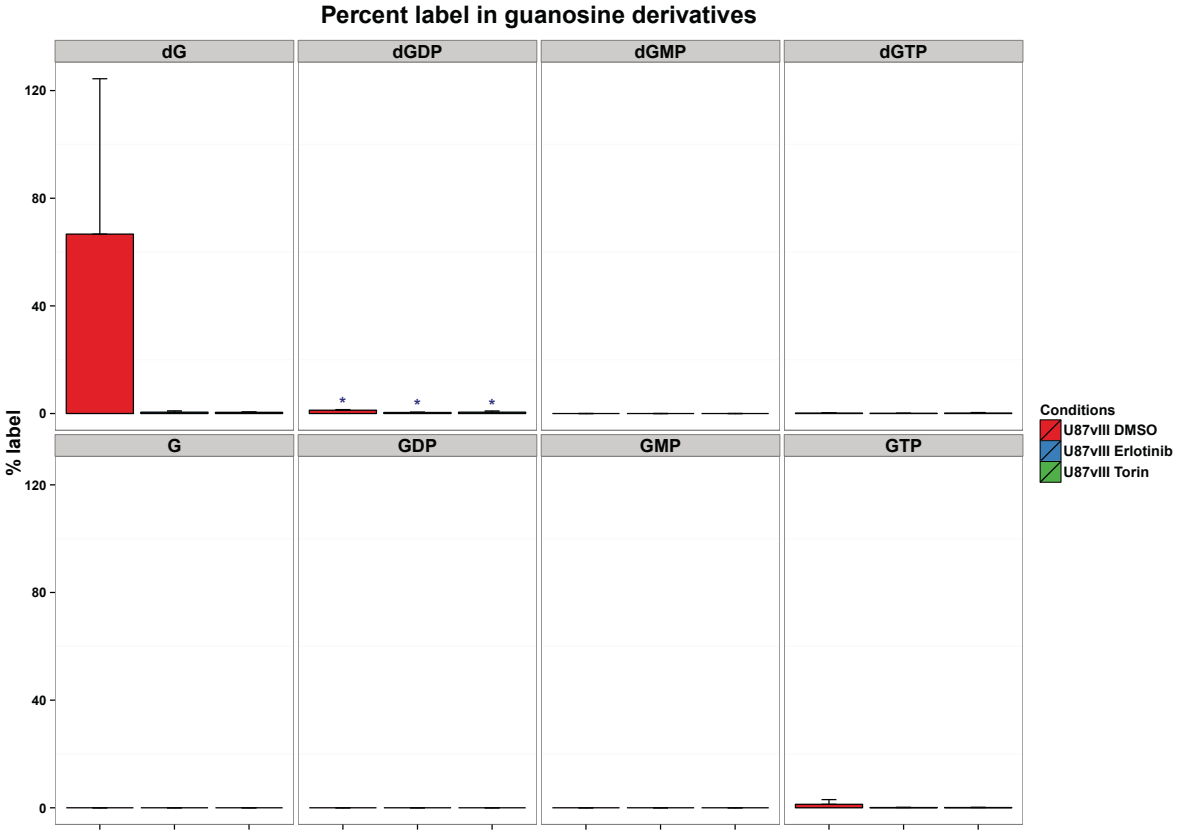
Percent label in guanosine derivatives
dG
dGDP
dGMP
dGTP
G
GDP
GMP
GTP
% label
120
80
40
0
Conditions
U87vIII DMSO
U87vIII Erlotinib
U87vIII Torin

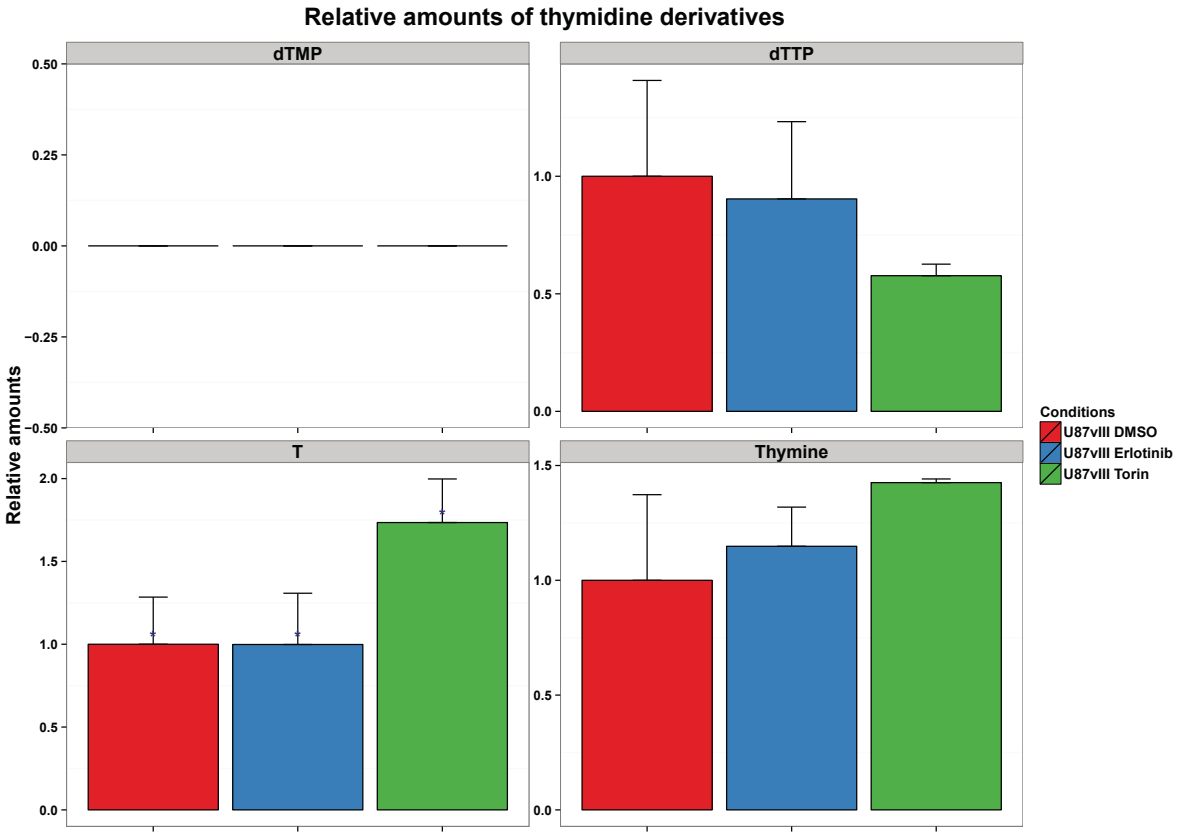
Relative amounts of thymidine derivatives
dTMP
dTTP
T
Thymine
Relative amounts
0.50
0.25
0.00
−0.25
−0.50
1.0
0.5
0.0
2.0
1.5
1.0
0.5
0.0
1.5
1.0
0.5
0.0
Conditions
U87vIII DMSO
U87vIII Erlotinib
U87vIII Torin

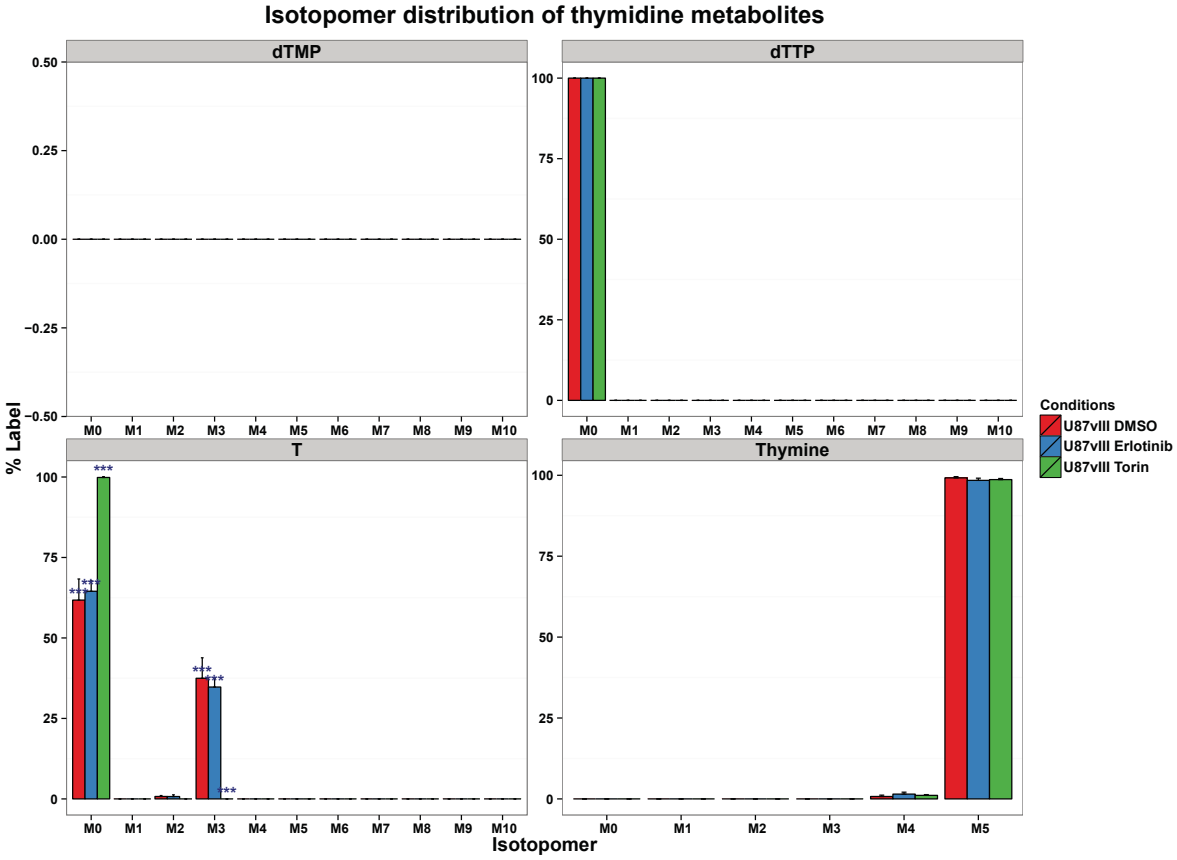
Isotopomer distribution of thymidine metabolites
dTMP
dTTP
T
Thymine
% Label
Isotopomer
M0
M1
M2
M3
M4
M5
M6
M7
M8
M9
M10
Conditions
U87vIII DMSO
U87vIII Erlotinib
U87vIII Torin

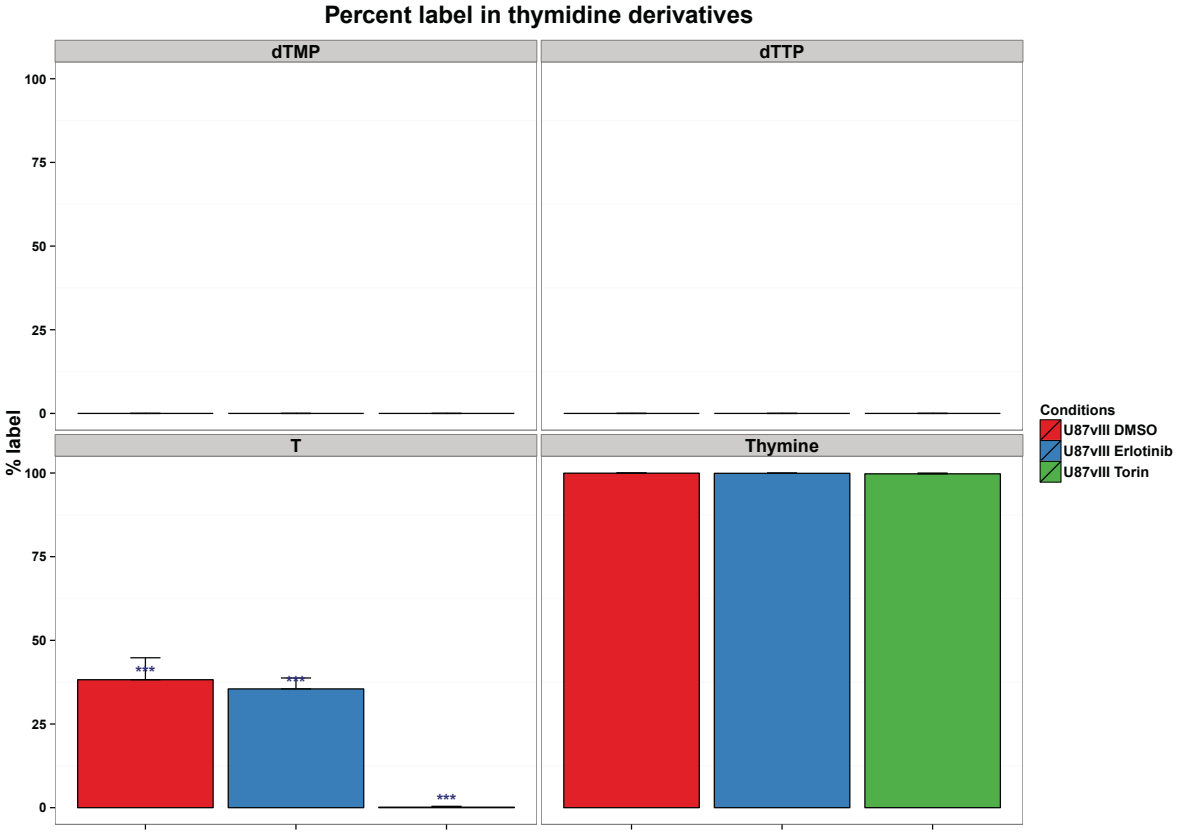
Percent label in thymidine derivatives
dTMP
dTTP
T
Thymine
% label
Conditions
U87vIII DMSO
U87vIII Erlotinib
U87vIII Torin

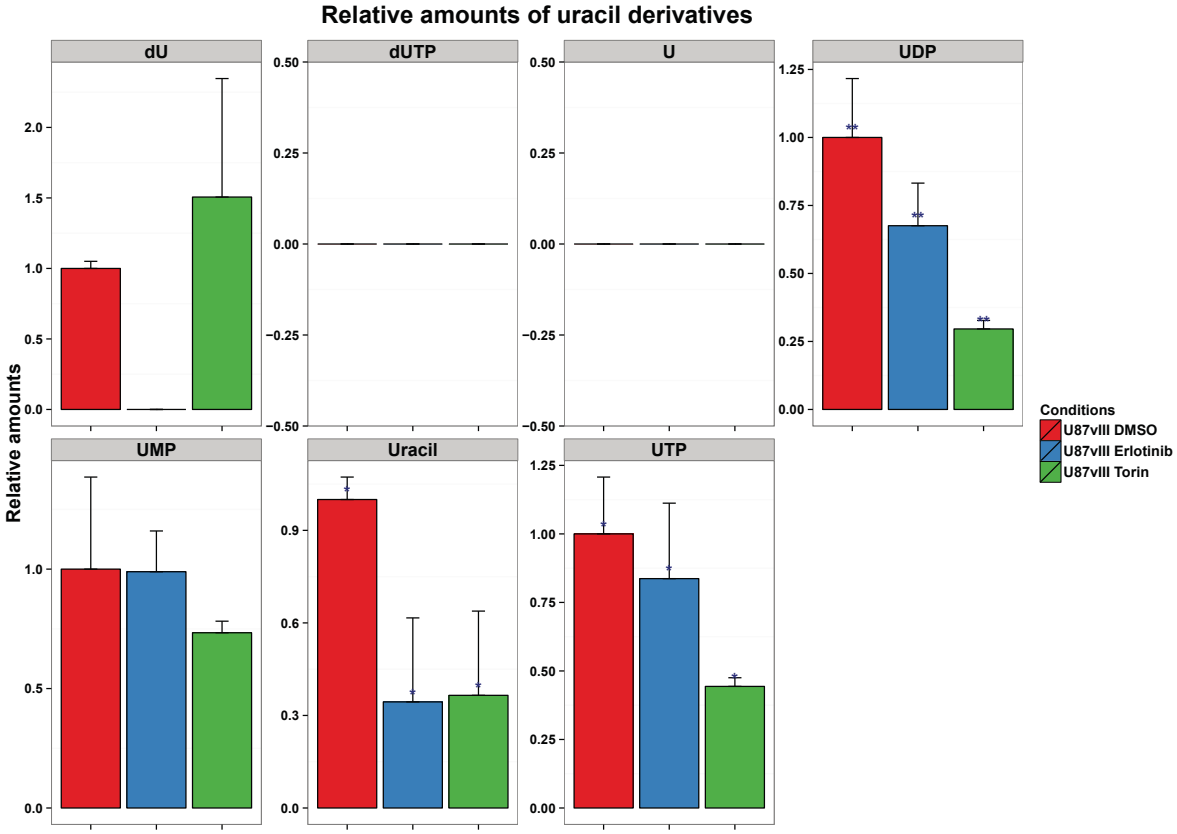
Relative amounts of uracil derivatives
dU
dUTP
U
UDP
UMP
Uracil
UTP
Relative amounts
Conditions
U87vIII DMSO
U87vIII Erlotinib
U87vIII Torin

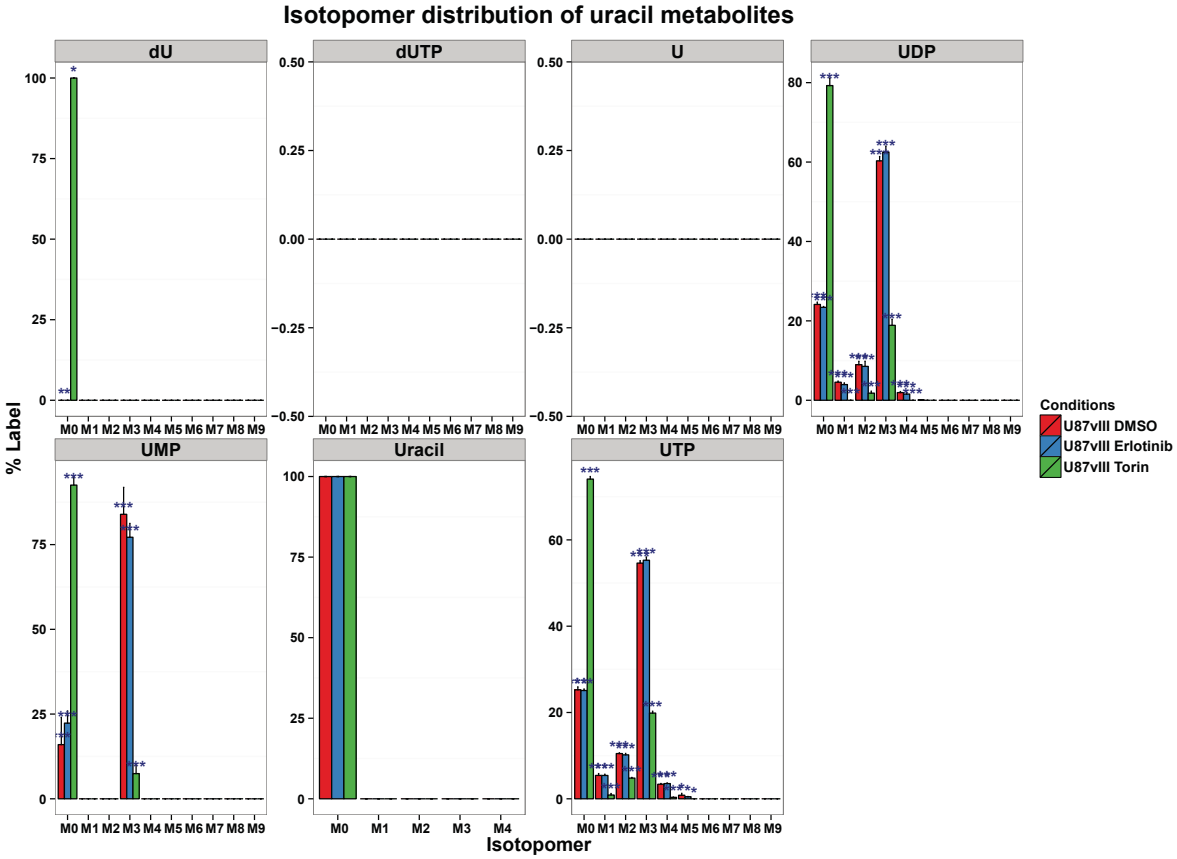
Isotopomer distribution of uracil metabolites
dU
dUTP
U
UDP
UMP
Uracil
UTP
% Label
Isotopomer
M0 M1 M2 M3 M4 M5 M6 M7 M8 M9
Conditions
U87vIII DMSO
U87vIII Erlotinib
U87vIII Torin

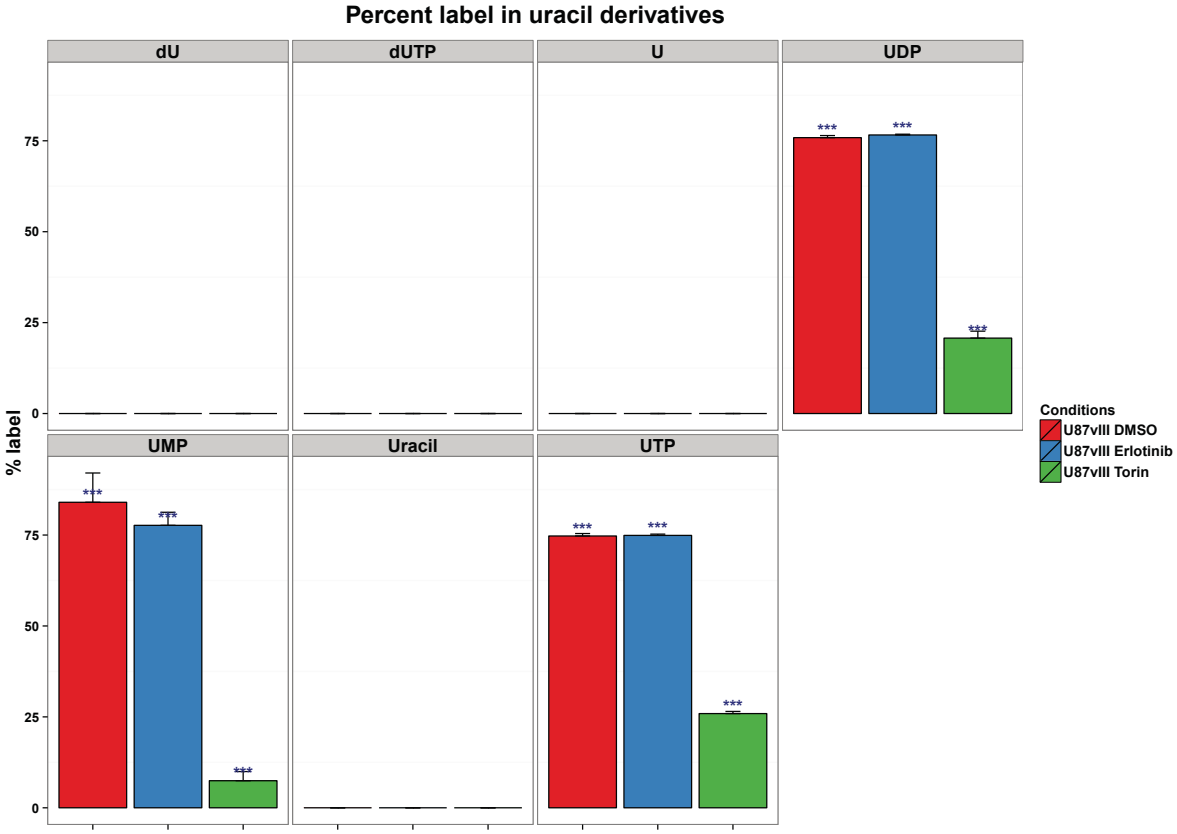
Percent label in uracil derivatives
dU
dUTP
U
UDP
UMP
Uracil
UTP
% label
0
25
50
75
***
Conditions
U87vIII DMSO
U87vIII Erlotinib
U87vIII Torin

APPENDIX III - Related to Chapter 4

Additional Mechanisms Mediating mTOR Inhibitor Resistance in GBM

INTRODUCTION

In Chapter 3 and 4, we described a unique co-dependency of GBM cells on xCT-mediated cystine uptake and glutathione synthesis upon mTOR kinase inhibition, and showed that targeting this metabolic co-dependency effectively induced tumor cell death through ferroptosis in GBM. Besides rewiring of metabolic pathways which serves as adaptive responses to cellular perturbations induced by targeted therapies, other mechanisms also contributes to tumor cell survival and development of drug resistance. Such mechanisms include, but no limited to, intrinsic heterogeneity of the tumor cell population, altered drug transport and metabolism, mutations in drug targets, oncogenic bypass and pathway redundancy, as well as deregulation of apoptosis and activation of pro-survival signaling pathways and autophagy. In addition, tumor microenvironment such as secreted cytokines and stromal cells also plays an important role in the resistance to different cancer therapies (Holohan et al., 2013; Huang et al., 2014). Therefore understanding the detailed mechanisms would be very important in guiding the correct decision of treatment strategies for cancer patients in the clinic, especially as drug resistance mechanisms usually vary in different cancers and different therapies. Here I want to present two studies resulted from collaborative efforts with other members from the Mischel lab as well as from our collaboration with the Heath lab at Caltech, which uncovered how two different resistance mechanisms - autophagy and oncogenic bypass pathways contribute to tumor cell resistance to mTOR kinase inhibitors in GBM.

RESULTS

Autophagy Induction Contributes to Tumor Cell Survival and Resistance to mTOR Kinase Inhibitors

To achieve better inhibition of mTOR and overcome resistance to the allosteric mTORC1 inhibitor rapamycin in GBM, we examined the anti-tumor effect of a second-generation mTOR kinase inhibitor CC214 both in vitro and in vivo using flank and orthotopic GBM xenografts. While CC214 dramatically suppressed signaling pathway activities downstream of both mTORC1 and mTORC2, inhibitor treatment only induced a cytostatic effect as no cell death was observed in xenograft tumors by TUNNEL staining (Fig. A3-1A). As inhibition of mTORC1 has been linked to autophagy induction, which is an important survival mechanism allowing tumor cells to degrade intracellular proteins to support metabolism under nutrient limitation (Chan, 2009; Efeyan et al., 2012), we tested the hypothesis that autophagy could be one mechanism mediating resistance to mTOR kinase inhibitor-induced cell death in GBM. Examination of autophagy markers showed significant induction of autophagic flux by CC214, especially in EGFRvIII expressing cells, which is consistent with their higher sensitivity to CC214 (Fig. A3-1B and C). Combination treatment of CC214 with the autophagy inhibitor chloroquine significantly suppressed GBM tumors in the brain and increased cell death (Fig. A3-1D). These data strongly suggest that autophagy is an important survival mechanism and contributes to the resistance to mTOR kinase inhibitors in GBM (Gini et al., 2013).

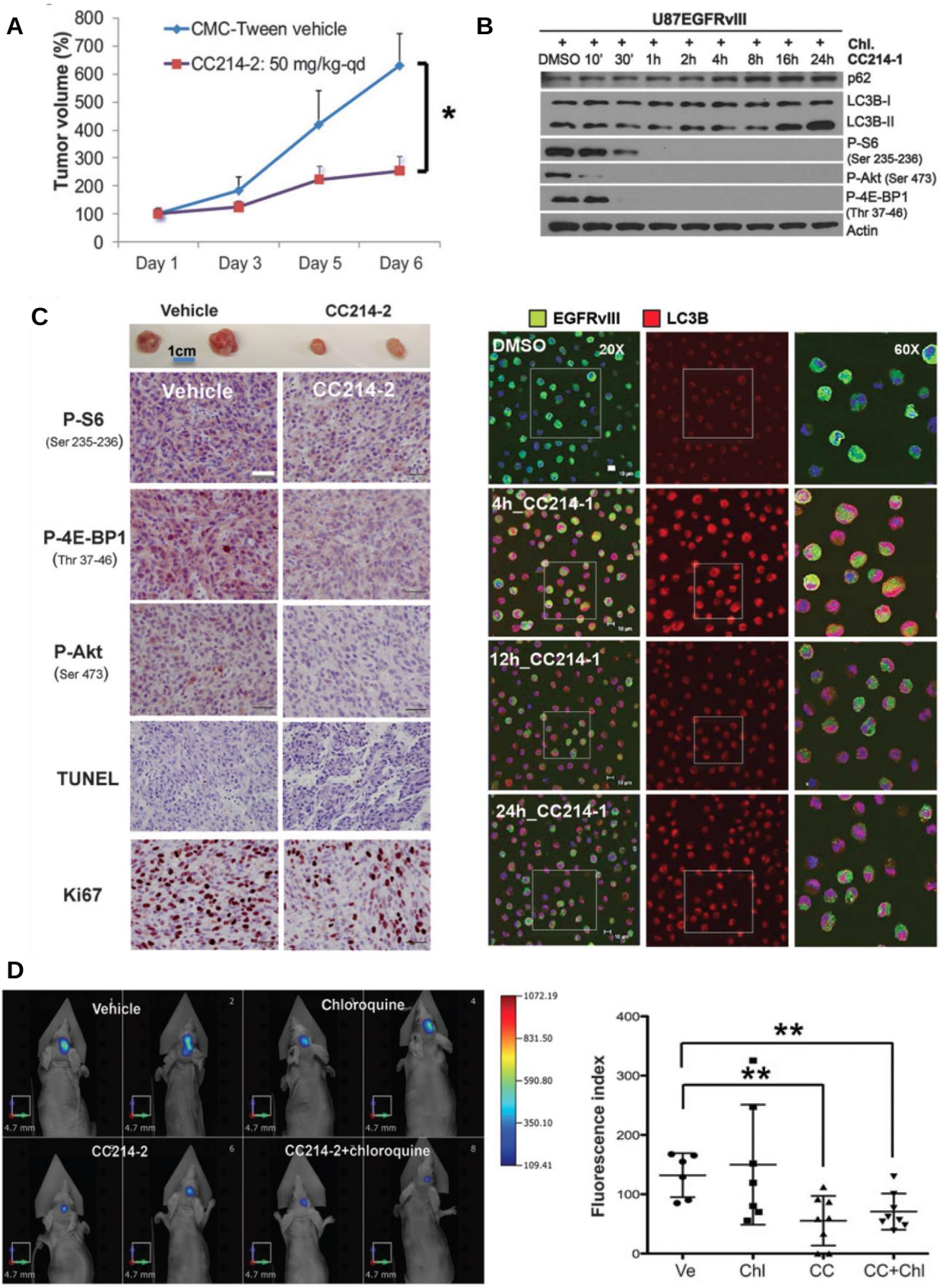
A
Tumor volume (%)
CMC-Tween vehicle
CC214-2: 50 mg/kg-qd
Day 1
Day 3
Day 5
Day 6
*
B
U87EGFRvIII
Chl.
CC214-1
DMSO 10' 30' 1h 2h 4h 8h 16h 24h
p62
LC3B-I
LC3B-II
P-S6 (Ser 235-236)
P-Akt (Ser 473)
P-4E-BP1 (Thr 37-46)
Actin
C
Vehicle
CC214-2
1cm
P-S6 (Ser 235-236)
P-4E-BP1 (Thr 37-46)
P-Akt (Ser 473)
TUNEL
Ki67
EGFRvIII
LC3B
DMSO
20X
60X
4h_CC214-1
12h_CC214-1
24h_CC214-1
D
Vehicle
Chloroquine
CC214-2
CC214-2+chloroquine
1072.19
831.50
590.80
350.10
109.41
Fluorescence index
**
**
Ve
Chl
CC
CC+Chl

Fig. A3-1. Autophagy Induction Mediates GBM Cell Survival and Resistance to mTOR Kinase Inhibitor CC214-1/2.

(A) Mice with U87EGFRvIII flank xenografts were treated with 50mg/kg/day CC214-2 through oral gavage for 6 days and tumor size was measured as well as immunohistochemistry was performed after tumors were taken out at day 6 to analyze activity of mTORC1 and mTORC2 signaling pathways and tumor cell proliferation/viability.

(B) Autophagy markers were analyzed by western blot in U87EGFRvIII cells treated with CC214-1 in the presence of chloroquine.

(C) Double immunofluorescence staining of EGFRvIII (red) and autophagy marker LC3B (green) was performed in GBM39 neurospheres comparing with or without CC214-1 treatment.

(D) In vivo combinatory treatment with CC214-2 and chloroquine was performed in GBM orthotopic xenografts. Tumor progression was evaluated using fluorescence molecular tomography.

Figure was modified and originally published by Gini *et al* (Gini et al., 2013). For detailed experimental procedures please refer to the original paper Gini *et al* (Gini et al., 2013).

Single-Cell Phosphoproteomics Reveal Adaptation to Alternative Signaling Pathways as Resistance Mechanism to mTOR kinase inhibitors

Altered signaling networks and induction bypass pathways is a common mechanism mediating resistance to kinase inhibitors in cancer (Holohan et al., 2013; Huang et al., 2014). To determine whether alternative signaling pathway activation also contribute to mTOR kinase inhibitor resistance in GBM, we established an in vivo mTOR kinase-resistant GBM model with patient-derived neurospheres, and performed single cell phosphoproteomics analysis using a Single Cell Barcode Chip (SCBC) platform developed in the lab (Heath et al., 2016; Yu et al., 2014) (Fig. A3-2D). Treatment of GBM xenograft tumors with CC214 showed an initial response phase, during which tumor growth and glucose uptake were significantly suppressed due to inhibition of both mTORC1 and mTORC2 (Fig. A3-2A and B). But by day 27, tumors regained rapid growth and elevated glucose uptake, suggesting an adaptive mechanism of resistance. Single cell phosphoproteomics analysis of control, responsive and resistant tumors revealed reactivation of both mTORC1 and mTORC2, which is consistent with IHC staining of tumor samples (Fig. A3-2C, E and F). More importantly, SCBC analysis uncovered that in the responsive tumors, while CC214 decreased signaling coordination associated with mTORC1/2, Erk and Src pathway was already activated, which persisted in the resistant tumor and possibly mediated sustained activation of mTORC1/2 downstream effectors. These suggest that combined inhibition of mTOR, Erk and Src pathways is required to achieve complete suppression of mTORC1/2 downstream pathways, while targeting any one or two pathways is not sufficient. We tested this hypothesis by performing different combination treatments on intracranial GBM xenograft tumors, and as expected, the best response was observed when inhibitors of all three pathways were combined, which successfully suppressed both signaling flux and tumor growth (Fig. A3-

2G and H). This study indicated that identifying and targeting independent signaling pathways would be the key to achieve the strongest anti-tumor effect with small molecule kinase inhibitors (Wei et al., 2016).

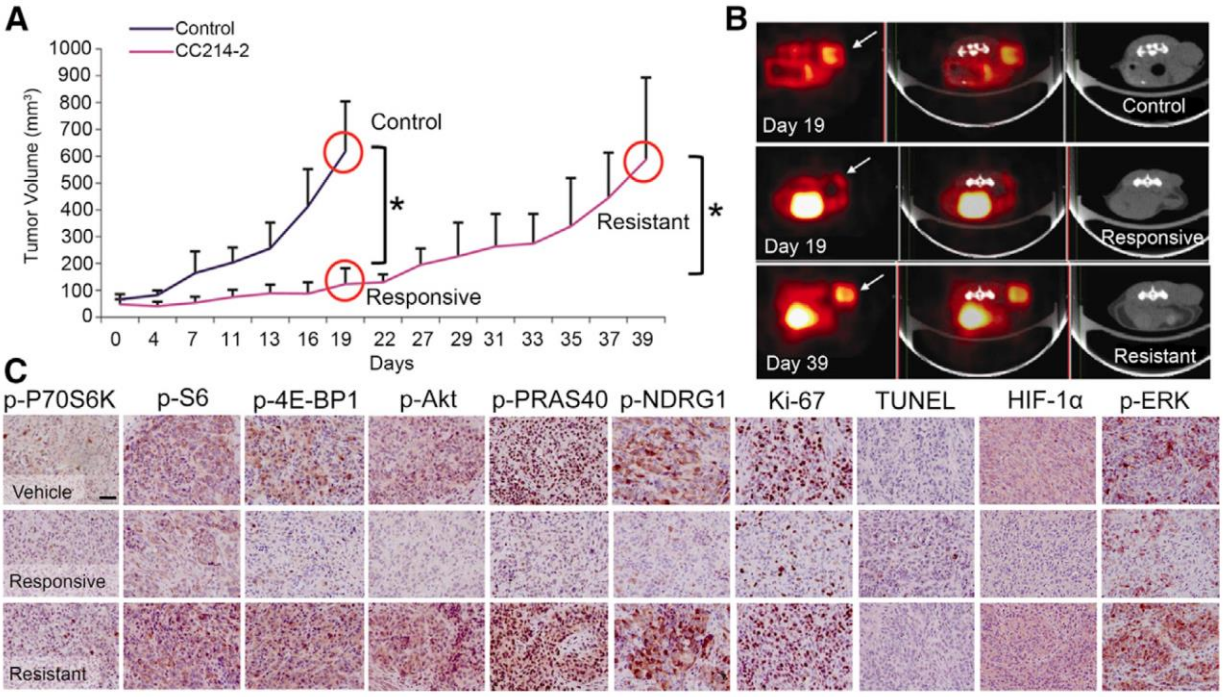

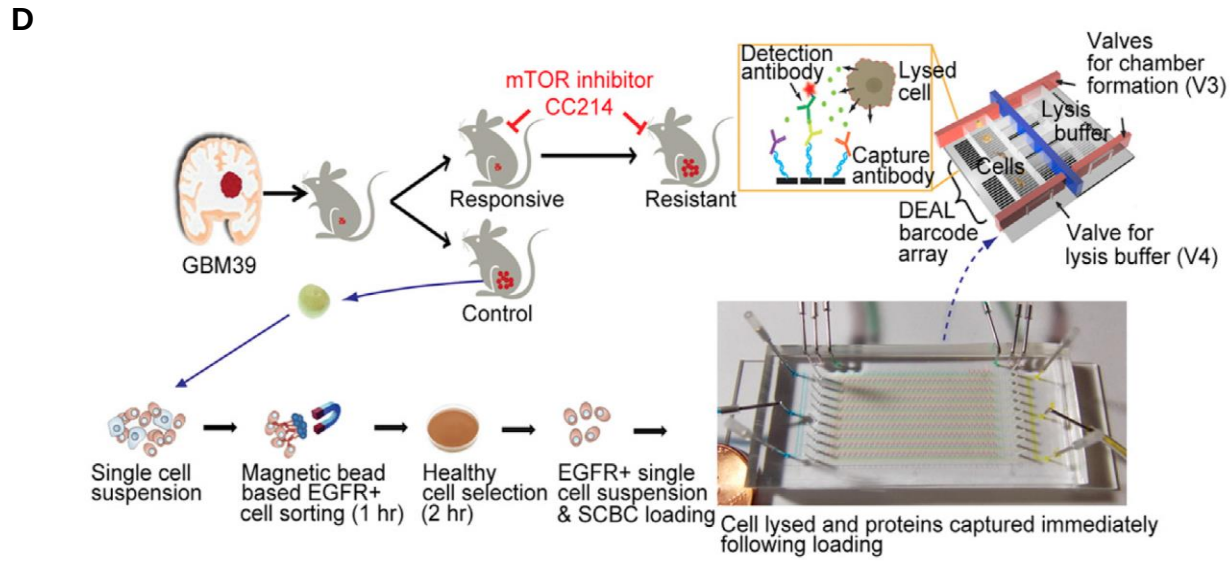

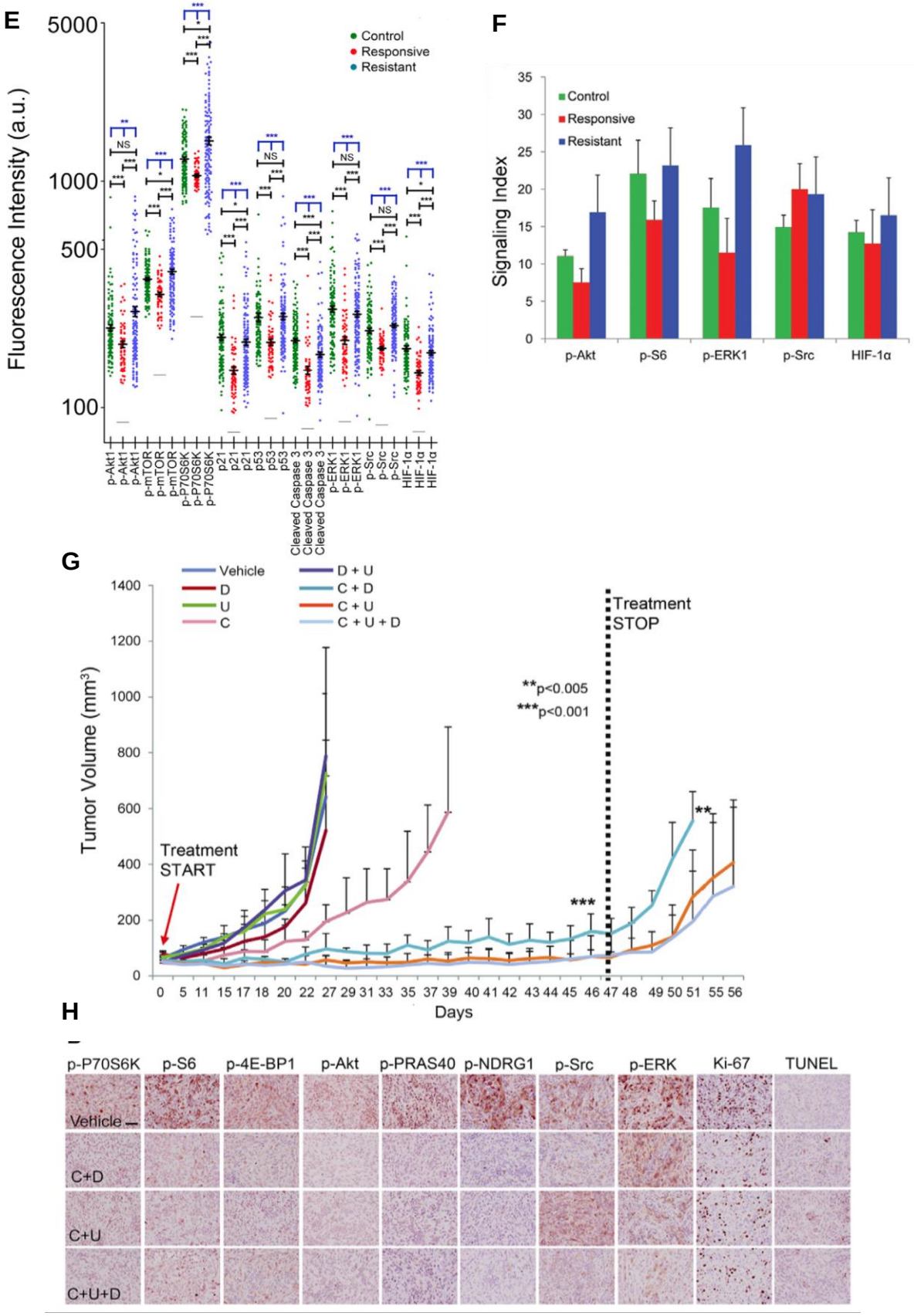
E
Fluorescence Intensity (a.u.)
5000
1000
500
100
Control
Responsive
Resistant
NS
p-Akt1
p-mTOR
p-P70S6K
p21
p53
Cleaved Caspase 3
p-ERK1
p-Src
HIF-1α
F
Signaling Index
35
30
25
20
15
10
5
0
Control
Responsive
Resistant
p-Akt
p-S6
p-ERK1
p-Src
HIF-1α
G
Tumor Volume (mm3)
1400
1200
1000
800
600
400
200
0
Vehicle
D
U
C
D + U
C + D
C + U
C + U + D
Treatment START
Treatment STOP
**p<0.005
***p<0.001
0 5 11 15 17 18 20 22 27 29 31 33 35 37 39 40 41 42 43 44 45 46 47 48 49 50 51 55 56
Days
H
p-P70S6K
p-S6
p-4E-BP1
p-Akt
p-PRAS40
p-NDRG1
p-Src
p-ERK
Ki-67
TUNEL
Vehicle
C+D
C+U
C+U+D

Fig. A3-2. Single-Cell Phosphoproteomics Analysis of mTOR kinase inhibitor-resistant GBM Tumors Revealed Activation of Src and Erk Pathways as Resistant Mechanisms.

(A) GBM39 flank xenograft tumors were treated with vehicle control or CC214-1 and tumor size was measured. Control (n=11) and responsive (n=7) tumors were collected for analysis at day 19 while resistant tumors (n=7) were collected at day 39. Results were shown as mean ± SD.

(B) ^{18}F-FDG, PET-CT and CT scans were shown comparing control, response and resistant tumors (n=4 for each condition).

(C) IHC staining for biomarkers of signaling pathways, cell proliferation and cell death on tissue samples collected from control, response and resistant tumors.

(D) A brief scheme of the workflow of Single Cell Barcode Chip (SCBC) analysis. Tumors were collected from experiment in (A) and digested into single cells, $EGFR^+$ cells were collected using conjugated antibodies and loaded onto SCBC where cells were lysed and phosphorylation of signaling proteins were analyzed.

(E) Data collected from SCBC analysis was presented as one-dimensional scatterplots with background subtracted (mean ± SEM). Grey bars indicate background of each protein assayed.

(F) IHC results for selected proteins from (C) were quantified and showed as mean ± SD as a comparison to SCBC data.

(G) GBM39 flank xenograft tumors were treated with mono- or combination therapies based on predictions from the SCBC analysis.Ttumor size was measured and quantified for each treatment. C: mTOR kinase inhibitor CC214-2, D: Src inhibitor Dasatinib, U: Erk inhibitor U0126.

(H) IHC was performed to look at inhibition of drug targets with the combination treatment. Figure was modified and originally published by Wei *et al* (Wei et al., 2016). For detailed experimental procedures please also refer to the original paper Wei *et al* (Wei et al., 2016).

DISCUSSION

Therapeutic resistance in cancer can usually be attributed to either intrinsic characters of the tumor, such as existing drug-insensitive populations or cells already harboring drug-resistant mutations within the tumor; or adaptive responses to drug treatments such as induction of survival mechanisms, activation of bypass or redundant signaling pathways, or acquisition of drug-resistant mutations. While drug resistant mechanisms in general fall into a few major categories across cancer, the specific response or survival pathways activated towards the same treatment usually differs in different cancer types, which could possibly result from the distinct driver oncogenes and tumor microenvironment that together determined the signaling and metabolic dependencies in different tumor cells. For instance, activating mutations of EGFR serve as driver oncogenes for both non-small cell lung cancer (NSCLC) and GBM, but these two cancers display complete different response and resistance mechanisms to EGFR inhibitors. EGFR inhibitors effectively suppress lung cancer progression in patients and induce apoptosis, albeit drug resistance usually arise through acquired mutations in EGFR that interferes with drug binding, or activation of the PI3K and Met pathway (Gazdar, 2009; Killock, 2015; Lin and Shaw, 2016). On the contrary, EGFR inhibitors are largely ineffective in GBM, showing only minimal suppression of tumor growth despite the downstream signaling pathways were effectively suppressed. In addition, GBM tumors employ a unique resistance mechanism to EGFR inhibitors by discarding the drug target through diminishing EGFR-containing extrachromosomal DNA (Nathanson et al., 2014). Similar phenomenon is also observed with mTOR inhibitors. While certain types of cancer are exquisitely sensitive to mTOR inhibition, such as renal cell carcinoma, GBM cells mostly survived by inducing autophagy and activate bypass pathways to drive tumor growth (Gini et al., 2013; Wei et al., 2016). More interestingly, it was found that mTOR

inhibition unexpectedly promoted tumor cell proliferation in pancreatic cancer. This is explained by the unique dependence on macropinocytosis for nutrient acquisition in pancreatic cancer cells, which is driven by Ras activation and also determined by the nutrient-limiting tumor microenvironment. Macropinocytosis relies on lysosome-mediated degradation of scavenged proteins, which is accelerated by inhibition of mTORC1 (Palm et al., 2015). All these indicate that it will be of great importance to study drug response and resistant mechanisms in different cancers, especially using in vivo and patient-derived tumor models as both tumor microenvironment and heterogeneity greatly contribute to therapeutic response and resistance. In addition, development of sensitive and accurate diagnostic platforms such as the SCBC described above will also be essential for assessing drug response and pinpointing the drug resistance mechanism in each individual patient so that the right treatment strategy could be determined to achieve the best anti-tumor effect. Therefore, despite that tumor cells could develop drug resistance through various mechanisms, it is still promising for us to achieve effective and prolonged tumor inhibition through rational designs of combination therapies targeting independent pathways, and inhibiting the exact resistance mechanisms using our increasing arsenal of anti-cancer therapies.

REFERENCES

Chan, E.Y. (2009). mTORC1 phosphorylates the ULK1-mAtg13-FIP200 autophagy regulatory complex. Science signaling *2*, pe51.

Efeyan, A., Zoncu, R., and Sabatini, D.M. (2012). Amino acids and mTORC1: from lysosomes to disease. Trends in molecular medicine *18*, 524-533.

Gazdar, A.F. (2009). Activating and resistance mutations of EGFR in non-small-cell lung cancer: role in clinical response to EGFR tyrosine kinase inhibitors. Oncogene *28 Suppl 1*, S24-31.

Gini, B., Zanca, C., Guo, D., Matsutani, T., Masui, K., Ikegami, S., Yang, H., Nathanson, D., Villa, G.R., Shackelford, D., *et al.* (2013). The mTOR kinase inhibitors, CC214-1 and CC214-2, preferentially block the growth of EGFRvIII-activated glioblastomas. Clinical cancer research : an official journal of the American Association for Cancer Research *19*, 5722-5732.

Heath, J.R., Ribas, A., and Mischel, P.S. (2016). Single-cell analysis tools for drug discovery and development. Nature reviews Drug discovery *15*, 204-216.

Holohan, C., Van Schaeybroeck, S., Longley, D.B., and Johnston, P.G. (2013). Cancer drug resistance: an evolving paradigm. Nature reviews Cancer *13*, 714-726.

Huang, M., Shen, A., Ding, J., and Geng, M. (2014). Molecularly targeted cancer therapy: some lessons from the past decade. Trends in pharmacological sciences *35*, 41-50.

Killock, D. (2015). Lung cancer: a new generation of EGFR inhibition. Nature reviews Clinical oncology *12*, 373.

Lin, J.J., and Shaw, A.T. (2016). Resisting Resistance: Targeted Therapies in Lung Cancer. Trends in cancer *2*, 350-364.

Nathanson, D.A., Gini, B., Mottahedeh, J., Visnyei, K., Koga, T., Gomez, G., Eskin, A., Hwang, K., Wang, J., Masui, K., *et al.* (2014). Targeted therapy resistance mediated by dynamic regulation of extrachromosomal mutant EGFR DNA. Science *343*, 72-76.

Palm, W., Park, Y., Wright, K., Pavlova, N.N., Tuveson, D.A., and Thompson, C.B. (2015). The Utilization of Extracellular Proteins as Nutrients Is Suppressed by mTORC1. Cell *162*, 259-270.

Wei, W., Shin, Y.S., Xue, M., Matsutani, T., Masui, K., Yang, H., Ikegami, S., Gu, Y., Herrmann, K., Johnson, D., *et al.* (2016). Single-Cell Phosphoproteomics Resolves Adaptive Signaling Dynamics and Informs Targeted Combination Therapy in Glioblastoma. Cancer cell *29*, 563-573.

Yu, J., Zhou, J., Sutherland, A., Wei, W., Shin, Y.S., Xue, M., and Heath, J.R. (2014). Microfluidics-based single-cell functional proteomics for fundamental and applied biomedical applications. Annual review of analytical chemistry *7*, 275-295.